In Vivo Physiology of Gap Junctions between Supporting Cells in the Organ of Corti

by

Pankaj Oberoi

S.B., Electrical Engineering
Massachusetts Institute of Technology (June, 1991)
M.S., Electrical Engineering
Massachusetts Institute of Technology (February, 1996)

SUBMITTED TO THE DIVISION OF HEALTH SCIENCES AND TECHNOLOGY
IN PARTIAL FULFILLMENT OF THE REQUIREMENTS FOR THE DEGREE OF

DOCTOR OF PHILOSOPHY

at the

MASSACHUSETTS INSTITUTE OF TECHNOLOGY

February 1999

Author .....
Division of Health Sciences and Technology
January 18, 1999

Certified by.....
Joe C. Adams
Associate Professor of Otology and Laryngology, Harvard Medical School
Thesis Supervisor

Accepted by.....
Martha L. Gray
Co-director, Division of Health Sciences and Technology

In Vivo Physiology of Gap Junctions between Supporting Cells in the Organ of Corti

by

Pankaj Oberoi

Submitted to the Division of Health Sciences and Technology
on January 18, 1999, in partial fulfillment of the
requirements for the degree of
Doctor of Philosophy

ABSTRACT

The majority of inner ear tissue is composed of non-sensory cells, known as supporting cells, yet little is known about their physiological roles in cochlear function. Gap junctions between the cochlear supporting cells form two gap junctional networks: the "epithelial network" in the organ of Corti and the "connective-tissue" network in the lateral wall. These networks appear to provide the anatomical substrates for the recirculation of K+ ions, which carry the transduction current, from the basolateral region of hair cells to the intrastrial space. While the existence of the gap junctional networks has been shown anatomically, little is known about their physiological properties or whether they serve the above suggested function.

In this work, physiological properties of the epithelial network were studied *in vivo* using several complementary methods: 1. direct on-line visualization of the movement of iontophoresed fluorescent dye; 2. electrophysiological measurements of resting potentials, cell impedance, mutual resistance, and sound-evoked responses; and 3. reversible interruption of the gap junctions using known uncoupling agents such as octanol, halothane, or a low pH artificial perilymph. To better interpret the physiological results, locations and densities of connexin 26 (Cx26), a gap junction protein, were mapped between cells in the organ of Corti.

Visualization of the dye showed: 1. the gap junctions are patent *in vivo* and 2. the movement of the dye was not always symmetric about the injection site, and often spread preferentially in the longitudinal direction. Resting potentials and evoked responses were graded with distance from the hair cells—the former became more negative and the latter decreased in amplitude. Cx26 was localized to the same regions as previously described in the rat (Kikuchi et al. 1995), but complex staining patterns showed that the staining was not uniform in all directions, and often denser in the longitudinal direction.

When injected into cells with dense longitudinal staining patterns for Cx26, dye spread more readily in the longitudinal direction. In other cells, neither preferential dye movement nor electrical gradients could be explained by the immunostaining results alone. These results suggest an intercellular current between the cells of the organ of Corti, which would be consistent with a potassium current away from the hair cells. Our results verified a functional gap junction network *in vivo* that can account for many hypothesized functions of the supporting cells, including potassium buffering.

Thesis Supervisor: Joe C. Adams
Title: Associate Professor of Otology and Laryngology, Harvard Medical School

Acknowledgements

I would like to express my sincere gratitude and thanks to the many people who have help me in my training at MIT and in my personal and academic growth.

First, I must thank my advisor Dr. Joe Adams for changing the direction of my career. A major turning point in my training came when I first took anatomy with Joe. The excitement of seeing how a complex network of tissue could produce such advanced function intrigued me. Joe's guidance has allowed me to appreciate a much broader view of how to approach problems. I have benefited from the years of advice, patience, criticisms, and incredible attention to detail that Joe has given me.

I am equally indebted to my thesis committee members, Drs. Denny Freeman, Chris Brown, Ed Mroz, and David Paul for their continual support and encouragement throughout my thesis. I thank Denny for helping me maintain the quantitative approach that can often be lost in such a project. I have benefited greatly from his vast technical expertise, questioning, and dedication to teaching. I am especially thankful to Chris for helpful advice and encouragement when a set of experiments or a particular approach did not work. His experimental insight kept me sane during long data droughts. Ed has been extremely helpful in making sure that I stay focused on my topic and not drift, as I have a tendency to do so many times. I am thankful for his ensuring I not lose sight of my goals as a graduate student--to graduate. Talks with David Paul were incredibly helpful to getting an idea of how the world views gap junctions, and his technical advice was critical to this thesis.

I owe special thanks to several people who have helped shape me to be who I am: Professor L. Gould, Dr. Bill Peake, and Dr. Nelson Kiang. Professor Gould helped me appreciate that when you want something, all you have to do is go and get it. His support and confidence in me during my undergraduate years will always be remembered. Bill's wit, humor, caring, and vast experience inspired me to continue with my education after my Masters. I am greatly indebted to Nelson for all the long conversations about how to think about problems and approach them. His excitement and drive for knowledge excited me about exploring new fields.

I am also indebted to all the people in the Eaton-Peabody Lab and Dept of Otolaryngology (MEEI) who have made this one of the best places to work and learn. Without these friends I would not have been able to keep my sanity long enough to graduate. I would like to thank Barbara Brugess for sharing her excitement with me when she found something new, and for all the lunch time conversation of how the Hensen cells are different when few people believed us. I am also indebted to her for all her help with cutting tissue. I would like to especially thank Diana Sands for the numerous things she does for the lab and has done for me. She is a great person.

Similarly, I have grown academically and personally because of my classmates in the Speech and Hearing Program and MEMP program. First, I'd like to thank Rick MacDonald for broadening my perspective on problems and showing me how to use the confocal microscope so I could have the nice images for this thesis. I am very thankful to Diane Ronan and AJ Aranyosi for their willingness to listen to me about my research. I thank my friends Sridhar Kalluri, John Iversen, Susan Voss, Tina Stankovic, Jason Sroka, Paul Dimitri, Quinton Gopen, Quentin Davis, Martin McKinney, Chris Long, Joyce Rosenthal, Janet Slifka, Greg Huang, Su Wooi Teoh, Ray Chan, Q, Irina Sigalovsky, and Ben Hammond for all their support and friendship.

I would like to thank the financial support provided by NIH grants awarded to the Speech and Hearing Program and Dr. Joe Adams.

My thesis would not have been possible without the support from outside the lab. I would like to thank my roommates Jay Youngclaus, Jeff Moeller, Larry Foley, Martin McKinney, and Sridhar Kalluri for making our apartment our home. I owe special thanks to Sridhar for all the conversations we shared on our way to work. It was an integral part of my day.

Finally, I would like to thank my parents, Raj and Baljeet, my Brother, Manish, and the rest of my family for their continued support. Although they didn't understand all the details, they supported me all the way. I would not have been able to finish in such a timely manner if it were not for all the love and affection of my wife, Jyoti, who maintained her faith in me and inspired me.

Dedicated to my wife,

Jyoti

for all of her patience and support.

Table of Contents

List of Figures

List of Tables

Introduction

By comparison to hair cells and auditory neurons, relatively little is known about the function of the non-sensory supporting cells that form the majority of tissue in the cochlea. Morphological studies have shown that they are highly differentiated and have different shapes (Lim 1980; Nagasawa et al. 1993; Spicer and Schulte 1994a; Spicer and Schulte 1994b; Spicer and Schulte 1996). Non-sensory cells in the organ of Corti contain a high density of structural components such as actin and microtubules (Attanasio et al. 1994; Flock et al. 1982; Kuhn and Vater 1995; Nagasawa et al. 1993; Nakazawa et al. 1995; Pack and Slepecky 1995; Slepecky and Chamberlain 1983; Spicer and Schulte 1994b), which suggests that their primary function is to provide mechanical support for the hair cells. Therefore, most studies of cochlear supporting cells have focused on their mechanical properties and micromechanics of the organ of Corti (Johnstone and Yates 1974; Khanna et al. 1998; Rhode 1971; Rhode 1974; Rhode 1978; Richter et al. 1998; Sellick et al. 1982; Zwislocki and Kletsky 1980). Very few studies have examined other physiological roles of supporting cells *in vivo* (Oesterle and Dallos 1986; Oesterle and Dallos 1989; Oesterle and Dallos 1990; Santos-Sacchi 1986; Santos-Sacchi 1987; Santos-Sacchi and Dallos 1983; Zwislocki et al. 1992). The goal of this thesis is to study the physiology of these cells *in vivo*: to examine roles, other than structural, that these cells may play in maintaining cochlear homeostasis.

Roles of supporting cells

Supporting cells have been much more extensively studied in other systems such as the brain (Kreutzberg 1996; Ransom and Orkand 1996; Reichenbach 1991; Steinhauser and Gallo 1996; Verkhratsky and Kettenmann 1996; Vernadakis 1988) and the retina (Celesia 1988; Newman and Reichenbach 1996; Palay 1991; Reichenbach 1989; Reichenbach et al. 1993). By examining what is known about supporting cells in other systems, it may be possible to better understand the functional roles of cochlear supporting cells. A brief description of what is known about other supporting cells will be followed by possible roles for cochlear supporting cells.

Glial cells, supporting cells in the central nervous system, provide many regulatory functions to maintain an adequate environment for the nerve fibers. Glial cells are known to take up

neurotransmitter (Barbour et al. 1991; Newman and Reichenbach 1996; Vernadakis 1988) and potassium (Barbour et al. 1991; Brew et al. 1986; Newman and Reichenbach 1996; Reichenbach 1991; Reichenbach et al. 1993) from extracellular spaces near the nerve fibers. Supporting cells also regulate extracellular environments by regulating pH, regulating intracellular volume through uptake of amino acids and, like macrophages, by removing waste produced by cell death (Bologa et al. 1987; Hoffmann 1992; Kazemi and Choma 1977; Kempski et al. 1991; Mountian et al. 1996; Pasantes-Morales et al. 1990; Pasantes-Morales and Schousboe 1989). During development, glial cells release growth factors that may affect plasticity and regeneration (Bhat 1995; Shao and McCarthy 1994). Microglia activated during pathological events such as inflammation, trauma, and ischemia act to protect the CNS environment (Aschner 1998a; Aschner 1998b; Benveniste 1992; Kreutzberg 1996; Norenberg 1994). While many signals are carried through the nerve fibers, interconnected networks of supporting cells also transmit signals through calcium waves and signaling molecules like cAMP and through electrical currents (Charles 1998; Deutsch et al. 1995; Nedergaard 1994; Nedergaard et al. 1995; Spray et al. 1993; Verkhratsky and Kettenmann 1996; Verkhratsky et al. 1998). Supporting cells have been shown to provide nutrients and metabolic trafficking to sensory cells (Bassnett et al. 1994; Goodenough et al. 1980).

An important function of non-sensory cells in the retina is potassium regulation. When potassium leaves sensory cells and neurons, it must be cleared away to prevent neuronal over-stimulation (Somjen 1979). Glial cells in the retina, called Müller cells, are thought to regulate the extracellular potassium via specializations of their morphology and identified potassium channels (Brew and Attwell 1985; Brew et al. 1986; Newman and Reichenbach 1996; Reichenbach et al. 1993). Müller cells traverse the layers of the retina from the region where the neurons and sensory cells are located to the vitreous layer. Their cell membranes at the region of the neurons, sensory cells (body of the Müller cell), and the vitreous layer (endfoot of the Müller cell) are highly permeable to potassium. Potassium currents enter through inward rectifying potassium channels and a sodium, potassium-ATPase at the body of the cell and to exit through potassium channels in the endfoot of the cell. Other glial cells, such as astrocytes in the brain, are

much smaller and provide spatial buffering[1] of potassium through networks of cells coupled by gap junctions (Enkvist and McCarthy 1994).

Many supporting cells, including those in the cochlea, are coupled through gap junctions. Gap junctions are intercellular channels that allow ions and small compounds (<2000 Da) to pass from one cell to another. Gap junctions allow signaling molecules, such as cAMP, Ca^{2+} and IP_3, to pass intercellularly, allowing cells to control and signal other cells (Bruzzone and Ressot 1997; Charles 1998; Paul 1995; Verkhratsky and Kettenmann 1996; Verkhratsky et al. 1998). In the lens of the eye, gap junctions between cells allow for the removal of waste and provision of nutrients for cells that are deep in the lens and do not have ready access to the extracellular space (Goodenough et al. 1980).

Potassium cycle in the cochlea

Potassium plays a key role in transducing acoustic energy into neural signals. Potassium passing through the transduction channels in the auditory hair cells causes a depolarization of the hair cell potential, which in turn causes the release of neurotransmitter that simulates fibers of the auditory nerve (see Dallos, 1996 for a review). Potassium exits the hair cells through channels along their basolateral surfaces (Santos-Sacchi et al. 1997). The potassium current, which is present even in silence, is driven by a large positive endocochlear potential (70 to 90 mV) from the apical side of the hair cells to their basolateral side. The stereocilia of the hair cells, which contain the transduction channels, sit in a fluid that is high in potassium (*endolymph*), while the basolateral surface of the hair cell is bathed in a fluid that is low in potassium (*perilymph*). To maintain the potassium current through the hair cells, the endolymphatic potassium concentration must be maintained high, and potassium must be cleared away from the area surrounding the basolateral surfaces of the hair cells. (For a review of these processes see Marcus 1986; Salt and Konishi 1986)

Regulation of potassium recycling (Figure 1) in the cochlea is essential for maintaining the sensitivity of the cochlea and normal hearing function. Tight junctions at the apical boundaries of cells lining the endolymphatic space (Forge 1984; Jahnke 1975a; Jahnke 1975b; Kikuchi and

[1] Spatial buffering is the movement of ions from areas of higher concentrations to regions of lower concentrations.

Hilding 1966) prevent extracellular diffusion of potassium between perilymph and endolymph. However, radioactive tracer studies have shown that potassium transported into the endolymph comes from the perilymph rather than from the blood (Konishi et al. 1978). It is well accepted that marginal cells of the stria vascularis, which are specialized to accumulate potassium through their basolateral surfaces and expel it through their apical membrane, are the principal source of endolymphatic potassium (Marcus 1986; Tasaki and Spyropoulos 1959). However, the extracellular space surrounding the basolateral surfaces of the marginal cells, the intrastrial space, is isolated from the perilymph via tight junctions between strial basal cells (Jahnke 1975b; Kikuchi and Hilding 1966; Marcus 1986). The perilymphatic potassium must reach the intrastrial space by some means other than extracellular diffusion.

The second challenge of maintaining a low perilymphatic potassium concentration is particularly important for the region surrounding the basolateral surfaces of the hair cells. Potassium leaving the hair cells must be dispersed rapidly because its accumulation extracellularly would cause hair cells to remain depolarized, and thus reduce the electrical drive for the flow of potassium into the hair cell. If the extracellular potassium concentration remained high over an extended period, it could lead to cell damage or neuronal death (Somjen 1979). The relatively large space of Nuel surrounding the outer hair cells could dilute the potassium and keep the extracellular potassium concentrations low. However, potassium concentration within these spaces can increase by as much as 1-3 mM during high level sound stimulation (Johnstone et al. 1989), which could cause the hair cells to remain depolarized.

Zidanic and Brownell (1990, 1992) measured extracellular potential gradients that indicated the existence of an extracellular current from the region of the hair cells to the lateral wall (extracellular current in scala vestibuli shown in Figure 1). They assumed that 50% of this current was carried by potassium ions. However, since sodium is the dominant cation in the perilymph and both sodium and potassium have the same mobilities, the current could be primarily be carried by sodium. Even if a significant extracellular current of potassium existed, tight junctions prevent an extracellular pathway to the basolateral surfaces of the strial marginal cells. Therefore, it has been hypothesized that potassium may pass from the basolateral region of the hair cells to the intrastrial space via an intercellular route (Kikuchi et al. 1995).

Intercellular potassium pathway in the cochlea

The basis for the hypothesized intercellular pathway shown in Figure 1 is the existence of two organized networks of non-sensory cells that contain specializations, which suggest that they perform homeostatic functions and potassium transport. Freeze-fracture, electron microscopy and immunohistochemistry showed that non-sensory cells in the mammalian cochlea are coupled to each other through gap junctions (Forge 1984; Gulley 1976; Iurato et al. 1976a; Iurato et al. 1976b; Jahnke 1975a; Jahnke 1975b; Kikuchi et al. 1995; Nadol et al. 1976), which may allow them to work in concert to provide functions that a single cell cannot accomplish alone. Kikuchi et al. (1995) found two distinct gap junctional cell networks. The *epithelial cell network* is composed of non-sensory cells of the organ of Corti including inner border cells, inner phalangeal cells, inner pillar cells, outer pillar cells, Deiters cells, Hensen cells, Claudius cells, Boettcher cells and root cells. The *connective tissue cell network* is composed of fibrocytes of the spiral ligament, cells lining scala vestibuli, strial basal cells, and strial intermediate cells.

At key sites within the networks, different cell types are specialized with high levels of proteins involved in ion, pH and fluid regulation, such as sodium, potassium-ATPase, inwardly rectifying potassium channels, the sodium, potassium, 2 chloride co-transporter, proton pumps, sodium proton exchangers, carbonic anhydrase, and the water-channel protein CHIP (Ichimiya et al., 1994; Schulte and Adams, 1989; Spicer and Schulte, 1991; Spicer and Schulte, 1996; Stankovic et al., 1997; Mizuta et al., 1997; Sakaguchi et al., 1998; Schubert and Adams, 1997). These specializations enable individual cell classes to perform highly specialized functions that contribute to the overall fluid and ion homeostasis of the cochlear environment. The location of these proteins within each network is integral to the potassium recycling pathway.

Connective tissue cell network and potassium regulation

Gap junctions among the cells of the connective tissue network provide a pathway by which potassium can pass through the tight junction barrier into the intrastrial space (Kikuchi et al. 1995). Electrophysiological studies showed that the ionic composition and resting potential of the intrastrial space is different from either the endolymph or the perilymph (Ikeda and Morizono 1989a; Ikeda and Morizono 1989b; Melichar and Syka 1987; Offner et al. 1987; Salt et al. 1987), which supports the idea that potassium cannot move extracellularly between the perilymph and

the intrastrial space. Gap junctions between type I fibrocytes and basal cells of the stria vascularis provide a pathway by which potassium can pass through the tight junction barrier (Kikuchi et al. 1995).

Basolateral surfaces of strial marginal cells contain a high concentration of sodium, potassium-ATPase; the sodium, potassium, 2 chloride co-transporter; and an active chloride channel, which allows for sustained potassium uptake from the intrastrial space (Wangemann et al. 1995). A sodium, potassium-ATPase and a sodium, potassium, 2-chloride co-transporter have also been localized to type II fibrocytes (Mizuta et al. 1997; Sakaguchi et al. 1998; Schubert and Adams 1997; Schulte and Adams 1989). This specialization of type II fibrocytes indicates that these cells are specialized for taking up potassium from the extracellular spaces. A sustained inflow of potassium into the fibrocytes could cause a lower potassium concentration in the extracellular spaces between the fibrocytes and the root cell processes, which are at the end of the epithelial cell network. The sustained activities of the pumps in both the marginal cells and the fibrocytes would cause a potassium current from type II fibrocytes to strial marginal cells.

Epithelial cell network and potassium regulation

A sustained potassium current into the type II fibyrocytes could draw potassium out of the root cell processes by lowering the extracellular potassium concentration. If the root processes have a high potassium permeability, similar to the endfeet of the Müller cells, the concentration gradient across the cell membrane of the root cells would cause potassium to exit the root cells. Potassium egress would create a potassium sink that would draw potassium from other cells within the epithelial cell network.

A mechanism for taking up potassium near the hair cells is necessary for completing the hypothesized intercellular pathway. Identification of an inwardly rectifying potassium channel in Deiters cells suggests that one of their functions is to allow potassium to enter Deiters cells from the extracellular spaces (Hibino et al. 1997). The intracellular potassium concentration in the Deiters cell and the resting potential would cause the potassium to flow outward when potassium channels are opened. However, if the localized extracellular concentration is increased by 5 mM, the localized membrane potential could shift, making it favorable for potassium to enter the cells (see Discussion of Chapter 2). Santos-Sacchi showed that the majority of the potassium channels in the outer hair cells are located at the base of the hair cells, where they abut Deiters cells and

where the extracellular space is relatively small compared to the spaces of Nuel (Santos-Sacchi et al. 1997). The potassium current could cause large changes in the potassium concentration in the localized spaces between the outer hair cells and Deiters cells, or the extracellular spaces near the inner hair cells. Under regular equilibrium conditions, potassium is taken up by the cells through sodium, potassium-ATPase, which is known to exist in the supporting cells, to counter the potassium flowing out of the cell. Therefore, if the outward potassium flux is decreased, then the active mechanism could cause a net uptake of potassium.

Gap junction physiology in the cochlea

The hypothesized intracellular potassium current is dependent on the properties of the gap junctions between the networked cells. Therefore, it is important to understand the physiology of these cells and the network as a whole. However, knowledge of supporting cell physiology is limited and restricted to cells near the hair cells: pillar cells, Deiters cells, and Hensen cells (Brown et al. 1983; Goodman et al. 1982; Oesterle and Dallos 1989; Russell and Sellick 1978; Zwislocki et al. 1992) or cells of the stria (Ikeda and Morizono 1989b; Melichar and Syka 1987; Offner et al. 1987; Salt et al. 1987). Knowledge of the basic properties of gap junctions among these cells is important for an understanding of what roles they play in the cochlear physiology.

Gap junctions

Gap junctions are channels formed by integral membrane proteins, called connexins, in adjacent cells. To date there have been fourteen different connexin proteins identified. Each hemichannel (called a connexon) is formed by six connexin subunits in a hexagonal lattice around an aqueous pore. A gap junction is formed when connexons in adjacent cells align symmetrically with a tight seal between the two cell membranes. Connexins with pairs of connexons do not need to be homotypic, and various combinations of different connexins can produce a large variety of different gap junction types. Cells usually express multiple connexins, which suggests that the makeup of connexons determine details of their functional features (Bennett and Verselis 1992; Bruzzone and Ressot 1997; Donaldson et al. 1997; Paul 1995).

Some important properties of gap junctions are their permeability and gating properties. Movement of ions and small compounds between cells can be controlled by modulation of gap

junction permeability and by properties of the gap junctions themselves (Bennett and Verselis 1992; Bennett et al. 1994; Goodenough 1978; Paul 1995). The permeability of particles through gap junctions is not only dependent on the size of the particle, but it is also dependent upon charge interactions between it and the pore, and the structure of the particle. Particles with similar sizes pass through gap junctions at different rates and the gap junction may be more permeable to one over the other. For example, neurobiotin has been shown to spread more readily than lucifer yellow (Zahs and Newman 1997). The time course of the changes in channel permeability can be very rapid, on the order of milliseconds. Other agents have been used to alter gap junction permeability. Octanol, halothane, and hexanol have been used to reversibly uncouple gap junctions (Deutsch et al. 1995; Muller et al. 1996; Pappas et al. 1996; Spray et al. 1985).

Dye-coupling studies

While the existence of cochlear gap junctions has been determined unequivocally, whether or not they are functional *in vivo* has not previously been determined. Intracellular injection of small fluorescent dyes that pass through gap junctions have been used to show functional coupling between cells by tracking the movement of the dye. All dye injection experiments in the cochlea to date have been done *in vitro*, or *in vivo* without direct visualization of dye movement.

The first study that attempted to show functional coupling in the cochlea using dye transfer resulted in no transfer of dye *in vivo* or *in vitro* (Santos-Sacchi and Dallos 1983). However, further studies in an extracted cochlear preparation *in vitro*, showed transfer of dye (Santos-Sacchi 1986) between Hensen cells and Deiters cells and pillar cells. Another attempt to study the functional coupling of supporting cells in the organ of Corti was performed using a lateral wall approach to the cells in the apical turns of a gerbil cochlea, Zwislock et al. (1992). In that study, unintentional filling of cells by a leakage current may have caused some unintentional spread of dye (see discussion in Chapter 1).

Electrophysiology

Direct measurements of cell impedance and coupling ratios were made between cells *in vitro* and *in vivo* with a lateral wall approach (Santos-Sacchi 1987). In that study, cell coupling *in vivo* was much lower than cell coupling between excised cell aggregates. Cell coupling was indirectly

measured though the measurement of intracellular responses to sounds (Oesterle and Dallos 1990). Oesterle and Dallos found that the magnitude of the intracellular supporting cell responses depolarized during tone bursts, which they attributed to a redistribution of potassium. The magnitude of the intracellular responses found by Oesterle and Dallos were smaller than the adjacent extracellular responses, which was contrary to other findings where the supporting cell responses were larger than extracellular recordings (Brown et al. 1983; Goodman et al. 1982; Russell and Sellick 1978; Zwislocki et al. 1992).

Significance to hearing loss

Recent studies found that mutations in human connexin 26 (Cx26) are accompanied by non-syndromic sensorineural deafness (Carrasquillo et al. 1997; Denoyelle et al. 1997; Kelsell et al. 1997; Zelante et al. 1997). Cx26 has been localized to all cells in the cochlea that are coupled by gap junctions (Kikuchi et al. 1995). It may therefore be the most abundant connexin type in the inner ear. If movement of ions between cochlear cells is critical for their normal functions, then a Cx26 mutation could disrupt intercellular communication and account for loss of hearing in ears with Cx26 mutations. The morphology of cochleas with Cx26 mutations is not known, but studying properties of cells coupled by Cx26 should provide a better understanding of their functional roles in the cochlea.

If the cochlear non-sensory cells are involved in potassium regulation and maintaining cochlear homeostasis, a disruption in the normal function of the gap junctional networks could lead to problems involving ionic imbalances. Endolymphatic hydrops, a condition of abnormally enlarged volume of scala media, occurs in Ménière's disease, in neural syphilis, meningitis, and acoustic trauma (Merchant et al. 1995). Although the mechanisms that result in increased endolymphatic volume in any of these various ear disorders are not well understood, an obvious means of increasing the volume of endolymph is increasing the osmolarity of the endolymphatic space. This would lead to increased endolymphatic volume as osmotic pressure pulled water from adjacent spaces to equalize the osmotic gradient. It seems likely that these diverse pathologies may all somehow achieve this common result by different mechanisms and may, therefore include ionic dysregulation as part of their disruption of cochlear function.

Goal of Thesis: Determine basic properties of the epithelial gap junction network

Little is known about the basic properties of cochlear gap junctional cell networks, such as the amount of coupling in an intact functioning cochlea. Determining the physical properties of gap junctional coupling of cochlear cells would establish the boundary conditions that constrain the physiological functions of the system. To characterize the proposed intercellular pathway for potassium, a detailed knowledge of the density and locations of gap junctions is needed, the patency of the gap junction network *in vivo* must be shown, and the basic properties of how well the cells are electrically coupled must be determined.

The goal of this thesis is to characterize the epithelial gap junctional cell network in the cochlea and answer basic questions about the functionality of the network. Several approaches are used to characterize the anatomical and physiological properties of the epithelial cell network. The work expands on previous knowledge of the gap junction network by examining the network in its intact state in an animal model with normal hearing sensitivity.

Dye Coupling experiments

Chapter 1 describes dye-coupling experiments in which the spread of dye between cells was visualized on-line and in real time in a normal functioning cochlea. These experiments addressed some shortcomings of previous studies. It was possible to inject all the cells in the epithelial cell network with Lucifer yellow, to observe spread of the dye, and to identify the cells to which the dye spread. The functionality of the gap junctions within the epithelial cell network was confirmed *in vivo*.

Electrophysiology experiments

Chapter 2 describes a series of electrophysiology experiments to quantify electrical properties of the epithelial cell network. In addition to measuring sound-evoked intracellular responses, cells' resting potentials were measured from the modiolus to the lateral wall to search for intercellular electrical gradients that may give rise to currents between the cells. The space constant for the network was calculated through the graded sound-evoked responses of the cells from the inner supporting cells to the root cells. Simultaneous recordings from pairs of cells were used to measure electrical coupling ratios by injecting current into one and measuring the

response in the other. Measurements of the cell input resistance, the intracellular responses to sound, and the coupling ratio, were analyzed to determine coupling resistance between the non-sensory cells. Standing and sound evoked currents were determined through these experiments.

Anatomical study

To compare the physiological results with the anatomy of the gap junctions of the epithelial cell network, the location and densities of gap junctions between cells were examined in greater detail than was previously done. The third chapter describes the anatomical connections using immunolocalization of an antibody to the gap junction protein connexin 26. An immunostained surface preparation was analyzed by taking optical sections through the entire thickness of the organ of Corti. In other experiments, structures of individual cells filled with fluorescent dyes were analyzed to determine the arrangement of the connections between cells.

Uncoupling the cell network

Uncoupling agents, such as octanol, halothane, and intracellular H+, have been used *in vitro* to change the coupling characteristics as one method for experimentally determining the functional role of the gap junctions. Santos-Sacchi showed that in isolated cell aggregates the coupling between cells is modulated by H+, and that the cells can be uncoupled with octanol (Santos-Sacchi 1991). Attempts were made to uncouple the gap junctions *in vivo* are described in Chapter 4. Dye coupling measurements were made during perfusion of the uncoupling agents. The physiology of the hearing, including intracellular responses were measured while these uncoupling agents were perfused through the cochlea.

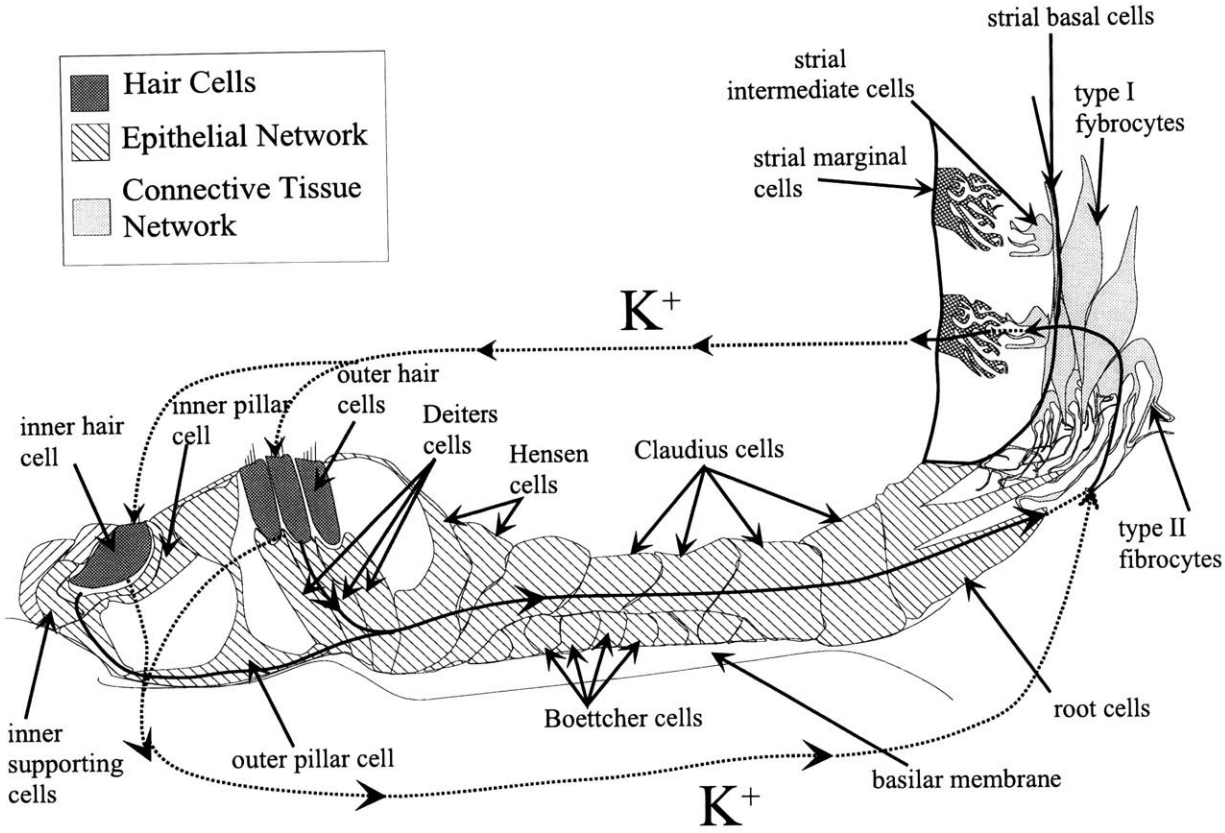

Figure 1. Hypothesized extracellular (dotted) and intercelluar (solid) potassium recycling in the cochlea. Potassium is expelled from strial marginal cells into the endolymph. The potassium then flows through the transduction channels in the hair cells and is expelled through their basolateral surfaces. In the extracellular pathway, the potassium diffuses from the region of the hair cell to the lateral wall. Any extracellular pathway to the marginal cells would be small because of tight junctions between strial basal cells. The two cell networks in the ear provide a possible intercellular pathway by which potassium can be cleared away from the basolateral surfaces of the hair cells and transported to the intrastrial space. The epithelial cell network contains the inner supporting cells, inner pillar cells, outer pillar cells, Deiters cells, Hensen cells, Claudius cells, Boettcher cells, and root cells. The connective tissue network includes the type I fibrocytes, type II fibrocytes, the basal cells and the intermediate cells. Potassium taken up by the Deiters cells can flow within the epithelial cell network to the root cells, where it is expelled. High levels of sodium, potassium-ATPase in the type II fibrocytes suggests they take up potassium. The potassium then flows within the connective tissue network to the intermediate cells where it is released into the intrastrial space.

1 Dye coupling among non-sensory cells in the organ of Corti

1.1 Introduction

The existence of gap junctions between supporting cells in the mammalian cochlea has been shown through freeze-fracture, electron-microscopy and immunohistochemistry (Forge 1984; Gulley 1976; Iurato et al. 1976a; Iurato et al. 1976b; Jahnke 1975a; Jahnke 1975b; Kikuchi et al. 1995; Nadol et al. 1976). Connexin 26 (Cx26), a gap junction protein, has been localized to junctions between adjacent cells which are organized into two networks in the cochlea: the *epithelial cell network* composed of non-sensory cells of the organ of Corti and root cells; and the *connective tissue cell network* composed of the fibrocytes of the spiral ligament, basal and intermediate cells of the stria vascularis, fibrocytes of the spiral limbus, and cells lining scala vestibuli (Kikuchi et al. 1995).

It is hypothesized that the epithelial cell network provides an intercellular pathway by which potassium is transported from the region of the hair cells to the lateral wall where the potassium is taken up by the connective tissue network (Kikuchi et al. 1995). Intracellular potassium within the connective tissue network is able to move into the intrastrial space from which it can be taken up by the marginal cells and passed into the endolymphatic space. One condition necessary to support the hypothesized current is that the gap junctions must be patent and must allow ions to pass between cells.

While the anatomical distribution of the gap junctions is known, not much is known about their functionality *in vivo*. In an extracted cochlear preparation *in vitro*, fluorescein, 6-carboxy-fluorescein, and equivocally Lucifer yellow spread between Hensen cells and Deiters cells (Santos-Sacchi 1986). In this preparation, the cells may not have been in their normal functioning condition because electrical measures of coupling showed a large difference between *in vivo* and *in vitro* coupling (Santos-Sacchi 1987). The cells studied were limited to a subset of the supporting cells in the epithelial cell network—Deiters cells, Hensen cells, and outer pillar cells. An attempt to study the functional coupling of these cells was performed using a lateral

wall approach to the cells in the apical turns of a gerbil cochlea (Zwislocki et al. 1992). Lucifer yellow (LY) was injected into supporting cells, but because of the approach to the cells, the transfer of dye could not be assessed until after the tissue was fixed and processed. Unintentional filling of cells by a leakage current may explain the apparent coupling of hair cells and supporting cells despite a lack of morphological evidence for gap junctions between these cells.

None of the previous coupling studies was able to study the entire intact epithelial cell network. The cell types that were studied in the previous preparations were limited to a few inner supporting cells, pillar cells, Deiters cells and Hensen cells. To determine if the cell network is an integral part of the potassium recirculation pathway, the entire network must be examined.

In the present study, LY was injected into the supporting cells of the organ of Corti *in vivo* in the basal turn of chinchillas. The advantage of this study over previous studies of dye coupling between supporting cells is that on-line filling of the injected cells and spread of dye to other cells was visualized. LY was imaged *in vivo* and the pattern of dye spread was analyzed to determine functional coupling. The tissue was then fixed, removed, and imaged at a higher resolution to determine the exact cells containing the dye. In the present study, all the supporting cells in the epithelial cell network, from the interdental cells to the root cells, were examined and found to show dye-coupling.

Some of the present results have been presented in abstract form (Oberoi and Adams 1996; Oberoi and Adams 1998).

1.2 Methods

Chinchillas weighing between 300g and 600g were anesthetized with 65 mg/kg of sodium pentobarbital i.p., with boosters given every 2 hours or as needed. Young animals between 3 months and 1 year were used because the bony part of the cochlea was less calcified and easier to shave away than in older animals. After the animal was anesthetized, the trachea was intubated and the head was firmly fixed at the snout and roof of the mouth. The rectal temperature was maintained between 36° and 38° C. Skin and muscle over the back of the skull was removed to expose the bulla and the occipital bone. The pinna was removed to allow for the placement of a sound source into the external canal. To visualize the round window and the hook of the cochlea while leaving the middle-ear apparatus intact, the dorsal-lateral portion of the bulla and several

septa were opened by shaving the bone. A ventro-lateral opening into the bulla was made to allow insertion of a fiber optic light source. Once the bulla was opened, a stiff bar from the head holder was attached to the temporal bone with dental cement to further reduce vibrations and to allow for longer cell holding times. The experiments were performed on a vibration isolation table and sound measurements were made in an electrically and acoustically isolated chamber.

A fiber optic light was placed against the first turn of the cochlea to trans-illuminate the bone and to determine the location of the spiral ligament and to assess the thickness of the bone (Figure 2). A portion of the otic capsule overlying scala tympani was shaved away with a knife to expose the basilar membrane (Brown and Nuttall 1984; Goodman et al. 1982). Once the bone was sufficiently thinned, a small hook was used to pick away the bone and enlarge the opening to about 2-5 mm in diameter. The opening allowed for visualization and access to the region of the cochlea best tuned to frequencies between 7000 and 9000 Hz. The positive pressure of the cerebrospinal fluid prevented most of the bone dust and shaving from entering the scala tympani. Blood coagulated when it entered scala tympani. The coagulated blood was removed with fine forceps or a microhook.

The experiments were performed in two different locations. The surgery and measurement of compound action potentials were performed in a soundproof, electrically isolated, heated chamber. After the surgery was completed another measure of the compound action potential thresholds were measured and the preparation was moved to another room with a vibration-free table. Heat lamps and heating pads were used to maintain the air temperature and the animal temperature.

All procedures with animals were approved by the Animal Care and Use Committee of the Massachusetts Eye and Ear Infirmary.

1.2.1 Monitoring cochlear function

Cochlear function was assessed by measuring the compound action potential (CAP) thresholds (iso-response contours) in response to tone bursts between 1 kHz and 30 kHz. Acoustic stimuli were produced by a 1 inch condenser microphone and measured using a ¼ inch microphone probe tube. The assembly was housed in a brass coupler that was sealed around the bony portion of the external ear (Kiang et al. 1965). Recordings were made with a silver

recording electrode placed on the round window and a Ag-AgCl reference electrode placed in the neck muscle. The responses were amplified 10,000 times by an AC-coupled amplifier (bandpass 10-100,000 Hz) and digitized with a 12 bit A/D converter with a 30 microsecond-sampling interval. The signal was averaged 16 times, with alternating polarity, at each sound pressure level, and the threshold was determined to be the level at which the peak-to-peak N1-P1 was 15 microvolts, which was above the noise.

The first measurement after opening the bulla was accepted as normal if the thresholds between 2 kHz and 14 kHz were below 40 dB SPL. In some cases, thresholds at frequencies above 12 kHz were elevated above 40 dB SPL. This was assumed to be due to trauma caused by opening the bulla. In these cases, the bone often appeared to be more ossified than normal and the otic capsule was more difficult to open. A second measurement of the CAP thresholds was taken after opening the otic capsule to assess cochlear damage during the surgical procedure. Data were included for analysis provided the CAP thresholds did not increase by more than 20 dB after opening the otic capsule and the thresholds were below 50 dB SPL.

The endocochlear potential (EP) was also used as an index of cochlear condition. The EP was measured by advancing the microelectrode through the organ of Corti into scala media. Since no CAP measurements could be taken after starting cell iontophoresis, EP measurements were used to monitor the condition of the cochlea periodically throughout these experiments. From other experiments, it was known that the advancement of the electrode through the organ of Corti could cause small increases in the CAP thresholds; therefore, the number of EP measurements was minimized.

1.2.2 Cell penetration and iontophoresis

Intracellular recording from cells and iontophoresis of dye into cells were performed using glass pipettes (1.2 mm OD; 0.6 ID) pulled with a vertical Narishige puller. Electrodes were filled with 6% lucifer yellow (Sigma) in 1 M LiCl, 5% lucifer yellow (LY) and 5% neurobiotin (Vector Lab SP-1120) in 1 M LiCl, or 4% lucifer yellow and 1% horseradish peroxidase (HRP) (Sigma) in 1M LiCl. The resistances of the electrodes were between 50 and 150 MΩ.

The electrode was manually advanced into the opening of the otic capsule with the aid of a dissecting microscope. While the electrode was extracellular in the perilymphatic space, the

capacitive compensation was adjusted to reduce the transient to a square pulse of current, and the series resistance of the electrode was eliminated using the bridge balance. A holding current of less than 10 pA was used to prevent spontaneous filling of cells when cells were penetrated. The electrode DC offset, or *tip potential,* was balanced to zero in the extracellular space.

Once the electrode was near the basilar membrane, advancement of the electrode was visualized with a compound microscope with long working distance objectives (Nikon 0.2 N.A. 10X and Nikon 0.4 N.A. 20X). The electrode impedance increased and the tip potential changed as the electrode encountered the basilar membrane. A *buzz* current was used while advancing the electrode to assist in penetrating the basilar membrane[2]. Penetrating the basilar membrane often caused a change in the impedance of the electrode. Sometimes the electrode resistance decreased, which was thought to be a slight breaking of the tip. Other times, the impedance increased, denoting a temporary clog since no dye could be seen upon an iontophoretic current. The electrode was considered intracellular when the electrode potential was large and negative, denoting a cell's resting potential. Cell membranes were penetrated by a buzzing current, or a small tap on the vibration isolation table. After penetration of a cell membrane, a steady resting potential was taken as a sign of a good seal between the electrode and the cell membrane. Poor seals were assumed to occur when the electrode potential wavered and then drifted back to zero within the first minute of penetration. Further advancement beyond the cells was accompanied by a large positive potential, corresponding to the endolymphatic potential.

Dye was iontophoresed into cells with a 10 Hz square-wave current (50% duty cycle) with the same polarity the dye to be injected. For the LY-only electrodes, -2 to -10 nA was used. When LY-NB or LY-HRP electrodes were used, LY was injected with a negative current and a positive 2 to 10 nA current was used to inject the NB or HRP. The iontophoretic current magnitude was determined by the properties of the individual electrodes. Electrodes with high impedances clogged easily, consequently lower currents were used for a longer durations with such electrodes.

Spread of LY was monitored and recorded during the injection. The dye was injected from 1 to 5 minutes depending on the apparent spread of the dye. Once the injected cell appeared to be

[2] The buzz current is a function of the Axoprobe, which provides for a function similar to capacitive ringing. The amplitude, duration, and frequency of the buzz current can be adjusted.

fully loaded, and the area of the injected dye did not appear to increase further, the iontophoretic current was stopped and the electrode withdrawn.

Multiple injections were made in each preparation and the locations of the injection sites were recorded to permit identification of the online injection sites with cells when the tissue was visualized in the surface preparations after the tissue was fixed. Different cells were systematically injected from an apical region to a more basal location along the cochlea, or vice versa. Enough distance separated the injected cells so the dye did not spread from one injection site to another. An attempt was made to use a single electrode for all the injections per preparation. However, after 4-5 injections, the fluorescence of the LY leaving the electrode appeared to be less bright, possibly indicating a lower concentration of dye.

1.2.3 On-Line Video Microscopy Imaging System and Image Processing

In vivo images of the organ of Corti were captured using an intensified Neuvicon tube camera (Cohu) or a low light sensitive CCD camera (Marshall electronics) mounted on a compound metallurgical microscope having a 20 mm working distance (0.4 n.a. 20x Nikon M Plan) objective and a 12X or 16X photo-ocular. Fluorescein isothiocyanate (FITC) sensitive filter cubes were used for imaging the LY. Photo-irradiation of the cells was reduced by using a Hamamastsu C2400 intensifier in the optical system (with the tube camera), and by shuttering the light source during image acquisitions. Grayscale images (8-bit) were acquired by averaging 64 or 128 frames of the output of the intensifier using the Image-1 software package by Universal Imaging.

Highlights on the surface view of the organ of Corti seen by trans-illumination of the otic capsule identified the injection sites. The brightfield surface view through the online imaging system, along with a cross-section of the same section of the organ of Corti adjusted to the same scale is shown in Figure 3. The bands seen in the surface view are generated by differences in the cell optical densities, and they guided the advancement of the pipette to the desired cell type. Recovery and identification of dye injected cells off-line using higher magnification and resolution verified the identity of the bands seen with the on-line optical system. Fluorescent images of the electrode were superimposed on the brightfield surface view so that cells of choice could be penetrated and filled with dye. Once a cell was penetrated, images were taken at timed intervals to track the spread of the fluorescent dye between cells.

The background fluorescent image of the pipette was acquired before cell penetration, or at the time of penetration. This image was subtracted from the remaining time series of images. A section of the subtracted image known to be background was used to compute the average and standard deviation of the noise in the image. Graylevels were clipped at 2-3 standard deviations above the noise of the signal to extract the fluorescent image of the spread of the dye. A time series of the on-line, subtracted, thresholded, and binary images is presented in Figure 4.

The thresholded and binary on-line images were analyzed to quantify the amount, direction, and shape of the dye spread. Outlines of objects were determined from the binary images and the following measurements were made on each fluorescent object at each time frame: area, total fluorescence, average fluorescence, center of object, orientation, length, breath, and elliptical form factor. The center of mass of the fluorescence was taken to be the weighted center of the object from the thresholded images. The length of the object was the longest chord through the object and the orientation was the angle of the major chord with respect to the x-axis. The breath of the object was the length of the longest chord perpendicular to the major chord. The elliptical form factor (EFF) was the ratio of the length to the breath. When the EFF equals 1, the object approximates the shape of a circle. The EFF was used as the indication of the asymmetry of the dye spread.

1.2.4 Surface preparations

After injection of the final cell of each experiment, an additional ½ hour elapsed before the tissue was fixed, to permit equilibration of dye within the tissue. The scala tympani was perfused with 10% formalin in 0.01 M phosphate buffer saline, pH 7.3 (PBS), to fix the tissue and the dye in the cells. When LY-NB was used, the time between injection and fixation was reduced to 10 minutes because of the extent of the spread of the NB. Warm 0.1% sodium nitrate in PBS was perfused intracardially to dilate the blood vessels and exsanguinate the tissue. This was followed by a perfusion of 10% formalin in PBS. The cochleas were removed and the oval and round windows opened. The fixative was gently perfused through the oval window, and the cochleas incubated in the fixative for two hours.

The lateral bone of the hook and basal turn of the cochlea were removed by shaving and picking away pieces of the bone. The organ of Corti and spiral ligament, at the site of the penetrations, was dissected out and the spiral ligament was removed. A surface preparation of

the organ of Corti was placed in a depression side in 1:1 glycerol and PBS. The fixed tissue was imaged using a compound microscope with a 100X (1.3 N.A) objective and a 40X (1.0 N.A.) objective for higher magnification and resolution. Under computer control, fluorescent images of the LY and the brightfield images were acquired at a number of focal planes to identify the injected cell types and to compare the pattern of dye spread to that visualized during the live preparation with that imaged in the fixed tissue. Auto-fluorescence was removed by adjusting the gain on the camera and image acquisition system so the nucleus of the brightest labeled cell was saturated and no signal was present in a region of the tissue where it was known that there was no dye present.

When the LY-NB or LY-HRP cocktail was used, a set of fluorescent images of the LY were acquired before processing the NB/HRP because the time required for processing the NB/HRP resulted in a weakened LY signal. After acquiring the LY images, the tissue was placed in 1:200 CY5 labeled streptavidin in 1% normal horse serum (NHS) for 1-2 days at 4°C in a light-free chamber. The tissue was then washed in 3 cycles of PBS at 15 minutes per cycle. The tissue was place in a depression slide in 1:1 glycerol and PBS and imaged with the CY5 filter set, LY filter set, and transmitted light at the same set of focal planes.

Several experiments were performed without using the on-line imaging system. The dye was injected the same way, but the electrodes and basilar membrane were visualized only with a dissecting microscope. The tissue was processed the same way, and the spread of the dye was determined from the surface preparations. Without the constraints of the on-line system, there was access to more cells and a larger area of penetration.

THIS PAGE INTENTIONALLY LEFT BLANK

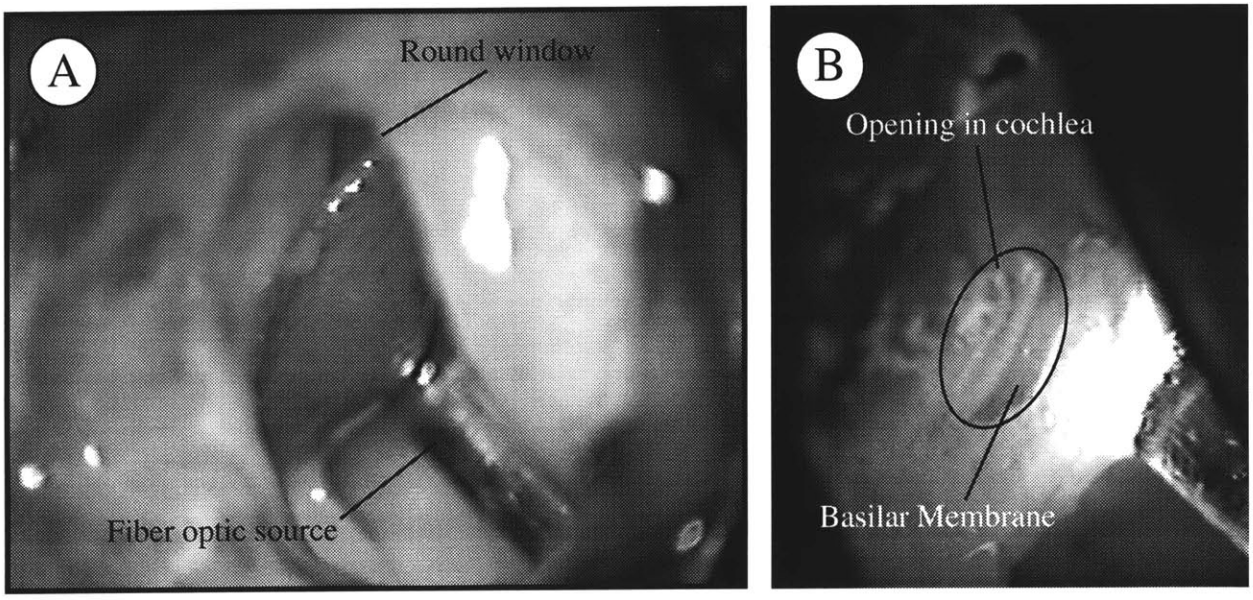

Figure 2. View of the basal turn of a chinchilla cochlea through a dissecting microscope. **(A)** Basal turn shown before opening the otic capsule. The fiber optic source (5 mm diameter) is seen against the side of the basal turn. **(B)** A hole has been made in the basal turn (shown at a higher magnification). Under trans-illumination, the basilar membrane can be seen through the opening.

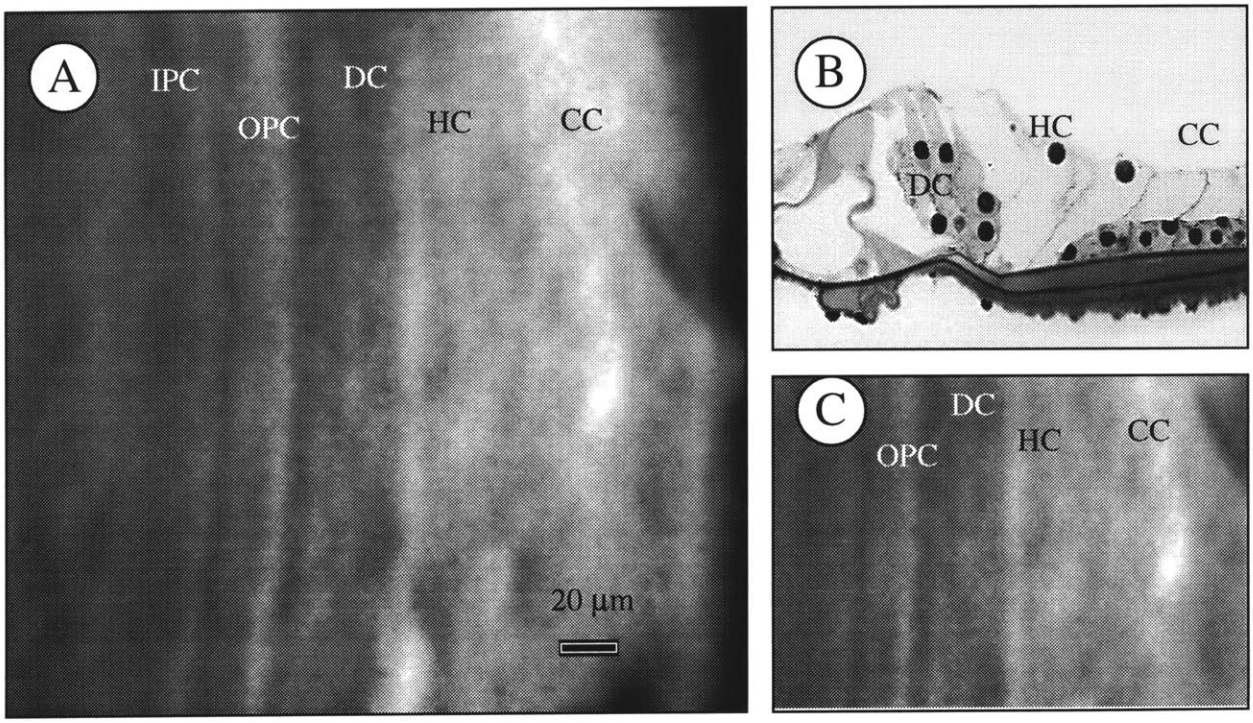

Figure 3. **(A)** Surface view of the in vivo preparation of the organ of Corti seen through an opening in the basal turn of the cochlea. The bands correspond to the different cell types. IPC inner pillar cell; OPC outer pillar cell; DC Deiters cell; HC Hensen cell; CC Claudius cell.**(B)** Cross-section through the same section of the organ of Corti at the same scale. The cross-section is aligned and shown at the same scale as the surface view in **(C)** to show that the landmarks seen in the surface view correspond to the designated cell types.

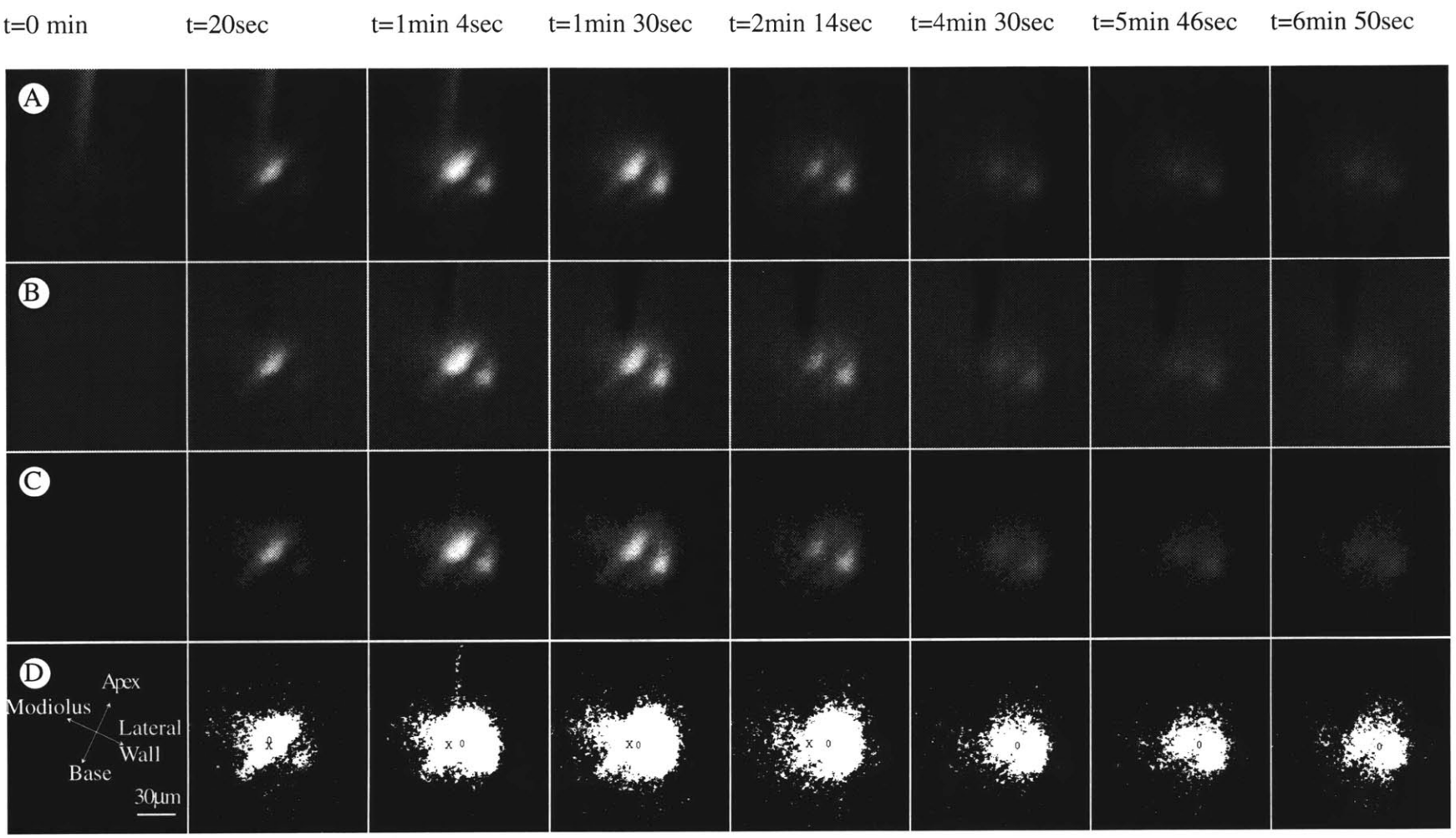

Figure 4. **(A)** Time series of on-line images of the spread of dye at from time t=0 to t=6min 50sec. LY was injected into a Claudius cell with a -2 nA current for 1min 30sec. At 2min, the pipette was withdrawn from the cell, and removed from the field of view. **(B)** Subtracted images: The image at t=0 was used as a background image and subtracted from the remaining time series. **(C)** Threshold Images: The standard deviation and mean were computed from the noise in the subtracted image. **(D)** Binary Images: The images were clipped at 3 standard deviations above the noise floor. The center of mass of the fluorescence was computed from the threshold images (**C**) and plotted as an O in the binary image. The site of injection is labeled with an X.

1.3 Dye-coupling results

The results presented are from experiments in which the condition of the cochlea was determined to be normal except where noted. The normal CAP thresholds for the chinchillas between 1,000 and 15,000 Hz was on average 25 dB SPL with a standard deviation of about 20 dB SPL. On average, there was less than a 5.0 dB shift in CAP thresholds after the cochlear opening was made. More than a 20 dB increase in the CAP threshold at the frequencies between 6 and 12 kHz was taken as a sign of a damaged cochlea and such cases were not included in the present analysis. Preparations with good CAP thresholds had EP measurements of 79.2 ± 3.2 mV (12 preparations).

1.3.1 Cell identification and resting potentials

Visualization of the organ of Corti while positioning the electrode permitted penetration of cells of choice. Tentative identification of cell types were made *in vivo* based on location of the bony shelf of the inner spiral lamina and the banded landmarks imaged on the basilar membrane. Since the organ of Corti is only one to three cell layers tall (Figure 3B), another criterion used to help distinguish between cell types was the insertion depth beyond the basilar membrane. Most impalements were restricted to the first cell encountered after the electrode was advanced beyond the basilar membrane. Cells believed to be Boettcher cells could be held only briefly, so the electrode was advanced to the next cell, which was assumed to be a Claudius cell. Hair cells were distinguished from supporting cells primarily by their depth in the organ of Corti. Some cells had higher electrical noise levels. These cells were thought to be hair cells because of their depth beyond the basilar membrane, and acoustic stimulation (usually a whistle) generated a large receptor potential. These cells were not held long enough to inject dye or make a stable measurement of the resting potential. In some cases, where cells could not be imaged well, and identification of cells could not be confidently made, the data were discarded.

On-line identification was useful for targeting collection of data uniformly across cell types. However, the final identification of all dye-filled cells was based on observations of surface preparations (shown in section 1.3.4). The following cell types were successfully impaled: inner supporting cells, inner pillar cells, outer pillar cells, Deiters cells, Hensen cells, Claudius cells,

Boettcher cells, and root cells. Eighty-three cells in twenty-one preparations were injected with LY and the spread observed on-line. Sixty-four of the injected cells were identified in the surface preparations.

A large, negative electrode potential indicated penetration of a cell. During the first few seconds after impaling the cell, a change of 2-5 mV in the cell's resting potential was assumed to be due to sealing of the membrane around the electrode, or clearing of the electrode tip. The cell's resting potential was measured as the stable potential reached after impalement. High impedance electrodes occasionally had fluctuations of 2-10 mV in their tip potential, so stable resting potentials were not obtained. For these cases, the cell's resting potential was recorded as the last measured potential in the cell minus the extracellular potential measured after backing out of the cell.

There was a 4 mV difference in the mean cell resting potentials from the supporting cells near the outer hair cells (Deiters cells) to the supporting cells further away towards the lateral wall (Claudius cells). Table 1 shows the mean resting potentials of the impaled cells and their standard deviations. Analysis of variance (ANOVA) on the entire population of resting potentials revealed a statistically significant difference in the measured resting potentials of the different cell types with a p-value of 0.043. Statistics between groups of cell types were computed using multiple Student t-tests between the groups (p-values shown in the last column of Table 1). The correction for multiple t-tests (Steel, 1961) showed that there was a significant difference in the Claudius cell and pillar cell resting potential to a 95% confidence level. The correction for the multiple t-test shows that the remaining comparisons are not statistically significant as the p-values for the t-tests suggest. There appeared to be a difference in the mean resting potentials of Claudius cells and all other cell types, but it was not statistically significant.

1.3.2 Analysis of the On-line Images

On-line images of LY injections showed that dye iontophoresed into a cell accumulated in the cell body and filled the impaled cell within 30 seconds of starting the iontophoretic current. Within one to two minutes of the start of the injection, dye spread to other cells, as seen in the time series of on-line images (Figure 4, Figure 5, and Figure 11). Despite a holding current, occasionally the LY leaked into cells after they were penetrated, spontaneously filling the cells.

Cell boundaries were not seen in the *in vivo* brightfield images (Figure 3A) because of limited magnification and resolution of the imaging system. In some cases, cellular details such as cell processes or filled cell bodies were seen in the fluorescent images if the plane of focus was adjusted (Figure 5 and Figure 6). However, most of the on-line fluorescent images were indistinct and lacked detail, making it difficult to identify individual cells. Superimposing outlines of cells, traced from a surface preparation at the same magnification as the on-line images, on the on-line fluorescent images aided in interpreting the spread of the dye (Figure 7). In this image, the dye accumulated in spaces comparable to the size and shape of the Deiters cells. Within one minute of the injection, the dye spread to at least three cells and was weakly present in another.

Since cell outlines were not distinct, the shape and total area of the imaged dye was analyzed to quantify the amount of spread. The area of the imaged dye as a function of time is shown in Figure 8 for each of the major cell types injected. These areas were computed from the binary images. In almost all of the graphs, the area of the fluorescence exceeded the area of a single cell. The large variability in the total area of spread was, in part, due to differences in the magnitude of the ionophoretic current and the duration of the current. However, in almost all cases, the area of the imaged dye was larger than the area of a single cell within 1 minute of the injection. In most cases the area of the dye increased during the injection, and then once the injection was stopped, the area leveled out or decreased to a different plateau, which was always larger than the size of a single cell. The area of the imaged dye decreased rapidly (IPC 54-4, HC 66-3, and CC 67-4) in a few cases. These cases had short holding times, and it is believed that the dye leaked out of the cells. In some cases (HC 74-5), dye abruptly disappeared, which is believed to be due to the cell bursting and the dye spreading away from the cell.

The shape of the imaged dye, quantified using the elliptical form factor (EFF), appeared to be asymmetric for injected pillar cells and symmetric for injected Claudius cells (Figure 9A). When the spread was asymmetric (EFF of greater than 1.5), the orientation of the elongated pattern was aligned with the longitudinal axis. Figure 9B shows the angle difference between the major axis of the imaged dye and the longitudinal axis of the cochlea (the longitudinal axis is the axis along the spiral of the cochlea). No clear pattern was observed for Deiters cells or Hensen cells (not shown). The angle difference is not significant for symmetrical spread because the major and

minor axes are similar in length, and small changes in the shape of the spread could have large changes in the angle of the major axis.

Increasing area of the imaged dye is believed to be representative of dye spread between cells. An alternate explanation is that it is blurring due to the imaging system. The point-spread function of the imaging system and the fluid interface of the tissue was analyzed in three preparations. Fluorescent beads (0.5 μm diameter) were placed on the basilar membrane in the same preparations in which dye spread was observed. The point-spread function was computed using the same algorithm as the outlines of the dye spread. The X-Y blurring was a maximum of 12 μm and blurring in the Z direction was 12-15 μm. Since the area of fluorescence was much larger than the point spread function, a change in the area of the fluorescence was not entirely due to blurring. The point spread function was mostly symmetric, so any asymmetry in the images of the accumulated dye was not likely due to the imaging system. Since the fluorescent beads were sitting on the basilar membrane, blurring of dye within the tissue could not be determined. There may have been some light channeling though the tissue that could have caused the apparent spread. Therefore, the patterns observed in the on-line images were compared to the images of the fixed tissue.

Changes in fluid level at the otic opening produced changes in the diffraction of the light, and caused lateral shifts of the imaged tissue. During heavy breathing motions and contraction of the stapedius muscle, the fluid level shifted between image acquisitions. In those instances, background subtraction was not performed, and consequently movement of dye could not be adequately analyzed. However, in these cases, the dye spread to beyond the area of a single cell, which confirmed that there was intercellular communication.

1.3.3 Extracellular Injection of Lucifer Yellow

To verify that the observed on-line spread of dye was intercellular, LY was iontophoresed into the extracellular spaces near the cells or in the tunnel of the Corti. The time series of on-line images showed no dye accumulation except for occasionally a small plume that disappeared once the current had stopped. Dye diffused away faster than the time required to acquire images. Extracellular injections were made for approximately 5 minutes, which were comparable to or longer than the duration of the intracellular injections. No labeled cells were seen in the surface

preparations of extracellular injections, which suggests that the cells do not take up dye from the extracellular spaces. Membranes of cells were not labeled by extracellular injections.

1.3.4 Analysis of the Off-line Images

Cell outlines and individual dye-filled cells were identified in surface preparations of the fixed tissue. LY was bound to the nucleus, cell membrane, and tubules in the processes of the pillar cells, Deiters cells, and Hensen cells. The dye was confirmed to be intracellular since the outlines of dye-filled cells were distinct and the extracellular spaces between cells lacked fluorescence (Figure 10). Decreasing the iris diaphragm of the condenser created sufficient contrast to permit brightfield visualization of cell borders. Superposition of brightfield and fluorescent images at the same focal plane allowed for exact cell identifications. The number of fluorescent nuclei was counted to quantify the amount of spread. Since the organ of Corti is a three-dimensional structure, the images were analyzed over the entire height of the organ to ensure all the cells were counted. Usually one cell was brighter than the other dye-filled cells, and it was assumed to be the injected cell since the highest concentration of the dye should be in the injected cell.

This was confirmed with 14 injections in which HRP and LY were simultaneously iontophoresed into a cell. The HRP was made fluorescent with a CY5 tag so the LY and HRP could be imaged at the same plane of focus with two different filter sets. HRP, which is too large to pass through gap junctions, remained in the injected cell, while the LY spread to adjacent cells. The brightest fluorescence for the LY coincided with the CY5 fluorescence (Figure 35). No other cells were labeled with the CY5.

At least one of each of the organ of Corti supporting cell types from the inner supporting cells to the root cells was injected and recovered. Counts of the number of cells to which LY spread are shown in Table 2 and Table 3. The tables are arranged with the columns in anatomical order from the modiolus (inner supporting cells) to the lateral wall (root cells). Each number represents the number of dye-filled cells counted for each of the supporting cell types for each injection. Cell counts for inner supporting cells, inner pillar cells, and outer pillar cells were subdivided into cells located basal to the injected cell and apical to the injected cell. No significant difference was seen between the total spread towards the apex or towards the base.

The dye consistently spread to a large number of cells when injected into the pillar cells and Claudius cells, but the amount of spread was variable when dye was injected into the Deiters and Hensen cells. In all but two cases of injected pillar cells more than 5 dye-filled cells were seen. Many cases of injections into Deiters cells and Hensen cells showed few dye-filled cells compared to injections into other cell types, which is believed to be in part due to short holding times for Deiters cells and difficulty in holding these cells. In four cases (gray) only the injected cell was recovered (3 injected Deiters cells and 1 injected Hensen cell). In all these cases, the cells' resting potentials returned to zero either abruptly or within the first minute of injection. In 12 cases out of the 39 injections into Deiters cells, Hensen cells, and Claudius cells, LY spread to 5 or fewer cells. Root cells were not held very long, and the electrodes often clogged up upon impaling them, so the spread was very limited and to only a few cells.

1.3.5 Spread of dye from the different cell types

Different patterns of dye spread were seen depending on the cell type injected. However, for the most part the patterns of spread seen in the on-line images were similar to the pattern of dye-filled cells recovered in the surface preparations. Since individual cells could not be seen in the on-line images, the surface preparations confirmed that dye spread to other cells, and confirmed the hypothesized movement of dye from one cell to another.

Impaling an equal number of all cell types was desired, but some cells were easier to hold, so more of those cell types were examined. Holding times for the cells were important for loading the cells with sufficient dye. The large size of the Claudius cells made them the easiest cells to penetrate and they had the longest holding times. Boettcher cells, which are the smallest cells in the organ of Corti, were difficult to hold and the resting potential were less stable with an abrupt return to the extracellular potential. Deiters cells were difficult to hold and were often lost within 2 minutes during poor penetrations.

Pillar cells

Dye injected into pillar cells initially spread in the longitudinal direction as shown by the EFFs. In the time series of on-line images shown in Figure 5, the dye is believed to be accumulating in the inner and outer pillar cells. The time series of images was taken at the plane of focus 15 μm above the basilar membrane. At 28 sec, the dye was seen in what was believed to

be the footplate (white arrowhead) of the injected pillar, with a streak towards the apex of the cochlea (black arrowhead). By 1 min 15 sec, the dye spread to two other distinct areas (hatched arrows) which are towards the base of the cochlea and modiolar from the site of injection (asterisk). This appeared to demonstrate spread toward the head of the outer pillar and the inner pillars. A series of optical sections through the organ of Corti showed dye accumulation near the reticular lamina (Figure 5D) with the same shape and size as the pillar cells seen from a surface view (Figure 10A). The images at the plane of the reticular lamina showed a lack of fluorescence (unfilled arrow in Figure 5D) that appeared to correspond to outer hair cells. Fluorescence surrounding the empty space (black arrowhead in Figure 5D) was possibly the processes of the outer pillar cell. The image at this plane shows that there are at least two cells filled with dye (white arrows). The lack of fluorescence is also apparent in the middle plane where the processes of the pillar cells are present (white arrow). This cell was confirmed to be an outer pillar cell in the surface preparation of the tissue (Figure 10). The surface preparation clearly showed multiple labeled inner pillar cells, inner supporting cells, and outer pillar cells. The pattern of dye-filled cells was primarily in the longitudinal direction.

Dye injected into what was thought to be the footplate of an outer pillar cell appeared to spread initially to the head of the pillar cell followed by spread to an adjacent cell in the longitudinal direction (Figure 11A-C). The initial longitudinal spread towards the base of the cochlea and to the modiolus was consistent with the anatomy of pillar cells, which have processes that project towards the base of the cochlea and to the modiolus. The white arrowhead corresponds to the footplate of the outer pillar cell, and the unfilled arrow shows the head of the outer pillar cell. In panel C there is another streak of fluorescence projecting back to the footplate (left). This appears to be an adjacent pillar cell that is being filled. This pattern of spread was the most common when outer pillar cells were injected. The on-line images looked similar to the recovered dye-filled cells (panel D). The brightest fluorescence was confirmed to be in the footplate (white arrowhead) and the head (unfilled arrow) of the injected cell, as shown in the surface preparation. The surface preparation showed that the dye spread primarily in the longitudinal direction. Just outside the field of view, nine inner pillar cells were faintly labeled. However, no dye was found in any Deiters cell or hair cell.

Although dye spread mainly in the longitudinal direction when injected into pillar cells, a decrease in the EFF after the first minute indicated that there was also a radial component to the

dye spread. The radial spread however was not symmetric about the injected cell, as seen from the cell counts (Table 2). In the case of an injected outer pillar cell, shown in Figure 12, dye spread to inner and outer pillar cells, but no Deiters cells contained dye. The left panels show fluorescent images with the brightest cell being an outer pillar cell. The upper panels (A and A') were taken at the same plane of focus, near the cuticular plate. Heads of pillar cells were filled with dye. Processes of outer pillar cells were seen around the first row of outer hair cells. Dye did not spread to outer hair cells or inner hair cells. Stereocilia of hair cells were seen in the brightfield image. The corresponding fluorescent image showed a lack of dye in that area. Dye was never found in inner or outer hair cells when supporting cells were injected. The lower panels (B and B') show the same tissue at 70 μm below the cuticular plate. The nucleus of the injected cell was outside the field of view, but the injected cell is labeled with an asterisk. The tunnel of Corti had faint background fluorescence, which was due to the out of focus fluorescence of the pillar cell footplates. At this plane of focus, inner pillar cells (black arrow) were labeled. Only a few inner supporting cells were labeled faintly, but the intensity of their fluorescence was above the auto-fluorescent levels of the cells. A distinct lack of fluorescence is apparent between the cells, confirming that the dye is located intracellularly. In this case, no dye-filled Deiters cells were seen. The dye spread primarily in the longitudinal direction to at least five cells in each direction. The radial spread was limited to two or three cells towards the modiolus and none towards the lateral wall.

Dye injected into inner pillar cells also showed a primarily longitudinal pattern of spread. In the radial direction, dye spread to outer pillar cells as well as inner supporting cells. A case in which an inner pillar cell was injected is shown in Figure 13. The top panels (Figure 13A and A') show the cells at the level of the cuticular plate. In the top panel, the brightest fluorescence is the phalangeal process of the injected inner pillar cell (white arrowhead) which surrounds an inner hair cell. There was no fluorescence in the area of the inner hair cells (white arrow). There was also one brightly-labeled head of an outer pillar cell (black arrowhead). At a plane of focus 12 μm lower (B and B'), the flask-like shape of the inner hair cells is present in the brightfield image (one is outlined). The fluorescence was contained in the body of the inner pillar cells, and no fluorescence was seen in the region of the hair cells. At a plane of focus 43 μm lower, a number of inner pillar cells and inner supporting cells contained dye. Dye spread to at least 10 inner pillar cells towards the base of the cochlea (right) and to 6 towards the apex of the cochlea

(left). Inner pillar cells form the proximal side of the tunnel of Corti. There were a large number of cells below the inner hair cells labeled in this plane of focus which were the inner supporting cells (unfilled arrows). Dye spread a distance of three cells in the radial direction towards the modiolus (top) and to only one cell, the outer pillar cell, in the radial direction towards the lateral wall. Dye-filled outer pillars from the same injection are shown in Figure 11D. Outer pillar cells adjacent to the injected inner pillar cell were very bright, but no dye-filled Deiters cells were present.

Deiters cells

When dye was injected into Deiters cells, dye usually spread initially in the longitudinal direction and accumulated in distinct locations approximately the size of single Deiters cells (Figure 6C). The two distinct accumulations in this image appear to be adjacent Deiters cells in the longitudinal direction. This pattern was seen in 5 preparations and in all these cases dye spread from the injected cell to a more apical cell. In this case, the phalangeal process of one cell was seen, but was faint (unfilled arrow) since the image was taken at a different plane of focus from the process.

Dye injected into Deiters cells spread to pillar cells in 5 out of the 7 cases when more than 5 labeled cells were recovered (Table 3). Dye injected into a Deiters cell spread to other Deiters cells and to outer pillar cells. One of these cases is illustrated in Figure 14. The upper panels (A and A') are at the level just below the cuticular plate. The Deiters cells' phalangeal processes were filled with dye. The brightest phalangeal process was from the injected Deiters cell. The heads of the outer pillar cells were also filled with dye. There appeared to be a bright accumulation of fluorescence between the phalangeal processes that initially appeared to be an outer hair cell. However, optical sections showed that this fluorescence was actually blurring from the bright labeling of Deiters cells at a lower plane of focus. Three rows of outer hair cells were seen in the brightfield image, but no fluorescence was localized within these cells. At 75 μm below the cuticular plate (B and B'), the labeled nuclei of the outer pillar cells and Deiters cells are seen. There was extensive spread of dye from the injected cell, which was a second row Deiters cell, to outer pillar cells, and other Deiters cells. There were 14 faintly labeled inner pillar cells outside the field of view of the images shown. No Hensen cells were labeled. In this case, dye spread equally in both the longitudinal directions to about six cells in each direction.

There was spread to the modiolus as far as the inner pillar cell, but the dye spread only to the third row of Deiters cells in the radial direction towards the lateral wall.

Hensen cells

On-line images of dye injected into Hensen cells appeared to show dye spreading in all directions and the accumulation was not restricted to the area of a single cell. In an example of an injection into a Hensen cell, shown in Figure 15, dye initially spread in the longitudinal direction, but by 3 minutes, dye appeared to spread in the radial direction as well. By the last on-line image, the center of mass of the fluorescence moved 9 μm towards the modiolus. The surface preparation showed that the pattern of the brightest dye-filled cells was similar to the pattern seen in the on-line images. The brightest cells in the surface preparation formed an elliptical pattern asymmetrical in the longitudinal direction. There were fainter dye-filled cells radial to the injection (Deiters and Claudius cells). Processes of the Hensen cell were seen in the surface preparation (white arrowhead).

Claudius cells

Dye injected into Claudius cells spread in all directions uniformly as shown by the EFFs, which are below 1.5 for most cases (Figure 9). About half of the time, the area of the imaged dye decreased after the injection stopped (Figure 8), while the other half the area remained constant or continued to increase. In all these cases, the average fluorescence level decreased. The combined increase in area and decrease in fluorescent intensity suggest that the dye was diffusing away from the injected cell. This is consistent with the fact that Claudius cells have fewer intracellular organelles than other cells in the organ of Corti for the LY to bind to, which would leave the dye free to diffuse to other cells. Even in cases of bright accumulations, which appeared to be nuclei of cells (Figure 4), the dye eventually diffused away. In a few cases, the amplitude of the iontophoretic current was increased, causing the average fluorescence to increase slightly. However, once the current stopped, the fluorescence level returned to the level before the increased current. This suggests that the additional injected dye diffused away.

Dye-filled cells recovered after an injection into a Claudius cell were uniformly located in all directions around the injected cell (Figure 16), similar to the elliptical pattern of spread seen in the on-line images. Lucifer yellow tended to bind primarily to the nucleus of the Claudius cells

because organelles are relatively sparse in these cells. Figure 16 shows recovered dye-filled cells after iontophoresis into a Claudius cell. The top panels are images at the level of Claudius cell nuclei. LY was bound to the cell membrane of the injected Claudius cell, and to nuclei of the other Claudius cells. Two nuclei, medial to the injected cell at the upper corner of the image (black arrowheads), are not labeled. Nuclei of Boettcher cells are seen 30 μm below the plane of the Claudius cells in the lower panels. There was extensive dye spread to Boettcher cells. The presumed electrode track through Boettcher cells appeared as a dark hole. An outline of the electrode track is superimposed on the brightfield image of the Claudius cells to confirm that the brightest Claudius cell was the impaled cell. While the spread of the dye appeared to be symmetrical in all directions around the impaled cell, the number of dye-filled cells in this case was slightly higher in the longitudinal direction than in the radial direction. However, across all Claudius cell injections, there was no difference in the longitudinal versus radial spread.

Other cells

The majority of cases of dye spread were seen among the cells in the middle of the epithelial cell network (inner supporting cells, pillar cells, Deiters cells, Hensen cells, and Claudius cells). There were a few cases in which the LY spread to the cells to the ends of the cell network (interdental cells and root cells). In one injection into an inner supporting cell, LY spread extensively to the modiolus and was found in the interdental cells which are at the medial end of the epithelial gap junction network. In this case, dye also spread towards the lateral wall to inner pillar cells and to outer pillar cells, but not to Deiters cells. At the other end of the epithelial gap junction network, root cells were filled with dye when LY was injected into an external sulcus cell or a root cell. It was not clear which cell was injected because the anatomy of the tissue at this section of the organ of Corti was complex when viewed from a surface view. Root cell processes extend into the lateral wall, where the tissue is thick, so it was difficult to identify cells in the brightfield images.

1.3.6 Iontophoresis of neurobiotin

The LY-NB cocktail was injected because NB is positively charged, which is opposite to the LY, and because it has been shown in other systems that the NB is more permeant through gap junctions. NB is not fluorescent, so its on-line spread could not be monitored, but the on-line

spread of LY was monitored. LY-NB was injected into cells in 5 different preparations. In all these cases, there was extensive spread of the NB. In the first 2 preparations the dye was injected for 4 minutes and allowed to spread for half an hour before fixation. In these cases, NB was present in all supporting cells in the first turn of the cochlea. No NB was detected in the second or third turns. Therefore, the remaining preparations were performed with a shorter duration between injection and fixation.

The recovered surface preparations showed massive spread of NB to all other cells, filling up the entire epithelial cell network, whereas the LY was found no more than 4 cells away from the injected cell type. The extensive spread of NB confirmed that the entire network could allow particles to pass between cells. In one preparation, shown in Figure 17, inner supporting cells, inner pillar cells, outer pillar cells, and Deiters cells contained a high concentration of NB when it was injected into an outer pillar cell (injection site 1). For an injected Claudius cell (site 3), the labeling of Claudius cells was very faint except for the injected cell, but the fluorescence was above the level seen in the second turn where no NB was detected. The fluorescence was brighter in the root cell processes than in the Claudius cells, suggesting that the dye accumulated there from an injection into the Claudius cells. In the later 3 preparations, only one or two cells were injected in each preparation. When the LY-NB was injected into a Claudius cell (Figure 18), the greatest amount of NB, but not LY, was present in root cell processes. The NB spread to the end of the gap junction network and accumulated in the root cell processes. The injection was made for 3 minutes at +5 nA. The tissue was fixed 5 minutes after the injection, and the spread of NB was seen to approximately 15 cells in each longitudinal direction (0.4 mm). Only four Hensen cells were seen labeled and no cells medial to them were seen labeled.

1.3.7 Cells with a lack of spread and unrecovered cells

As mentioned earlier, there were a few cases of impaled cells that were quickly lost or the resting potential returned to zero. The cells may have been lost because of incomplete sealing of the cell membrane around the electrode or movement of the electrode with respect to the tissue. When a cell was lost, the measured potential returned to the extracellular potential. If the potential returned to zero abruptly, then it was assumed that the electrode had come out of the cell. In most cases the cell was not severely damaged and could be penetrated again, or the dye was still contained in the cell. A slowly increasing potential back to the extracellular potential

was interpreted as a sign of severe damage to the cell and the cell membrane. The on-line images of dye injected supported the notion that there was not a very good seal with the electrode because dye was imaged diffusing away from filled cell. During severe damage, dye was observed to leak out of the cell as the resting potential returned to zero. Once the iontophoretic current was stopped, dye disappeared from the injected cell as well. The recovered cells in the surface preparation for these injections showed either no dye-filled cells, or only a single dye-filled cell, which was taken to be the injected cell.

1.3.8 Deteriorated cochleas

Dye did not always see spread between cells when the CAP thresholds at the frequencies near the cochlear opening (7-9 kHz) was elevated above 50dB threshold. In several cases, dye did spread when the CAP thresholds were elevated above 70dB SPL. In these cases, the cochlear microphonic[3] and the EP were normal. When the EP was below 65 mV, the CAP thresholds were elevated, and the physiology of the cochlea was thought to be deteriorated. In this state, the cells were hard to hold, and once they were impaled, the resting potentials were more depolarized than normal. In these cases, the cells appeared to be uncoupled, as evidenced by the finding that the dye did not spread to other cells.

[3] The cochlear microphonic was observed visually on the oscilloscope during acquisition of the tone-evoked CAP thresholds. The observations were a qualitative assessment of the cochlear microphonic, and there may have been a 10 or 20 dB SPL error in the microphonic response.

Cell Type	Number of Cells	Average Resting Potential (mV)	Standard Error	P value Difference from Claudius Cells
Inner Pillar Cell	11	-75.55	1.99	0.009
Outer Pillar Cell	14	-78.93	2.44	0.019
Deiters Cell	23	-76.43	1.73	0.015
Hensen Cell	13	-77.38	1.80	0.055
Claudius Cell	20	-82.95	1.98	
Boettcher Cell	2	-80.00	4.00	

Table 1. Average resting potentials for the cell types which were injected with lucifer yellow. The resting potentials used are ones from experiments in which the hearing was known to be good through either the CAP thresholds, or measurement of EP. The rows are arranged by supporting cell type from the modiolus to the lateral wall. Averages and standard deviations of resting potentials from injected cells ANOVA showed that there is a significant difference in the cell populations ($p<0.043$). Further significance testing between the Claudius cell population and the other cell populations using Student's t-test are shown in the last column.Based on the correction for multiple t-tests, the only significant difference was between inner pillar cells and Claudius cells.

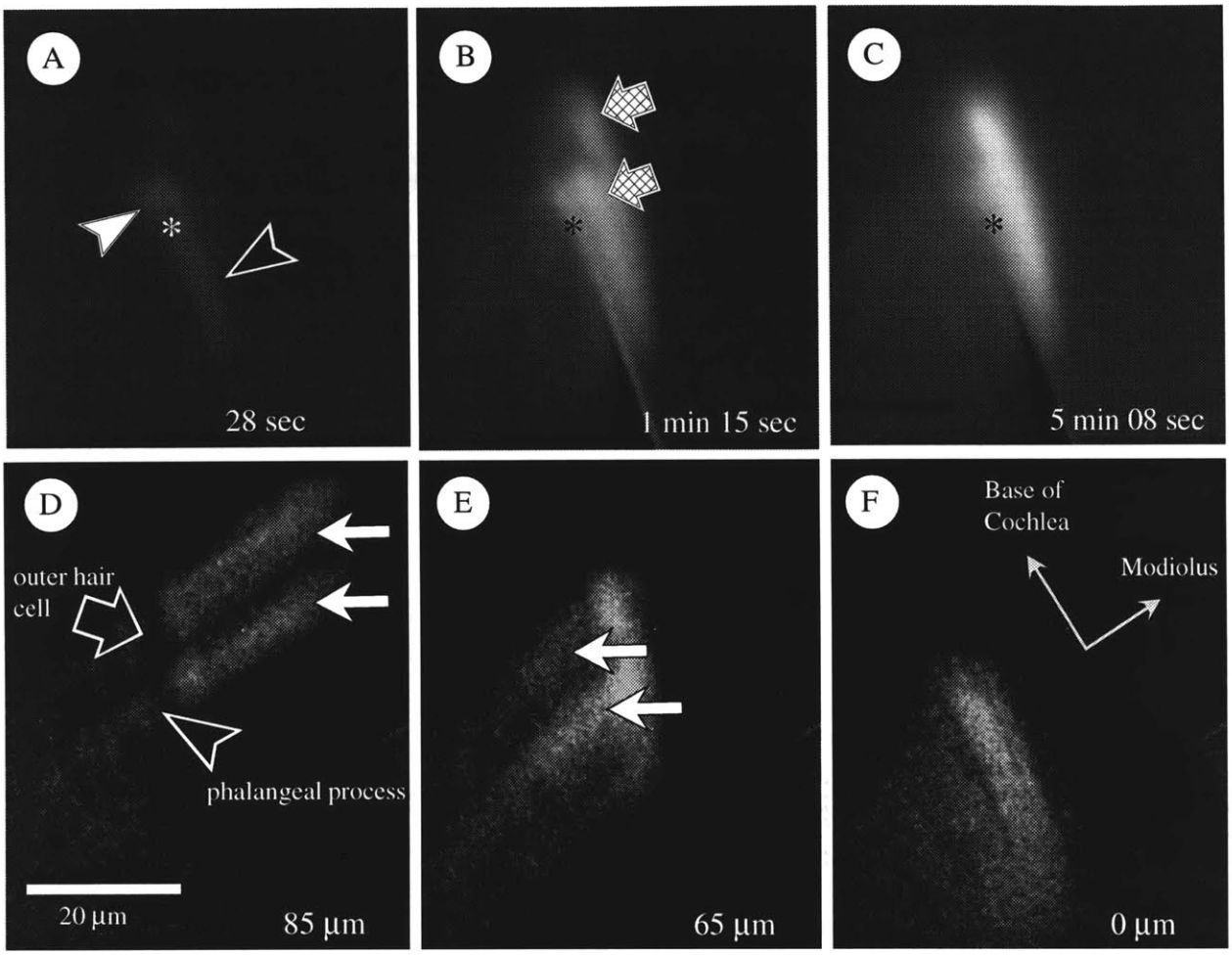

Figure 5. **(A-C)** Time series of background-subtracted on-line images from an injection into an outer pillar cell (white arrowhead). The plane of focus is near the basilar membrane (10 µm). The asterisk marks the site of injection. The dye spread towards the modiolus and to the base of the cochlea to a second cell within 1 min of the injection (hatched arrows). Out of focus blurring caused an apparent spread towards the apex of the cochlea (black arrowhead). The injection lasted 2min. **(D-F)** A series of images from the same preparation taken at different focal planes from the reticular lamina **(D)** to the basilar membrane **(F)** to identify the structure of the cell being injected. At the reticular lamina, the heads of two pillar cells can be seen (arrow). There is a lack of fluorescence lateral to the cells, which is believed to be an unlabled outer hair cell (unfilled arrow). Twenty µm lower **(E)**, the phalangeal processes of the pillar cells are present (white arrows). At the level of the basilar membrane **(F)**, distinct cells cannot be seen.

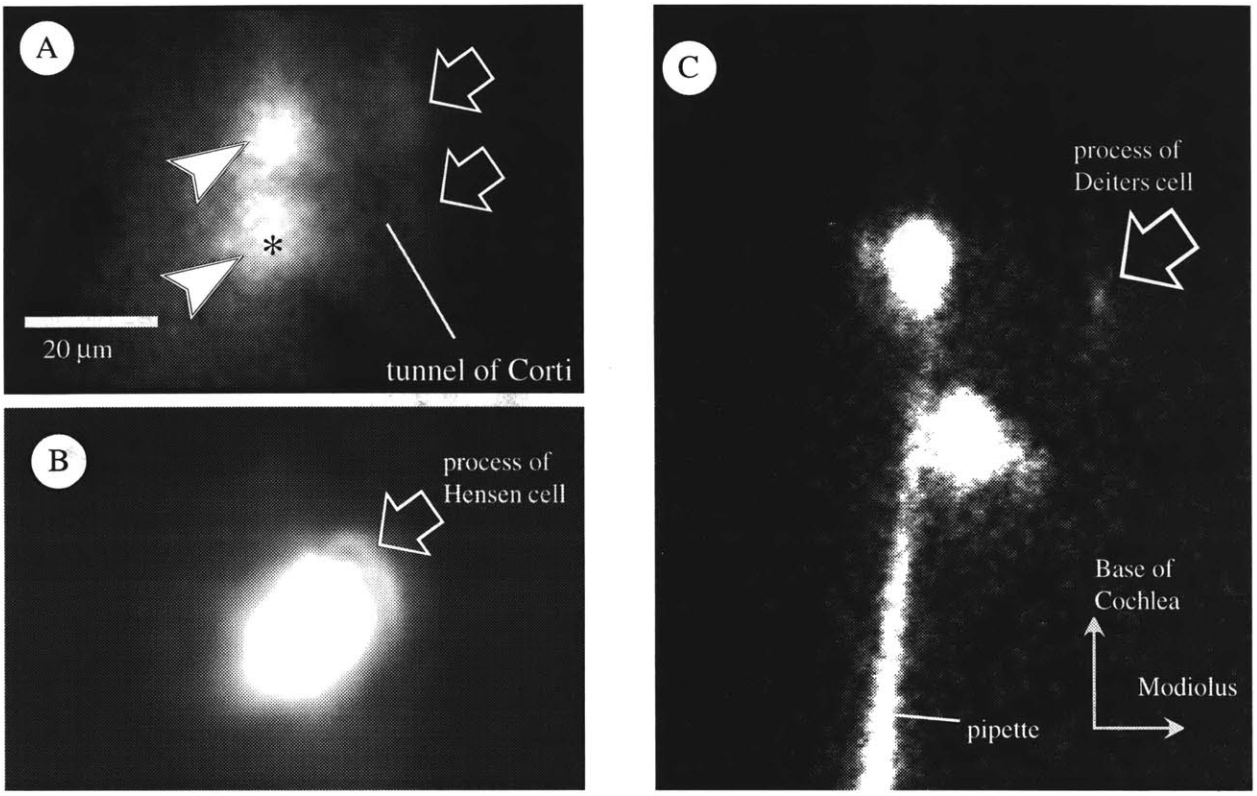

Figure 6. **(A)** Background subtracted on-line images from an injection into an outer pillar cell (white arrowheads; asterisk labels injected cell). The image was taken 1min 20sec after the injection was completed. Inner pillar cells were filled with dye (unfilled arrows). **(B)** Injection into a Hensen cell (2min 04sec after injection). The body of the cell was saturated with dye, but a process of the cell can be seen (unfilled arrow). **(C)** Injection into a Deiters (1min 30sec after injection). The pipette is shown impaling one cell, and a second cell apical to the first one is seen labeled. The unfilled arrow is pointing to the phalangeal process of the cell.

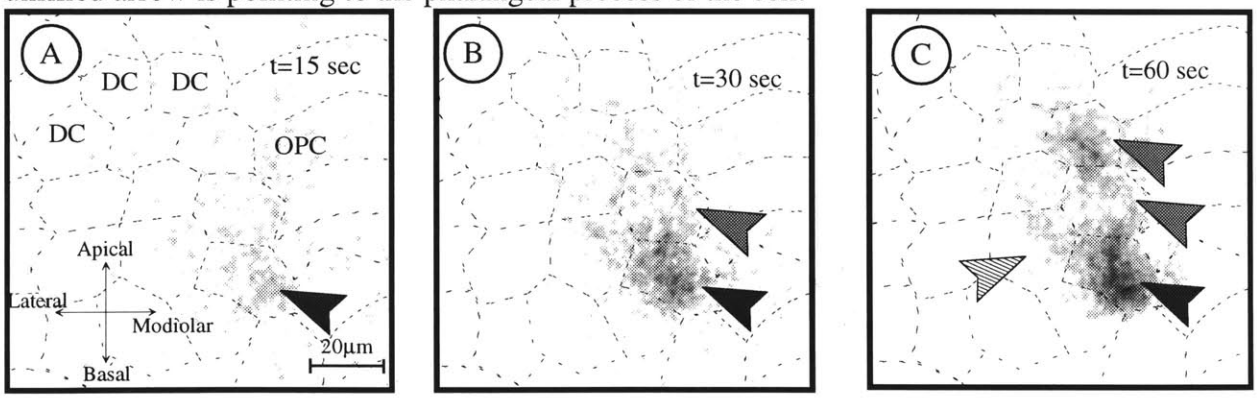

Figure 7. On-line images of dye-spread at the indicated times during an injection of LY at t=0 sec. The images were inverted to render the fluorescence dark for ease of illustration. The injection site is a first row Deiters cell. The injected cell filled by t=15 sec and later the dye spread to nearby Deiters cells. The black arrowhead indicates the injected cell; the gray arrowheads indicate distinctly labeled cells; the hatched arrowhead shows a weakly labeled cell. Cell boundaries can only be inferred in vivo. The dotted lines are an overlay from a surface preparation taken after fixation of the tissue that is included to aid interpretation of off-line analysis of the images.

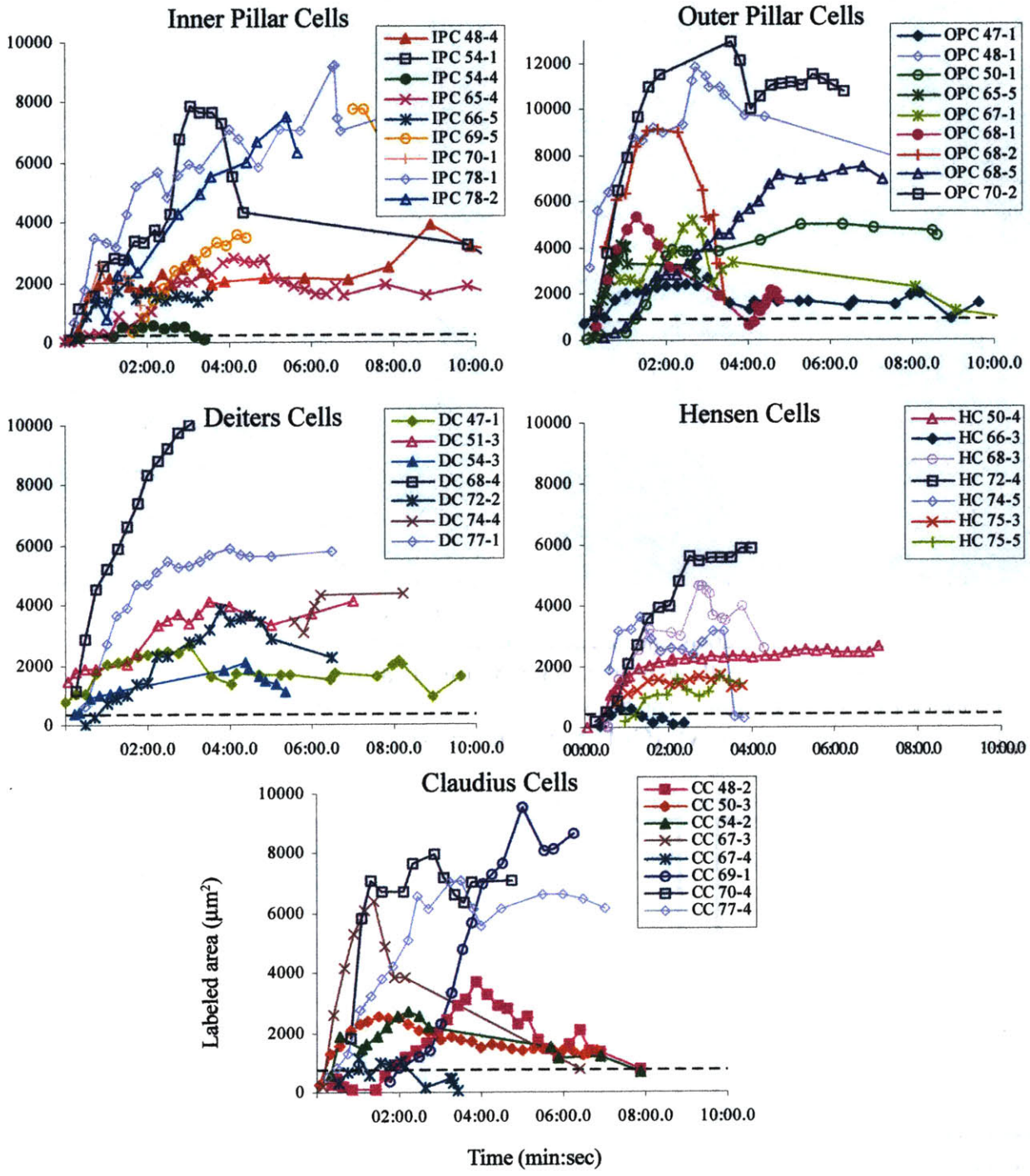

Figure 8. Area of the imaged dye (μm^2) as a function of time. The dotted line in each graph is the approximate single cell area for the injected cell type (measured from surface preparations). Inner pillar cell: 380 μm^2, outer pillar cell: 680 μm^2, Deiters cell: 450 μm^2, Hensen Cell: 530 μm^2, Claudius cell: 700 μm^2.

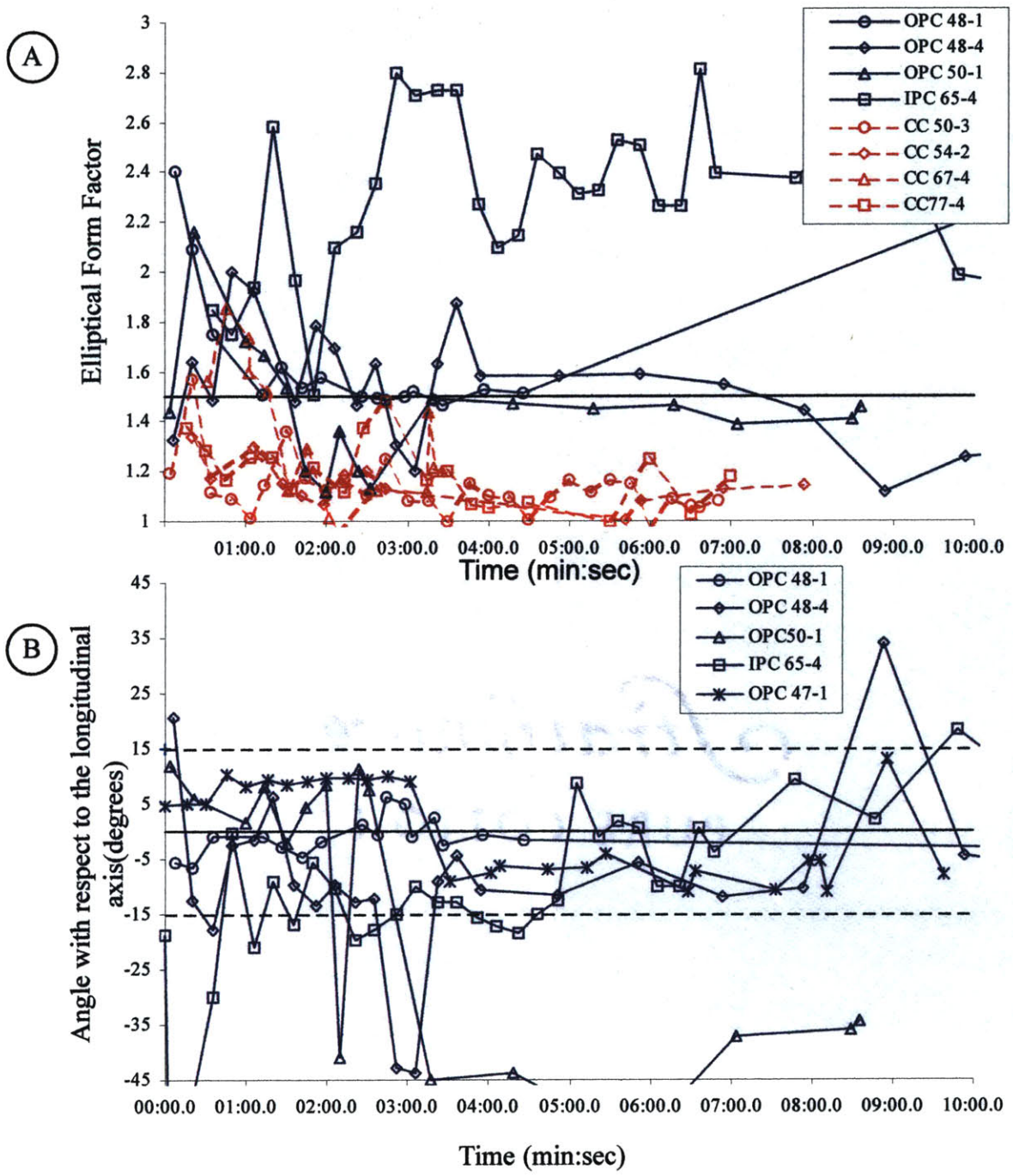

Figure 9.**(A)** Elliptical form factor (EFF) of the imaged dye as a function of time during the iontophoresis. The EFF is the major axis of the object vs. the minor axis. Representative EFFs for pillar cells are shown in the solid lines and the EFFs for Claudius cells are shown in the dashed lines. A solid line is drawn at 1.5, which indicates an elliptical object with a 3:2 major to minor axis. **(B)** Orientation of the imaged dye with respect to the longitudinal axis as a function of time for pillar cells. When the EFF is greater than 1.5, the orientation of the dye injected into the pillar cells is aligned with the longitudinal axis to within 15 degrees. When the shape was symmetrical, the orientation is not a significant feature, so no data was shown for the Claudius cells, which had a symmetical spread upto 1.3 EFF. The value for OPC50-1 at 6 min was -60 degrees.

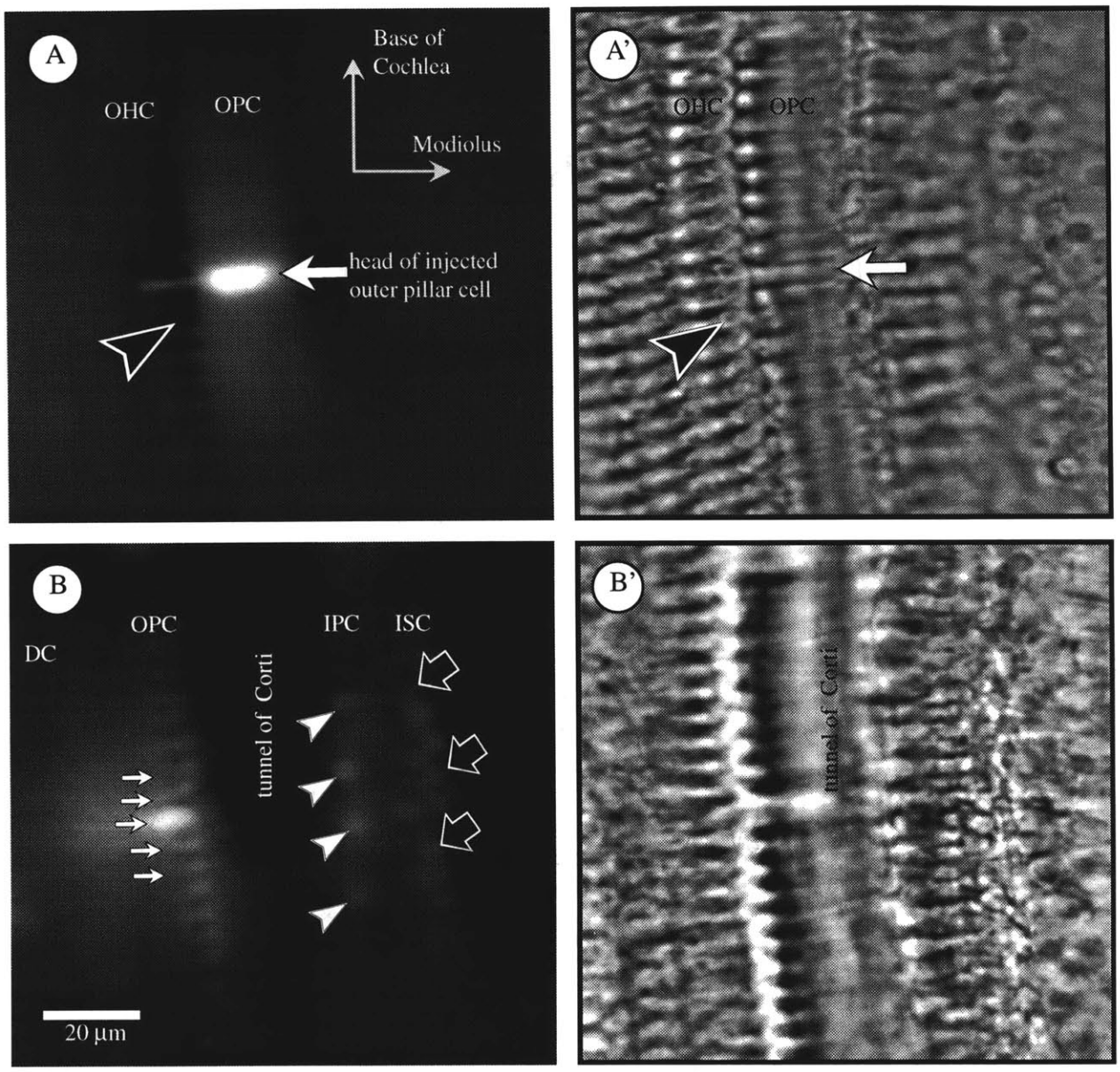

Figure 10. Two focal planes of a surface preparation recovered from the injection shown Figure 5. Adjacent fluorescent (**A** and **B**) and brightfield images (**A'** and **B'**) are at the same focal plane. **(A)** An image near the reticular lamina shows the brightest cell is an outer pillar cell (white arrow). There is exclusion of dye at the first row of outer hair cells (black arrowhead). **(B)** Nuclei of the inner supporting cells (unfilled arrows) and inner pillar cells (white arrowheads) are present at 54 µm below the reticular lamina. In the same image, filled outer pillar cells are present (white arrows).

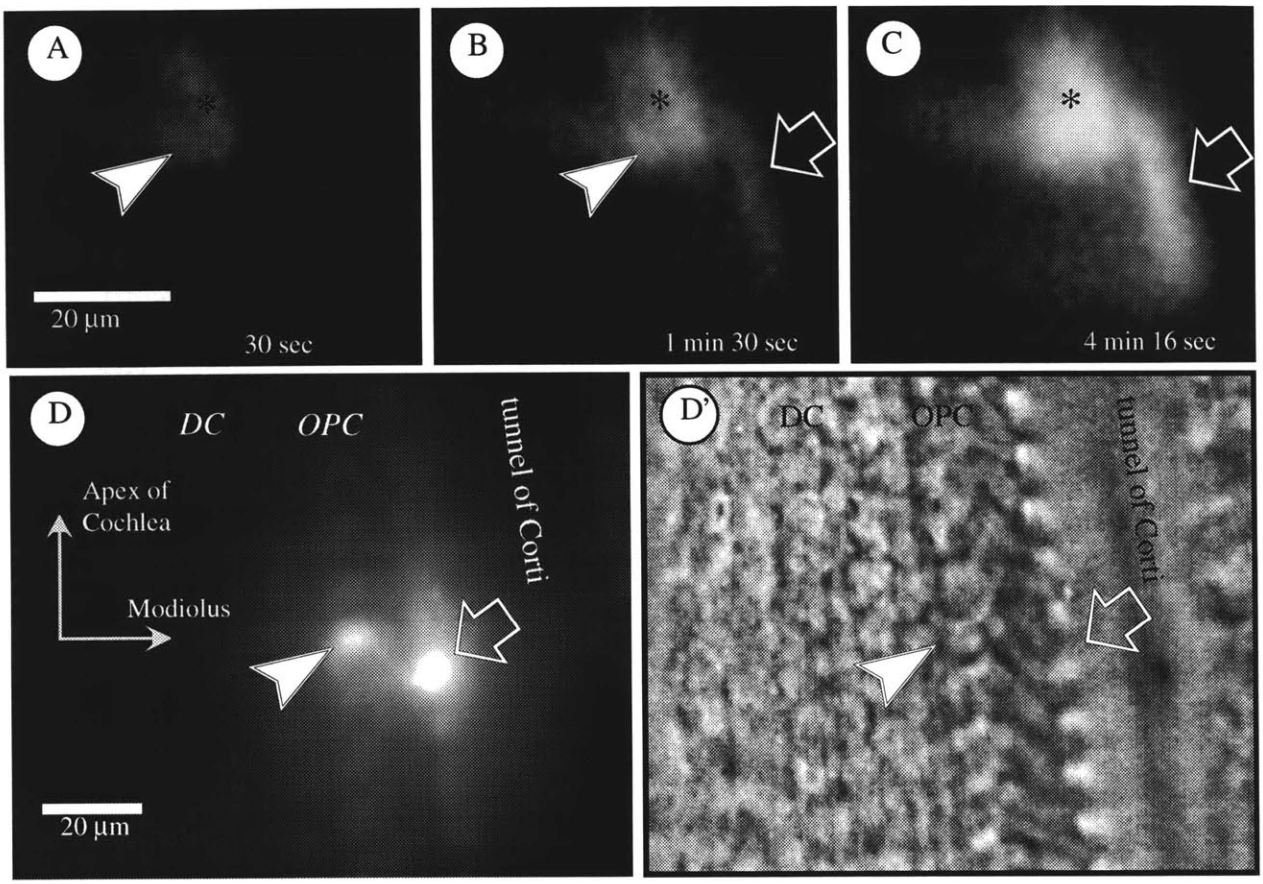

Figure 11. **(A-C)** Time series of background subtracted on-line images of an injection into an outer pillar cell. The asterisk shows the site of injection, which is the foot of the pillar cell. The dye spreads to the base of the cochlea and towards the modiolus to the inner pillar cell and the head of the outer pillar cell. **(D and D')** The surface preparation of the same tissue shows a similar pattern of fluorescence. The fluorescent image **(D)** shows multiple cells labeled in the longitudinal direction. The corresponding brightfield image is shown in **D'**. The footplates (white arrowhead) and heads (unfilled arrow) of the outer pillar cells are clearly labeled in the surface preparation. The corresponding arrows and arrowheads for the injected cell are also shown in the on-line images.

Unit	Injected Cell	Inner SC (A)	Inner SC (B)	Inner Pillar (A)	Inner Pillar (B)	Outer Pillar (A)	Outer Pillar (B)	Deiters (1)	Deiters(2)	Deiters(3)	Hensen	Claudius	Boettcher	Root Cells
37-2	Inner SC	4	5	2	3									
48-3	Inner SC	6	3	4	5	1								
78-1	Inner SC	+50	+50	14	12	10	7							
54-1	Inner Pillar	3	3	4	3	3	3							
54-4	Inner Pillar			4	4	1								
65-3	Inner Pillar			3	1									
65-4	Inner Pillar	8	12	6	7	7	4	2						
66-4	Inner Pillar	3	3	4	1	4								
68-6	Inner Pillar	4	6	1	1									
70-1	Inner Pillar	7	7	3	3	3	2							
72-1	Inner Pillar	18	14	11	7	7	5							
32-10	Outer Pillar			5	4	9	8							
37-2	Outer Pillar					4	6							
47-1	Outer Pillar			2	3	5	6							
47-10	Outer Pillar			1	2	3	7							
48-1	Outer Pillar	6	6	5	5	5	5							
48-4	Outer Pillar	3	4	4	4	5	5	3						
50-1	Outer Pillar		2	5	6	4	5							
65-1	Outer Pillar					1	1							
65-5	Outer Pillar	12	15	5	5	5	8							
66-5	Outer Pillar	2		2	2	7								
68-1	Outer Pillar			2		1	3							
71-1	Outer Pillar	4	6	6	7	5	6	14	10	9				
78-2	Outer Pillar	9	8	7	8	9	12	15	11	13				
81-4	Outer Pillar					2	3	2						
94-3	Outer Pillar			1	2	3	5							
95-3	Outer Pillar		1	2	2	3	2							

Table 2. Number of cells counted in the surface preparation after injection into inner supporting cells, inner pillar cells, and outer pillar cells. The columns are arranged in anatomical order from the modiolus to the lateral wall (inner supporting cells to the root cells). The inner supporting cell, inner pillar cells, and outer pillar cells are subdivided into the number of cells apical to the injection site (**A**) and number of cells basal to the injection site (**B**). The Deiters cells are subdivided by their row number. The dark outlined rows indicate that the dye spread to five or fewer cells. For one case of an injected inner supporting cell (78-1), more than 50 inner supporting cells were labeled in both the apical and basal directions.

Unit	Injected Cell Type	Inner SC	Inner Pillar	Outer Pillar	Deiters (1)	Deiters(2)	Deiters(3)	Hensen	Claudius	Boettcher	Root Cells
65-6	Deiters (1)										
78-3	Deiters (1)			4	12	8	10	14			
95-1	Deiters (1)			4	1						
54-3	Deiters (2)										
69-3	Deiters (2)										
74-4	Deiters (2)		14	14	13	13	13	47			
77-2	Deiters (2)						1				
78-4	Deiters (2)					2	1				
94-36	Deiters (2)	8	8	9	7	5	1				
95-2	Deiters (2)			6	5	6	4	3			
81-5	Deiters (2)				4	3	3				
68-5	Deiters (3)			6	6	10	9	10			
70-4	Deiters (3)						2	3			
77-1	Deiters (3)						2	5			
78-4	Deiters (3)					3	2	1			
50-3	Hensen						3	4			
50-4	Hensen						2	3			
68-3	Hensen				4	6	10	16	19		
69-5	Hensen					3	9	25	4		
70-3	Hensen							3			
71-3	Hensen							4			
72-2	Hensen							8	6	20	
74-7	Hensen							1			
75-3	Hensen										
77-3	Hensen						3	9	3	2	
54-2	Claudius								6		
65-7	Claudius								5		
66-2	Claudius								5	12	
68-2	Claudius							8	9	2	
68-4	Claudius							5	4	34	
71-2	Claudius							6	16	73	
72-3	Claudius							2	16	53	
72-4	Claudius							3	21	62	
74-3	Claudius								2	2	
74-8	Claudius								2	11	
77-4	Claudius								15	+100	
66-6	Clauidus								2	3	
95-4	Clauidus								1	1	
79-4	Claudius							3	8	20	2
78-5	Root Cells								1		2
69-6	Root Cells								2		3

Table 3. Number of cells counted in the surface preparation after injections into Deiters cells, Hensen cells, Claudius cells, and root cells. The columns are arranged in anatomical order from the modiolus to the lateral wall (inner supporting cells to the root cells). The Deiters cells are subdivided by their row. The dark outlined rows indicate that the dye spread to five or fewer cells. Gray rows represent units in which the injected cell was the only dye-filled cell in the surface preparation.

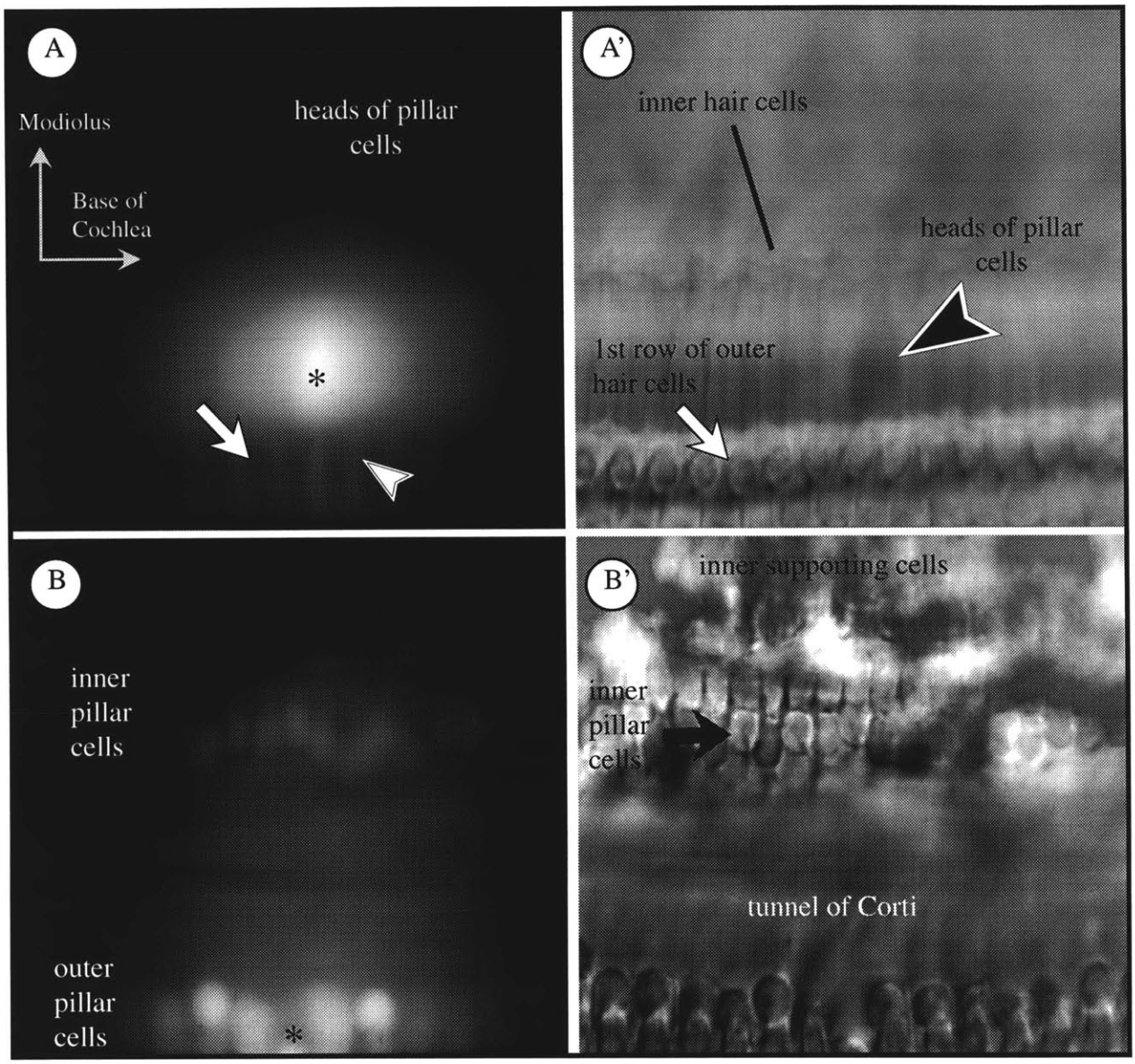

Figure 12. Two focal planes of a surface preparation after injection of an outer pillar cell. Adjacent fluorescent (**A** and **B**) and brightfield images (**A'** and **B'**) are at the same focal plane. The injected cell (asterisk) is the brightest cell labeled in **A** (focus is at the apex of the pillar cells). The heads of the outer pillar cells (black arrowhead) and processes of the pillar cells (white arrowhead) are labeled; however, the outer hair cells stand out because of their lack of dye (white arrow). The hair cells can be seen in **A'**. The focal plane through the base of the cells **(B)** shows dye is in the outer pillar cells and inner pillar cells (black arrow).

THIS PAGE INTENTIONALLY LEFT BLANK

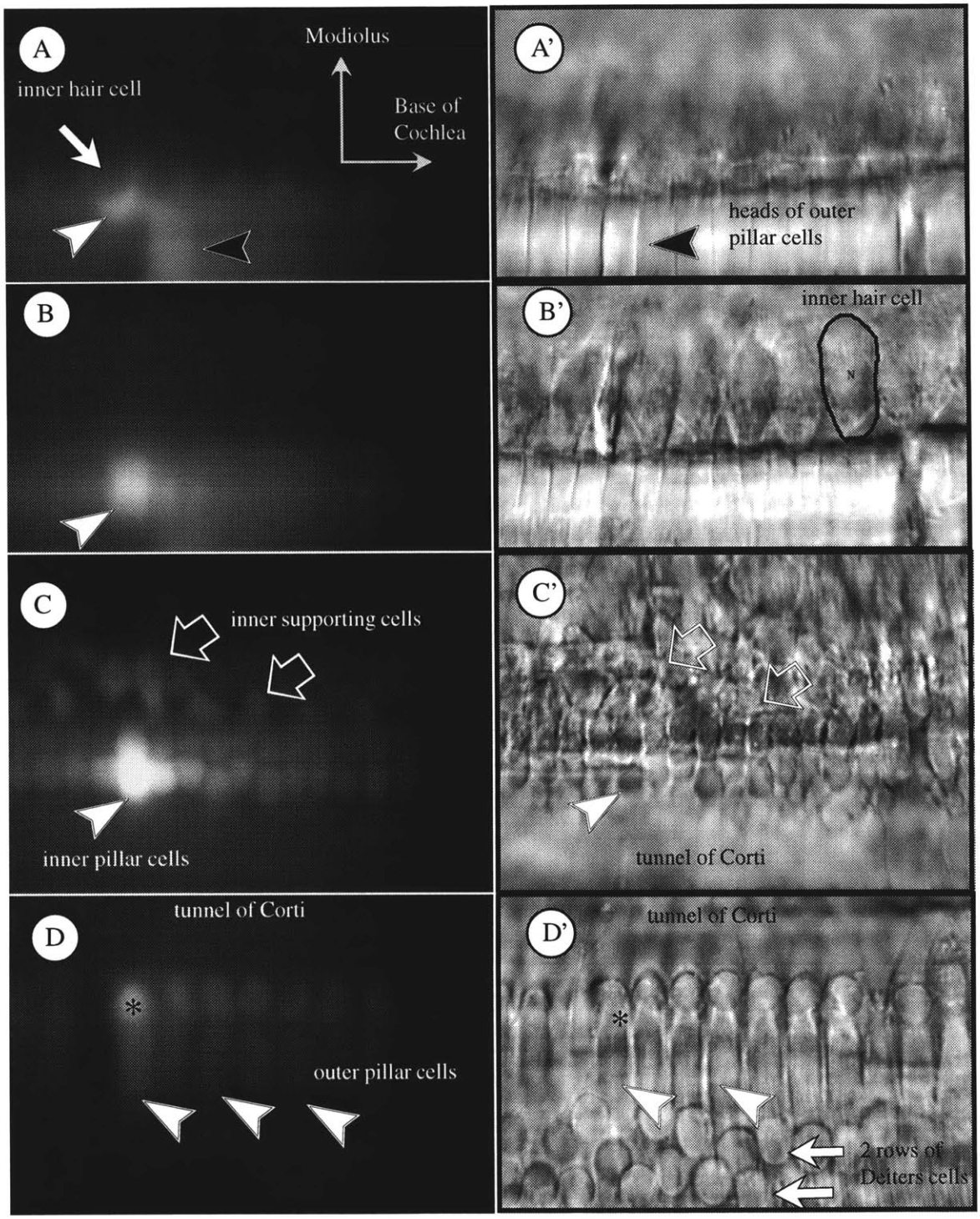
A
inner hair cell
Modiolus
Base of
Cochlea
A'
heads of outer
pillar cells
B
B'
inner hair cell
N
C
inner supporting cells
inner pillar cells
C'
tunnel of Corti
D
tunnel of Corti
outer pillar cells
D'
tunnel of Corti
2 rows of
Deiters cells

Figure on Previous Page

Figure 13. Surface preparations of an injection into an inner pillar cell. (**A** and **A'**) Images at the cuticular plate show the phalangeal process of an inner pillar cell (white arrowhead) and the heads of outer pillar cells. (black arrowhead). Dye is excluded from the inner hair cells (white arrow). (**B** and **B'**) 15 μm below the cuticular plate. Cell bodies of inner hair cells (one is outlined) and their nuclei (N) can be seen in the brightfield image. Dye is contained within the body of inner pillar cells (white arrowhead). (**C** and **C'**) Images 16 μm above the basilar membrane. The base of the inner pillar cells are filled with dye, and the brightest cell is the injected inner pillar cell. Inner supporting cells, which are directly below the inner hair cells, are also seen filled with dye (unfilled arrows). (**D** and **D'**) Images at 16 μm above the basilar membrane, but the image is shifted towards the lateral wall and the view is of the outer pillar cells. The base of the outer pillar cells are filled with dye (white arrowhead). The brighest outer pillar cell is the one adjacent to the injected inner pillar cell. The brightfield image shows the two rows of Deiters cells (arrows), but none are filled with dye.

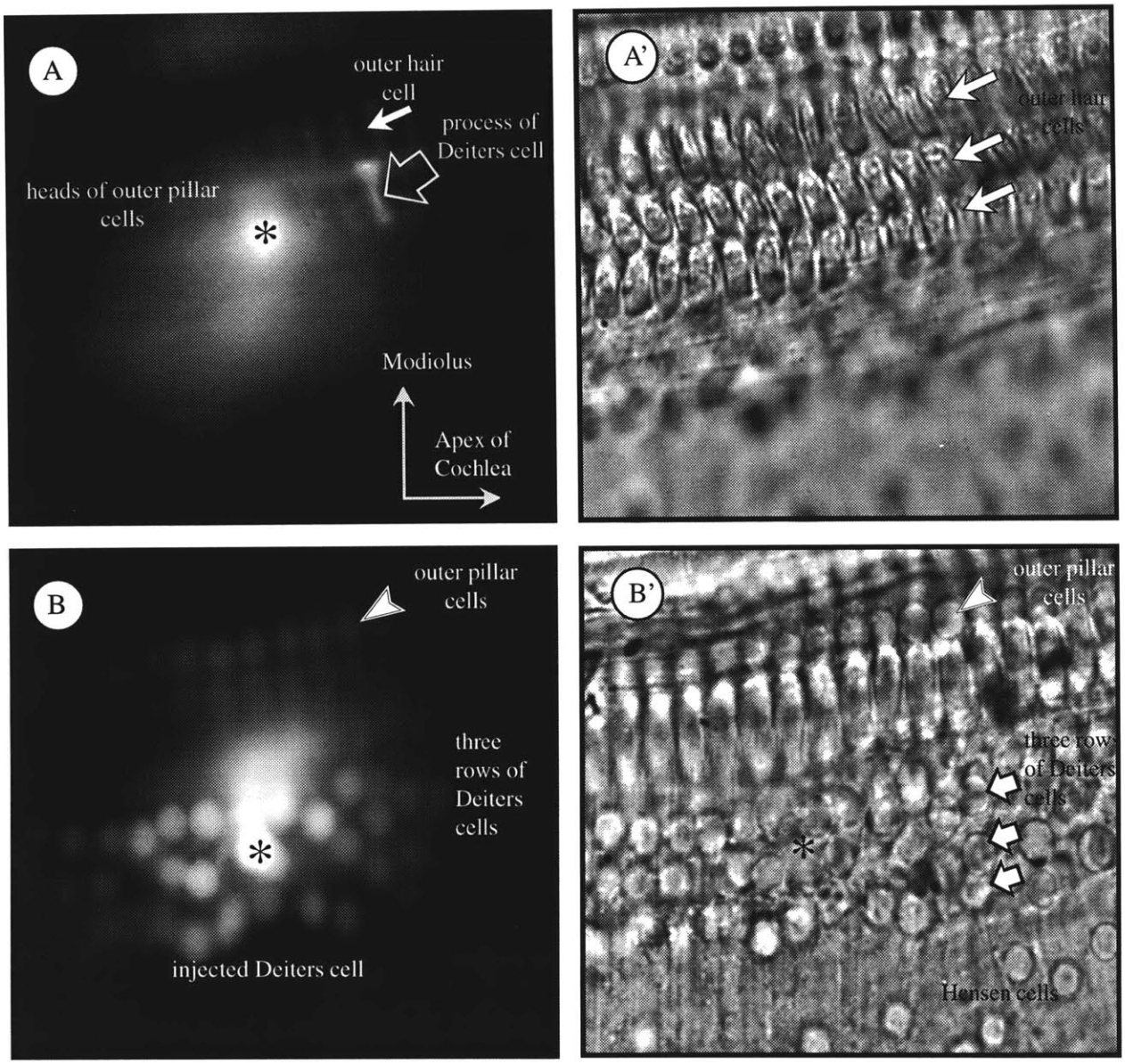

Figure 14. Two focal planes of a surface preparation after injection into a second row Deiters cell. **A**. Phalangeal processes of Deiters cells (unfilled arrow) is visible when the focal plane is at the reticular lamina. The three rows of outer hair cells can be seen in **A'** (white arrows), they are obvious because of their excusion of dye **(A)**. The bright spot is the nucleus of the injected cell (asterisk). The nuclei of all three rows of Deiters cells are labeled in **B** (75 µm below the culicular plate) and are seen in **B'** (bold white arrows). The outer pillar cells also contain dye as shown by the white arrowheads **(A,B)**.

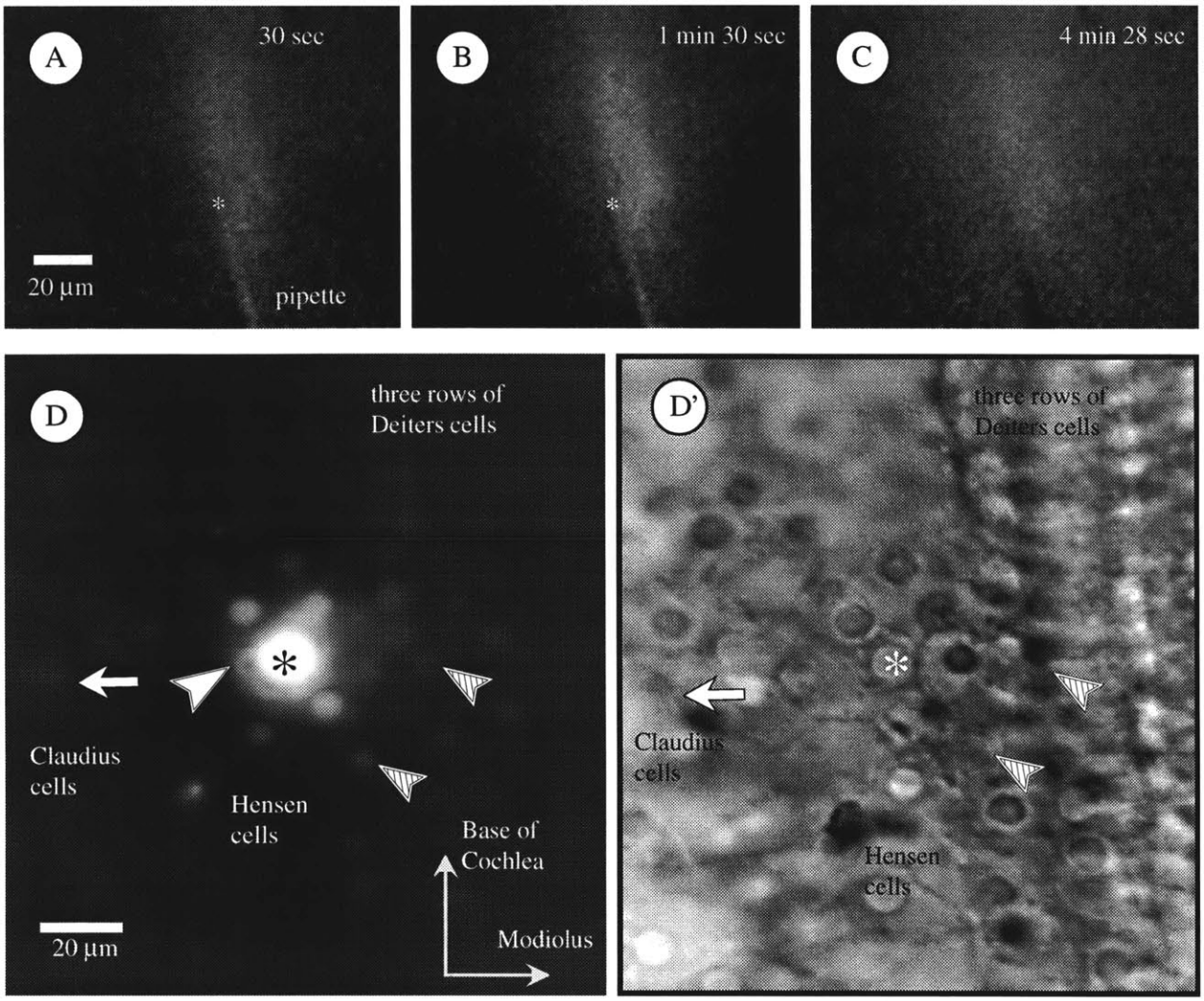

Figure 15. (**A-C**) On-line images of an injection into a Hensen cell. Initially the spread appears to be in the longitudinal direction. After 5 minutes of the injection, the dye appears to have spread more uniformly in all directions. The pipette can be seen in **A** and **B**, and a shadow of the pipette after it is withdrawn out of the cell and out of the field of view in **C**. The site of injection is marked with an asterisk. (**D** and **D'**) Surface preparation of the injected cell at the same plane of focus. The dye is contained in two cells at the brightest fluorescent level (asterisk). Other dye-filled Hensen cells, Claudius cells, and Deiters cells are present. Examples of two faintly labeled Deiters cells are shown with striped arrowheads. A faintly labeled Claudius cell is shown with a white arrow. The fluorescence is faint because the nuclei are out of focus. A process of a Hensen cell can be seen (white arrowhead). This Hensen cell is adjacent to the third row Deiters cell and sends a process to the apical surface of the organ of Corti.

THIS PAGE INTENTIONALLY LEFT BLANK

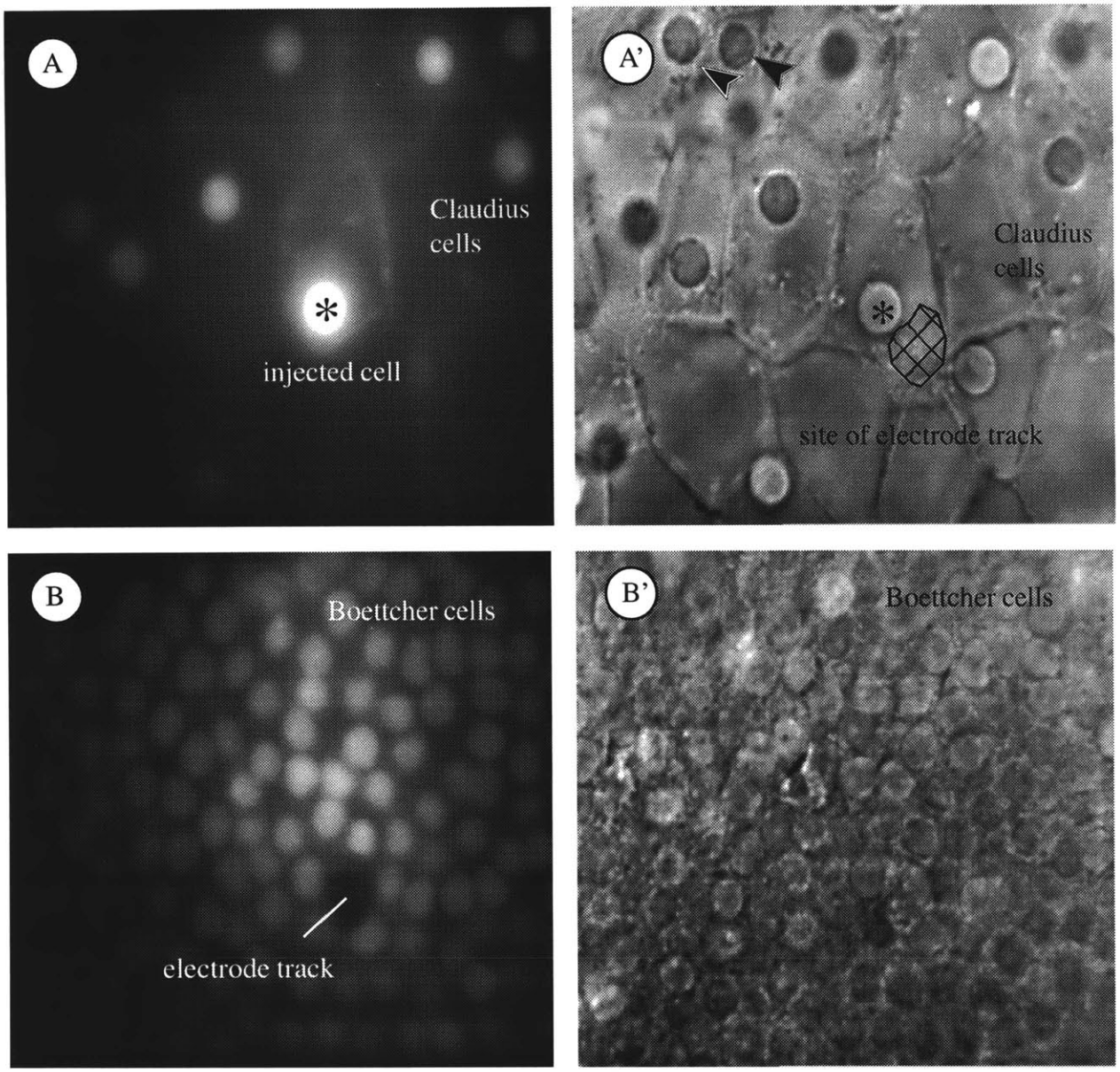

Figure 16. Two focal planes of a surface preparation after injection into a Claudius cell. Dye spread to many Claudius cells (**A**) and Boettcher cells (**B**). Labeled nuclei of Claudius cells can be seen in the fluorescent image in **A** with the brightest one corresponding to the injected cell (asterisk). Dye did not accumulate in two cells seen in the brighfield image (black arrowheads). Panel **B**, 15 μm below **A**, shows labeled Boettcher cell nuclei. The presumed electrode track is seen as a lack of fluorescence in **B**. A mesh outline of the track is overlayed on the brightfield image (**A'**) to show the site of injection.

THIS PAGE INTENTIONALLY LEFT BLANK

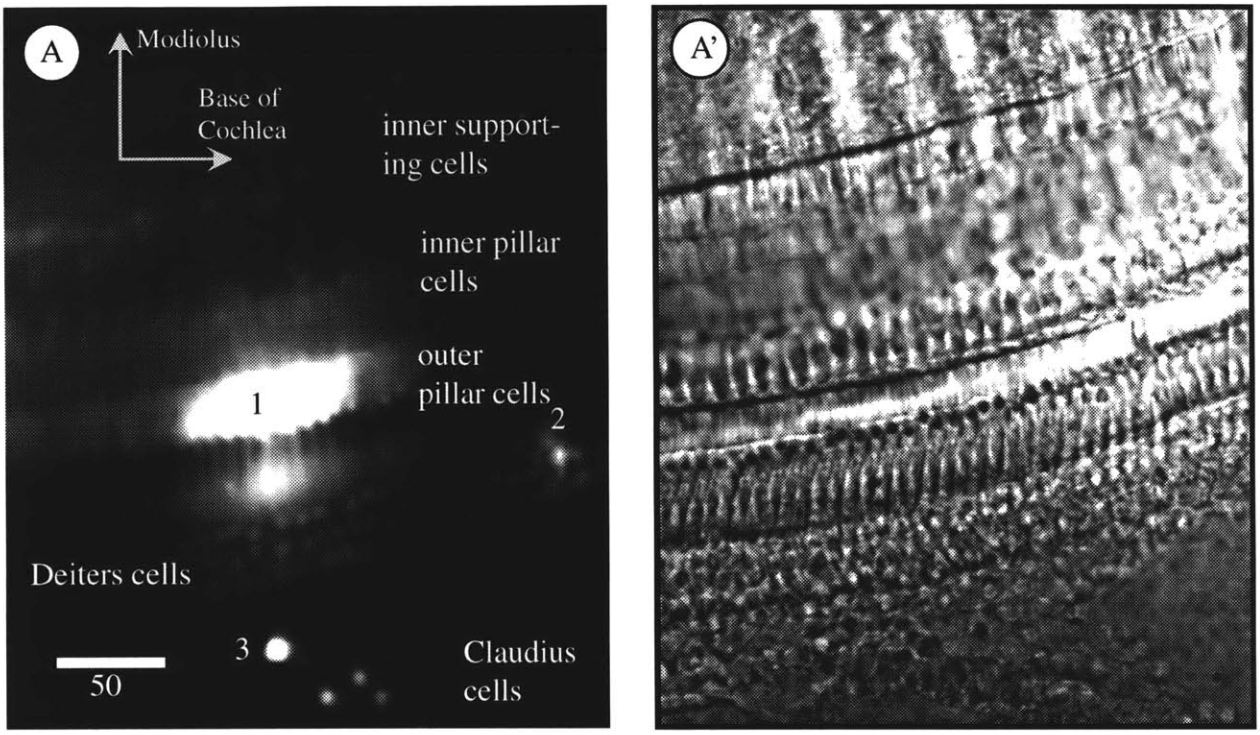

Figure 17.Fluorescent image of CY5-labeled neurobiotin (**A**) and the corresponding brightfield image (**A'**). Several injections were made in a single prepration. The spread was massive and spread to almost all cells in the epithelial gap junction network. The neurobiotin injection sites were: 1. outer pillar cell, 2. Deiters cell, and 3. Claudius cell.

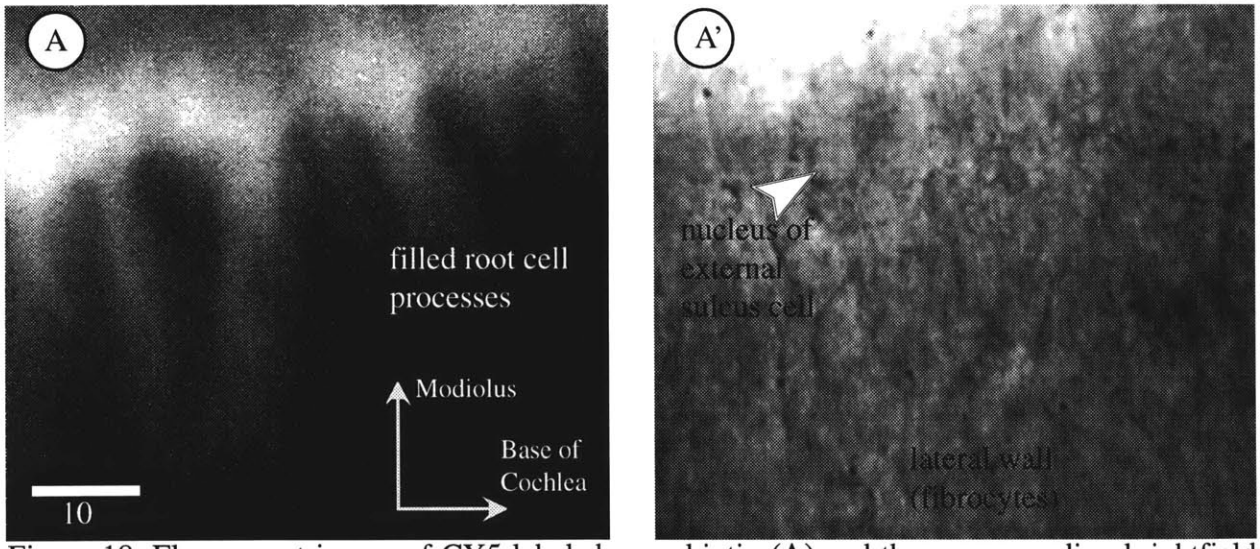

Figure 18. Fluorescent image of CY5-labeled neurobiotin (**A**) and the corresponding brightfield image (**A'**). The processes of the root cells are filled with the neurobiotin. The bright band of fluorescence across the top of the field is the accumulation of neurobiotin in the external sulcus cells and root cells.The brightfield image shows the lateral wall and images of the fibrocytes. Processes of root cells are at the lateral end of the epithelial gap junction network. No dye is seen in the fibrocytes or in the extracellular spaces. The injection was made in a Claudius cell for 3 minutes at +5nA. The concentration of neurobiotin in the Claudius cells was much lower and slightly above the autofluorescence of the tissue.

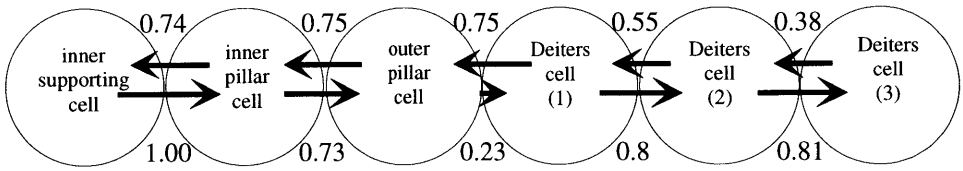

Figure 19. Schematic representation of supporting cells that are coupled in the radial direction along with the probability of dye spread between the cells. For each case where there were more than two LY-filled cells of a given cell type, the number of cases in which the dye spread towards the modiolus and towards the lateral wall were counted. The probabilities are given above and below with arrows facing the right representing movement towards the lateral wall. The junction with the largest noticable difference was between outer pillar cells and Deiters cells. LY spread from Deiters cells to outer pillar cells in 6 out of 8 cases (prob=0.75). LY spread from outer pillar cell to Deiters cell in only 5 out of 21 cases (prob=0.23). The probabilites were computed from in Table 2. The lengths of the arrows represent the probability for the direction of the movement of LY.

1.4 Discussion

This study was the first to document the spread of dye between cells in an intact cochlear epithelial cell network in real time. The preparation permitted documentation of the direction in which the dye spread and how fast the dye spread to adjacent cells. The dye often spread to an area larger than the size of a single cell within one minute of the injection. While specific cells could not be identified in the on-line images, the surface preparation images permitted identification of dye-containing cells and confirmed that the dye spread in a manner consistent with results of the on-line images. Spread from each supporting cell type in the organ of Corti cochlea confirmed that the intercellular pathway from the interdental cells to the root cell processes was functional. On-line imaging of the dye verified that its apparent spread seen in the surface preparations occurred in normally functioning cochleas. These dye-coupling experiments verified that gap junctions between cells in the epithelial cell network are patent in a normal cochlea with good hearing, in agreement with the hypothesized intercellular pathway for potassium recycling.

1.4.1 Comparison of on-line results and surface preparation

The long-working distance objective and our approach to the cochlea allowed visualization of cells on the basilar membrane in real time. However, poor quality of the on-line images made it difficult to make quantitative measures of the dye spread. One of the biggest problems was the lack of resolution of cell boundaries in the brightfield images. The resolution limitation was due in part to the loss of power of the fluorescence caused by the air-fluid interface between the objective and the perilymph in the opening of the cochlea. From the on-line images, it was possible to get a qualitative measure of the spread of dye and then a quantitative measure from the surface preparations.

Less dye spread was observed in the on-line images than was observed in the off-line images. This was probably due to less refractive problems and to greater light gathering efficiency of the optics used when imaging the surface preparations. During the experiments, light levels were kept low and the light was shuttered to reduce photobleaching and photo-irradiation of the cells, so only high concentrations of dye could be imaged. Dye may have been spreading to other cells

and accumulating in concentrations that were too low to be imaged. This reduced imaging ability on-line may have been the cause for the plateau in the area of dye spread seen during the iontophoresis (Figure 8).

The differences in the area and intensities between different cases of injections of given cells types may be due to differences in the amount of injected dye, as well as differences in light levels between different preparations. If the dye was diffusing rapidly, then the concentration of dye several cells away may not have reached a level that could be imaged on-line. This would also cause the intensity of the image to plateau. This pattern is consistent with what was seen when injecting Claudius cells. When injected into Deiters cells and pillar cells, the LY bound to the abundant intracellular organelles, which created a high intracellular concentration that was readily imaged. The fluorescent intensities did not decay as fast as they did with the Claudius cells, which have few organelles to bind the dye within the cells.

The combination of on-line and off-line images showed that the dye moved intercellularly through the gap junctions and not via an extracellular pathway. When dye was injected into the spaces of Nuel, it diffused away rapidly to levels below which could be imaged. The recovered tissue from these injections showed no dye-filled cells. On the other hand, on-line images of intracellular injections showed dye confined to specific areas. The surface preparations showed convincingly that the dye was intracellular because the nuclei were the brightest parts of the images. There was no sign of dye in the extracellular spaces between the cells. If dye injected into a cell were to leave the cell, then the extracellular dye concentration would remain low since the extracellular spaces are large. It is unlikely that an adjacent cell would take up significant dye. Since the LY was seen to spread as far as 10 cells away from the injected cell, it is most likely that the dye took an intercellular pathway from the injected cell to remote cells.

Our images of intracellular LY were similar to most images shown by Zwislocki et al. (1992). However, their image of the phalangeal processes of the Deiters cells was very different from our results. In the present study, completely filled phalangeal processes of injected Deiters cells were consistently recovered, and in cases with a large amount of spread, processes of the adjacent Deiters cells were filled. In the image of the Deiters cell processes shown by Zwislocki et al. (Figure 14, Zwislocki et al., 1992), processes are not filled and only the membranes, or the spaces between the processes are filled. One way to explain the differences in the staining

patterns between Zwislocki et al. and the present results may be that Deiters cell and pillar cell membranes in their material was autofluorescent. In another of their figures (Figure 20, Zwislocki et al., 1992), they showed autofluorescence of the outer hair cells and Deiters cells. Another possible explanation of their results is that extracellular LY bound to the Deiters cell process on the outside of the plasma membrane. In the present experiments, it was possible to eliminate the autofluorescence from the tissue by adjusting the gain of the imaging system above the autofluorescence level of tissue in cases where no dye was injected. In the present study, the presumed filled processes of outer pillar cells, inner pillar cells, and Hensen cells were well above the autofluorescence level of adjacent unfilled cells. Therefore, it is likely that the previous results were artifact.

1.4.2 Patterns of dye spread

A key finding in this study is that the gap junctions between adjacent cells in the entire epithelial cell network was found to be patent. In no case was there a single injection in which the entire network from the interdental cells to the root cells were filled because the amount of LY to be injected would have been too large. Some of the LY bound to the intracellular organelles, so larger concentrations of dye were needed for larger spread and the dye did not spread across the entire organ of Corti. However, by combining the results from the different injections, it was shown that the entire network is patent. Neurobiotin was seen in many more cells with a single injection than was seen following LY injections. This is in keeping with other reports (Zahs and Newman 1997) that NB spreads more readily through the gap junctions than does LY. NB was present in all cell types when injected into just two or three cells, further supporting the finding that the entire epithelial gap junction network is functional.

Several patterns of dye spread were observed. 1. At the junction between outer pillar cells and first row of Deiters cells, LY tended to spread more often from Deiters cells to outer pillar cells (6/8) than in the reverse direction (5/21). 2. LY injected into pillar cells tended to spread preferentially in the longitudinal direction. 3. LY injected into Claudius cells spread uniformly in all directions and usually spread to a large number of cells.

No distinct patterns of spread were observed when LY was injected into Deiters cells or Hensen cells. Occasionally there was uniform spread, and at other times, there appeared to be a

preferred movement. Since the number of LY-filled cells was usually fewer than 10 cells, it was difficult to determine the pattern of spread.

Can the electrical gradient between cells account for differences in radial dye spread?

In the present work, resting potentials of supporting cells were found in the same range as other studies (Oesterle and Dallos 1989; Russell and Sellick 1978; Zwislocki et al. 1992). There appears to be a gradient in resting potentials from the supporting cells underneath the hair cells to the lateral wall, with the cells further away being more negative. Such a gradient is consistent with the hypothesis that potassium ions flow intracellularly from the supporting cells near the hair cells to the root cells. Another explanation for the observed electrical gradient is that Claudius cells may be less likely to be damaged upon penetration, so their measured resting potentials more accurately represent the actual resting potential.

If there were a positive current from outer pillar cells to root cells, then electrodiffusion would cause the LY to spread medially and NB to spread laterally. Assuming that the current from pillar cells to root cells is uniform, then the current density from outer pillar cells to Deiters cells would be larger than the current density between adjacent Hensen cells or adjacent Claudius cells. The area of contact and number of gap junctions between outer pillar cells and Deiters cells is smaller at the pillar-Deiters junction. A larger current density at this site is one possible explanation for the preferential movement of LY between outer pillar cells and Deiters cells and not between Hensen cells and Claudius cells.

The radial movement of LY is summarized in Figure 19. There appeared to be directional movement of dye at the outer pillar cell and Deiters cell junction. In 21 cases where multiple outer pillar cells were filled with dye, there were only 5 cases of LY-filled Deiters cells. In 8 cases where first row Deiters cells were filled with dye, there were 6 cases with LY-filled outer pillar cells. Using a Student t-test, the difference in the spread was significant with a p-value of 0.0082. This difference in spread could be explained by a positive current from outer pillar cells to Deiters cells. No difference in resting potentials between these cell types was found, so there may be alternate explanations for the preferential movement, such as anatomical differences between this junction and other junctions in the organ of Corti, for example the content of specific connexin molecules.

When NB was injected into pillar cells, there was considerable amount of spread to Deiters cells (injection #1 in Figure 17). When Deiters cells were injected, there was some spread to outer pillar cells, but the majority of the spread appeared to be to other Deiters cells lateral to the injected cell (injection #2 in Figure 17). Movement patterns of both the LY and NB suggest that a current may be influencing the direction of the spread. Further evidence that a current may exist is that when NB was injected into Claudius or Hensen cells, it appeared to accumulate in root cells and external sulcus cells (Figure 18), which are at the end of the gap junction network. In this case, there was little NB found in Claudius cells, Hensen cells, or Deiters cells. NB spread laterally in the same direction as the putative positive current. This pattern would be predicted by an electrodiffusive flow given the existence of the resting potential gradient.

The lack of preferential radial movement of LY between other cell types may be due to a lower current density between those cells. Another explanation for the lack of a radial movement of dye from the other cell types is that there is no intercellular current as suggested by the findings of a gradient in the resting potentials. The results are suggestive, but do not provide compelling evidence for or against the presence of a current. They do, however, confirm the patency of the cell network, which could allow currents if they existed.

Anatomical correlates of dye spread

The on-line images showed strong longitudinal dye coupling among inner supporting cells and pillar cells. This longitudinal pattern of dye was also seen in the surface preparations. There were no obvious resting potential gradients in the longitudinal direction, but evidence for such gradients was not systematically sought. The endolymphatic potential does have a longitudinal gradient, but over the region of the cochlea in which this study was performed, it would be less than 1 mV (Salt et al. 1989). The existence of a gradient in the endolymphatic potential does not necessarily generate an intercellular gradient in the longitudinal direction. The finding that the dye was present in equal numbers of cells in both longitudinal directions from inner and outer pillar cells suggest that there is no longitudinal potential gradient.

The initial longitudinal direction of the dye spread was different for pillar cells and Deiters cells. Dye injected into pillar cells appeared to spread rapidly towards the base of the cochlea whereas dye injected into Deiters cells appeared to spread more readily towards the apex of the

cochlea. This apparent directional spread during the initial time after the injection may have been due to spread of dye within the injected cell. The shapes of the cells are different and the apparent spread could be due to the different directions taken by the apical processes of the two cell types. The phalangeal process of pillar cells project towards the base of the cochlea whereas the process of the Deiters cells project towards the apex of the cochlea. Dye spreading within a single cell to the apical surface would appear to spread in the direction taken by the apical processes.

The longitudinal spread may have been due to the presence of a high density of gap junctions between these cells in the longitudinal direction (Chapter 3). Minimal spread of LY from outer pillar cells to Deiters cells may be partially explained by the relatively few gap junctions between them over a very small area of contact when compared to the number of junction between homotypic cells. If there were coupling and little quantities of LY spread between these cells, then the resulting low concentrations of LY may not be imaged. However, this argument would imply that the movement of LY from Deiters cells to outer pillar cells be equally low, but this was not seen. Therefore, there must be other mechanisms that allow LY to move preferentially from Deiters cells to pillar cells, such as directional coupling or an intercellular current. The finding that NB readily spreads from outer pillar cells to Deiters cells, in the opposite direction as the LY, is consistent with the hypothesis that there is a current from outer pillar cells to Deiters cells. A possible explanation for directional spread of LY from Deiters cells to outer pillar cells is that gap junctions between these cells are directional and allow dye to pass through more easily in one direction than the other direction. This directionality has been shown when heterotypic connexons form the gap junction pore (Robinson et al. 1993; Verselis et al. 1994). However, there is no immunohistochemical evidence to date that multiple connexin proteins are co-localized to the same junction to suggest that such gap junctions exist morphologically in the cochlea.

LY injected into Claudius cells, and occasionally into Hensen cells, spread uniformly in all directions, indicating a different pattern of spread. Uniform spread is consistent with anatomical findings that these cells are uniformly connected to other cells in all directions. Preferential radial movement of LY among Hensen cells and Claudius cells was not found to be statistically significant.

1.4.3 In vitro vs. in vivo studies

The present results generally agree with results from the *in vitro* dye coupling experiments of Santos-Sacchi (1986) and dye coupling between supporting cells shown by Zwislocki et al. (1992). However, the present study extended these findings by ensuring that dye injections were made in normally hearing ears so as to eliminate the possibility that the results could be due to artifacts of damaged ears or *in vitro* conditions. Santos-Sacchi (1987) found higher electrical coupling ratios *in vitro* (0.6) than *in vivo* (0.1), which suggests the cells *in vivo* function differently than the cells *in vitro*. It is known that gap junctions are highly labile, and small changes in the cellular environment could cause changes in the coupling between cells (for review see Bruzzone and Ressot 1997). The only previous *in vivo* dye coupling study (Zwislocki et al. 1992) was performed without visualization of the tissue and dye spread was analyzed using the surface preparation after fixation of the tissue. In the present study, on-line monitoring showed that in some cases dye was unintentionally injected into cells despite the use of a holding current. Because the experiments of Zwislocki et al. were done without on-line monitoring, there is uncertainty that all dye-filled cells in that study were intentionally filled.

1.4.4 Coupled outer hair cells?

In this study, no dye-filled hair cells were ever seen in the surface preparations. This is in contrast with the previous study of Zwislocki et al. (1992), which claimed coupling between hair cells and supporting cells, despite the lack of anatomical data to support the presence of gap junctions (Gulley 1976; Kikuchi et al. 1995). Dye spread to hair cells in that study could have been due to inadvertent filling of cells as the electrode passed through the tissue. The authors concluded that there was dye coupling between outer hair cells and supporting cells based on weakly fluorescent Hensen cells when a bright outer hair cell was observed (Zwislocki et al. 1992). However, there was no mention of dye-filled Deiters cells, through which the dye must have passed if it spread from the hair cells to the Hensen cells.

Inadvertent filling of cells could explain their results. For the measurement of AC responses from the hair cells, their electrode passed through Hensen cells. They rejected the idea that the dye had spilled into the cells by claiming that the dye density was too high in the supporting cells. However, in the present study it was found that dye concentration can get quite high within

a cell in a very short time. Despite a holding current, spontaneous filling of cells was observed in our earlier experiments. In these experiments, LY filled cells in as little as 5 seconds. Cells that inadvertently filled without any injection were more weakly labeled than the intentionally injected cells within the same surface preparation.

Zwislocki et al. claimed that dye spread was directional because they did not find it in outer hair cells when supporting cells were injected, but always found it in supporting cells when hair cells were injected (Zwislocki et al. 1992). Their interpretation was that there is a direct current from outer hair cells to supporting cells, which is carried by potassium. It is this current which they suggest may be one of the driving forces for the flow of the dye. However, since they used LY, the flow LY from the hair cell to the supporting cell would be impeded by the potassium current and should accumulate in the hair cell since it has a charge opposite to potassium. Their hypothesized current would cause the flow of dye from supporting cell to hair cells, which was not seen. This directional flow is inconsistent with their findings that multiple outer hair cells were filled when a single hair cell was injected. Since outer hair cells do not contact each other, there cannot be direct coupling between the cells. This would imply that the current flows from the injected hair cell to the supporting cell, and back into adjacent hair cells. This would be a direct contradiction of their conclusion that the spread was directional from hair cells to supporting cells. Possible explanations for their results are that the cells are autofluorescent, or that the outer hair cells appear to be fluorescent because of blurring from fluorescence of the Deiters cells (Figure 11). In the present study, autofluorescence was suppressed by reducing the gain on the imaging system until no fluorescence was seen in regions where it is known that there was no dye injected, for example half a turn away from the site of injection. By optically stepping through the tissue at 1 micron steps, it was possible to distinguish where the fluorescence was intracellular, and in which planes the fluorescence was outside the boundaries of the cells.

In the present study, no dye coupling was found between outer hair cells and supporting cells. No anatomical evidence for gap junctions between outer hair cells and Deiters cells has been shown in the mammalian cochlea. In this study, only a few putative hair cells were penetrated, but they were not held long enough to inject dye. The first cell that could be held after penetrating the basilar membrane was usually a Deiters cell rather than an outer hair cell. No dye was ever visualized in a hair cell in any of the surface preparations. In fact, the absence

of dye from the hair cells was striking. In the present experiments, no evidence was found which suggested that the cells take up dye from the extracellular spaces. It is therefore concluded that the dye found by Zwislocki et al. in the Hensen cells came from the electrode as it passed through enroute to the outer hair cells.

1.4.5 Lability of the gap junction network

The condition of the cochlea appeared to play a role in the spread of the dye. When the CAP thresholds were elevated, the dye did not always spread. The lack of spread was usually found when the EP was low and intracellular resting potentials from the injected cells were low. When the EP was normal and the CAP thresholds were elevated between 20 and 40 dB SPL, LY was observed to spread. When the EP was below 50 mV, cells were difficult to hold and the dye was confined to one cell. This finding is different from those of Zwislocki et al. (1992), who found massive dye spread from Hensen cells to Deiters cells when the EP was very low (22 mV). Since the lateral wall approach was used in that study, the lower EP levels could have been due to disruption of the scala media and the stria vascularis by the electrode passage through the lateral wall, while perilymphatic spaces remained intact. If this is true, the gap junction network may have still been intact. The CAP thresholds and EP were not systematically altered to rigorously test these hypotheses.

Low EP in preparations in the present study may have been caused by a disruption in the gap junction network. Since the gap junctions are known to be function even without the EP *in vitro*, one possible explanation for the low EP when there is lack of spread is that the gap junction networks are essential for generation of the EP. If the gap junction networks are required to generate the EP, then a degenerated state of the supporting cells may have caused a reduction in the EP.[4] It is known that when ouabain is perfused in the perilymph, the EP falls to a negative value within 10 minutes of the perfusion (Marcus et al. 1981). If ouabain blocks the sodium, potassium-ATPase in the type II fibrocytes, then it may prevent the flow of potassium into the intrastrial space where it is taken up by the strial marginal cells for transport into the endolymph.

---

[4] An attempt was made to uncouple the gap junction network using known uncoupling agents Octanol, Halothane, and arachidonic acid (AA). In most of the results the dye coupling was not affected by the perfusion of any of these uncoupling agents. However, Octanol has been shown to uncouple Hensen cells *in vitro* (Santos-Sacchi, J. 1991). Since these agents bind to the cellular matrix, it is thought that *in vivo*, the concentration of agent required to uncouple the cells may not get high enough near the cells. The agents may stick to the matrix of the basilar membrane. These results will be explored further in Chapter 4.

Many of our preparations where the EP was degraded there was a lot of bleeding during procedure of opening the otic capsule. Some constituents in the blood may have thereby entered the perilymph and disrupted the cell network. The cells may also have been altered by small changes in the intracellular pH, which may have uncoupled the cells.

It is known that gap junction permeabilities can be modulated by a large number of different factors. Some of the variability in the amounts of dye spread may have been due to changes in the permeability of the gap junctions between cells. We were not able to systematically determine which factors caused a change in the gap junction permeabilities. In two earlier preparations, traumatizing sounds louder than 90 dB SPL were applied to the cochlea for 2 hours. Dye was injected in cells before and after the sound stimuli. Dye always spread to fewer cells after the traumatizing sound. Further investigations of the effects of sound on gap junction permeability are necessary to better understand the network.

1.4.6 Summary

The results of this study can be summarized as follows:

1. The entire epithelial gap junction network from interdental cells to root cells was found to function *in vivo* as verified by visualization of LY and NB spread between these cells.
2. The primary direction of the spread of LY was in the longitudinal direction for injected pillar cells. However, the spread was uniform in all directions when it was injected into Claudius cells. Deiters cells and Hensen cells showed both longitudinal and radial movement of dye.
3. There appeared to be preferential spread of LY from Deiters cells to outer pillar cells. LY only occasionally spread from outer pillar cells to Deiters cells, whereas when there was spread from Deiters cells it usually spread to outer pillar cells.
4. Accumulation of neurobiotin in root cells along with a statistically significant movement of LY from pillar cells to Deiters cells suggest that an electrical gradient may affect the movement of injected dyes.
5. No dye transfer was found between supporting cells and hair cells.

2 Electrical gradients in the epithelial cell network in the organ of Corti

2.1 Introduction

Cochlear function relies on an electrical potential difference between the endolymphatic space and hair cells' resting potential. This potential difference provides the driving force for the receptor current through the transduction channels in the hair cell. When sound is present, the receptor current is modulated, causing the hair cells to depolarize and release neurotransmitter. The receptor current is primarily carried by potassium because potassium is the dominant cation in the endolymph. Potassium entering hair cells through transduction channels exits the cell through channels in their basolateral surfaces. After exiting, potassium is recycled back to endolymph, which preserves the high endolymphatic potassium concentration necessary for sound transduction.

There are several possible mechanisms for recycling potassium from the basolateral surfaces to the endolymph (Figure 1). Radioactive tracer studies showed that potassium is recycled from the perilymph to the endolymph directly rather than the blood (Konishi et al. 1978). However, tight junctions between the apical surfaces of the cells lining the endolymphatic space (Jahnke 1975b) prevent potassium from diffusing between the two spaces. Standing and sound-evoked extracellular currents in scala tympani (Zidanic and Brownell 1990; Zidanic and Brownell 1992) suggest the presence of an extracellular potassium current from the hair cells to the lateral wall, as shown in Figure 1. An intercellular pathway has been suggested based on (1) anatomical evidence of cell networks (Kikuchi et al. 1995) and (2) high concentrations of sodium, potassium-ATPase at the junctions of the networks (Schulte and Adams 1989), and (3) the patency of the gap junctions among the cells of the epithelial cell network (Chapter 1). However, the relative importance of intercellular versus extracellular recycling is not known. This chapter describes electrical aspects of the supporting cells in the epithelial cell network that appear to be part of an intercellular potassium recycling process.

There has been limited evidence concerning the idea of potassium recycling through the epithelial cell network. Supporting cells depolarize during tone bursts, but hair cells do not show this response (Oesterle and Dallos 1990). This depolarizing DC potential is thought to be due to a redistribution of potassium. The depolarization can be due to an accumulation of potassium in the spaces of Nuel (Johnstone et al. 1989), or by potassium uptake by the supporting cells (Santos-Sacchi 1991). ATP-dependent inwardly rectifying potassium channels found in Deiters cells (Hibino et al. 1997) provide anatomical evidence in support of the hypothesis that Deiters cells are specialized to take up potassium.

A potassium sink is thought to exist in the region of the type II fibrocytes because they contain a high density of sodium, potassium-ATPase. Sustained potassium taken up by the type II fibrocytes in the lateral wall could cause a decrease in the extracellular potassium concentration surrounding those cells. Lower extracellular potassium would increase the concentration difference across the distal processes of the root cells, which extend into the region of the type II fibrocytes, and would cause additional potassium to exit the root cells. This could generate a potassium concentration difference or current between the Deiters cells, where potassium is taken up, and the root cells, where potassium is expelled.

In the present study, resting and sound-evoked potentials were measured in the radial direction to seek evidence for intercellular currents within the epithelial cell network. Intracellular potentials were studied systematically along the radial axis by recording from inner supporting cells, inner pillar cells, outer pillar cells, Deiters cells, Hensen cells, and Claudius cells. Resting potentials were measured to determine if there are "standing" potential gradients that may indicate an intercellular current. Sound-evoked potentials were measured to determine how sound influenced these gradients. These intracellular measurements were compared with extracellular measurements to determine the relative importance of the two recycling pathways.

Measurements of electrical coupling properties of the cells in the supporting cell network were also made in the present study by simultaneously impaling pairs of cells to measure mutual resistance. The mutual resistance is the ratio of the voltage response in one cell to a current injected into the other cell. The space constant, a measure of coupling, was computed from sampling the mutual resistance between pairs of cells at increasing separation distances. The space constant was also computed by analysis of the sound evoked responses. At high sound

levels, it is assumed that a small region of the cochlea is stimulated evenly along the longitudinal direction. A uniform stimulation in the longitudinal axis would the two dimensional network of cells to be modeled as a one dimensional model. In the one dimensional case, the potential decreases exponentially with distance from the source. Electrophysiological and sound-evoked results were used to compute the network's space constant to quantify the coupling between these cells *in vivo*.

2.2 Methods

A detailed description of the methods for opening the cochlea and measuring the cochlear condition are described in Chapter 1. Chinchillas weighing between 300g and 600g were anesthetized with 65 mg/kg of sodium pentobarbital, i.p., with a booster given every 2 hours or as needed. After the animal was anesthetized, a tube was placed in the trachea and the head was firmly fixed at the snout and roof of the mouth. The rectal temperature was maintained between 36° and 38° C with heat lamps and a heating pad. Skin and muscle over the back of the skull was removed to expose the bulla and the occipital bone. The pinna was removed to allow for the placement of a sound source into the external canal. To visualize the round window and the hook of the cochlea while leaving the middle-ear apparatus intact, the dorsal-lateral portion of the bulla and several septa were opened by shaving the bone. A second ventro-lateral opening was made to allow insertion of a fiber optic light source (Figure 2). After the bulla was opened, a stiff bar from the head holder was attached to the temporal bone using dental cement to further reduce vibrations and to allow for longer cell holding times. The experiments were performed on a vibration isolation table in an electrically and acoustically isolated chamber. The otic capsule was opened in the basal turn to expose the basilar membrane. The cochlear opening allowed for recordings from cells with a best frequency between 7000 and 9000 Hz.

2.2.1 Monitoring cochlear function

Cochlear function was assessed by measuring the compound action potential (CAP) thresholds (iso-response contours) in response to tone bursts between 1 kHz and 30 kHz with a rise and fall time of 1 msec, which were presented through a calibrated, closed acoustic system with a 1 inch condenser microphone system (Kiang et al. 1965). Baseline CAP thresholds were

measured after opening the bulla. A second measurement of the CAP thresholds was taken after opening the otic capsule to determine cochlear damage during the surgical procedure. Experiments were performed in preparations in which the CAP threshold in the frequency range between 6000 and 10000 Hz did not increase by more than 20 dB SPL. The endocochlear potential (EP), another measure of cochlear condition, was measured during the experiment by advancing the microelectrode into scala media through the organ of Corti. The average EP in 28 preparations was 81.2mV with a standard deviation of 3.2 mV.

2.2.2 Electrical recordings

Intracellular recordings and iontophoresis of dye into cells were performed using glass pipettes (1.2 mm OD; 0.6 ID; omega dot) pulled with a vertical Narishige puller. Electrodes were filled with 2M KCl or 0.45M KCl, mixed in with 0.05M Tris (pH 7.5), and 4% Methyl Blue. The resistance of the electrodes was between 20 and 100 MΩ. Dual-barrel theta-glass electrodes were used in some preparations to measure the impaled cell's voltage response to a current stimulus. Some dual barrel electrodes had higher resistances, in which case a 3M KCl electrode solution was used. A reference Ag-AgCl wire was placed in a neck muscle. The recording electrodes were connected to a high input impedance, capacity compensated, low-gain microelectrode amplifier (Axon Instruments, AxoProbe 1A) with an active bridge circuit and DC-offset. The output of the amplifier was passed through a low-pass anti-alias filter with a cutoff of 1000 Hz (part of the AxoProbe), amplified with a precision amplifier, and sampled at a sampling frequency of 2560 Hz. The signal was averaged on a data acquisition board and stored in a computer. The responses were also monitored on an oscilloscope during the acquisition.

Within each experiment, intracellular recordings were made from several different types of supporting cells. The cell type was identified using the landmarks on the basilar membrane (Figure 3). An electrode was mounted on a Narishige manipulator to allow for precise radial movements. A radial sweep across the organ of Corti produced a set of measurements from cells separated radially by successively moving the electrode from the modiolus to the lateral wall, or from the lateral wall to the modiolus. The initial cell type in a radial sweep was tentatively identified by its location and the locations of the remaining cells were measured with respect to the initial cell.

A large and negative potential indicated penetration of a cell. During the first few seconds after impaling the cell, there was usually a small change in the cell's potential that was assumed to be due to sealing of the membrane around the electrode, or clearing of the electrode tip. The cell's resting potential was measured as the stable potential that resulted after this time period.

Sound-evoked measurement

Series of tone bursts were presented over a range of frequencies, levels, and durations. Responses to frequencies between 500 and 12000 Hz were measured at levels between 30 dB SPL and 80 dB SPL. Tone duration of 50 msec with a 1 msec rise and 1 msec fall time. The off time was usually 200 msec for the 50 msec stimuli. Long duration stimuli between 500 and 10000 msec were occasionally used, after which the tone was off for 2 to 3 times the duration of the tone burst. The responses were averaged between 4 and 32 times to enhance the signal to noise ratio. For the longer duration tone bursts, fewer averages were taken because of limited holding times. Measurements were made near the cell in the extracellular space just before or after impaling the cell.

Electrical measurements

Cell input resistance was measured using either a single-barrel or a dual-barrel electrode. With a single-barrel electrode, cell input resistance was measured by injecting a known current (I1) into the cell and measuring the change in the potential ($\Delta V1$). Since the electrode resistance is non-linear at higher injection currents, cell resistance measurements with single-barrel electrodes were made using 1 nA current pules of 100 msec duration. When dual-barrel electrodes were used, current was injected into one barrel and the voltage response was measured from the second barrel. Currents between –5 nA and 5 nA were used with the dual-barrel electrodes. The electrode resistance (single-barrel electrode), or the resistive coupling (dual-barrel electrode) was measured outside the cell in the perilymph either before or after impaling the cell and was subtracted from the measured intracellular response to determine cell impedance.

Simultaneous impalement of two cells with single barrel electrodes was necessary to measure the mutual resistance. Square pulses of current ranging between -20 and 20 nA were injected into one cell (I1), and the steady state change in voltage was measured in the second cell ($\Delta V2$). The

entire range of currents was not always used because the electrodes often blocked at higher currents. After measurements from the initial pair of cells, the second electrode was withdrawn from the second cell, and moved radially a known distance to sample responses from another cell while the first cell was held. A radial sweep measured the mutual resistance as the second electrode was moved relative to the first electrode. The voltage response in the extracellular space was measured to determine the electrical coupling between the electrodes. The extracellular responses were subtracted from the intracellular responses in all the mutual resistance data presented.

Statistical analysis

Analysis of variance (ANOVA) and Student t-tests were performed on the raw data to determine statistically significant differences in the responses of the different cell types. All statistical tests were made at the 95% level of confidence. Multiple t-tests were performed on the pooled resting potential data to determine significantly different resting potentials. The significance level was corrected for false positive when performing multiple t-tests (Steel, 1961).

2.2.3 Cell labeling and histology

Lucifer yellow (LY) and horseradish peroxidase (HRP) were injected into some cells for verification of cell type and distances between recording sites. An electrode solution of 2% LY in 1M LiCl provided for a low impedance electrode (between 40 and 80 MΩ) which allowed for electrical recordings and labeling of cells. LY was iontophoresed into the cell for 1 minute after making the electrical measurements. The LY was recovered in the surface preparation as shown in Chapter 1. In a few cases, 1% HRP was added to the LY-LiCl solution to fill the cell. The HRP was iontophoresed with a 1-15 nA current. To image the HRP after the cochleas were dissected, the tissue was bathed in biotinylated tyramine (BT) and H_2O_2 for 10 minutes followed by 1:200 CY5-strepavadin overnight. The fluorescent labeled cells were well above the autofluorescent levels of the tissue.

Dye-filled cells confirmed the cell types and distances between cells in several of the radial sweeps. Distances between the nuclei of the dye-filled cells were on average the same as the distances the electrode was moved during the experiment. Small variations in the differences

between the measured distances and movement were thought to be due to differences in the impalement sites with respect to the location of the cells' nuclei.

2.3 Results

Impaled cells were classified based on visual cues from the landmarks found on the basilar membrane (see Chapter 1). Presumed hair cells were distinguished from supporting cells by a larger receptor potential in response to sound than seen in supporting cells, the insertion depth of the electrode beyond the basilar membrane, a greater than 45 degree phase lead in the AC response with respect to the extracellular response for inner hair cells, and a lower resting potential than the supporting cells. These properties of hair cells have been shown in previous literature (Russell and Kossl 1991; Russell and Sellick 1983). HRP and LY were used to mark a number of cells to verify the recording cell types. Twenty-six out of thirty-two recovered dye-filled cells were found to have been correctly identified during the experiments. Three of the misclassifications were between Hensen cells and Claudius cells. Another two misclassifications were between Deiters cells and Hensen cells. The sixth misclassification was an outer pillar cell that was misclassified as a Deiters cell.

2.3.1 Resting potentials

The supporting cell resting potentials decreased along the radial direction of the organ of Corti. The resting potential data consisted of two samples: 1) Cells measured from 35 preparations (pooled data: Table 4), and 2) Thirty-seven *radial sweeps* obtained from 22 preparations (radial sweep data: Figure 20) in which, multiple cells were measured along the radial dimension. The pooled data were all the cells in which sound evoked responses were measured and were often sampled in an arbitrary order. Results from the pooled data and the radial sweep data showed similar trends despite inter-preparation variability present in the pooled data. The pooled data showed a potential difference of about –7 mV from Deiters cells to Claudius cells, and the average radial sweep resting potential gradient was –8.3 mV over the same region. A linear least-squares fit was done for each set of sweep measurements to determine the gradient of the resting potential. The histogram of the slopes shows that in all but

three cases the gradients were negative from the region of the hair cells to the lateral wall (Figure 20A). This indicates that the trend observed in the average is present in the individual sweeps.

An ANOVA revealed that the average pooled resting potentials were significantly different ($p=0.021$) among four cell types: pillar cells, Deiters cells, Hensen cells, and Claudius cells. Student's t-tests were performed on pairs of data sets to determine if there are significant differences in the mean resting potentials of the different cell types and then were corrected for multiple t-test. Based on the correction for multiple t-test, there was a significant difference in the average resting potentials of Claudius cells and pillar cells and Deiters cells. There was not a significant difference between the average resting potentials of other cell types. Despite a lack of significance between resting potentials of Hensen cells and Claudius cells, the average radial sweep (Figure 20C) appeared to show a potential difference between these cells. The sweep data also indicated a potential difference between proximal Claudius cells (near 100 μm) and distal Claudius cells (near 200 μm).

The micropipette's angle of approach did not always permit measuring from the entire range of cells from the region of the hair cells to the lateral wall. Limited access to cells was the main reason for differences in the total number of cells of each cell type and one of the reasons for the limited range of the sweeps. Fewer cell measurements at the ends of the organ of Corti was the primary reason for the larger standard error below $x=0$ and for $x>150$ (Figure 20C).

2.3.2 Sound-Evoked DC Responses to Tone Bursts

Examples of sound-evoked waveforms from a Hensen cell and the corresponding extracellular space are shown in Figure 21. At the onset of the tone, there was a rapid change in the intracellular potential (*on-DC*). The on-DC response was measured 4 msec after the onset of the tone. The potential at the end of the tone (*end-DC*) was taken 4 msec before the end of the tone. The *slow-DC* is the difference between the on-DC and end-DC. The intracellular supporting cell slow-DC was positive, but the corresponding extracellular slow DC was negative. At the end of the tone burst, the potential dropped rapidly, and then slowly returned to the resting potential of the cell. The *off-DC* potential was measured 4 msec after the tone was turned off and the slowly returning potential is termed the *after-potential.* Sound-evoked responses to tone frequencies below 1,000 Hz consisted of an AC response component superimposed on a DC

component (Figure 21B). The magnitude and phase of the AC response will be discussed in Section 2.3.3.

Waveforms from cells sampled during a radial sweep are shown in Figure 22. The inner hair cell response was not a part of the sweep, but was measured in the same preparation just before the radial sweep in a nearby region of the cochlea. The corresponding extracellular responses (shown below the intracellular responses) were always smaller (about half the response) than the intracellular responses. The intracellular supporting cell responses had a positive slow-DC potential and a large off-DC potential. The extracellular responses, however, showed little change during the tone bursts except for a small negative slow-DC potential. A slow-DC potential was seen in the hair cell at high levels, but it had a very fast time constant. The hair cell and extracellular responses appeared to return to rest rapidly after the tone was turned off. The after-potential in the supporting cell responses appeared to last as long as 150 msec.

Similar to the resting potentials, the DC potential measurements were arranged as two data sets: 1) pooled cells collected across 35 preparations (Table 5 and Figure 23); and 2) twenty-nine radial sweeps in which four or more cells were sampled per sweep (Figure 24 and Figure 25). The transmembrane potential responses were computed by subtracting the extracellular response from the intracellular response. The pooled data measurements were sorted by cell type and arranged in anatomical location from the region of the hair cells to the lateral wall. The radial sweeps were shifted such that 0 μm corresponded to the presumed first row Deiters cell (region near the outer hair cells). Each of the radial sweeps (right column) was linearly interpolated to 5 μm sampling, and averaged and plotted with the standard error in the left column. Sound-evoked gradients were present in both the pooled and radial sweep measurements from inner pillar cells to Claudius cells. The distance between the pillar cells and the Claudius cells was about 130 μm, and the gradients measured from the radial sweeps were measured as a function of radial distance the electrode was translated.

DC Potentials across the basilar membrane

The intracellular on-DC and end-DC potentials decreased from the region of the hair cells to the lateral wall (Figure 23 and Figure 24). The intracellular on-DC and end-DC pooled data had a potential difference of –0.192 and –0.207 mV, respectively, between pillar cells and Claudius

cells. A histogram of the slopes of linear fits to the radial sweep data showed that in all but 4 cases the potential gradient was negative, with a median slope of –0.183 and –0.202 mV per 100 μm (histograms in Figure 24). The intracellular off-DC and slow-DC remained constant from the region of the hair cells to the lateral wall. The sweeps had small slopes, and the average sweep did not change much. The intracellular slow-DC was constant at about 0.3 mV, which explains why the gradients in the on-DC and end-DC were similar.

The radial functions of the transmembrane on-DC and end-DC potentials (Figure 25) were different from the intracellular radial functions (Figure 24). The transmembrane responses were near zero in the region of the hair cells and then increased at about 50 μm. Beyond 50 μm, the transmembrane responses appeared to level off. Deiters cells transmembrane potentials were near zero because the extracellular responses near these cells were often larger than the intracellular responses, as indicated by negative transmembrane on-DC measurements (Figure 23). The intracellular slow-DC was usually positive (see pooled data), but the extracellular slow-DC was close to zero or slightly negative.

The mean pooled transmembrane on-DC, and transmembrane end-DC of Deiters cells and Claudius cells were significantly different when corrected for the multiple t-test. The p-values for the t-test between Deiters cells and Claudius cells are shown in the figure. While the intracellular on-DC was had a p-value of 0.038, it was not determined to be significant. No significant differences were detected in the off-DC or slow-DC potentials (see Figure 23 for p-values). At the proximal (pillar cells) and distal ends (Claudius cells) of the averaged sweeps, the standards errors were large because fewer cells were sampled from these regions.

Slow-DC and After-potentials

The slowly increasing DC potential during the tone stimulus and the after-potential appeared to be exponential in nature. The time course of these responses were analyzed by fitting the response during the tone to the equation:

$$V = V_e - (V_e - V_i)e^{\left(-\frac{t-t_{on}}{\tau}\right)} \qquad (3.1)$$

and the response after tone to the equation:

$$V = V_o e^{\left(-\frac{t-t_{off}}{\tau}\right)}. \qquad (3.2)$$

Exponential fits for a Deiters cell response and the adjacent extracellular response are shown in Figure 26A. The on and off time constants for exponential fits for the Deiters cell response were 32 msec and 55 msec respectively. The initial and final potentials V_i, V_e, and V_o (1.7, 2.01, and 0.46 mV respectively) were similar to the on-DC, end-DC, and off-DC potentials. The fit for the extracellular response had on and off time constants that were 39 msec and 25 msec respectively. The magnitude of the extracellular slow-DC and after-potential was small.

In about 10 percent of the intracellular recordings in response to a 50 msec tone bursts, the slow-DC was fit by an exponential with a time constant much larger than 1000 msec, as shown in the example in Figure 26B. The final potential (V_e) was 125 mV for this example, which is not physiologically possible. The rising DC appeared to be better fit by a linear slope rather than an exponential. The on time constants for intracellular response to tone bursts of 50 msec were measured for the 80 dB SPL cases. No noticeable differences in the on time constants were seen among the different types of supporting cells. The mean on time constant for all the supporting cells, using only the time constants below 1000 msec, was 23.8 msec. The off time constants were usually twice as long as the on-time constants with a mean value of 44.3 msec. Hair cell on and off time constants were on average 3.3 and 12.1 msec, respectively.

Tone bursts greater than 400 msec (Figure 27A) were used to determine the accuracy of the exponential fits measured with the 50 msec tone bursts. The slow DC potential continued to increase monotonically during the long tone duration, but never reached an asymptote. Time constants of exponential fits to these responses were dependent on the duration of the tone bursts. The responses to 50, 1000, and 3000 tone bursts from the same cell had time constants that were 24.5, 803, and 1130 msec. It is not likely that the response was a single exponential on the order of tens of milliseconds. In a few cases when a 15 second tone burst was used, the response continued to increase, and appeared to plateau at about 8 seconds with a maximal depolarization of 4.6 mV. The extracellular response, however, remained flat during the longer duration bursts and had the same range of time constant as the short duration responses.

The intracellular response in presumed hair cells was very different from the supporting cell responses for long duration tone bursts. Two inner hair cells were held long enough to perform

the long duration tone stimuli. Outer hair cells were not held long enough to perform the same long duration experiments. The responses shown in Figure 27B are from the same inner hair cell shown in Figure 22. During the first 50 to 100 msec the response was flat, or increased and then after about 100 msec, the response slowly decreased. At the end of the tone burst, the inner hair cell was hyperpolarized by a few millivolts and then the potential returned to the cell resting potential with a time constant of approximately 250 msec. In response to short duration tone bursts of 50 msec, inner hair cells were depolarized after the tone.

2.3.3 AC Responses

The intracellular AC magnitudes in response to 1000 kHz tone bursts (Figure 28) decreased from the region of the hair cells to the lateral wall. For each sweep, measurements beyond the Deiters cells ($x>0$ μm) were fit with a linear slope. The median of the slopes was –0.335 mV per 100 μm. The extracellular magnitude was larger than the intracellular magnitude near the region of the hair cells (transmembrane AC magnitude: Figure 28B), but beyond the Deiters cell, the intracellular Hensen cell and Claudius cell AC magnitudes were always larger. A decreasing transmembrane magnitude was present beyond the Deiters cells.

The intracellular phase did not change in the radial direction (Figure 28C). A lack of change in the phase indicated predominantly resistive coupling between cells. A change in phase would have indicated some capacitance between cells. The phase of the AC component from cells in the radial direction was taken with respect to the phase of a Deiters cell within each individual sweep. If a measurement near the Deiters cells was not taken in a given sweep, a linear interpolated phase for a measurement at 0 μm was used. Phase changes measured in individual sweeps were between $\pm .1\ \pi$ radians. A slight phase lead in the Claudius cell with respect to the Deiters cell was seen in 4 of the 13 cases. One possible explanation for the phase lead may be a change in the electrode capacitance due to accumulation of residual tissue on the electrode as it is withdrawn from one cell and is moved to another position. Sweeps were separated by direction of the sweep—forward sweeps (modiolus to lateral wall, plotted as solid lines), and reverse sweeps (lateral wall to modiolus, plotted as dotted lines). There was no correlation between the sweep direction and phase lead of Claudius cells. The phase lead and the range of phase changes could be explained by the low sampling rate and noise of the response. Since the 1000 Hz was close to the Nyquist sampling rate, a small signal to noise ratio could account for apparent phase

shifts.[5] Further away from the Deiters cell, the signal to noise ratio decreased because the AC magnitude was smaller, so the noise in the phase would increase. In 4 sweeps, a 500 Hz tone was used, and the phase response in those sweeps showed no phase lead of Claudius cells and smaller variances because of twice as many samples per cycle of the response. It is concluded that there is no change in the phase between cells within the cell network.

The phase lead of the extracellular response was measured by subtracting the intracellular phase from the extracellular phase (Figure 28D). The extracellular response lagged the intracellular response in all regions except near the hair cells. The extracellular phase lag increased with distance from the region of the hair cells. The median extracellular phase lag near 150 μm was .14π radians. This is equivalent to a time delay of 0.07 msec at a frequency of 1000 Hz. The extracellular phase measurements near the hair cells usually led the intracellular phase of the Deiters cells and pillar cells in that region, suggesting that the current flows from the hair cell to the supporting cell via an extracellular path.

The magnitude and phase of the extracellular response near the hair cells was often larger than the intracellular response. A scatter-plot of the AC magnitude difference and phase difference between the cells and their corresponding extracellular measurements are shown in Figure 29. The lower right quadrant, corresponds to a larger extracellular AC magnitude and an extracellular phase lead. Most transmembrane pillar cell responses were located in the lower right quadrant. Hensen cell and Claudius cell transmembrane responses were located mostly in the upper left quadrant, corresponding to a larger intracellular AC magnitude, and an extracellular phase lag. Deiters cell responses were split between the two quadrants. Assuming a linear, causal system, an extracellular phase lead and larger extracellular magnitude could be due to a signal reaching the extracellular space before the intracellular. This suggests that the temporal path for the current generating the response is from the extracellular spaces near the hair cells, then intracellular, and then to other extracellular spaces.

[5] The phase of a cosine at 1000 Hz, sampled at the same rate as our data, was compared to a cosine with varying amounts of noise added in. With a signal to noise ratio of 10, the phase shifted by as much as .07 π radians. The signal to noise ratio of the responses from Claudius cells were occasionally smaller than 10.

2.3.4 Extracellular Responses

The extracellular AC and DC responses near Deiters cells and the tunnel of Corti were often larger than the intracellular measurements from Deiters cells and pillar cells, as shown by the negative transmembrane potentials (Figure 23 and Figure 29). To determine the potential profile of the extracellular space in this region, extracellular measurements were made by backing out an electrode from the region of the hair cells at about 80 μm beyond the basilar membrane (Figure 30). The extracellular response was smaller with increasing distances from the region of the hair cell to scala tympani. These results suggest that there is a potential gradient within the extracellular spaces of the tunnel of Corti and near the outer hair cells and Deiters cells. The intracellular on-DC from a Deiters cell in the same preparation, shown as a dashed line, was lower than the maximum extracellular potential.

2.3.5 Frequency dependence

The sound-evoked responses were dependent upon frequency of the tone bursts. The best frequency was defined as the frequency with the largest intracellular on-DC magnitude at 80 dB SPL. The iso-intensity frequency functions for three cells from a radial sweep are shown in Figure 31A. The on-DC and slow-DC frequency response curves show a peak at the best frequency, which was near 9 kHz for these cells. The responses decreased more rapidly at frequencies above the BF than for frequencies below CF. At frequencies above 10 kHz, the intracellular on-DC and slow-DC responses were comparable to the extracellular responses, which suggests that these responses are just a reflection of the extracellular response at frequencies above 10 kHz. The compound action potential thresholds at 10 and 12 kHz were normal for this preparation (near 25 dB SPL).

2.3.6 Coupling measurements

Cell input resistance

The average cell input resistance of the supporting cells measured using a single-barrel electrode was 14.99 ± 8.67 MΩ (Table 6). No statistically significant difference was found between the cell input resistance of the different cell types. Measurements of the cell input resistance using a dual-barrel electrode averaged 1.17 ± .86 MΩ. Three cases where a range of

currents pulses from –5 nA to 5 nA were used in alternating polarity are shown in Figure 32. The cell resistance is the slope of the linear fit through the measured voltages. There was a slight inward rectification. The cell resistance was higher for depolarizing currents versus than for hyperpolarizing currents. The cell resistance measurements were all measured as the response to depolarizing currents.

Mutual resistance

Measurements of mutual resistance are shown in Figure 33. The mutual resistance was taken as the slope of the least-squares linear fit to the voltage responses in cell two to the currents injected into cell one (ΔV2/I1). The solid line (filled squares) shows the linear fit through the measured response in cell two (ΔV2) to a current injected into cell one (I1). The dashed line (open circles) shows the linear fit through the measured response in cell one (ΔV1) to a current injected into cell two (I2).

Several properties of the mutual resistance measurements were observed in several pairs of cells. 1) The mutual resistance measurement depended on the cell being injected. For the examples shown in Figure 33, the response in cell two was about 4-8 times larger than the response in cell one. In this case, cell one was more modiolar than cell two, but the larger mutual resistance measurement was not always due to current injected into the more modiolar cell. 2) Slopes calculated independently for depolarizing and hyperpolarizing currents often showed an asymmetric response about the current axis for many pairs of cells. For the two cases shown, the depolarizing current into cell one produced a larger response than the hyperpolarizing current, which was generally true when an asymmetry was present. However, the responses from current injected into cell two did not show such a large asymmetry. 3) A saturating non-linearity was seen in response to large currents in 4 out of 10 coupled cells with a large mutual resistance (greater than 0.1 MΩ). The responses in panel B (filled squares) appeared sigmoidal—a leveling off or a decrease in the mutual resistance was found at the large amplitude current injections. The response (ΔV2) was approximately the same for currents above 10 nA, and was about the same for currents below –12 nA.

To control for time dependence in the measurements, or changes in electrode impedances, the current amplitudes were injected in an indiscriminate order. Measurements at a given current

amplitude were taken just after impalement of the cells and then remeasured at the same current amplitude after all the initial data had been collected (usually 15-20 minutes after impaling the cell). Measurements in Figure 33B show that the two potential measurements at the same current level were similar, and there was no significant change in the response after 20 minutes of holding the cells. For example, two responses with a I1 current of -19 nA, separated by 22 minutes, were similar in value, indicating little if any temporal change. Therefore, the asymmetries and non-linearities are likely not due to temporal changes in the coupling or electrodes.

Mutual resistance decreased as the distance between the pair of cells increased (Figure 34). Mutual resistances from experiments in which a radial sweep was performed and the dye-filled cells were recovered are connected by dashed lines in Figure 34A. The mutual resistance measurements were measured using current injected into cell one. The solid lines represent visual fits to the data using a theoretical model for a two-dimensional lamina (see Discussion). The remaining mutual resistances measured from other preparations are shown in Figure 34B. Cases in which the cells were labeled and recovered (panel A) showed a slightly higher mutual coupling than cells which were not labeled (panel B).

A set of dye-filled cells recovered from one preparation are shown in Figure 35. The mutual resistance between 1a and the sweep of cells 2a, 3a, and 4a from Figure 35 are shown as circles in Figure 34A. The mutual resistance and distance between 1b and 2b was .5 MΩ and 38 μm respectively. Cells 1c and 2c were separated by 80 μm and showed little mutual resistance (.03 MΩ).

There was a large variability in the measurements of mutual resistance, but the majority of the mutual resistances were above 0.001 MΩ. The two cases in which the mutual resistance was below 0.001 MΩ were considered uncoupled. These cells also showed a weak sound-evoked response further suggesting degraded physiology. Some of the variability may have been due to inaccurate measurements of separation distances. For instance, in cases where the actual distances between the nuclei of the labeled cells were measured from histology, the estimated distances during the experiment were usually smaller than the actual distances. This suggests that the exact separation distances were usually underestimated.

When two electrodes were used, it was difficult to visualize the exact location of both electrodes because of fluid distortions produced by two electrodes. The method for determining the distance between pairs of cells was to move the electrode a known distance in the extracellular space under visual observation and to take that distance as the separation of the electrodes when they were in the cells. In 6 cases, cell one was held as long as possible while the second electrode sampled response from cells at about 30 μm steps. The separation between the initial cell pair (cell one and cell two) was estimated and the distance of the remaining cells relative to cell two was taken to be the distance moved by the electrode manipulator. In three of these preparations, it was possible to measure the intercellular distances because the cells were labeled. In these experiments, electrode one was filled with a HRP-LY cocktail and electrode two was filled with LY. Figure 35 shows the recovered cells from one preparation (CH113). Cells 1a, 1b, and 1c were three cells in which the HRP was recovered, indicating that they were cell one in our mutual resistance measurements. The HRP was made fluorescent and was confined to a single cell whereas the LY appears to have spread to adjacent cells. The LY injected cells 2a, 3a, and 4a were determined from the brightness of the fluorescence of their nuclei and from LY precipitate found at the BM under the cell which is indicative of impaled cells. The distance between 2a, 3a, and 4a was similar to the distance the electrode was moved during the experiment.

Cell Type	Number	Average Resting Potential (mV)	Standard Error	Range	
				max	min
Inner Hair Cells	3	-52.70	6.11	-46	-58
Outer Hair Cells	3	-66.67	4.86	-76	-54
Inner Supporting Cells	9	-82.22	2.39	-92	-68
Inner Pillar Cells	17	-82.53	2.01	-98	-63
Outer Pillar Cells	19	-83.58	1.99	-102	-69
Deiters Cells	82	-79.73	0.75	-96	-58
Hensen Cells	81	-81.27	0.84	-106	-64
Claudius Cells	120	-86.77	0.79	-110	-62
Boettcher Cells	9	-89.56	4.02	-112	-74

Table 4. Measurements of resting potentials from cells of the organ of Corti. The data are pooled from 35 preparations.

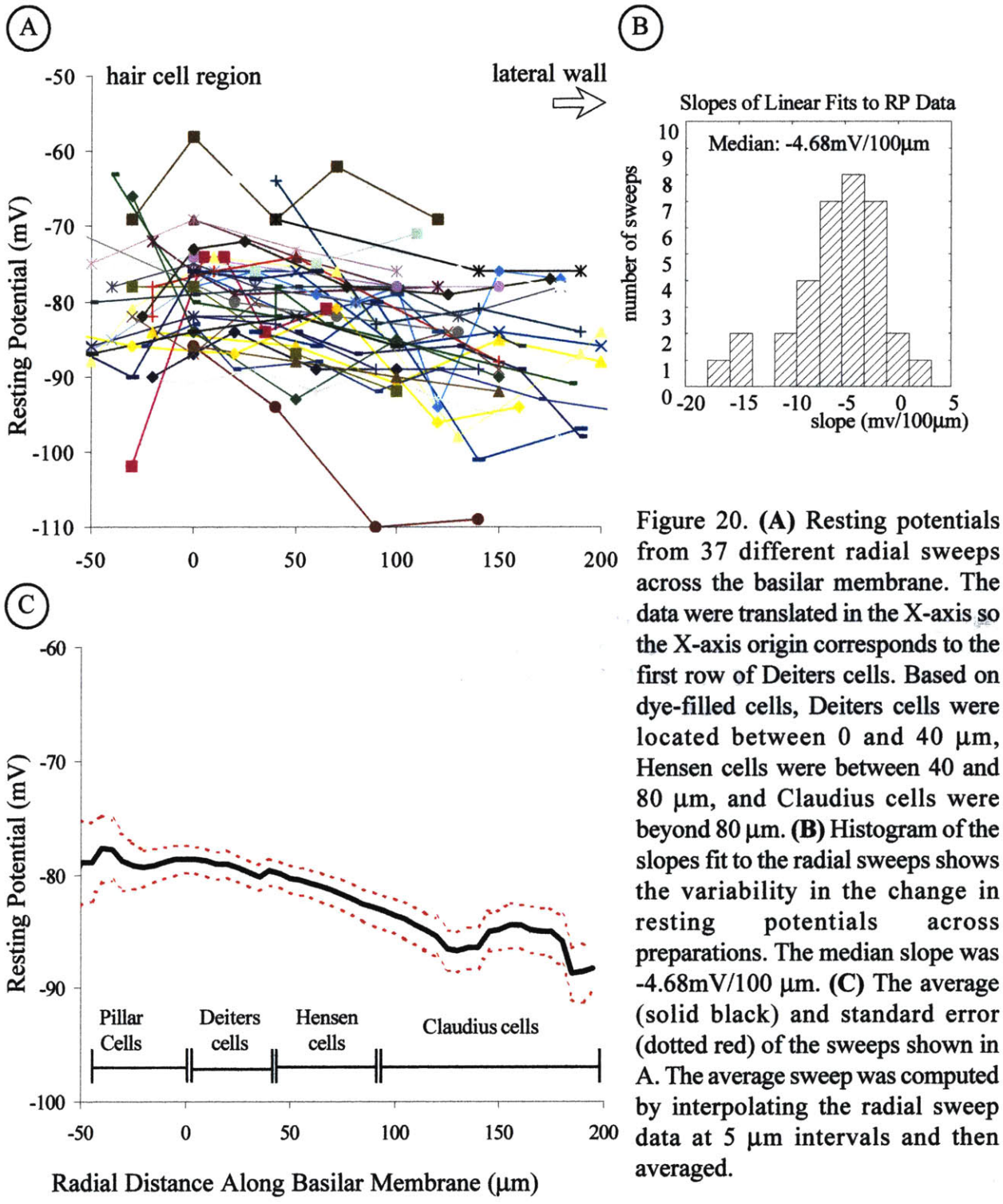

Figure 20. **(A)** Resting potentials from 37 different radial sweeps across the basilar membrane. The data were translated in the X-axis so the X-axis origin corresponds to the first row of Deiters cells. Based on dye-filled cells, Deiters cells were located between 0 and 40 µm, Hensen cells were between 40 and 80 µm, and Claudius cells were beyond 80 µm. **(B)** Histogram of the slopes fit to the radial sweeps shows the variability in the change in resting potentials across preparations. The median slope was -4.68mV/100 µm. **(C)** The average (solid black) and standard error (dotted red) of the sweeps shown in A. The average sweep was computed by interpolating the radial sweep data at 5 µm intervals and then averaged.

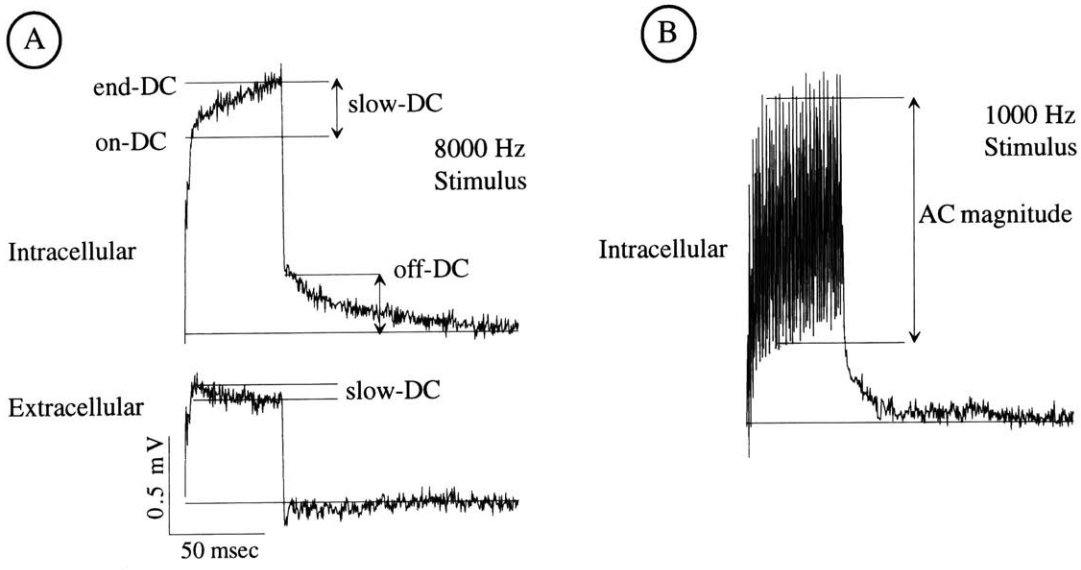

Figure 21. Typical responses from a presumed Hensen cell in response to a 50 msec tone burst at 8000 Hz (**A**) and 1000 Hz (**B**). The corresponding extracellular response just outside the cell is shown below the intracellular response in **A**. The tone burst was at 80 dB SPL for all these cases. The on-DC, end-DC, off-DC, slow-DC, and AC magnitude are the primary parameters used to analyzed the responses to tone bursts.

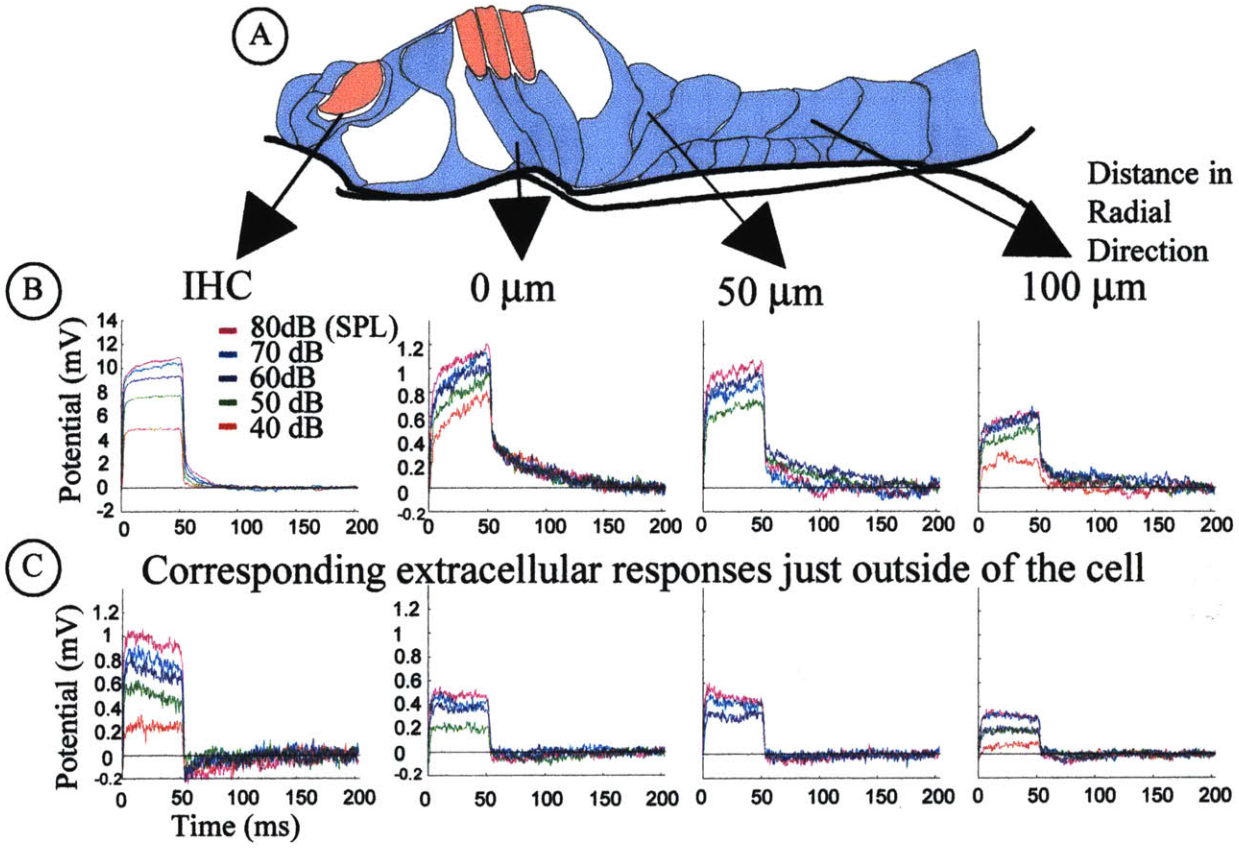

Figure 22. **(A)** Schematic cross-section of the organ of Corti used to show the recording sites. **(B)** Intracellular response from a presumed inner hair cell, Deiters cell, Hensen cell, and Claudius cell within a single preparation. First the measurements were made from the inner hair cell, and the electrode was moved to a Deiters cell in an adjacent region slightly more basal in the cochlea. Then the electrode was translated 50 and 100 µm in the radial direction where further recordings were made. The responses are for a 50 msec tone burst at 8 kHz over a range of sound pressure levels from 40 dB SPL to 80 dB SPL. The scale of the inner hair cell response is 10 times larger than the remaining scales. The responses decrease as the measurements are made further away from the hair cell. The decrease is present in responses over the entire range of levels. **(C)** The response in the fluid just outside the cell from which the responses are shown directly above. The decrease is also seen in the extracellular response, but it is not as large. The intracellular response was always larger than the extracellular response in this case.

Cell Type	On DC			End DC			Off DC			Slow DC		
	Intra.	Extra.	*Trans.*	Intra.	Extra.	*Trans.*	Intra.	Extra.	*Trans.*	Intra.	Extra.	*Trans.*
Inner Hair Cell (3)												
Average	6.260	1.838	*4.422*	6.670	1.616	*5.055*	1.250	-0.329	*1.579*	0.411	-0.222	*0.632*
Standard Error	0.356	0.100	*0.456*	0.289	0.080	*0.368*	0.652	0.049	*0.602*	0.068	0.021	*0.088*
Outer Hair Cell (3)												
Average	2.444	0.917	*1.527*	2.475	0.752	*1.723*	0.100	-0.233	*0.333*	0.031	-0.165	*0.196*
Standard Error	0.076	0.362	*0.435*	0.124	0.328	*0.451*	0.118	0.101	*0.151*	0.048	0.053	*0.053*
Inner Supporting Cell (4)												
Average	1.411	0.516	*0.895*	1.637	0.393	*1.244*	0.169	-0.091	*0.260*	0.226	-0.123	*0.349*
Standard Error	0.422	0.129	*0.433*	0.322	0.094	*0.329*	0.169	0.069	*0.138*	0.155	0.070	*0.166*
Inner Pillar Cell (8)												
Average	1.263	0.992	*0.271*	1.613	0.961	*0.652*	0.283	-0.088	*0.371*	0.351	-0.030	*0.381*
Standard Error	0.178	0.152	*0.241*	0.275	0.182	*0.332*	0.122	0.053	*0.103*	0.110	0.034	*0.116*
Outer Pillar Cell (11)												
Average	1.345	1.299	*0.045*	1.554	1.210	*0.344*	0.279	-0.222	*0.501*	0.209	-0.089	*0.299*
Standard Error	0.106	0.197	*0.169*	0.136	0.186	*0.166*	0.083	0.063	*0.072*	0.060	0.026	*0.061*
Deiters Cell (52)												
Average	1.319	1.049	*0.291*	1.621	0.981	*0.660*	0.281	-0.086	*0.366*	0.302	-0.068	*0.369*
Standarad Error	0.078	0.082	*0.084*	0.098	0.082	*0.089*	0.050	0.029	*0.052*	0.035	0.016	*0.039*
Hensen Cell (32)												
Average	1.198	0.555	*0.644*	1.457	0.509	*0.948*	0.195	-0.008	*0.203*	0.259	-0.046	*0.305*
Standarad Error	0.087	0.046	*0.070*	0.109	0.043	*0.093*	0.041	0.017	*0.042*	0.031	0.015	*0.032*
Clauidus Cell (57)												
Average	1.153	0.550	*0.603*	1.430	0.510	*0.920*	0.256	-0.003	*0.259*	0.277	-0.040	*0.317*
Standarad Error	0.062	0.040	*0.046*	0.078	0.037	*0.060*	0.032	0.017	*0.025*	0.025	0.010	*0.023*

Table 5. Measured intracellular, extracellular, and transmembrane DC responses to a 50 msec tone burst at 8 kHz with a 80 dB SPL intensity. The transmembrane response is the intracellular response minus the extracellular response. The number of cases are below the cell type.

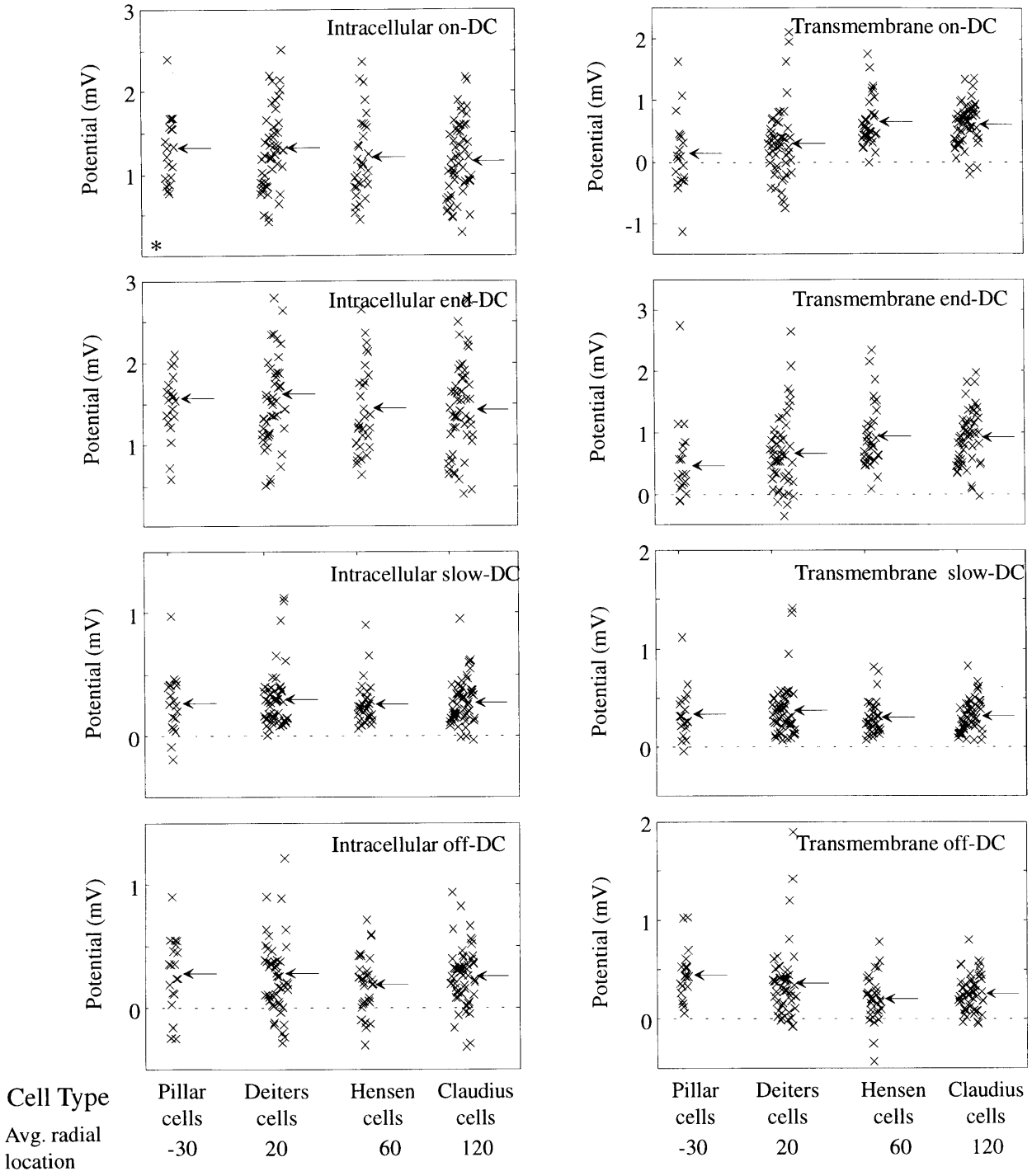

Figure 23. Scatter plots of the intracellular and transmembrane DC magnitudes from the pooled data set, sorted by cell type. The mean values of the magnitudes are shown with arrows. The mean values and standard errors for each measurement are given in Table 6. The statistical significance in the difference between the Deiters cells and Claudius cells mean responses were tested with a Student's t-tests and then corrected for multiple t-tests. The only significant difference was in the transmembrane on-DC and slow-DC between Claudius cells and Deiters cells.

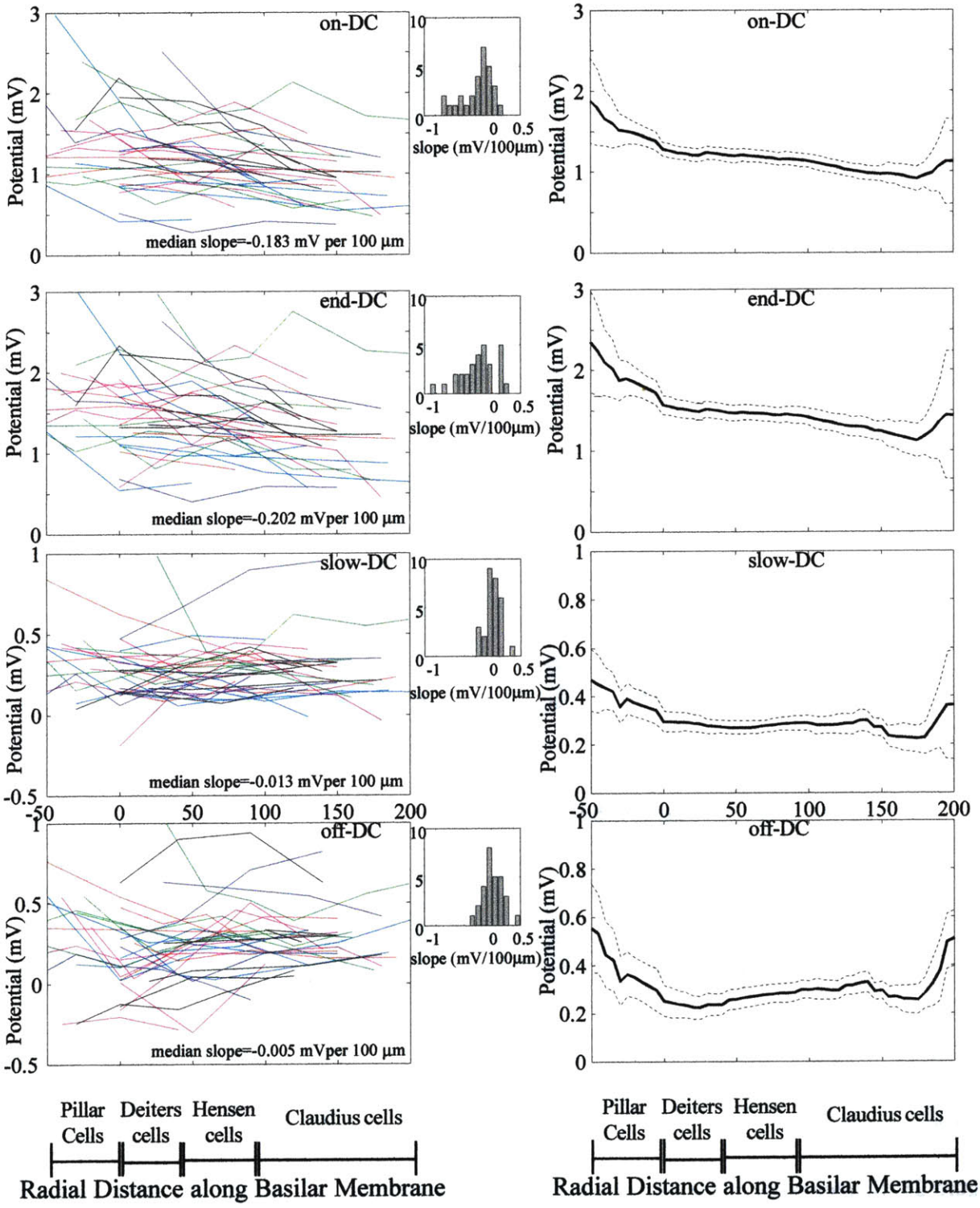

Figure 24. Intracellular DC measurements from 29 radial sweeps where 4 or more cells were sampled (left column). Linear fits to the data were used to compute the slope of the gradient from the Deiters cells to the Claudius cells. Histograms of the slopes are shown in the middle column. Using a linear interpolation between the measurements within a given sweep, the average sweep (solid lines) measurements were computed along with the standard error (dashed lines).

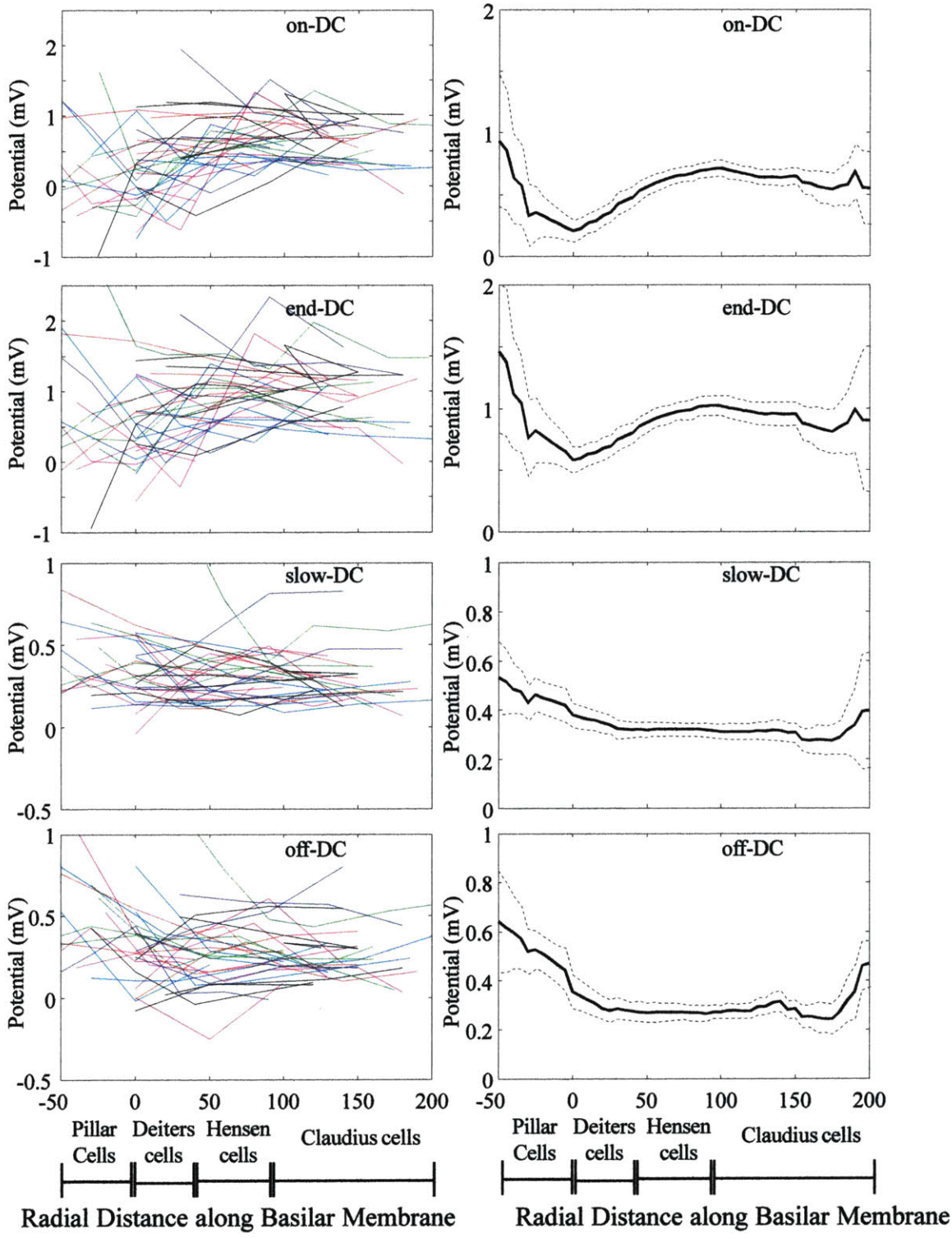

Figure 25. Transmembrane DC measurements from 29 radial sweeps where 4 or more cells were sampled (left column). Using a linear interpolation between the measurements within a given sweep, the average mean sweep measurements were computed along with the standard error (right column).

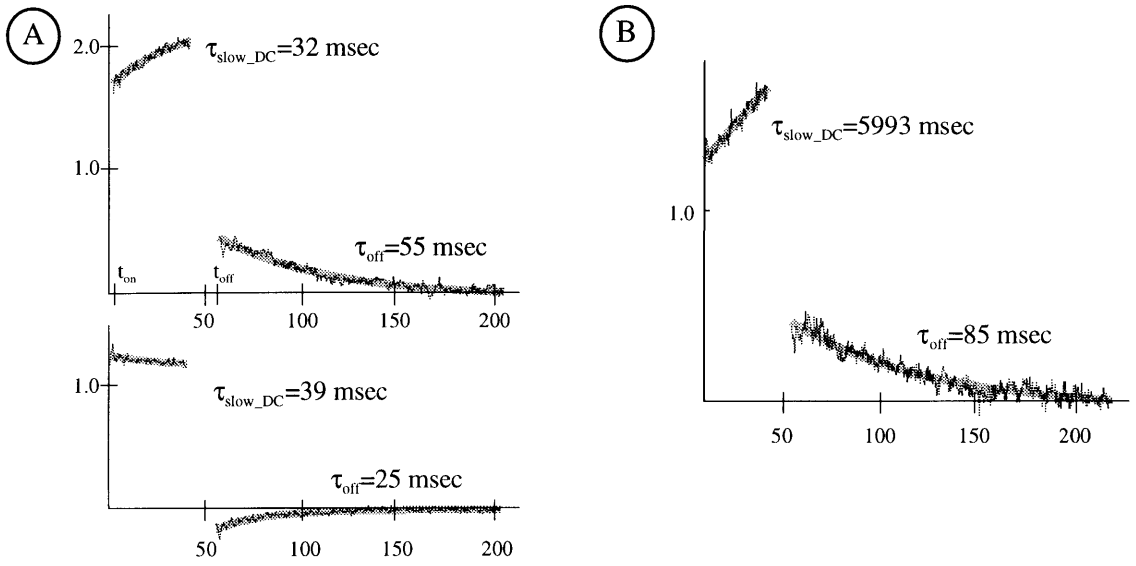

Figure 26. Exponential fits to responses during the tone and after the tone to model the slowly rising DC potential and after-potential. **(A)** Example of a good exponential fit to both the rising DC and after-potential. Top figure is a Deiters cell intracellular response, and the bottom curve is the extracellular response. **(B)** Another Deiters cell showed a long time constant of 6 seconds, appeared to have a better linear fit.

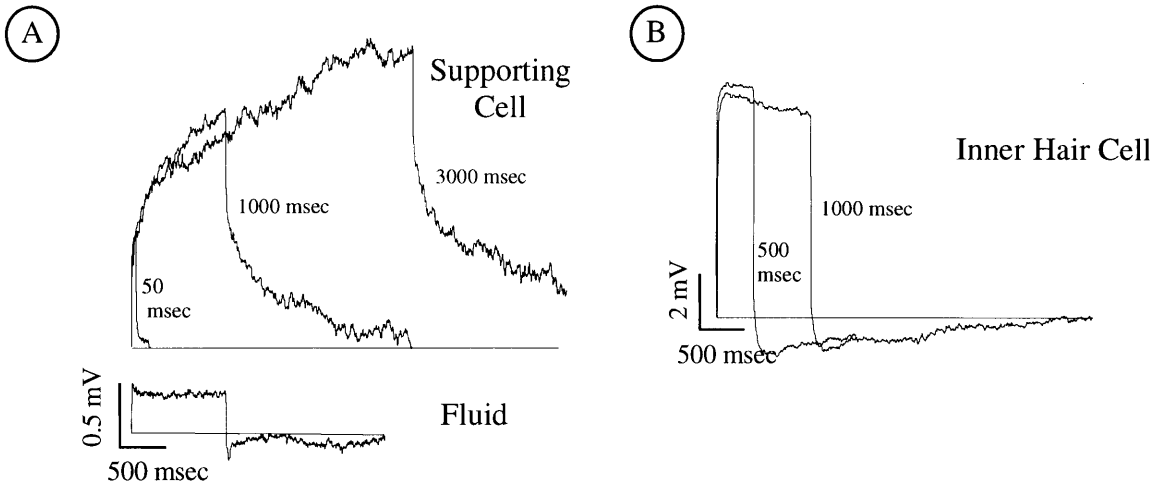

Figure 27. Time waveforms from long duration tone bursts. **(A)** Responses from a Claudius cell in response to 50, 1000, and 3000 msec tone bursts. The corresponding extracellular fluid response for 1000 msec is shown directly below. **(B)** Responses from an inner hair cell (same as in Figure 27) in response to 500 msec and 1000 msec tone bursts. All tone bursts were at 8 kHz at 70 dB SPL.

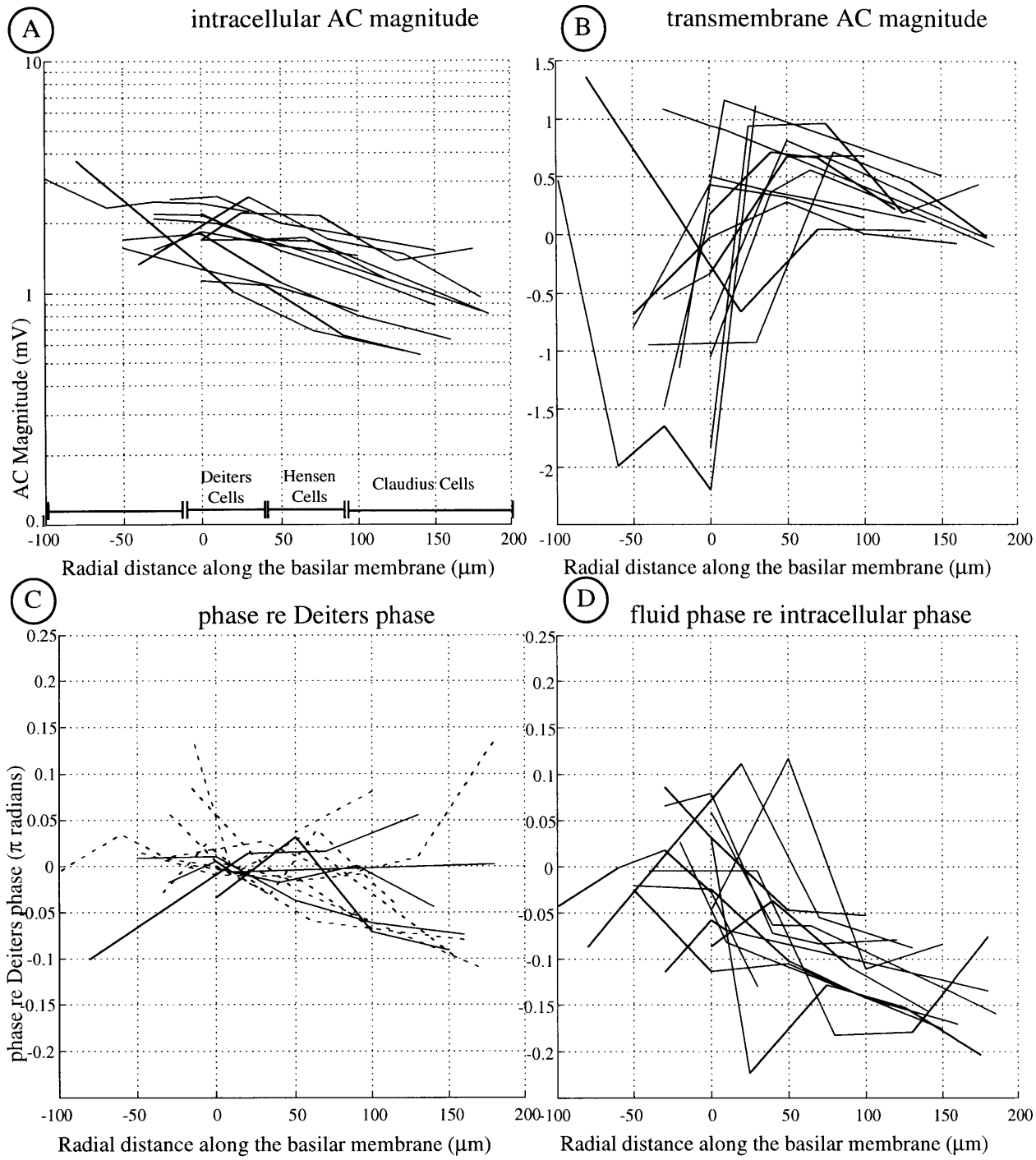

Figure 28. **(A)** Intracellular AC magnitude as a funciton of radial distance for 13 radial sweeps. **(B)** Transmembrane AC magnitude as a funciton of radial distance for the same sweeps. **(C)** Intracellular phase re Deiters phase as a function of radial distance. The absolute phase was shifted so that the approximate phase at the Deiters cells was at 0 phase. The phase leads for positive numbers and lags for negative values. **(D)** Fluid phase re intracellular phase as a function of radial distance. For positive values the fluid leads the intracellular response and for negative values the fluid lags the intracellular phase.

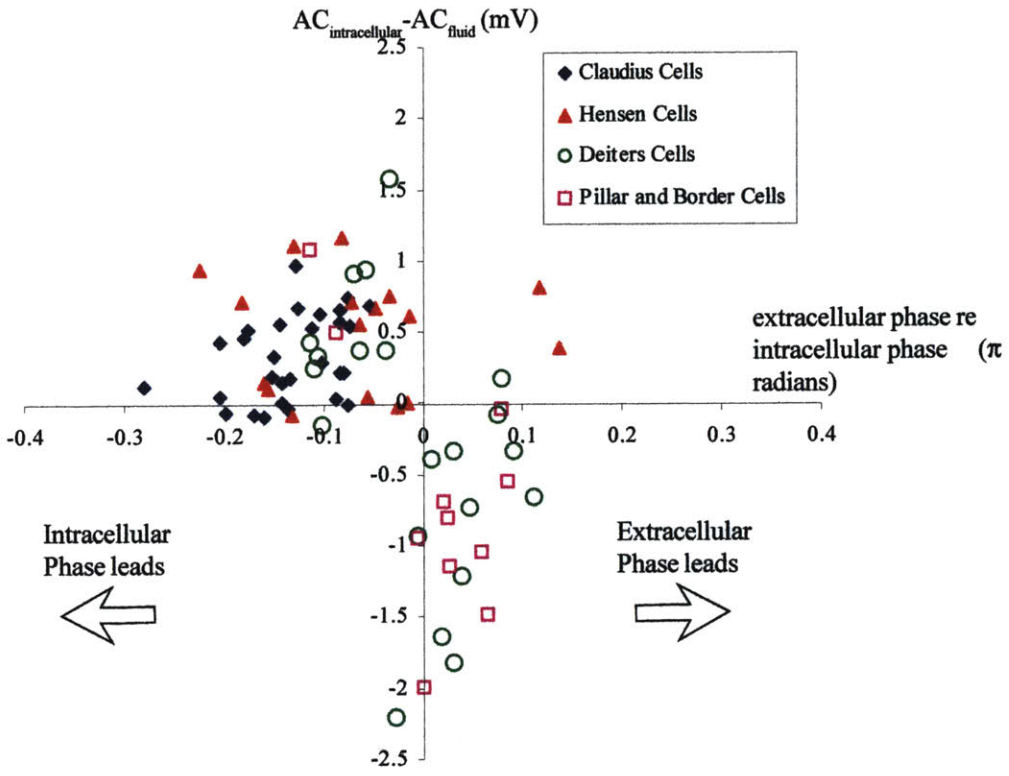

Figure 29. Scatter plot of transmembrane AC magnitude versus the intracellular phase lead with respect to the fluid phase. Measurements were made using a 1000 Hz tone at 70 dB SPL. The lower right quadrant indicates a larger extracellular magnitude and an intracellular phase lag. The upper left quadrant indicates a larger intracellular magnitude and an intracellular phase lead.

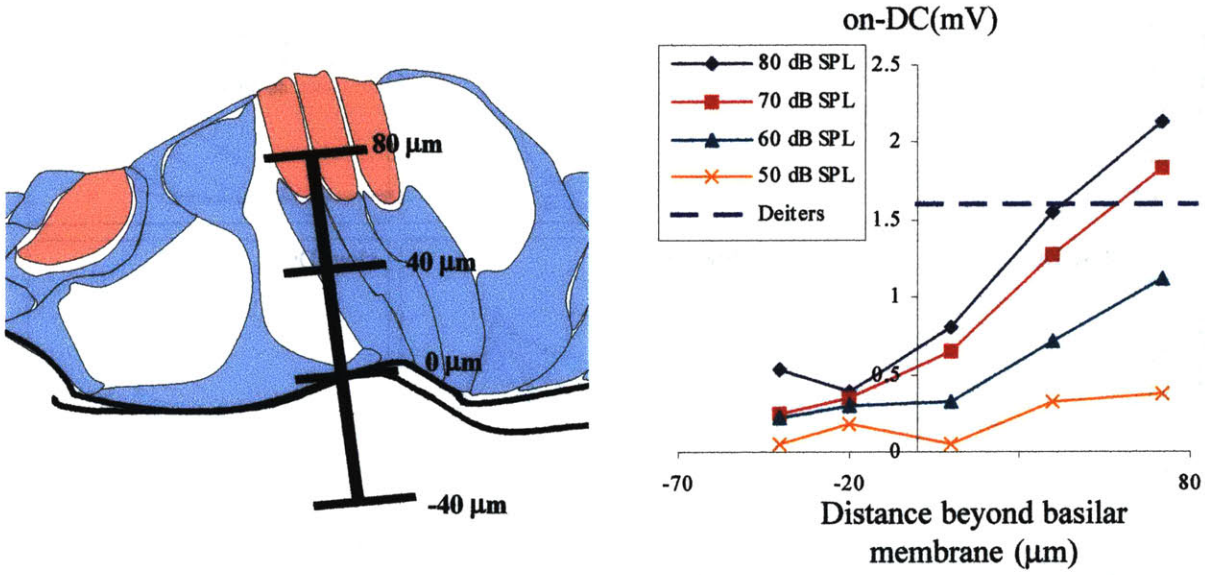

Figure 30. **A**. Schematic diagram of the assumed extracellular measurements taken in the region of the tunnel of Corti. **B**. On-DC measurements from the extracellular spaces near the hair cells and Deiters cells (X>0), and within scala tympani (X<0). The dashed line shows the value of the intracellular Deiters cell on-DC measurement in response to a 80 dB SPL tone burst. The Deiters cell was measured while the electrode was being advanced and was penetrated near a depth of 30 µm.

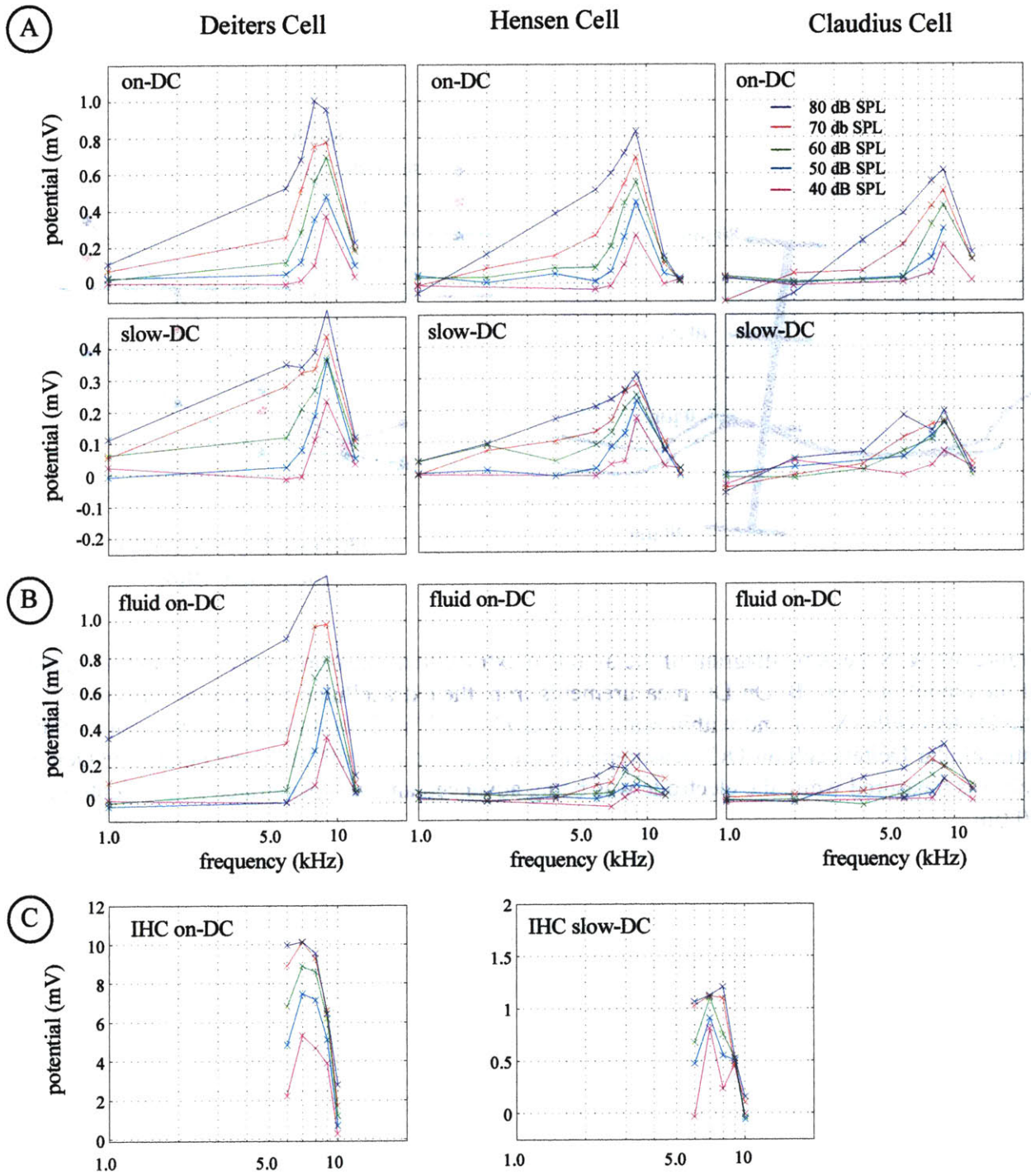

Figure 31. Iso-intensity response curves which show the frequency dependence of the DC potentials for several cells from a radial sweep. **(A)** Intracellular on-DC and slow-DC from a Deiters cell, Hensen cell, and Claudius cell from a radial sweep at locations 0, 40, and 100 μm. The intensity ranged from 40 to 80 dB SPL. The best frequency for this sweep was 9 kHz. **(B)** Corresponding extracellular on-DC response. **(C)** Intracellular on-DC and slow-DC from an inner hair cell from another preparation. The best frequency is 7 kHz.

	Number	Average Impedance (Mohms)	Standard Error	Range	
Single Barrel Electrodes					
Pillar Cells	6	19.67	4.52	33.00	6.00
Deiters Cells	3	5.78	4.63	15.00	0.34
Hensen Cells	9	13.55	3.22	30.00	2.00
Claudius Cells	13	16.98	3.68	44.29	1.12
Total	32	14.99	2.07	44.29	0.34
Dual Barrel Electrodes					
Total	22	1.17	0.18	4.12	0.26

Table 6. Cell resistance of impaled cells from 12 preparations. Resistance was measured with single-barrel and dual-barrel electrodes.

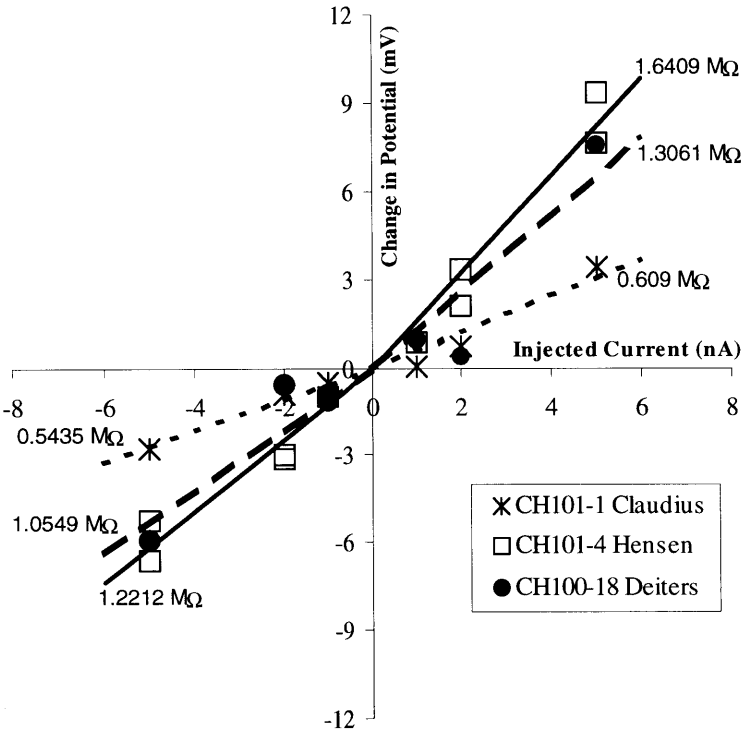

Figure 32. Cell resistance of three different cells using a dual barrel electrode. Positive and negative current were applied with one barrel and the voltage response was measured with the second barrel. Separate linear fits are shown for depolarizing and hyperpolarizing currents. The solid line is a linear fit from a Hensen cell (squares): 1.64 MΩ for depolarizing currents and 1.22 MΩ for hyperpolarizing currents. The dashed line is the linear fit from a Deiters cell (filled circles): 1.31 MΩ for depolarizing currents and 1.05 MΩ for hyperpolarizing currents. The dotted line is the fit from a Claudius cell (asterisk): 0.61 MΩ for depolarizing currents and 0.54 MΩ for hyperpolarizing currents.

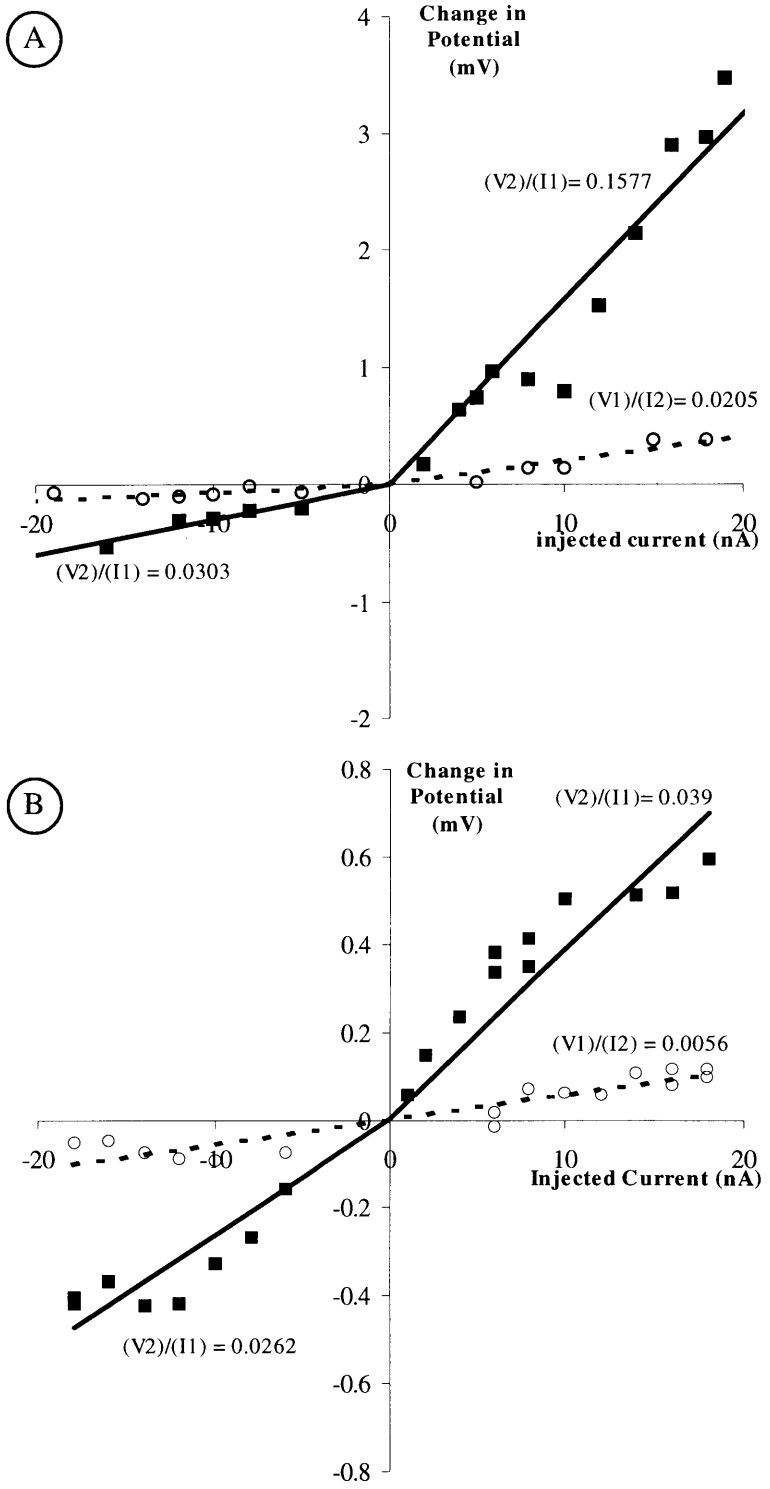

Figure 33. Two examples of current-voltage relationships between pairs of cells. The squares (solid lines) are voltage measurements in cell 2 in response to a current injected into cell 1. The open circles (dotted lines) are voltage measurements in cell 1 in response to a current injected into cell 2. Measurements were taken in a pseudo-random order. Several currents (I2=18,19 nA and I1=-19, 8,6 nA) were repeated at the beginning and at the end of the set of measurements to determine temporal effects. Slopes of the linear fits to the data are the mutual resistances.

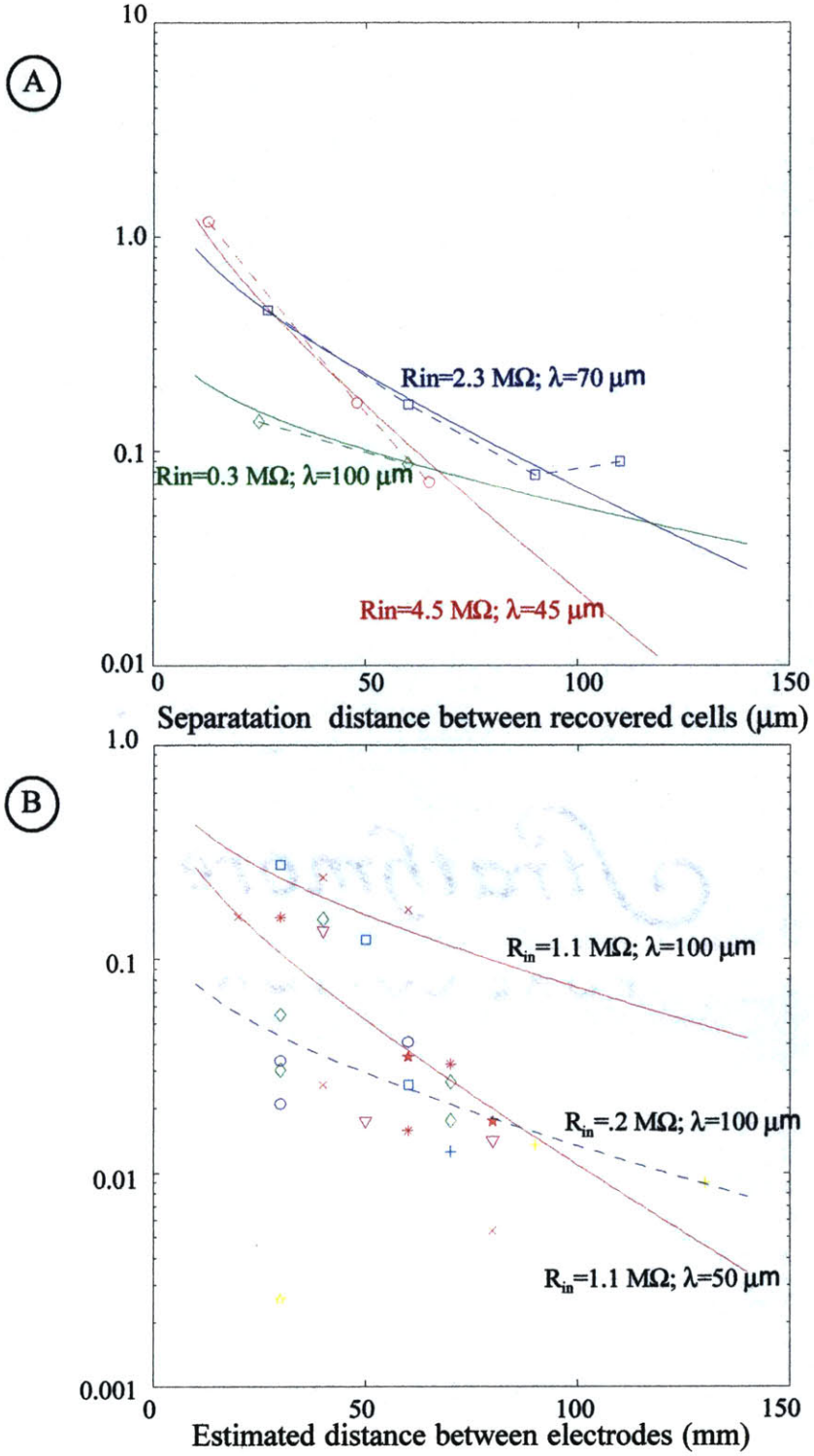

Figure 34. Measurements of mutual resistance as a function of separation distance between the cells. **(A)** Measurements from marked cells recovered from three different preparations (circle-CH113; square-CH111; diamond-CH112). The solid lines are throretical fits (Equation 3.1) to the data (shown are the membrane resistances and the space constant). **(B)** Mutual resistance measurements from unfilled cells. Each symbol represents a different preparation. The mutual resistance was computed using the depolarizing currents because the electrodes passed positive currents better than negative currents. Theoretical curves based on Equations 3.3-3.5 are superimposed on the data.

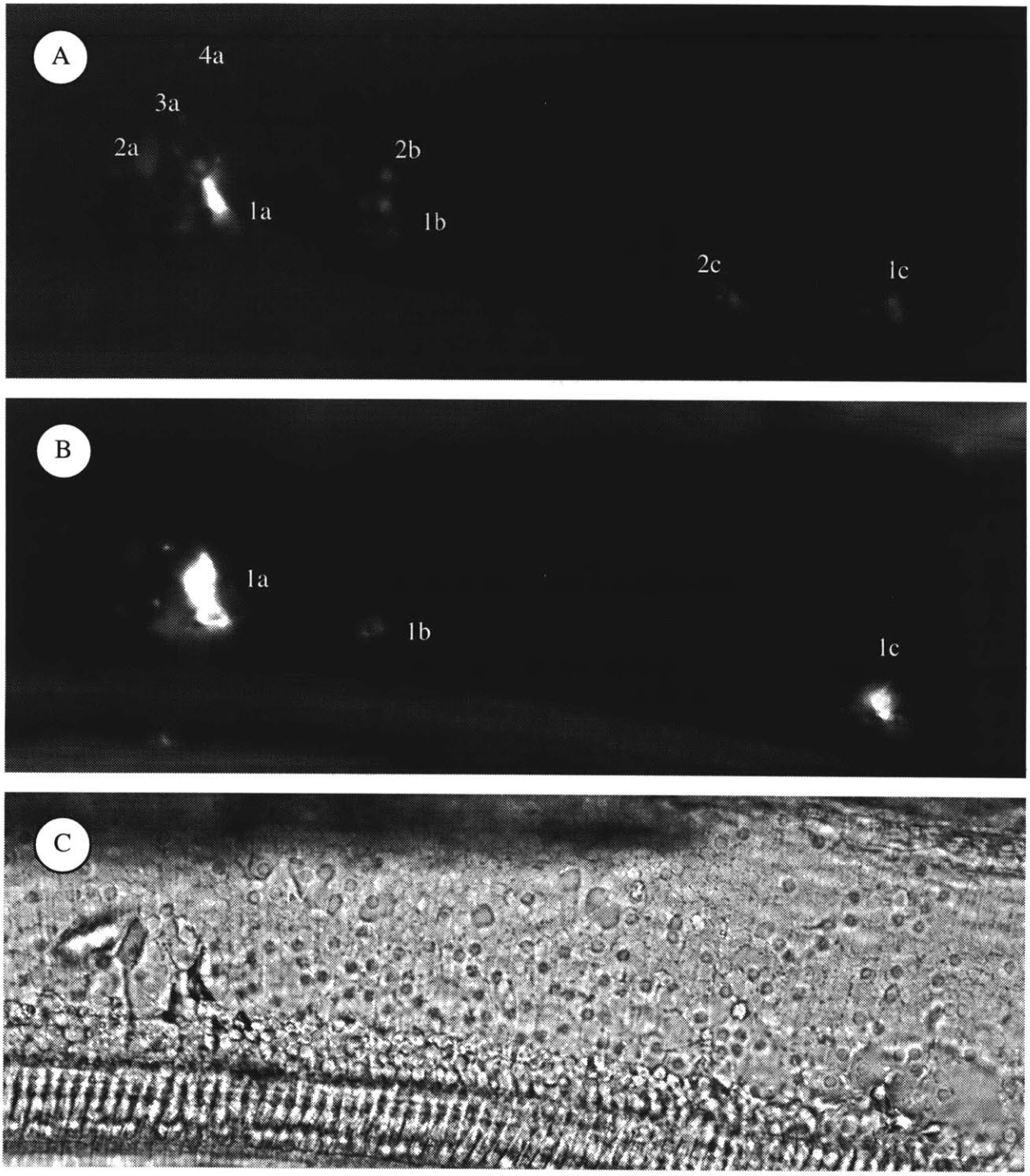

Figure 35. Surface view of filled cells recovered from mutual resistance measurement from experiment CH113. Electrode one was filled with am HRP-LY cocktail, and the second electrode was filled with just LY. (A) FITC image shows LY-filled cells. (B) CY5-SA bound to the HRP. Image using the CY5 filter set shows three cells that electrode one impaled. (C) Brightfield image of the surface view shows 1a and 1c are Hensen cells and 1b is a Deiters cell. Mutual resistance between 1a and 2a, 3a, and 4a are shown in Figure 23.

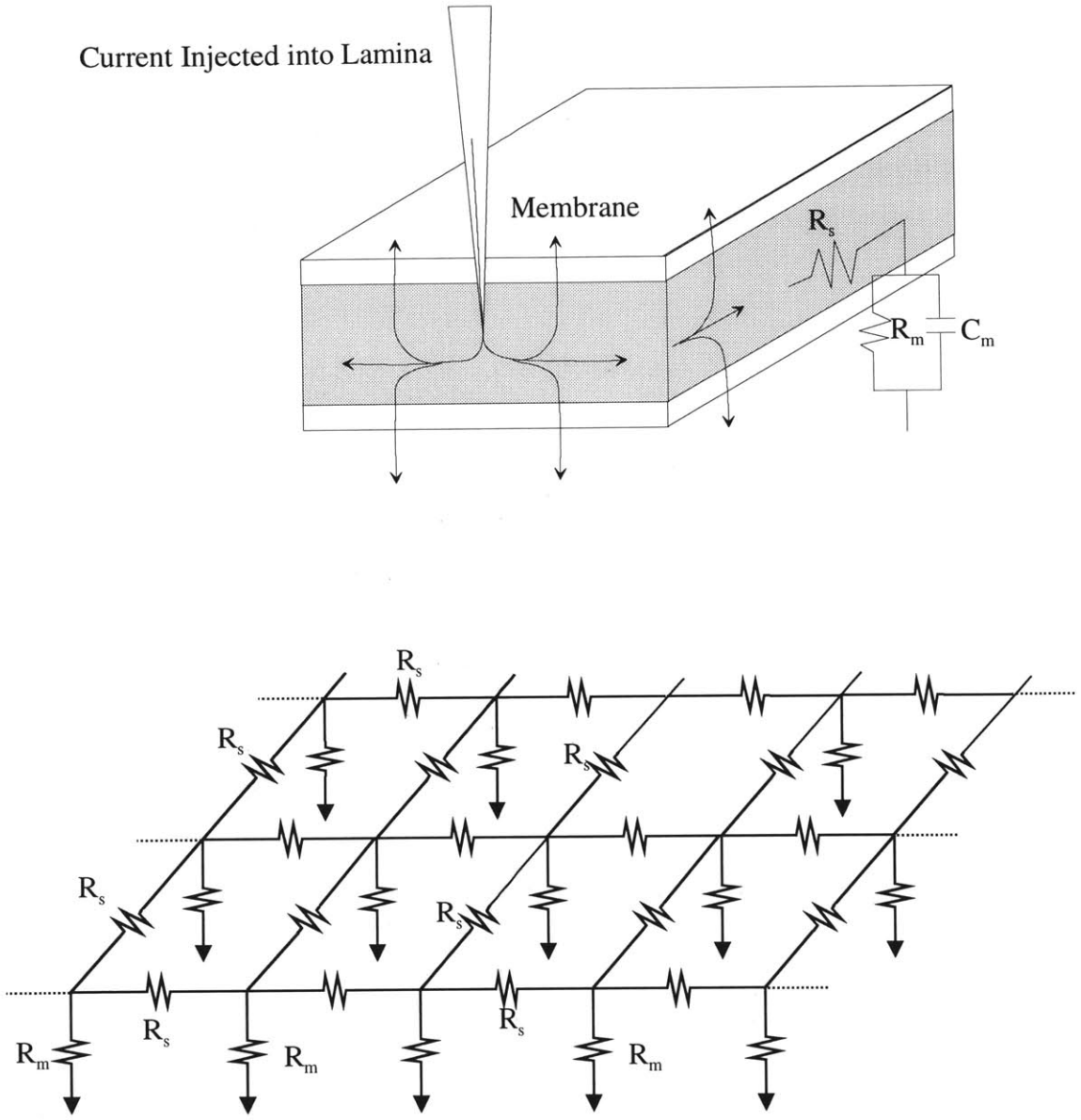

Figure 36. Schematic diagram of current injected into a 2-D lamina. Current spreads laterally within the lamina and through the membrane. The lateral resistance is R_s, the membrane resistance is R_m, and the membrane capacitance is C_m. In the bottom is a discretized uniform square grid model of a sheet of networked cells. The resistance between the cells is R_s and the resistance across the cell membrane is R_m.

2.4 Discussion

Previously measured extracellular potential gradients in the radial direction from the modiolus to the lateral wall in scala typmani were thought to be generated by currents as a part of potassium recycling in the cochlea (Zidanic and Brownell 1990; Zidanic and Brownell 1992). In the present study, standing and sound-evoked potential differences between cochlear supporting cells were analyzed as a function of radial direction from the inner supporting cells to the Claudius cells. These potential differences suggest an intercellular current that may play a role in potassium recycling. Intracellular currents produced by potential differences would be carried by potassium and would be a significant portion of the total potassium current. Through measurement of the magnitude and phase of the intracellular and extracellular responses near the hair cell region, data from the present study suggest that there is no direct coupling between hair cells and supporting cells.

2.4.1 Standing currents

In the present study, resting potentials from a large range of cochlear supporting cell types were measured and found to be within the range of resting potentials reported in previous studies. Unlike previous studies, the present study found a significant difference in resting potentials between certain supporting cell types. Initial reports of supporting cell resting potentials and responses to sound were anecdotal in hair cell studies (Brown and Nuttall 1984; Goodman et al. 1982; Russell and Sellick 1978; Weiss et al. 1974). Later studies directly examined supporting cell responses (Oberoi and Adams 1998; Oesterle and Dallos 1989; Oesterle and Dallos 1990; Santos-Sacchi 1987; Zwislocki et al. 1992). No statistically significant differences were measured among supporting cells resting potentials from the apical turn of the guinea pig, whose resting potentials were between –50 and –92 mV (Oesterle and Dallos 1989). In the gerbil apical turn, supporting cell resting potentials were between –60 and –100 mV (Zwislocki et al. 1992). While they did not convincingly show differences in resting potential, they suggested that within a given preparation there were potential differences between supporting cells. The average resting potentials measured in Chapter 1 were between –75 and –83 mV and the average potential difference between Deiters cells and Claudius cells was statistically significant.

An important finding in the present study was a -7 mV potential difference in the average resting potentials from the region of the hair cells (Deiters cells) to Claudius cells. A similar potential difference was measured in Chapter 1, but the average resting potentials were 4-6 mV more depolarized than the measurements from the present chapter. The main difference between the two experiments was the electrode solution used to make measurements. In the dye-coupling experiments, LiCl was used as the electrolyte, and KCl was used as the electrolyte in the present study. Although the electrode tip potentials were zeroed in the extracellular space, different tip potentials could be generated after the electrode was inside the cell, depending on the electrode solution. The electrodes used in the study in Chapter 1 also contained LY, which may also alter tip potentials of electrodes inside the cells.

In the present study, no systematic measurements in the longitudinal direction were performed, so the possibility of a small resting potential difference between cells in the longitudinal direction cannot be ruled out. Within a given preparation, similar cell types separated in the longitudinal direction appeared to have similar resting potentials.[6] Therefore, it is assumed that an intercellular potential difference only exists in the radial direction, and that resting potentials are similar in the longitudinal direction.

Resting potential difference between coupled cells

Cochlear supporting cells studied in the present study are coupled by gap junctions, so their resting potentials should be the same unless there are mechanisms to generate the differences. Other studies have shown that electrically coupled cells can have different resting potentials. Supporting cells in the basilar papilla of the alligator lizard are coupled to hair cells through gap junctions (Nadol et al. 1976), yet hair cells were more depolarized than the supporting cells (Weiss et al. 1978). Potassium entering hair cells would tend to flow to supporting cells because of the potential difference between these cells. The potential difference measured between Deiters cells and Claudius cells in the present study would tend to move potassium from Deiters cells to Claudius cells through the network of gap junctions. The observed standing potential gradient between cochlear supporting cells may be generated by several mechanisms: 1) a

[6] If longitudinal potential differences exist, then they are much smaller than the differences seen in the radial direction. Since the apex and base of the cochlea are separated by 20-30 mm, the potential gradient that may exist between adjacent longitudinal cells would be much smaller than the measured gradient in the radial direction (200 μm).

difference in potassium or other ion concentrations, 2) a current between the cells, 3) different membrane mechanisms that maintain different resting potentials within each cell type, 4) differences in the damage due to penetrations, causing a larger leakage current in some cells than other cell types, or 5) a combination of several of the mechanisms mentioned. Although mechanism 4 cannot be ruled out, it is unlikely since holding times for cells were usually longer than 10 minutes and a significant leak current would damage the cell, causing the resting potential to go to zero.

Concentration gradients as a mechanism for potential difference

A change in the intracellular or extracellular potassium concentration can account for potential differences between Deiters cells and Claudius cells. A cell's resting potential is close to the potassium equilibrium potential across the basolateral surface, so a change in the potassium equilibrium potential would change the resting potential. If the intracellular Deiters cell potassium concentration is 130 mM, and the perilymphatic potassium is 3 mM (Salt and Konishi 1986), then the Deiters cell's potassium Nernst equilibrium potential is -98 mV. A decrease in the potassium Nernst equilibrium potential by 7 mV, could be the result of an increase in intracellular potassium concentration by 40 mM or a decrease in the extracellular potassium concentration by 0.6 mM.

If the intracellular potassium concentration in Claudius cells or root cells were 40 mM larger than in Deiters cells, then potassium would tend to move towards the hair cells, opposite to the proposed potassium recycling. A current generated by such a potassium concentration gradient (using Fick's Law $\Phi=-D\ \Delta c/\Delta x$) would be about 20 nA[7] towards the Deiters. Without an active mechanism to pump an equivalent amount of potassium between the cells, a concentration gradient can not be maintained. No such electrogenic mechanism is known to exist that pumps potassium between cells. Given this magnitude is larger than most physiological currents, it is unlikely that the potential difference from Deiters cells to Claudius cells is due to an intracellular potassium concentration difference.

[7] The flux was calculated using Fick's Law for Diffusion with a separation distance of 200 μm and concentration difference of 40 mM. The current was computed by multiplying the flux by the cross-sectional area of the tissue for a 15 μm thick section. The area was approximated to be 1000 μm^2. The effective cross-sectional area would be lower because the pores of the gap junctions are only a fraction of the total area.

Assuming the extracellular potassium concentration decreases by 0.6 mM from the extracellular space near the hair cells to the extracellular space near the root cells, then the potassium current through a 15 μm thick section of the cochlea would be 3 nA.[8] This potassium current is six times larger than the potassium current through the hair cells at rest. If the 0.6 mM concentration difference exists only in the microenvironment near the type II fibrocytes and root cell processes, where the extracellular space is much smaller than scala tympani, the extracellular flux could be much smaller. A flux generated by diffusion would not cause a net current because an anion would diffuse with the potassium to maintain charge neutrality, or a different cation would diffuse towards the modiolus, so the diffusion currents cannot be compared to the extracellular currents measured by Zidanic and Brownell (1990).

Intercellular current due to potential differences

If the intracellular ionic concentration is the same within all supporting cells, then the equilibrium potential between the cells is zero. An intercellular potential difference would generate a net intercellular current. A –7 mV drop across 10 cells with radial resistance of R_s=3 MΩ, would generate a current of 233 pA through a single cell at rest given no leakage current.[9] The intercellular current would be carried primarily by potassium since it is the dominant cation. This current is the same order of magnitude as the standing current through the hair cells, which may be as high as 500 pA (Zidanic and Brownell 1990).

Differences in membrane permeabilities can generate potential differences

Differences in resting potentials can exist if there are differences in the cell membrane permeabilities. A cell's resting potential is usually depolarized compared to the potassium equilibrium potential, and depends on the cell membrane's permeability to different ions. If the potassium equilibrium potential is the same in both Deiters cells and root cells, and if the root cell membranes are more permeable to potassium, then the resting potential of the root cells would be closer to the potassium equilibrium potential (they would be more hyperpolarized). The

[8] Computed using Fick's Law for Diffusion. The extracellular potassium current through a 15 μm thick section of scala tympani would be on the order of 3 nA given a potassium concentration gradient of 0.6 mM and an extracellular area about 10 times larger than the supporting cell area.

[9] Assuming the average width of a cell is 15 μm, then for a 1 mm thick section of cochlea the current would be 0.2 μA.

potential difference between cells would cause a current between them. Since the potassium permeabilities of supporting cells are not known, we cannot be sure whether differences in membrane permeabilities are the mechanism by which potential differences are generated.

Comparison of Intracellular and Extracellular Standing Current

In a previous study, the extracellular current measured in a 1 mm wedge of cochlea was found to be 0.8-1.6 μA (Zidanic and Brownell 1990). This suggests that the total standing extracellular current is about 4-8 times larger than an intercellular current (0.2 μA), which would be generated by differences in resting potentials. The standing extracellular potential gradient between the region of the hair cell and the lateral wall was at a maximum of 1.0-1.4 mV, which was much smaller than the intercellular gradient observed in the present study. Yet the total extracellular current was larger since the resistance of the perilymph is much lower than the resistance through the gap junctions (2 S/m measured by von Bekesy, 1951) and the area of scala tympani is larger than the area of the cell network.

While the total extracellular current (~1 μA) is likely to be larger than the total intracellular current (~200 pA), the intercellular potassium current may be larger than the extracellular potassium current. Assuming the total currents are carried primarily by sodium and potassium, and the ionic currents are proportional to their concentrations, the intracellular potassium current is calculated to be about nine times larger than the extracellular potassium current since 90% of the intracellular current is potassium (0.18 μA) and only 2% of the extracellular current is carried by potassium (0.02 μA). It therefore appears that the intracellular pathway for potassium recycling could play a major role in potassium recycling in the resting state.

2.4.2 Circuit model of the epithelial cell network

A single layer network of cells can be modeled as a two-dimensional lamina with a lateral resistance, and a membrane resistance and capacitance, as shown in Figure 36. Current injected into the lamina spreads laterally within the lamina and leaks across the membrane. The magnitude of the current at any location depends on the lateral and membrane resistances. Given an isotropic lamina, the current spreads uniformly in all directions from the injection site within lamina, as well as out the membrane. If the lateral resistance were non-uniform, the current

would spread non-uniformly. Infinite lateral resistance along one axis, an extreme case of a non-uniform lamina, would allow the current in only the perpendicular axis. If the current spreads laterally in one dimension of the sheet, the lamina can be modeled as a leaky cable. The rate at which the current decays from the site of injection will depend on the ratio of the lateral resistance to the membrane resistance. For a steady-state current, time effects are eliminated, so the membrane capacitance can be ignored.

Uniform 2D Model

In a continuous uniform lamina, with membrane resistance R_m (Ω m^2) at the top and bottom of the sheet and a radial resistance of R_s (Ω), part of the current spreads radially along the sheet and some current leaks though the membrane. Given a current injected i_o at the origin,

$$\frac{V_r}{i_o} = R_s \frac{K_o(r/\lambda)}{2\pi} \qquad (3.3)$$

describes the mutual resistance between the origin and any point, where K_0 is the zeroth order modified Bessel function (Jack, et al., 1975) (Lamb and Simon 1976). The space constant is given by $\lambda^2 = R_m/R_s$.

A more accurate model of a cell network is a discretized conducting lamina. For simplicity, the epithelial cell network was modeled as a uniform square grid network with equal resistances between cells (Figure 36). In this model, current spreads equally in all radial directions. However, from the dye coupling experiments and the anatomical data presented in Chapter 3, it is clear that not all regions of the epithelial network are uniformly coupled in all directions. Therefore, the data were examined with a uniform model and a model with stronger longitudinal coupling (along the spiral of the cochlea) than radial coupling (from the hair cell region to the lateral wall).

Equation 3.3 predicts an infinite voltage at the origin and cannot be applied at the injection site, and the cell input resistance cannot be obtained from this equation. With the approximation that the network is a square grid, the input resistance, r_{in} (Ω), can be used to calculate the membrane resistance, r_m (Ω), and series resistance, r_s (Ω), with the space constant using

$$r_{in} = \frac{2r_m}{\pi}\left(\frac{\gamma}{\gamma+4}\right)K\left(\left[\frac{4}{4+\gamma}\right]^2\right) \qquad (3.4)$$

where $K(x)$ is the complete elliptic integral of the first kind, and $\gamma=r_s/r_m$. Given the average cell spacing between the cells to be D,

$$\gamma = 2\cosh\left(\frac{D}{\lambda}\right) - 2\,. \qquad (3.5)$$

It has been shown that the continuous model approximates the discrete cell network to within 5% or 10% if the space constant is greater than one cell diameter (Detwiler and Hodgkin, 1979). However, as the number of cells that are connected increases, the approximation is worse for small space constants less than a few cell diameters

Uniform 1D Model

The two-dimensional model can be simplified into a one-dimensional model if the same current is applied along the entire y-axis at x=0. One dimension of the continuous sheet model could be modeled using a cable model in which the voltage decays exponentially from the injection with a space constant of λ (Lamb and Simon, 1976).

$$v_x = \frac{r_m}{\lambda} i_o e^{-|x|/\lambda} \qquad (3.6)$$

The membrane resistance is r_m and the injected intracellular current is i_o. The space constant is the same for both the 1-D and 2-D models.

Simplifying assumptions

Modeling the epithelial cell network as a uniform network was based on an analysis of cell coupling between Müller cells. Coupling between networked Müller cells was analyzed by making mutual resistance measurements as a function of distance. The two dimensional network was simplified into a one-dimensional network by stimulating the retina with a slit of light to eliminate the response gradients in the y-direction. The response in the x-direction was used to characterize the space constant and compare it to the mutual resistance measurements to obtain the cell membrane resistance.

With some simplifying assumptions, the sound-evoked responses can be used to simplify the two-dimensional epithelial cell network into a one-dimensional cable model. The assumptions are (1) Part of the current leaving the hair cells is taken up by the supporting cells. (2) The current into the supporting cells is derived mainly from the outer hair cells. (3) The current input to the cell network is at the Deiters cells, which we denote as the x-axis origin. (4) At high sound pressure levels, the amount of current through the hair cells over a localized longitudinal region around the stimulus frequency is the same. Similar to using a slit of light to stimulate the retina, at a high sound level, the longitudinal axis of the cochlea is stimulated simultaneously, and at the region of the stimulating frequency. For cells near the center of this region (best frequency), the current flows primarily in the radial direction, eliminating the longitudinal axis of the model. The space constant of the cell network was computed by measuring the cell responses in the radial direction.

2.4.3 Measures of Network Coupling: Sound-Evoked Gradients

The on-DC and AC responses in the supporting cells and extracellular spaces are thought to be a direct reflection of hair cell responses (Assumption 3). The on-DC and AC responses were analyzed in the radial direction (one-dimension) to determine the network properties of the epithelial cell network, based on the assumption that there are no potential differences in the longitudinal direction.

The AC magnitude response decreased as a function of distance from the hair cell region. Space constants were computed by exponential fits to be between 100 and 300 μm for the AC measurements shown in Figure 28. The space constant is a ratio of the membrane resistance per area to the radial resistance. If the surface area of a cell is near 5000 μm^2 (40 x 40 x 15 μm) then the membrane resistance is 2 to 18 times larger than the radial resistance. Therefore, ions would tend to move in the radial direction rather than across the cell membrane. The intracellular phase did not change along the radial direction, which suggests that the capacitive effects caused by the adjacent cell membranes can be ignored, and the network can be modeled as purely resistive in the radial direction. The combination of a long space constant and little change in the phase implies that the gap junctions provide a low resistance pathway for current.

The on-DC potentials as a function of distance from the hair cells varied much more than the AC measurements. Variability between measurements caused poor exponential fits to the on-DC potentials, making it difficult to measure a space constant. The DC response variations could be explained by a weakness in the assumption that the sound stimulates a region of the cochlea uniformly. The iso-intensity curves (Figure 31) shows that above best frequency (BF) the on-DC response decreases more rapidly than below BF even at 80 dB SPL. The cochlea is tonotopically mapped, and higher frequencies correspond to a more basal cochlear location. Therefore, there may be some longitudinal effects where current flows from an apical region towards the base of the cochlea. The AC responses were measured with 1000 Hz tone bursts, which is well below the BF of the recording site, so the longitudinal excitation was uniform, and therefore a better representation of a one-dimensional network.

The equations for the cable model assume that the network is longer than several space constants to avoid boundary effects. However, the space constants measured using the AC responses are equal to or greater than the width of the organ of Corti. Therefore, at the root process, or the end of the cell network, the resistance of the root cell membranes must be taken into account to correctly model the network. If the resistance of the root cell membranes does not match the gap junctional resistance, the space constant could be miscalculated from the measured responses (Weiss 1996). It seems likely that the root cell membrane resistance is higher than the gap junction resistance membrane, so the space constant could be artificially larger than the space constant that would be observed if the width of the organ of Corti was much larger than the space constant.

2.4.4 Measures of Network Coupling: Mutual Resistance

Estimates of the resistance between the cells (series resistance) and the resistance of the cell membrane can be obtained from the mutual resistance measurements. Modeling the cell network as a two dimensional lamina, the resistance between the cells and across the cell membranes can be computed using Equations 3.3-3.5. Theoretical curves (based on Equations 3.3-3.5) for the mutual resistance as a function of separation distance were superimposed on the measured mutual resistances (Figure 34). In panel A, the measurements were taken within a radial sweep, and theoretical fits were made visually to the data. The space constants were 70, 45, and 100 μm with input resistances of 1.2, 2.4, and .4 MΩ. From these measurements, the cell membrane

resistances (r_m) were 54, 38, and 29 MΩ and the series resistances (r_s) were 2.8, 4.5, and 1.2 MΩ. In the lower panel, the data were measured from many different preparations, so 3 theoretical curves were superimposed to show the range of possible values. When the space constant was changed from 50 μm to 100 μm, the slope of the curve became less steep. The input resistance parameter shifted the entire curve along the y-axis and showed a range between 1.1 and 0.2 MΩ. The range of space constants and input resistances appear to cover a range of measurements, even though there was a large variability in the mutual resistance measurements.

The large variation in the mutual resistance could be due non-uniform coupling between cells. Dye-coupling experiments showed that dye injected into pillar cells spread primarily in the longitudinal direction, implying stronger coupling in that direction (Chapter 1). Strong longitudinal coupling was consistent with the dense immunostaining for connexin 26, a gap junction protein, in the longitudinal direction. If the longitudinal resistance were larger than the radial resistance, in the square grid model, then the mutual resistance measurements would decrease more rapidly in the radial direction than in the longitudinal direction. Equations 3.3-3.5 would underestimate the actual radial space constant and overestimate the longitudinal space constant. The radial resistance measured from these measurements would be larger than the actual resistance. Non-uniform coupling could explain the differences in the space constant measured with the sound-evoked responses and with electrically-evoked responses. The space constants measured from the AC magnitudes were larger (greater than 100 μm) than the space constants measured from mutual resistance measurements (40-100 μm).

Due to constraints in the experimental setup, coupling was not systematically measured in the longitudinal direction. Recovered dye-filled cells showed that the pairs of cells were not only separated radially, but there was also some longitudinal separation. Therefore, part of the variance in the electrical coupling measurements could be due to differences in radial and longitudinal separations.

The series resistance was calculated to be between 1.2 and 4.5 MΩ from the mutual resistance measurements. The series resistance was used to determine the current between cells given a potential difference between cell. The space constants of the network were derived from the mutual resistance measurements to give a qualitative measure of the coupling between the

cell. These space constants were smaller than those measured with sound, but within the same order of magnitude.

Directional coupling?

Non-uniform coupling and differences in the membrane resistances could account for differences in the mutual resistance measured from pairs of cells. Mutual resistance was higher when current was injected into one cell than when it was injected into another cell for many cases. There may be several explanations for this apparent directional coupling. One possible explanation is that the cells are coupled by gap junctions that have a higher conductivity in one direction than the other (Robinson et al. 1993; Verselis et al. 1994). In these cases where there is directional coupling, the gap junction is composed of two different subunits (connexons) made of different gap junction proteins (connexins). However, there is no evidence of different connexins co-localized at the same junction in the organ of Corti.

A second, more plausible explanation for the directional mutual resistance is differences in the cell input resistance. Cell input resistance is dependent on both the cell membrane resistance and the amount of coupling to other cells. Cochlear supporting cells appear to be highly differentiated, and probably contain different types and numbers of membrane channels that would cause differences in their membrane resistance. If one cell in a pair of impaled cells has a lower membrane resistance, then a larger portion of the current injected into that cell would exit through the cell membrane rather than passing to the coupled cell. If the other cell in the pair had a high membrane resistance, then the majority of the current would pass through the cell network to coupled cells. The difference in the cell membrane resistances would generate directional coupling. Evidence in the present study suggests that the cell membrane resistances can vary by more than an order of magnitude. The range of cell input resistances measured using double-barrel electrodes was between 0.26 and 4.12 MΩ. Since the input resistances were not measured during the mutual resistance measurements, a direct correlation between the directional coupling and input resistance could not be assessed.

A third explanation is a difference in the amount of coupling between cells. If cell one were coupled to many more cells than cell two, then the current from cell one would spread in many more directions than the current from cell two. Therefore, less current spreads towards cell two

from cell one. There is anatomical evidence to support differences in the amount of coupling between different cell types. Such a difference in coupling could exist between Hensen cells and other cells, such as Claudius cells. Many Hensen cells have an irregular geometry and can be coupled to many other cells. Processes of Hensen cells extend to cells that are not directly adjacent to them (Chapter 3). Claudius cells, Deiters cells, and pillar cells, however, have more regular geometries, and may be coupled to only a few cells. If, in addition to differences in numbers of coupled cells, the coupling is non-uniform, then the current injected into cell one could spread primarily to a direction other than towards cell two. From the dye-coupling studies, the pillar cells appear to be more highly coupled in the longitudinal direction. If the current were injected into an outer pillar cell, one might expect to see a smaller current in the adjacent Deiters cell than in the adjacent outer pillar cell.

A fourth explanation is that the cells may contain different membrane protiens that may be voltage dependent. If the channels in the membrane are voltage dependent, then a current of one polarity may elicit a larger coupling resistance than a negative current. Polarity dependent differences could also be due to differnces in cells' ability to handle chloride. When a positive current is applied, the current is carried by potassium, which is the dominant positive ion. Cells are usually well equipped to handle potassium increases. Since the intracellular potassium concentration is already large, the applied currents may not change the intracellular potassium concentration by much. When a negative current is applied, chloride is injected into the cell. The intracellular chloride concentration is regularly low, and an inflow of chloride may alter the normal function of the cells. Differences in cells' abilities to handle cations and anions could also be the cause for the differences in the input resistance measured using positive and negative currents.

2.4.5 Comparisons of coupling and resistance measures to previous reports

Patency of the gap junctional network was shown through direct measurement of dye coupling (Chapter 1) and the present study found a range of values for the mutual resistance and the gap junctional resistance between supporting cells *in vivo*. Only a few studies have examined the electrical coupling properties of cochlear supporting cells (Mammano et al. 1996; Oesterle and Dallos 1989; Santos-Sacchi 1987; Santos-Sacchi 1991) or the membrane characteristics of supporting cells (Mammano et al. 1996; Santos-Sacchi 1991). The only previous study to

measure the *in vivo* electrical properties was limited to Hensen cell in the apical turn. There have been many studies of coupling between supporting cells and epithelial cells in other systems (Brew et al. 1986; Duncan et al. 1988; Lamb and Simon 1976; Muller et al. 1996).

A larger coupling ratio, defined as the voltage drop in cell two versus the voltage drop in cell one due to an injected current in cell one, was found *in vitro* (0.6) than *in vivo* (0.1) (Santos-Sacchi 1987). When the compartmentalization of the cochlear fluids was disrupted by tearing the stria vascularis and Reissner's membrane, the coupling ratio increased to 0.455. These findings were explained as greater coupling when the cochlea was damaged or *in vitro* than *in vivo*. However, findings in the present study suggest that supporting cells are highly coupled *in vivo*, as determined by the large space constant and low gap junction resistance between cells.

There are several possible explanations for the previous results of low coupling ratio *in vivo*. The cell input resistance from isolated Hensen cells was 1.06 GΩ, and the input resistance of coupled Hensen cells was 0.5 MΩ. Such a low input resistance for the coupled cells implies that there is a low resistance pathway away from the cell. This suggests that the gap junctional resistance is much lower than the membrane resistance. If the cells are coupled to 10 cells, then only 1/10 of the lateral current will pass to any adjacent cell, producing a coupling ratio of 0.1 if all the current goes through the gap junctions. However, some current goes through the cell membrane, so a 0.1 coupling ratio would be possible with fewer coupled cells.

Damage to the cochlea could cause a higher coupling ratio. When cells are removed from the cochlea or the cochlear environment is damaged, membrane proteins may degenerate. This may cause an increase in the cell membrane resistance, which in turn would cause more current to pass through the gap junctional networks. The increased cell membrane resistance would cause only a small change in the cell input resistance if the gap junction resistance were much lower than the membrane resistance, as found in the present study. Santo-Sacchi found that cell input resistance was similar for *in vivo* and *in vitro* preparations, so an increased membrane resistance could explain differences in the coupling ratios. If cochlear damage uncoupled some of the cells, then a larger current would pass to the remaining coupled cells.

Cell resistances

In the present study, cell input resistance measured using single barrel and double barrel electrodes differed by about a factor of ten. Previous reports using single barrel electrodes found the input resistance to be on average 17.1 MΩ (Oesterle and Dallos 1989), but with dual barrel electrodes, Hensen cells were found to have an input resistance near 0.5 MΩ (Santos-Sacchi 1987). The cell input resistance measurements are thought to be overestimated using single barrel electrodes because the electrode resistance is in series with the cell resistance. The non-linear resistance of many single barrel electrodes could cause an inaccurate measurement of the cell input resistance. The double-barrel electrodes have a larger tip than the single barrel electrodes, so it is possible that the lower input resistance measurements measured with such electrodes are due to a larger leakage current caused by cell damage due to the electrode penetration. In the present study, the input resistance was determine to be between 0.4 and 4.0 MΩ from theoretical fits to the mutual resistance measurements. The electrodes were single barrel, so the leakage current was thought to be minimized, although it could not be eliminated. This suggests input resistance measurements using single barrel electrodes over-estimate the cell input resistance. The average cell input resistance measured in the present using double barrel electrodes was 1.17 MΩ, which is probably more accurate than the measurements using single barrel electrodes.

The cell membrane resistance computed from the mutual resistance measurements in the present study (30 to 60 MΩ) was much lower than previous measurements *in vitro* using whole cell voltage clamp of single cells (1.03 ± 0.563 GΩ) (Santos-Sacchi 1991) or uncoupled cells (212 ± 94 MΩ) (Mammano et al. 1996). In those studies, the detergents used to isolate cells and the process of removing cells from the cochlea could have damaged cell membrane proteins, so the cell membrane resistance could be higher than the membrane resistance measured *in vivo*. These measurements were made on apical Hensen cells, so differences between basal and apical Hensen cells could account for some differences between the present study and previous studies. The membrane resistance of the endfeet of Müller cells were found to have a membrane resistance of 12 MΩ (Mobbs et al. 1988). Membrane resistance of other cells, such as the epithelial cells in the lens of the eye, were 1.94 Ωm^2 (Duncan et al. 1988). Based on a cochlear supporting cell dimension of 50 x 30 x 15 mm, the membrane resistances in the present study are

between 1.0 and 2.0 Ωm^2. Therefore, the membrane resistance measurements in the present study are similar to other coupled cells, but lower than previous measurements from Hensen cells.

2.4.6 Sources of AC and DC potentials

The origins of supporting cell sound-evoked responses are generally accepted to be in part a reflection of hair cell currents. However, it is still unknown how this may happen. Previous experiments show contradictory results that have generated different hypotheses as to how the responses are generated. Some studies found sound-evoked supporting cell AC and DC responses to be equal to or smaller in magnitude than the extracellular responses (Oesterle and Dallos 1989; Oesterle and Dallos 1990; Russell and Sellick 1978). This implied a lack of direct coupling between the hair cells and the supporting cells and that the supporting cell responses were generated by passive flow of hair cell generated currents across the supporting cell membranes. Other measurements from gerbil supporting cells in the base (Goodman et al. 1982) and the apex (Zwislocki et al. 1992) reported larger intracellular responses than extracellular responses. Goodman et al. explained their results by suggesting that the network or supporting cells could provide a pathway with a smaller decrement than the extracellular space. Zwislocki et al. suggested that there was electrical and dye coupling between hair cells and supporting cells that allowed direct current from the hair cells to the supporting cells. The two suggested mechanisms are: i. Current flows out of the hair cell, into the extracellular space and then across the cell membrane through non-specialized membrane or channels. ii. Current flows directly from the hair cell to the supporting cells through gap junction or gap junction-like channels that electrically couple hair cells to supporting cells.

The results from the present study shed new light on the generation of intracellular supporting cell responses. The results do not definitively show a current path from the hair cells to the supporting cells, but do show how the results from previous studies can be reconciled. In the present study, the transmembrane DC-on and AC potentials were often negative for pillar cells and Deiters cells (cells near the region of the hair cells), indicating that the extracellular responses were larger than the intracellular responses. The extracellular spaces near these cells were examined and the responses were dependent on the depth of the electrode beyond the basilar membrane. These responses were similar to previous extracellular potential and

potassium concentration measurements made from the tunnel of Corti (Johnstone et al. 1989). When the electrode was in scala tympani, the response was much lower than the extracellular response on the other side of the basilar membrane in the tunnel of Corti. The basilar membrane probably acts as a significant impedance to the free diffusion of potassium as evidenced by the drop in the extracellular DC response as the electrode crossed penetrated it into the tunnel of Corti. Upon further advancement of the electrode, the extracellular response increased, and at a depth near where the hair cells would be expected (80 μm), the response was larger than responses measured intracellularly from Deiters cells in the same region of the cochlea. Therefore, the contradictory results from previous studies could be explained by differences in the locations of extracellular measurements. The present findings support mechanism (i) as the way supporting cell responses are generated.

If there is electrical coupling among supporting cells, then the responses should be transmitted along the cell network. In the present study, the on-DC and AC responses were observed in cells remotely located from the hair cells, and they were larger than the extracellular responses. This finding differed from the previous study (Oesterle and Dallos 1990) where smaller intracellular on-DC and AC responses were observed in Hensen cells. The most plausible way to reconcile a larger intracellular potential than an extracellular potential is that it's source is through electrical coupling. Current enters cells near hair cells, and the responses of those cells are smaller or equivalent to the extracellular response. For regions remotely located to the hair cells, the extracellular response decays faster than the intracellular response, so the pathway of least resistance would be through an intercellular pathway.

Evidence from the AC responses supports mechanism (i) as the mechanism by which the supporting cells reflect hair cell responses. Some of the AC responses in the present study were larger in the extracellular space than in the supporting cells near the hair cells. If these supporting cells were electrically coupled to the hair cells, then their responses should be in between the hair cell responses and the extracellular responses. Gap junctions provide a low resistance pathway between cells. If supporting cells were coupled to hair cells via gap junctions, then the intracellular phase of the supporting cells near the hair cells would be similar to the hair cell phase. The extracellular responses near the hair cells have been shown to lag the hair cell responses (Russell and Sellick 1983). A scatter plot of the transmembrane AC magnitude and

fluid phase relative to the intracellular phase (Figure 29) showed that responses where the transmembrane AC magnitude was negative, the intracellular phase lagged the extracellular phase. These findings are consistent with current flowing from the hair cell to an extracellular space, and then into the supporting cell. Since the phase of inner hair cells leads the extracellular phase by 90 degrees, direct coupling between inner hair cells and inner supporting cells would also be supported by a 90 degree phase lead in the inner supporting cells. None of the responses observed showed a greater than 30 degree phase lead with respect to the extracellular phase.

Mechanism for potassium current flow into Deiters cells

What is a possible mechanism by which potassium is taken up by the Deiters cells and supporting cells around the inner hair cells? Under steady-state equilibrium conditions, there is no net potassium current in or out of the cell. Given the potassium equilibrium potential of –98 mV, a cell resting potential of –78 mV, and a membrane resistance of 50 mΩ, the amount of current exiting the cell due to the concentration gradient across the cell is 400 pA. Active mechanisms, such as sodium, potassium-ATPase, are thought to supply an equal inward current to maintain equilibrium. Potassium released from the hair cells increases the extracellular potassium concentration, which in turn changes the potassium equilibrium potential. If the extracellular potassium increases by 1 mM, then the potassium equilibrium potential would increase by 8 mV. This would decrease the outward potassium current to 240 pA, but the active mechanism would still take up 400 pA, so the net flux would be inward. The larger extracellular potential would further reduce the outward flow of potassium, so the net inward current would be larger. The average current through an outer hair cell at 80 dB is about 400 pA[10], so a significant portion of the current could be taken up directly through an active mechanism in the Deiters cell.

It has generally been thought that the large spaces of Nuel prevent the extracellular potassium concentrations near the hair cells from getting large. The spaces surrounding the hair cells can be divided into two types of spaces: the relatively large spaces of Nuel and the smaller cleft spaces between the hair cells and the supporting cells abutting them. If the potassium concentration in

[10] The maximal conductance though an outer hair cell is thought to be 28 nS. Given a 150 mV drop between scala media and outer hair cell resting potential, the maximal current would be intracellular 4.2 nA. At 80 dB SPL, the channels may not be maximally open and the average conductance would be about 2.8 nS. 400 pA is a conservative average current through the outer hair cells at 80 dB SPL. Brownell (1986) reported that the average current through an outer hair cell is about 500 pA, which is close to our approximation.

the spaces of Nuel can increase significantly in response to loud sounds, then the potassium concentration in small spaces would increase as well, probably by a larger amount. It has been shown that the majority of the potassium channels through which potassium exists outer hair cells are located in the basal portion of the outer hair cell (Santos-Sacchi et al. 1997), which sit in the Deiters cup in close proximity to the Deiters cell. A large increase in potassium concentration in the region between Deiters cells and outer hair cells could cause a localized depolarization of the Deiters cell membrane and potassium could be taken up by non-specific or inwardly rectifying potassium channels that have been identified in the Deiters cells (Hibino et al. 1997). A high extracellular potassium concentration would cause potassium to flow into the Deiters cells through such channels.

The Deiters cells' cups surround the base of outer hair cells and come in close apposition to the outer hair cells. If the hair cell is a cylinder of diameter 8 μm, and the cup surrounds the lower 10 μm of the hair cell and the average space between the hair cell and the cup is 50 nm, then the volume between the hair cell and the Deiters cup is 1.4×10^{-11} cm^3. If, for a 10 msec tone burst, all the potassium expelled by the hair cell were to accumulate within this space (4×10^{-12} C, or 4.14×10^{-17} moles of potassium), the concentration in that region would increase by 3 mM. The potassium equilibrium potential would increase by about 20 mV, and would reduce to outward flow of potassium to close to zero. If potassium were free to diffuse away from this space, then it would take 100 msec for half of it to diffuse 10 μm, or 1 msec to diffuse 1 μm given a diffusion coefficient of 10^{-5} cm^2/s. However, since the Deiters cells surround these spaces, the diffusion coefficient may be higher. The approximation that all of the potassium in 10 msec accumulates in that area may not be entirely valid, but even if half the potassium accumulates there, then the potassium equilibrium potential would increase by 12 mV, and thereby have a significant effect on the potassium current out of the Deiters cell. If the spaces between the cells are smaller (on the order of 25 nm), then the potassium concentration could increase by as much as 7 mM, and the potassium equilibrium potential could increase by 30 mV. If the potassium equilibrium potential were to become higher than the Deiters cell's potential, potassium would passively flow into the cell.

Sound-evoked potential gradients

An important finding of the present study was an intracellular sound-evoked gradient within the epithelial cell network. There was a statistically significant potential gradient in the on-DC measurements of -0.183 mV per 100 μm from the Deiters cells to the Claudius cells. A gradient in the AC magnitude was observed to be –0.335 mV per 100 μm. Both of these gradients are consistent with an intercellular potassium current in the radial direction from the cells near the hair cells to cells near the lateral wall. If the distance from the Deiters cells to the root cells is 200 μm, and the gradient extends to the root cells, and then the DC potential difference between these cells is -0.366 mV. Given that there are 15 cells with a 3MΩ resistance between them, the current due to this potential gradient would be 8 pA. This is a small fraction of the current that is thought to be taken up by Deiters cells or currents through hair cells. If the resistance between the cells were actually lower, then the current would be higher. Even with a radial resistance of 1 MΩ, the current would only be 24 pA. The on-DC potential was measured 4 msec after the tone was turned on, so it may not represent an accurate measure of a sound-evoked current. The AC response magnitude, decreased 0.67 mV, corresponding to a 16 to 32 pA current, which is still significantly smaller than the current through the hair cells.

Our hypothesis is that the DC and AC responses are electrically transmitted between cells in the radial direction, which produced the observed graded response. Measures of the on-DC and AC responses indicate that the cell network is highly coupled. Results showed that the intracellular on-DC response in cells far from the hair cells was larger than the corresponding extracellular response. A larger intracellular response could be generated by active processes, such as pumps or a current flow into or out of the cell. It is unlikely that sound induces the rapid onset of an active process in cells remotely located from the hair cells. A more plausible explanation is that the intracellular response spreads from the cells close to the hair cells to the cells further away with less decrement than the spread in the extracellular space. The intracellular response of Deiters cells is slightly smaller than the extracellular response near the hair cells, but the intracellular Claudius cell response is larger than the corresponding extracellular response. This suggests that an intercellular current from Deiters cells to Claudius cell is through a less resistive pathway than the corresponding extracellular pathway.

Our results showed that the phase of the AC response of supporting cells lagged the hair cell responses, and there was no phase shifts between supporting cells along the radial direction. This indicated that the coupling between supporting cells was mostly resistive, and there was very little capacitance between them. If the AC responses are generated by a flow of receptor current across the supporting cell membrane through non-specialized membrane patches, then the coupling could be due to just the phase shift in the extracellular space as the measurements are made further away from the hair cells. This idea is supported by the fact that the phase difference between the intracellular and extracellular spaces is consistent throughout the organ of Corti.

Slow-DC Potentials

The origin of the slow DC has not been clearly identified, but several possible mechanisms may contribute to this response. 1. An increase in the extracellular potassium concentration (up to a 1 mM change in the region of the outer hair cells, and 3 mM near the inner hair cells) during long duration and high intensity sounds (Johnstone et al. 1989) can cause a depolarization in the cell membrane potential. The change in potassium concentration of 0.5 to 1.0 mM (approximate in response to a 80 dB SPL tone Johnstone et al. 1989) could change the potassium equilibrium potential by 8 mV, which in turn would depolarize the cell's membrane potential. The rate of increase of the slow-DC potentials observed in the present study were similar to the rate of potassium accumulation in the spaces of Nuel, where potassium concentration increases monotonically during the first 3 sec of the tone burst, and then levels off (Johnstone et al. 1989). The potassium was cleared away from the spaces with a time constant of 2 to 3 sec, which was similar to the observed off-DC time constants. 2. An alternate explanation is that supporting cells take up some of the potassium released by the hair cells. In the previous section, it was shown that there could be considerable potassium taken up by the Deiters cell, which would cause the cell to depolarize. 3. The slow DC response could be due to a combination of extracellular potassium accumulation and potassium uptake.

Extracellular potassium accumulation could cause supporting cells near hair cells to depolarize during the tone bursts. Hensen cells and Claudius cell are located remotely from hair cells, and the diffusion half time for potassium to diffuse from the extracellular space near the hair cells to the extracellular space near the Claudius cells would be 10 seconds given a distance of 100μm. Since the slow-DC is present in Claudius cells at about the same time and rate of

depolarization as in Deiters cells, it is thought that the response is carried by an intercellular current. The magnitude of the slow-DC is the same in cells along the organ of Corti, which is consistent with a current through a primarily resistive network with a low resistance. This suggests that our calculations of the resistance between cells may have been overestimated.

In a previous study by Oesterle and Dallos, little or no slow-DC potential was found in Hensen cells, which led them to hypothesize that the slow-DC could be primarily due to potassium accumulation (Oesterle and Dallos 1990). These results are not consistent with the idea that the Hensen cells are coupled to the Deiters cells, in which the response was present, and are in conflict with the findings in the present study. The previous measurements were made in the apical turn of a guinea pig and the present study was done in the basal turn. It is known that there are difference in the morphology of apical and basal Hensen cells (Merchan et al. 1980; Schiff and Christiensen-Lou 1967; Spicer and Schulte 1994a; Spicer and Schulte 1994b). Chapter 3 shows that there are differences in the density of the gap junction protein connexin 26 (Cx26) between Hensen cells in the basal and apical turns. In the apical turns, the density of immunostaining for Cx26 was lower and the cells appeared to be poorly coupled. This could explain the lack of a slow-DC potential in apical Hensen cells.

2.4.7 Summary

The graded sound-evoked responses from the Deiters cells to the lateral wall confirm that there is electrical coupling between the supporting cells in the epithelial cell network. Space constants measured from the graded responses suggest that the cells in the network are highly coupled with a much lower resistance between cells than across the cell membrane. Electrical impedance measurements of coupling were consistent with the sound-evoked gradient. The resistance between the cells was found to be about one-tenth the resistance across the cell membrane.

The present study found evidence to suggest an intercellular standing current that is smaller than the previously observed extracellular current. However, since these currents may be carried by different ions, the intercellular potassium current could be on the order of 200 pA, which is close to previously measured standing current through the hair cell. While the standing current appeared to be significant, based on the resistance measurements, the sound-evoked gradient could have been generated with little current. However, these findings are inconsistent with the

findings that the slow-DC potential and off-DC potential responses did not decrease from Deiters cells to the lateral wall.

The findings in the present study provide further evidence to support the idea of an intercellular potassium current between the supporting cells in the organ of Corti. The findings suggest the following potassium pathway as described in Figure 1. Potassium exits the hair cells at the basolateral surfaces, where it is extracellular. Some of the potassium is taken up by the supporting cells adjacent to the hair cells, and some of the potassium spreads extracellularly. Once taken up by the supporting cells, the potassium spreads through the gap junctions to other cells since they provide a low resistance pathway. The electrical gradient between Deiters cells and Claudius cells suggests that potassium taken up by Deiters cells would move preferentially towards Claudius cells.

3 Anatomical substrates for coupling of non-sensory cells of the organ of Corti

3.1 Introduction

The organ of Corti is a complex three-dimensional structure composed mostly of non-sensory *supporting cells*. The majority of what is known about the function of supporting cells has been inferred from their morphology and cyctochemistry. Much of the focus on supporting cells has been on their structural role in the micromechanics of the cochlea (Johnstone and Yates 1974; Laffon and Angelini 1996; Lim 1980; Rhode 1978; Richter et al. 1998; Sellick et al. 1982). The locations of many ion regulating proteins and the identification of intercellular networks imply that the supporting cells play a major role in ion homeostasis in the cochlea, similar to the role performed by Müller cells in the retina and glial cells in the brain (Hibino et al. 1997; Ichimiya et al. 1994; Kikuchi et al. 1995; Sakaguchi et al. 1998; Schulte and Adams 1989; Stankovic et al. 1997).

Freeze fracture, electron microscopy, and immunohistochemistry have been employed to show the structural substrates for coupling between non-sensory cells in the cochlea (Forge 1984; Gulley 1976; Iurato et al. 1976a; Iurato et al. 1976b; Jahnke 1975a; Jahnke 1975b; Kikuchi et al. 1995; Nadol et al. 1976). Kikuchi et al. (Kikuchi et al. 1995) found that the presence of the gap junctions identifies two distinct cell networks within the cochlea: the *epithelial cell network* and the *connective tissue cell network*. The *epithelial cell network* is composed of non-sensory cells of the organ of Corti including interdental cells, inner border cells, inner phalangeal cells, inner pillar cells, outer pillar cells, Deiters cells, Hensen cells, Claudius cells, Boettcher cells, and root cells. The *connective tissue cell network* is composed of the fibrocytes of the spiral ligament, the cells lining scala vestibuli, strial basal cells, strial intermediate cells, and strial marginal cells.

Previous studies have examined the functional coupling of the cells in the organ of Corti through dye coupling (Chapter 1, Santos-Sacchi 1986, Santos-Sacchi and Dallos 1983, Zwislocki et al. 1992), electrical coupling (Chapter 2, Santos-Sacchi 1987, Santos-Sacchi 1991), and

sound-evoked responses (Chapter 2, Oesterle and Dallos 1989, Oesterle and Dallos 1990). Direct visual observation of the intercellular movement of dye has shown that the gap junctions are patent *in vivo* (Chapter 1). However, the dye often spread in preferred directions depending on the injected cell type, which suggests that the cells are not uniformly coupled. Electrophysiological studies (Chapter 2) also suggest that cell membrane and coupling resistances are not uniform. Further investigation of the anatomical substrates for coupling is needed to determine if the preferential movement of dye and the range of intercellular resistances can be explained by the locations and densities of gap junction between the cells.

In this study, the presence of connexin 26 (Cx26), a gap junction protein, was documented in the cells of the chinchilla organ of Corti to determine if their locations could account for the physiological results presented in Chapters 1 and 2. Immunohistochemical localization of Cx26 was used to identify the sites of gap junctions. A three-dimensional map of the immunostained junctions was created through optical sectioning. Optically sectioning the tissue allowed the examination of the single specimen in many planes of sections so that distinctive spatial relations of the cells and their connections could be illustrated to best advantage. This study revealed non-uniform coupling with a higher density of staining between particular cell types. The locations of the highest density of gap junctional staining was connections congruent with the physiological measures.

3.2 Methods

3.2.1 Immunohistochemistry

Surface preparations for immunohistochemistry were generated using the same procedure as Kikuchi et al. (1995). Chinchillas (body weight 300 to 600 g) were deeply anesthetized with 65 mg/kg of Nembutal and then perfused intracardially with warm 0.01 M phosphate-buffered saline (PBS), pH 7.3 containing 0.1% sodium nitrite, and then with 10% formalin in PBS. The middle ears were opened, and the round window was perforated. The stapes was removed and fixative was perfused through the scalae. The middle ears were immersed in fixative for 2 hours and then washed in PBS to remove the fixative. The bony part of the bulla was removed and the cochleas were placed in 0.12M ethylenediamine tetra-acetic acid (EDTA, pH 7.0) and stirred for

several days until all the bone was decalcified. The decalcified cochleas were bisected through the modiolus using a razor blade. The half turns were isolated with fine jeweler's forceps. Reissner's membrane and the tectorial membrane were removed. The lateral wall was dissected out using a razor blade.

Each half-turn was processed as a whole mount through the immunostaining sequence. Specimens were placed in 5% normal horse serum (NHS) and 0.03% Triton X-100 in PBS for 1 hour, then placed directly into the rabbit polyclonal (Ab9770) [11] in 1% NHS-PBS (1:15,000) with 0.01% Triton X-100 and agitated overnight. The tissue was placed in 1:400 biotinylated donkey anti-rabbit IgG (Jackson) in 1% NHS-PBS for 1 hour, Vectastain ABC reagent (Vector) for 1 hour. For a brown reaction product, the tissue was then placed in 3,3'-diaminobenzidine tetrahydrochloride (DAB)-H_2O_2 substrate medium and monitored using a dissecting microscope (for about 5 minutes). Alternatively, for a fluorescent reaction product, the tissue was placed in CY5 linked to streptavidin (1:1500) in PBS for 1 hour. The fluorescently labeled tissue was placed in fluorescein isothiocyanate (FITC) labeled phalloidin (1:500) in PBS for 1 hour and pyronin Y (1:1000) in PBS for 15 minutes. The combination of the phalloidin and pyronin were used as counterstains to identify cells when imaging the Cx26 reaction product in the surface views with the confocal microscope. Copious washing in PBS separated each of the above steps.

To image the fluorescent tissue, it was placed in a slide well with 50% glycerol in PBS and coverslipped and imaged. For the brown reaction product tissue, the half-turns were dehydrated in a graded series of ethyl alcohol, cleared in propylene oxide and embedded in Polybed 812 (Polysciences) in a slide mould. The half turns were cut out of the plastic slides. The plastic on either side of the organ of Corti was thinned and the specimen was then remounted on a glass slide.

3.2.2 Dye-filled cells

Iontophoretic injection of dyes was performed in anesthetized chinchillas (65 mg/kg of sodium pentobarbital i.p., with boosters given every 2 hours or as needed) with the same exposure as described in Chapters 1 and 2. Electrodes filled with 1% horseradish peroxidase (HRP) in 1M LiCl and 2% lucifer yellow (LY) were used to impale cells in the organ of Corti.

[11] Antibody was given to us by David Paul and described by Goliger and Paul, 1994.

The dye was iontophoresed into cells in the basal portion of the cochlea corresponding to the best frequency region between 7000 and 9000 Hz. After the injections, the tissue was fixed with a perfusion of 10% formalin in PBS into the scalae and immersed in the fixative for 2 hours at room temperature. The bony part of the otic capsule was shaved away using a scalpel and the basal turn of the cochlea was removed. The tissue was placed in 5% NHS with 0.03% Triton X-100 for 30 minutes, BT and H_2O_2 for 10 minutes, and then CY5-strepavadin (1:500) overnight. The tissue was placed in 50% glycerol in PBS and coverslipped. The tissue was imaged successively using brightfield illumination and epi-illumination through CY5 and FITC-lucifer yellow filter sets.

Tissue from two cochleas was place in 1% osmium tetroxide in 0.1M cacodylate buffer, pH 7.3 for 10 minutes, dehydrated, embedded in Polybed 812 (Polysciences), and then cut at 2 micron serial sections in the plane of the basilar membrane from the cuticular plate to the basilar membrane. The cut tissue was mounted on glass slides, stained with toluidin blue for 3 minutes, and coverslipped. The serial sections were examined for structures that correspond to those seen in the dye-filled material.

3.2.3 Imaging acquisition and processing

Brightfield and fluorescent images

Brightfield and some fluorescent images were acquired with a Hamamatsu 12 bit CCD camera mounted on a Nikon microscope and imaged with a 100x 1.3NA oil immersion objective. Images were digitally acquired and a background image was subtracted away to correct for shading and noise. Brightfield and fluorescent images of surface preparations were taken at 1 μm or 0.5 μm optical sections through the tissue. Images were acquired and pre-processed using the MetaMorph (Universal Imaging, PA) software package. The remove haze function[12] A nearest neighbor algorithm in the MetaMorph software was used to reduce blurring of the images. Some additional image processing was done using Picture Publisher (Micrografx, Inc.) to brighten the images and enhance the edges using an unsharp mask filter with a filter size of 10.

[12] The remove haze function is a nearest neighbor algorithm. The images from the adjacent planes (n-1 and n+1) are added together, and then blurred with a low-pass filter. The blurred image is scaled and subtracted from the center plane (n) to get the haze removed image. The parameters for the blurring and the scaling values were adjusted to give the clearest center image as determined by the author. Different parameters were used for different sets of images.

Confocal images

Surface views of the organ of Corti were taken with a BioRad MRC 500 confocal unit attached to an inverted Nikon microscope with a 100x 1.3 N.A. oil immersion objective. Images were taken at 1 μm optical sections through the entire organ of Corti. Images obtained with three successive fluorescent filter sets (Rhodamine, FITC, and CY5).

Two software packages were used to reconstruct the anatomical structures of the supporting cells and the Cx26 immunostaining between them. Cell outlines were rendered by tracing contours around cells using SegmentView (Andrew Dobsenecki, MIT). The locations of the gap junctions were superimposed on these renderings. The confocal surface view images were loaded into VoxBlast (Vaytek Inc.), rendered with different opacities to show the three-dimensional structure and imaged in different cross-sectional planes.

3.3 Results

Surface views of the organ of Corti immunostained for Cx26 showed staining among cells extending from the inner sulcus cells proximally to the root cells distally, as previously reported in the rat organ of Corti (Kikuchi et al. 1995). Staining was seen in both the radial and the longitudinal directions, but some cells showed staining primarily between homotypic cells in the longitudinal direction (pillar cells) and in others it was uniform in all directions (Claudius cells and inner sulcus cells). A complete rendering of the three-dimensional localization of the Cx26 was not possible with just the surface views, and radial cross-sections were needed to appreciate the complexity of the patterns of coupling. A combination of surface views and cross-sections was used to document the three-dimensional coupling between cells.

Radial cross-sections (Figure 37) showed differences between cells in the basal turn (A) and cells in the third turn (B). The most noticeable differences were the absence of Boettcher cells in the upper turns and the change in the shape of Hensen cells between these locations. The paraffin sections of the organ of Corti show the densest staining between Boettcher cells, however in the apical turns these cells are not present. Instead, in the apical turns dense staining was located between Deiters cells, Hensen cells, and Claudius cells.

3.3.1 Inner supporting cells

Computationally reconstructed cross-sections of the inner portion of the organ of Corti stained for phalloidin (green) and immunostained for Cx26 (red) are shown in Figure 38A and Figure 40A. The outline of an inner hair cell (IHC) was traced from brightfield images of the same tissue and the outline was superimposed on the fluorescent image in white (Figure 38A). Staining with phalloidin was found in inner pillar cells, outer pillar cells, the cuticular plate, and stereocilia of the hair cells. The majority of immunostaining among inner border cells and inner phalangeal cells was above (white arrow) and below the inner hair cell (black arrowheads). Optical sections of a different surface preparation (brown DAB reaction product) showed punctate staining between the border cells primarily in the longitudinal direction at the plane of focus of the inner hair cell stereocilia (Figure 38B). Staining was present among inner phalangeal cells along the entire length of the inner hair cell (Figure 38A; black arrowheads and white arrow). In the surface view, at a plane of focus below the IHC cell body (Figure 38C), staining was present between inner pillar cells (IPC) and inner phalangeal cells (IPh). Cx26 immunostaining was uniform along the entire perimeter of the inner sulcus cells and the entire height of the cell (Figure 38 D and white arrowhead in Figure 38A). Very little staining was present among inner border and inner phalangeal cells at the level of their nuclei (Figure 38D).

3.3.2 Inner and outer pillar cells

A rendering of cells traced from surface views optically sectioned at 1 μm intervals is shown in Figure 39E. Locations of the gap junctions were superimposed on the rendering and shown as lines. Surface views of the tissue from which the rendering was made are shown in Figure 39A-D. Immunostaining was present at the base of the cells and along the basolateral surfaces of the heads of outer pillar cells. The majority of the immunostaining among inner pillar cells and outer pillar cells was present between homotypic cells in the longitudinal direction at their base (black and white arrows Figure 39C,D and white arrowheads in Figure 41E). Confocal fluorescent images (Figure 41E) showed more distinct staining because of less blurring in the optical system. Staining was detected along the base of the tunnel of Corti in the reconstructed cross-sections of the same fluorescent tissue (white arrowhead in Figure 41A). Strong immunostaining was present over the entire area of contact between the bases of inner and outer pillar cells. Immunostaining between adjacent inner pillar cells was present along the basal portion of the

cells, and little or no staining was present between their heads or phalangeal processes. The majority of the staining between heads of the outer pillar cells occurred along the basolateral side and the basal most place where adjacent heads met (Figure 39B, black arrowhead). There was no noticeable staining between adjacent outer pillar cells along the main part of the heads. The staining between heads of outer pillar cells took the form of short segments (black arrows in Figure 38C, Figure 40D, and white arrows in Figure 41B). In the computationally reconstructed cross-sections, the staining appeared to be confined to a line along the bottom of the pillar head (black arrowheads in Figure 39E, white arrow in Figure 41A).

3.3.3 Deiters cells

Immunostaining was present between first row Deiters cells and outer pillar cells at the base of the cells (just above the basilar membrane) and between processes of Deiters cells and heads of outer pillar cells at the reticular lamina. The immunostaining found between these cells at their basal appositions appeared to be less than the immunostaining found between inner pillar cells and outer pillar cells. Immunostaining between processes of Deiters cells and outer pillar cells and between processes of Deiters cells at the reticular lamina was punctate and appeared as 2 or 4 dots (Figure 40C).

In a rendered view (Figure 40B) and a reconstructed cross-section (Figure 40A and Figure 41A), immunostaining was localized primarily at two places along the Deiters cell body: the base of the cell near the insertion with the basilar membrane (unfilled arrows in Figure 40E and hatched arrowheads in Figure 41E,F) and the apical part of the cell body, above the nucleus (white arrows in Figure 40D and hatched arrows in Figure 41C). The highest density of punctate staining occurred at or just below the cups of the Deiters cells, which can be seen in the reconstructions and the renderings (white arrows in Figure 40A,B and hatched arrows in Figure 41A) and paraffin sections (white arrows in Figure 37). In series of optical sections, there was no staining at the level of outer hair cell nuclei (Figure 41B), but at a plane of section 5 μm lower (Figure 40D and Figure 41C), there was dense immunostaining present. At a plane of section 8 μm lower, at the level of the nucleus of the Deiters cells (Figure 41D), immunostaining was sparse and none was seen in the cross-section. The staining at the base of the cells occurred a within 5 μm of the basilar membrane, and appeared as short linear segments around the cells (Figure 40E, arrows), whereas the staining near the Deiters cups was more punctate.

The main difference between the Deiters cells in the basal turn and in higher turns was that in the 2nd and 3rd turns, processes of the last row of Deiters cells forms the other tunnel. In the apical turns, dense linear segments of immunostaining was localized between the last row of Deiters cells along the outer tunnel (Figure 41B, white outlined arrow) primarily in the longitudinal direction. This longitudinal coupling was also present in the rendering of the last row of Deiters cells in the basal turn in Figure 40B.

3.3.4 Hensen Cells

Several patterns of staining were present in Hensen cells stained for Cx26. This suggests that there may be more than one subtype of Hensen cell. Differences in immunostaining were seen between Hensen cells in the basal of the cochlea (Figure 40F-H) and Hensen cells in the apical turns of the cochlea (Figure 41B-F). Within each turn, there were several types of Hensen cells as distinguished by their structure, location, and density of Cx26 immunostaining. In the basal turn, four types of Hensen cells could be distinguished: tectal cells, cells intensely stained for phalloidin, cells lightly stained for phalloidin, and lateral Hensen cells. In apical turns, there were three types of Hensen cells: roof Hensen cells, outer Hensen cells, and lateral Hensen cells (see Table 7 for a summary).

The following traits distinguished distinct types of Hensen cells. Tectal cells, which cover the upper part of the outer tunnel in the basal turns of the cochlea, had sparse Cx26 staining at junctions with the third row of Deiters cell processes at the level of the reticular lamina. There was no longitudinal staining between these cells. Adjacent to the tectal cell, distally, at the apical surface of the organ of Corti, were two types of Hensen cells distinguished by their staining for phalloidin. The intensely stained cells appeared to have a sheath of actin at their apical surface. The reconstructed perspective view of Hensen cells (Figure 40G) showed that the apical portion of the Hensen cells forms a contour that is not smooth, but has peaks and valleys. The intensely stained cells (IH) are present at the peaks and the lightly stained cells (LH) are in the valleys. Banded regions of immunostaining between certain cells were apparent in the surface view. In the longitudinal direction, immunostaining was not present, or was weak between IH and LH cells. The LH cells had a high density of Cx26 staining with adjacent LH cells. The center of the IH cells appeared to have staining, but the computationally reconstructed cross-section (Figure 40F) showed that the immunostaining occurred at the junction with the cells beneath them (black

arrowhead). It appears that the cells beneath the IH cells are LH cells since they do not stain intensely for phalloidin, and some of the LH cells appeared to extend to the area underneath IH cells. The cells underneath the intensely staining cells had substantial Cx26 staining at their boundaries in the radial direction as well as in the longitudinal directions. The lateral Hensen cells, another Hensen cell type, lateral to the IH and LH cells (labeled as H in Figure 40F,H) showed short linear staining for Cx26 along the entire perimeter of the cell. This pattern of immunostaining spanned the entire height of the organ of Corti from the basilar membrane to the scala media. These connections were between homotypic cells, and between lateral Hensen cells and LH cells.

Sections through the surface view of the Hensen cell region in apical turns revealed different staining patterns from those in the basal turn. This suggests that the apical cells may represent different subtypes from those presented in the basal turn (Figure 41 and Figure 42) or that they are the same cell types with a different organization. A series of images, from a specimen employing the brown DAB reaction product, taken at 5 μm intervals through the surface preparation from the reticular lamina to the basilar membrane are shown in Figure 42. The nuclei of the roof Hensen cells were at the level of the cuticular plate (Figure 42, 0 μm). These cells showed no immunostaining and were similar to the tectal cells in the base, with the exception that they did not form the top of the outer tunnel of Corti, but instead were situated on top of the Deiters cells that form the outer tunnel. There was little to no Cx26 immunostaining between homotypic outer Hensen cells, whose nuclei are located at 10 μm and 30 μm lower. Cx26 immunostaining was present at low concentrations between the last row of Deiters cells and outer Hensen cells (Figure 42, 0-25 μm). At the region of the Deiters cups, where the outer hair cells sit (Figure 42, 30-50 μm, and Figure 37), staining was denser between outer Hensen cells and Deiters cells. Reconstructed confocal images also showed little staining between the outer Hensen cells in the apical turn (Figure 41). There was dense staining between Hensen cells near the base of the organ of Corti (Figure 41E,F). At this level, the staining pattern appeared as thick linear segments.

Surface views (Figure 40H) showed the complex and tortuous structure of the Hensen cells and suggest that they contact many cells. Nine Hensen cells filled with HRP revealed further complexities in their structure. In 4 cases, processes projected from the Hensen cells to Deiters

cells. These cells were thought to be a subset of the lateral Hensen cells. Processes were present at the level of the cups of the Deiters cells (Figure 43A), and at the base of the Deiters cells (Figure 43B,C). At the base of the cell, Hensen cell processes extended to the third and second row Deiters cells near their insertion into the basilar membrane. In other cases, the processes ran along the basilar membrane and extended to cells as far as three cells in each longitudinal direction. These processes wrapped around the base of the Deiters cells near their insertion into the basilar membrane, as shown in Figure 43C (white arrow). No more than three processes from a single cell were seen at this level. At the level of the Deiters cell cups, Hensen cell processes extended to the third row of Deiters cells and enveloped them. Other smaller processes extended to other Hensen cells. The 4 dye-filled cells appeared to contact 16, 10, 18, 15 cells, respectively, in two of these cases, LY was injected simultaneously with the HRP, and the LY was found in the adjacent Deiters cells and Hensen cells, indicating they were coupled to the cells they contacted. In two other of the nine cases, the dye-filled Hensen cells had no basal processes, but instead sent a process to the tectal cell (Figure 44). In the remaining 3 cases, the cells had no processes and extended from the basilar membrane to scala media similar to the lateral Hensen cells (H) shown in Figure 40. By their location, it appeared that all of these cells were the lateral Hensen cells. It is certain that these cells were not tectal cells, but since they were not counterstained for phalloidin, it could not be determined conclusively if they were IH or LH cells.

The properties of cell morphology seen in dye-filled cells could be recognized in semi-thin plastic sections. An unstained organ of Corti was serially cut at 2 μm surface sections and then stained with toluidin blue (Figure 45). Cells with processes extending to Deiters cells and wrapping around the bases of Deiters cells were more darkly stained with toluidin blue, indicating a denser cytoplasm. These processes were similar to the processes seen in the HRP-filled Hensen cells, extending from the Hensen cell region to the Deiters cells near the Deiters cups (Figure 45A). At a lower plane of section, the same cell extended processes to the second and third row Deiters cells and wrapped around a Deiters cell at its insertion into the basilar membrane, similar to the processes seen in Figure 43C. These darkly stained cells were sparse, being separated longitudinally by about 5 cells. About one third of the last row of Deiters cells had these processes around their bases.

3.3.5 Claudius cells, Boettcher cells, external sulcus cells, and root cells

Claudius cells and Boettcher cells showed Cx26 immunoreactive sites along their entire cell surfaces at appositions with other cells (Figure 46). In the region where Claudius cells are above the Boettcher cells, the computationally reconstructed cross-section showed staining between Claudius cells and Boettcher cells (white arrow in Figure 40F). Boettcher cells stained for phalloidin at the cell membrane, which tended to mask the immunostaining, which is consequently not well defined in Figure 40F.

Fluorescent images of external sulcus cells and root cells showed a linear staining pattern between the external sulcus cells and processes of the root cells. Shorter linear segments were seen among root cell processes. Brightfield and fluorescent images of these cells are shown in Figure 47.

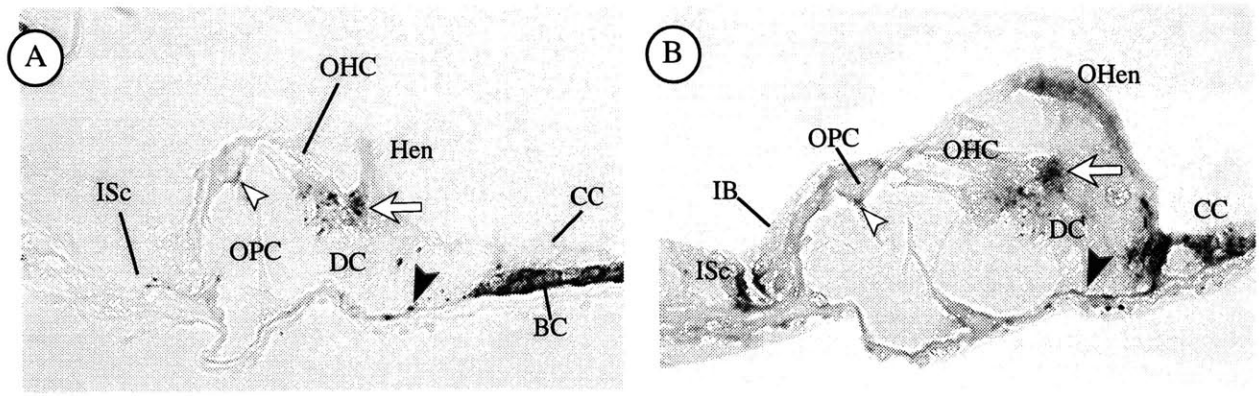

Figure 37. Paraffin sectioned chinchilla cochlea immunostained with anti-Cx26 antibody (1:40K); 10% formalin fixation. The intensity of stain was adjusted to show the densest staining in the organ of Corti. The images are from the same cross-section and were processed simultaneously. **(A)** In the basal turn, the densest staining is seen in the Boettcher cells (BC), at the base of the outer hair cells between Deiters cells (arrow), between the third row of Deiters cells (DC) and Hensen cells (Hen), at the base of Deiters cells (filled arrowhead), and at the bottom of the head of the outer pillar cell (OPC, unfilled arrowhead). The staining at the bottom of the head of the outer pillar cell is between adjacent outer pillar cells in the longitudinal direction. **(B)** In the apical turn the densest staining is seen between the 4th row Deiters cells (DC) and the Claudius cells (CC), at the base of the outer hair cells (OHC), and between inner border cells (IB) and inner sulcus cells (ISc). There is diffuse brown reaction product in the outer Hensen cells (OHen). It's diffuse cytoplasmic distribution distinguishes it from punctate reaction product present at junctions of cells and it is considered to be a non-specific reaction product.

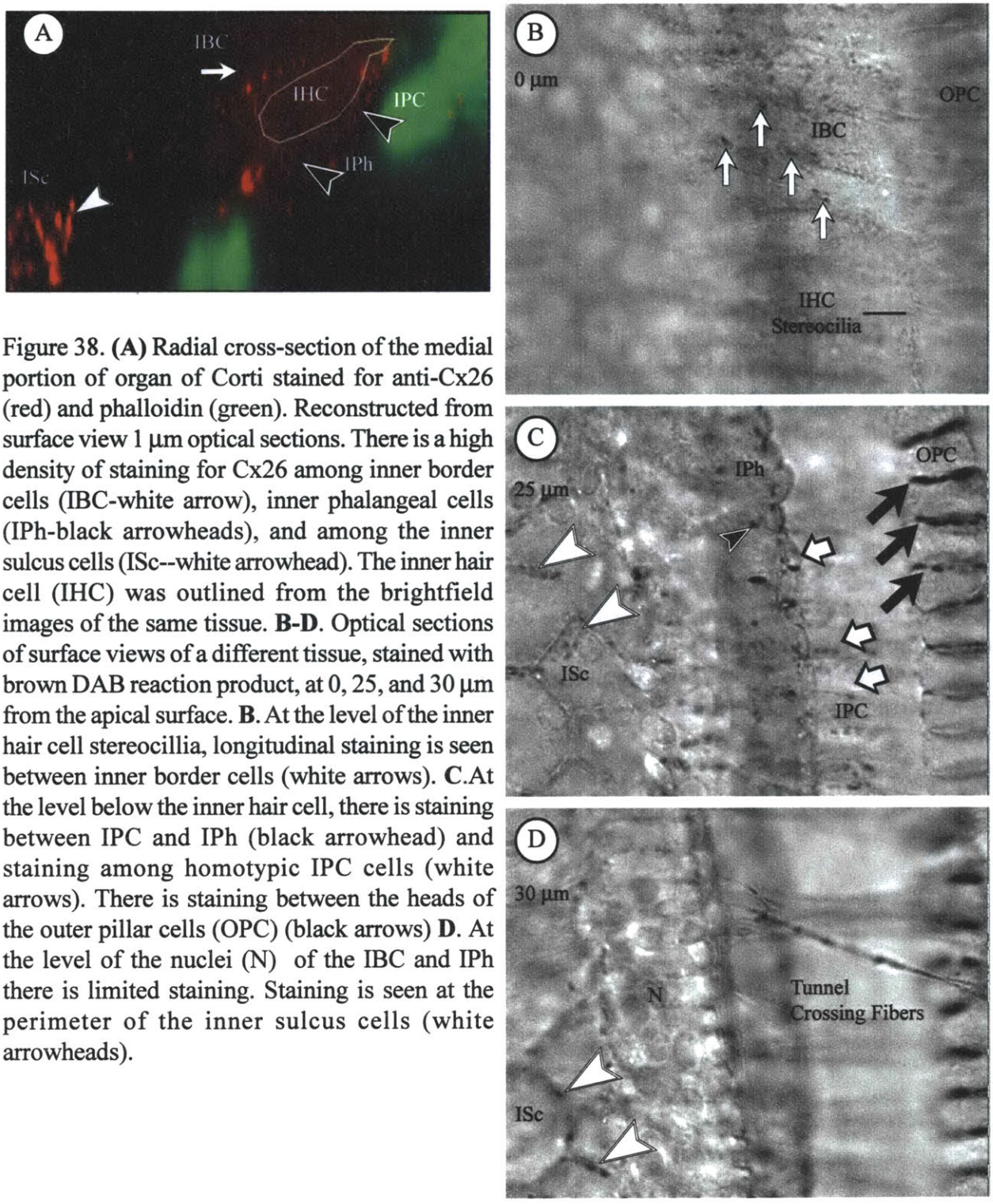

Figure 38. **(A)** Radial cross-section of the medial portion of organ of Corti stained for anti-Cx26 (red) and phalloidin (green). Reconstructed from surface view 1 µm optical sections. There is a high density of staining for Cx26 among inner border cells (IBC-white arrow), inner phalangeal cells (IPh-black arrowheads), and among the inner sulcus cells (ISc--white arrowhead). The inner hair cell (IHC) was outlined from the brightfield images of the same tissue. **B-D**. Optical sections of surface views of a different tissue, stained with brown DAB reaction product, at 0, 25, and 30 µm from the apical surface. **B**. At the level of the inner hair cell stereocillia, longitudinal staining is seen between inner border cells (white arrows). **C**.At the level below the inner hair cell, there is staining between IPC and IPh (black arrowhead) and staining among homotypic IPC cells (white arrows). There is staining between the heads of the outer pillar cells (OPC) (black arrows) **D**. At the level of the nuclei (N) of the IBC and IPh there is limited staining. Staining is seen at the perimeter of the inner sulcus cells (white arrowheads).

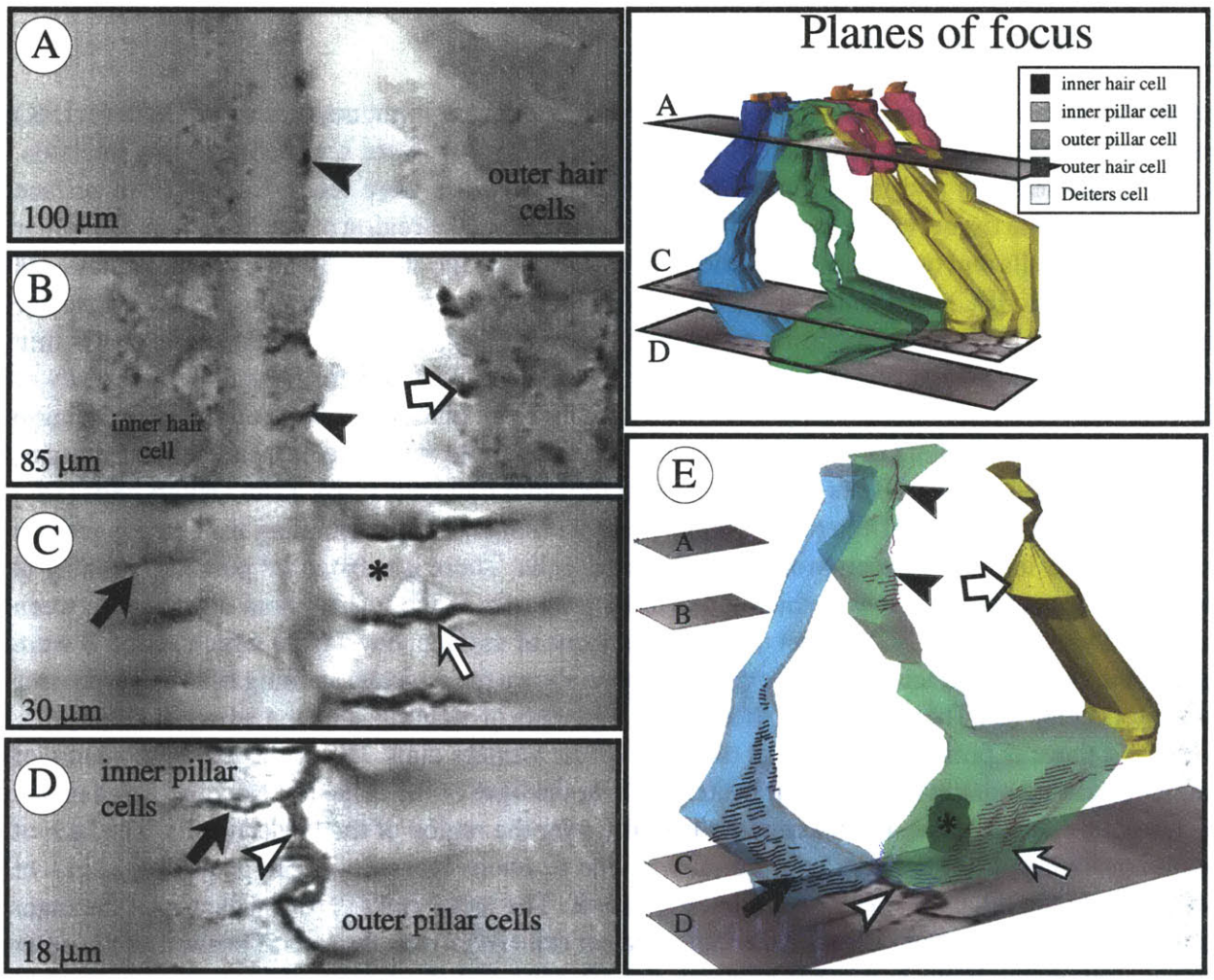

Figure 39. Optical sections at 100 (**A**), 85 (**B**), 30 (**C**), and 18 µm (**D**) with respect to the basilar membrane of a plastic embedded surface preparation immunostained for connexin 26. Images show the region between inner pillar and outer pillar cells. Three dimensional surfaces of cells are reconstructed for orientation (upper right panel) and the immunostaining is mapped onto the surface (**E**) to display locations of gap junctions. **A,B,E**. Vertical punctate reaction product is present between apical sections of adjacent outer pillar cells (black arrowhead) above 90 µm. Some immunostaining is present between Deiters cups (fat white arrow). **D,E**. Dense reaction product is present between adjacent inner pillar and outer pillar cells (white arrowhead). **C,D,E**. Staining between adjacent homotypic inner pillar cells (black arrow) and outer pillar cells (white arrow) is present along the entire surface of the base of the cells. The nucleus of the outer pillar cell is labeled with an asterisk.

(Caption for figure on next page)

Figure 40. Confocal images from the basal turn of the cochlea immunostained for Cx26 (1:15K) (red) and counterstained for phalloidin (green). Surface views were scanned at 1 μm intervals. Radial cross-sections and three-dimensional perspective views were reconstructed from surface views of the same tissue. **(A)** A reconstructed cross-section of the region of the inner hair cell, pillar cells, Deiters cells and outer hair cells. The phalloidin stained the stereocilia, the cuticular plate, the inner pillar cell (IPC), and outer pillar cells (OPC). Some immunostaining is present above the inner hair cell (IHC), corresponding to staining between adjacent inner border cells (IBC- thin white arrow). The no staining is present between tectal cells (T), which form the upper boundary of the outer tunnel. No immunostaining was localized at the level of the outer hair cells (OHC). Staining is present between Deiters cells (DC) at the Deiters cups (bold white arrow), and near the base of the cells (unfilled arrow). **(B)** Perspective view of the outer hair cells (OHC) and Deiters cells (DC) looking at the third row of Deiters cells from the outer tunnel. Immunostaining for Cx26 is present at the reticular lamina between processes of Deiters cells. There is substantial punctate staining at the Deiters cups (white arrow), which looks to be primarily in the longitudinal direction between adjacent Deiters cells. **(C-E)** Subset of optical sections of surface views from which **A** and **B** were generated. **(C)** The surface view at the cuticular plate shows the punctate staining between processes of Deiters cells. **(D)** There are some short linear segments of staining between adjacent outer pillar cells, and there is punctate staining at the level of the Deiters cups. **(E)** Short linear segments of immunostaining are presnet between Deiters cells at the base of the cells. **(F)** Reconstructed cross-section of the same tissue, but taken more laterally over the region of the Hensen cells. The lack of immunostaining in the Deiters cell region was due to photo bleaching from acquiring stacks of images from the tunnel of Corti region shown in **A-E**. The tectal cell (T) forms the top of the outer tunnel. An intensely stained (for phalloidin) Hensen cell (IH) forms the lateral portion of the outer tunnel. Immunostaining is present between the IH cells and the lightly stained (for phalloidin) Hensen cells (LH) below them (black arrowhead). Immunostaining appears to be localized to cell boundaries along the entire length of the LH cells. Lateral to the LH and IH cells of the outer tunnel are Hensen cell (H) that span the entire height of the organ of Corti and are immunostaining along their entire lengths. Boettcher cell (BC) boundaries are darkly stained for phalloidin, which masks the immunostaining for Cx26. Claudius cells (CC) appear to have immunostaining at appositions with the Boettcher cells (white arrow). **(G)** Perspective view of the tissue viewed from the third row of outer hair cells. The tissue has a contour with the three IH cells forming peaks in the tissue, and the LH cells in the valleys. Immunostaining is present along the entire surface of the LH_2 (white arrowhead). **(H)** Surface view looking through the entire tissue shows the complex structures of the Hensen cells. The LH cells appear to have strong immunostaining in the longitudinal direction with other LH cells (white arrowhead). The immunostaining seen within the center of the IH cells (black arrowhead) is actually staining between the IH and LH cells at their basal appositions as shown in the cross-section **F**. The immunostaining at the junction of Hensen cells and Claudius cells appears to be along the entire cell perimeters.

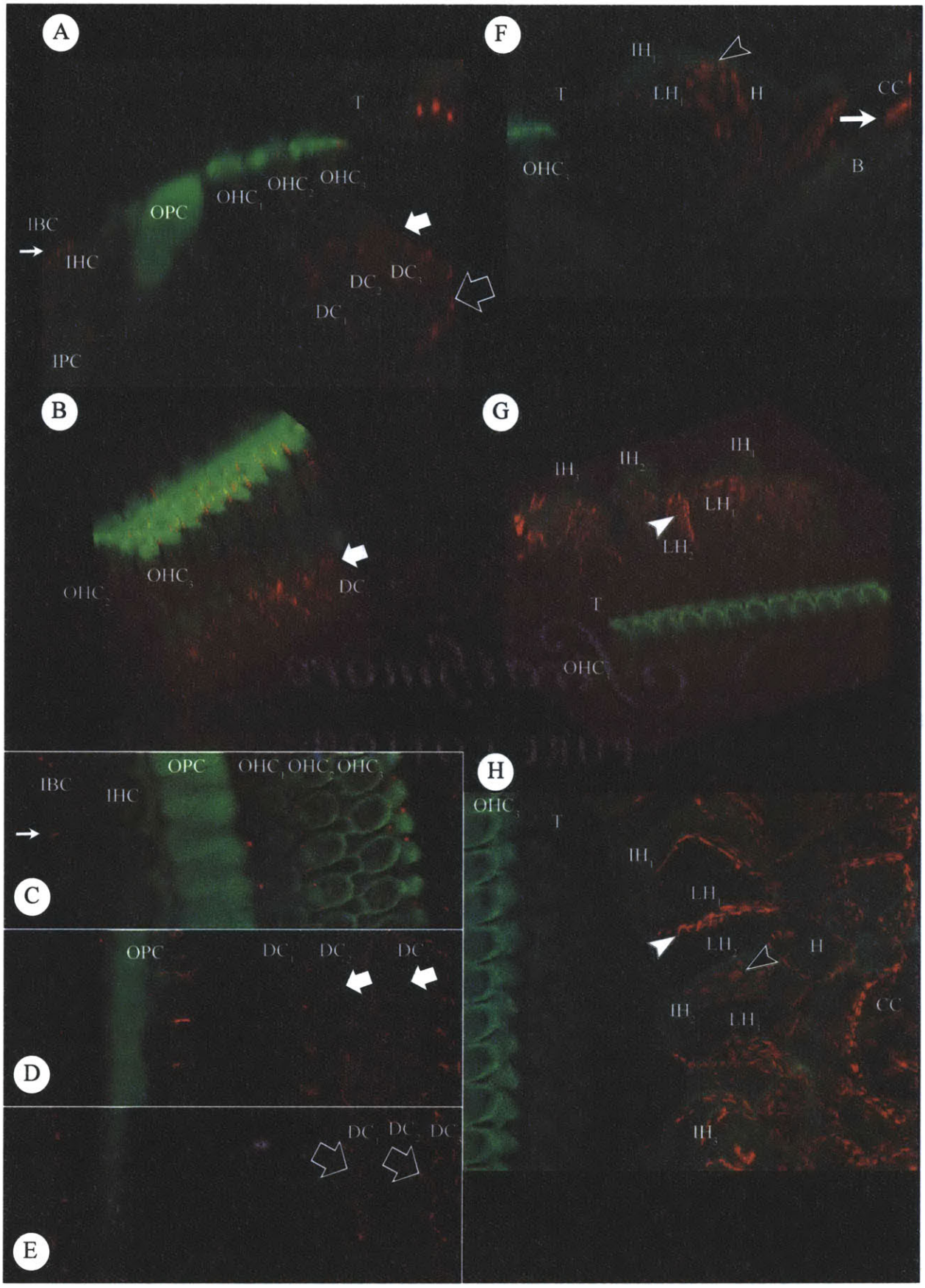
A
T
OHC1
OHC2
OHC3
OPC
IBC
IHC
DC2
DC3
DC1
IPC
B
OHC3
OHC2
DC
C
OPC
OHC1 OHC2 OHC3
IBC
IHC
D
OPC
DC1 DC2 DC3
E
DC1 DC2 DC3
F
IH1
T
LH1
H
CC
OHC3
B
G
IH1
IH3
IH2
IH1
LH1
LH2
T
OHC3
H
OHC3
T
IH1
LH1
LH2
H
IH2
LH1
CC
IH3

(Caption for figure on next page)

Figure 41. Confocal images from the third turn of a chinchilla cochlea immunostained for Cx26 (1:15K) (red) and counterstained for phalloidin (green) and pyronin Y (blue). **(A)** Radial cross-section was reconstructed from optically sectioned surface views separated by 1μm. Labeling for pyronin Y is not shown for the sake of simplicity. Phalloidin labels the heads and feet of the outer pillar cells (OPC), and the cuticular plate. The cell bodies of the three rows of outer hair cells (OHC) were unstained for both phalloidin and Cx26. There was some phalloidin staining at the Deiters cups (black arrowhead) and at the base of the Deiters cell (DC). Immunostaining is present along the basolateral surface of the head of the outer pillar cell (white arrow) and the base of the outer pillar cell (white arrowhead). Immunostaining is present between adjacent Deiters cells at their cups (hatched arrow), along the outer tunnel (unfilled arrow), and at their bases (hatched arrowhead). **(B)** Optical section at the level of the nuclei (N) of the first two rows of outer hair cells and the nuclei of the outer Hensen cells (OHen). There is immunostaining between outer pillar cells (white arrows) and among the last row of Deiters cells (unfilled arrows). Phalloidin staining is present at the level of the Deiters cups around the outer hair cells (black arrowhead). **(C)** Optical section 5 μm below **B** through the Deiters cups and the nuclei of the third row of outer hair cells (N). Dense punctate staining was present between Deiters cells, oriented primarily in the longitudinal direction. **(D)** Optical section at the level of the nuclei of the Deiters cells (N) shows little staining among the Deiters cells. **(E)** Optical section near the base of the cells. Immunostaining is present between bases of adjacent outer pillar cells. There is immunostaining between the bases of the Deiters cells (hatched arrowhead). Immunostaining is localized between Deiters cells and Hensen cells and among Hensen cells. **(F)** At a plane of section below the pillar cell, the nuclei of the cells beneath the basilar membrane are stained with the pyronin. The base of the Deiters cells show some immunostaining (hatched arrowhead), and binding of phalloidin. There is dense staining between Hensen cells.

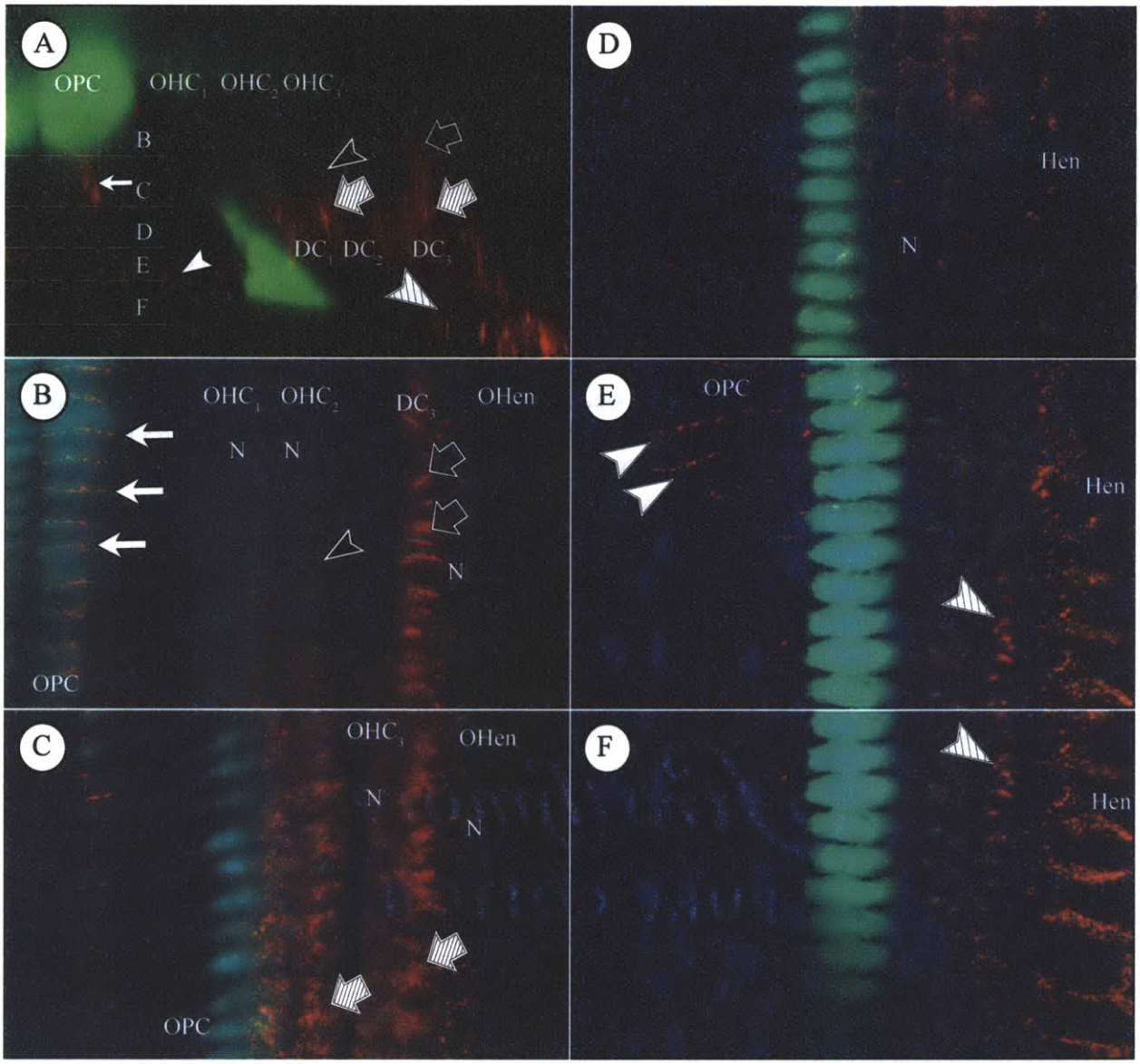
A
OPC
OHC1 OHC2 OHC3
B
C
D
E
F
DC1 DC2 DC3
D
Hen
N
B
OHC1 OHC2
DC3
OHen
N N
N
OPC
E
OPC
Hen
C
OHC3
OHen
N
N
OPC
F
Hen

Figure 42. Surface view of outer tunnel of Corti from the third turn of a chinchilla cochlea immunostained with anti-Cx26(1:15K) using a brown DAB reaction product. Optical sections were taken at 5 μm intervals from the endolymphatic surface to the basilar membrane. **0 μm**. The nucleus (N) of cells similar to the tectal cells in the base are seen. There is staining between the processes of the third row Deiters cells (bold white arrows). **10-25 μm**. One set of nuclei (N) of the outer Hensen cells (OHen) is present. Immunostaining is present between the last row of Deiters cells that forms the undersurface of the tunnel (white arrows). **25-35 μm**.The nuclei (asterisk) of the third row of outer hair cells (OHC) are present. Immunostaining is present between the Deiters cell (DC) at the level of the Deiters cups (black arrowheads) beneath the second row of hair cells. Another set of outer Hensen cell nuclei is present. There is weak staining between the Deiters cells an the outer Hensen cell. **45-55 μm**. The body of the Deiters cells below their nuclei (asterisk at 45 μm) show weaker staining. There is staining between Deiters cells and Hensen cells and among the Hensen cell in the longitudinal direction (black arrows).

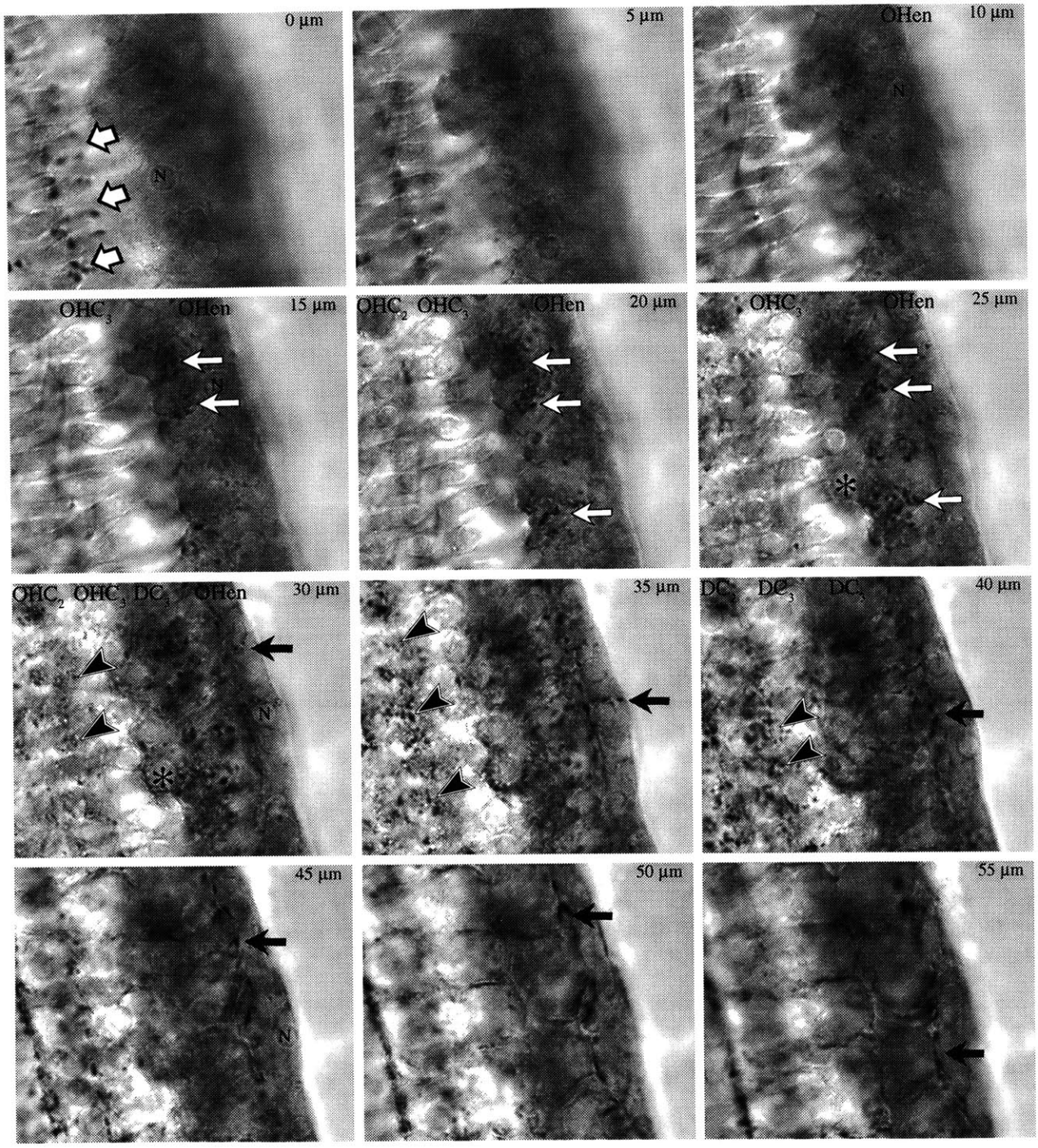
0 µm
N
5 µm
OHen
10 µm
N
OHC3
OHen
15 µm
N
OHC2
OHC3
OHen
20 µm
OHC3
OHen
25 µm
*
OHC2
OHC3
DC3
OHen
30 µm
N
*
35 µm
DC3
DC3
DC3
40 µm
45 µm
N
50 µm
55 µm

Cell	Location/Description	Phalloidin	Cx26 Staining
Tectal Cells	basal turn; roof of outer tunnel.	Little if any at the cell borders	Weak punctate staining with phalangeal processes of 3rd row Deiters cells; occasional staining with other tectal cells in the longitudinal direction.
Cells Intensely Stained for Phalloidin	basal turn; lateral to tectal cells; form peaks at the top of the outer tunnel	Intensely stained for phalloidin; mostly stains the apical surface of the cell	Long linear segment staining with adjacent lightly phalloidin stained cells. Staining at junctions with lightly stained for phalloidin cells underneath them.
Cells Lightly Stained for Phalloidin	basal turn; lateral to tectal cells; forms valleys in the apical contour of the outer tunnel; located underneath the intensely stained cells.	Weakly stained for phalloidin	Strong staining with adjacent lightly stained cells
Lateral Hensen Cells	basal turn; lateral portion of the outer tunnel; appeared to extend the entire height of the organ of Corti.	Weak Staining	Short linear segments of staining along the entire perimeter and height of the cell.
Roof Hensen Cells	apical turn; at the level of the cuticular plate, similar level as the tectal cells; situated on top of the phalangeal process of the 3rd row Deiters cells	Weak Staining	No immunostaining
Outer Hensen Cells	apical turn; lined the apical part of the organ of Corti lateral to the outer tunnel; not clear if they extended to the base of the organ of Corti; cells appear to contain lipid droplets	Apical membrane lightly stained.	Occasional staining with adjacent cells in the longitudinal direction and weak staining between these cells and the 3rd row Dieters cells.
Lateral Hensen Cells	apical turn; adjacent to Deiters cells, at a level below Deiters cell nuclei.	Weak to no staining	Staining appeared as linear segments. The staining was densest at the base of the cell between adjacent Hensen cells and between Deiters cells and Hensen cells.

Table 7. Summary of different types of Hensen cells observed.

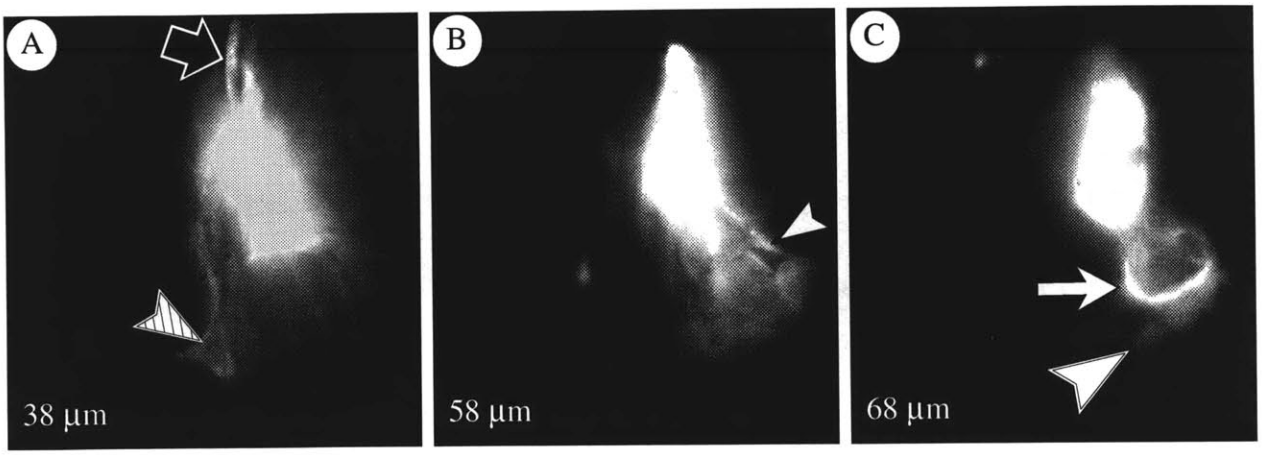

Figure 43. Optical sections through a surface view of fluorescently-labled HRP-filled Hensen cell at 38, 58, and 68 µm from the apex of the cell. The nucleus was centered at 32 µm and the basilar membrane was at 74 µm. **(A)** At the level of the Deiters cup, there is a process (striped arrowhead) projecting to a third row Deiters cell. Some processes project to other Hensen cells (unfilled arrow). **(B)** There are processes extending to different third row Deiters cells near the base of the cell (white arrowhead). **(C)** A process of the cell wraps around the base of a third row Deiters cell (white arrow) and sends processes to second row Deiters cells (white arrowhead).

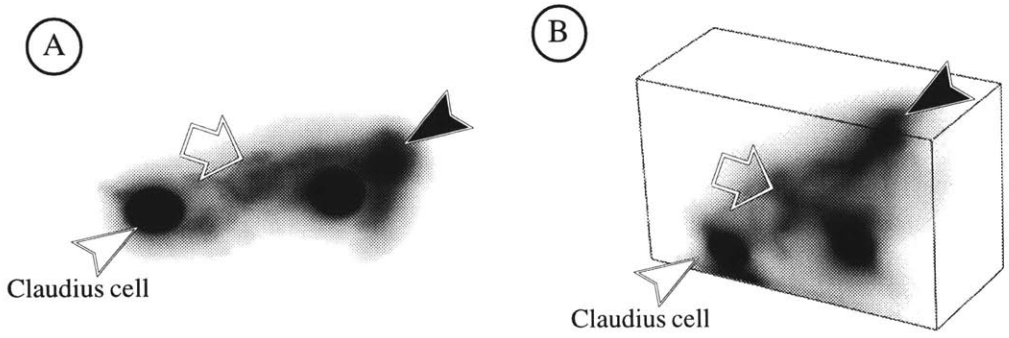

Figure 44. Three-dimensional rendering of lucifer yellow (LY) filled cells.**A**.Surface view of LY injected into a Hensen cell. The images were thresholded and inverted to show the two brightest cells. The optical sections were superimposed to show the dye spread to a Claudius cell (white arrowhead). The surface view shows processes of the Hensen cells that extend to the reticular lamina (black arrowhead) and a process that extend to other Hensen cells (unfilled arrow). **B**. Optical sections were reconstructed to show a 3D perspective view of the dye-filled cells. A process to the reticular lamina is present (black arrowhead), and the level of proceses to other Hensen cells are shown with an unfilled arrow.

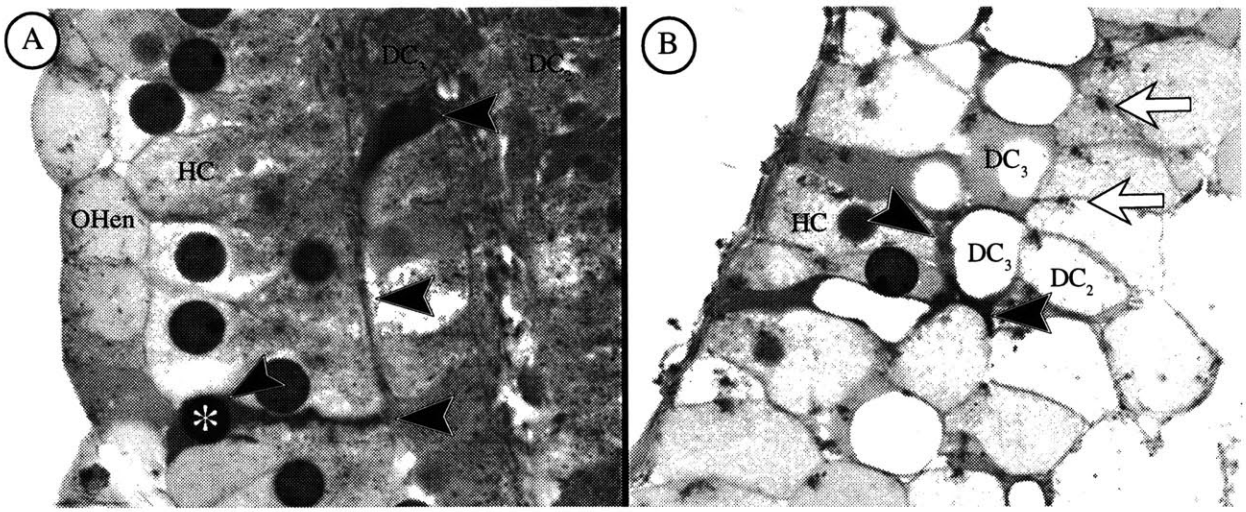

Figure 45. Plastic sections cut at 2 μm thickness in the plane of the surface view through the region of the Hensen cells. The tissue is taken from the end of the basal turn and is stained with toludin blue. **(A)** Section at the level just below the Deiters cell cups, but above their nucleus. The Hensen cell (HC) nuclei are present. A darker Hensen cell (black arrowheads, the asterisk marks the nucleus) sends a processes to second and third row Deiters cells similar to the HRP-filled cell in Figure 40. The outer Hensen cells (OHen) are seen lateral to the Hensen cells with nuclei at this plane of section. **(B)** At the base of the Deiters cells, the same darker Hensen cell is seen enveloping third row Deiters cells (DC_3). This plane of section is 4 μm above the basilar membrane. The white arrows indicate microtubules in the second row of Dieters cells.

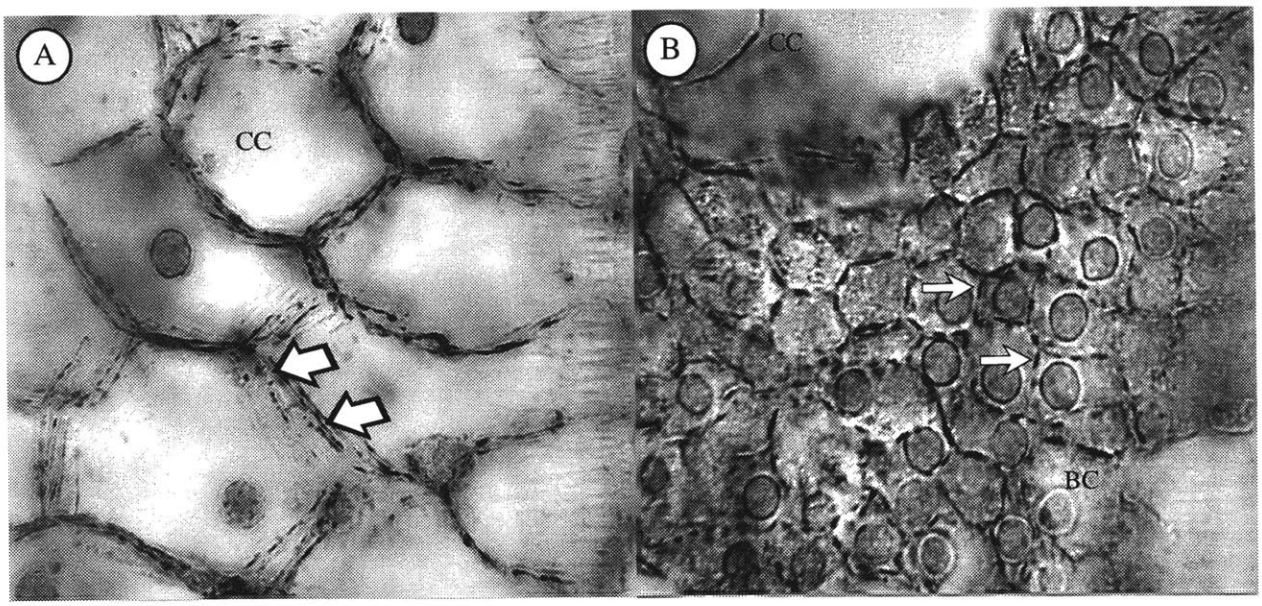

Figure 46. Surface view of Claudius cells (CC) and Boettcher cells (BC) immunostained with anti-CX26 (1:15K). **(A)** Several sections were superimposed to show the depth of the staining. Linear arrays show the staining along the surface of the Claudius cell appositions (white arrows). There is both linear and punctate staining. **(B)** Plane of focus of the Boettcher cells. There are short linear segments of staining between Boettcher cells (white arrows).

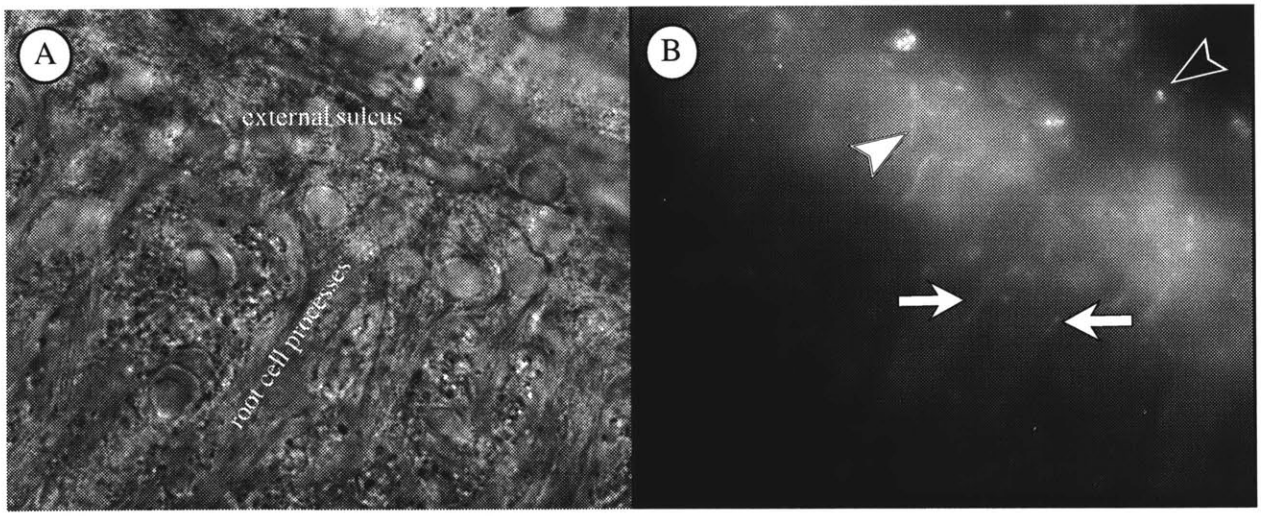

Figure 47. Brightfield (**A**) and flourescent (**B**) surface views at the same plane of focus of the lateral wall showing the external sulcus cells, and the root cell processes (white arrows) extending into the lateral wall. Fluorescent immunostaining with anti-Cx26 (1:15K) shows a linear staining pattern among the external sulcus cells (white arrowhead) and processes of the root cells (white arrows). There is some punctate-like staining among the Claudius cells (black arrowhead).

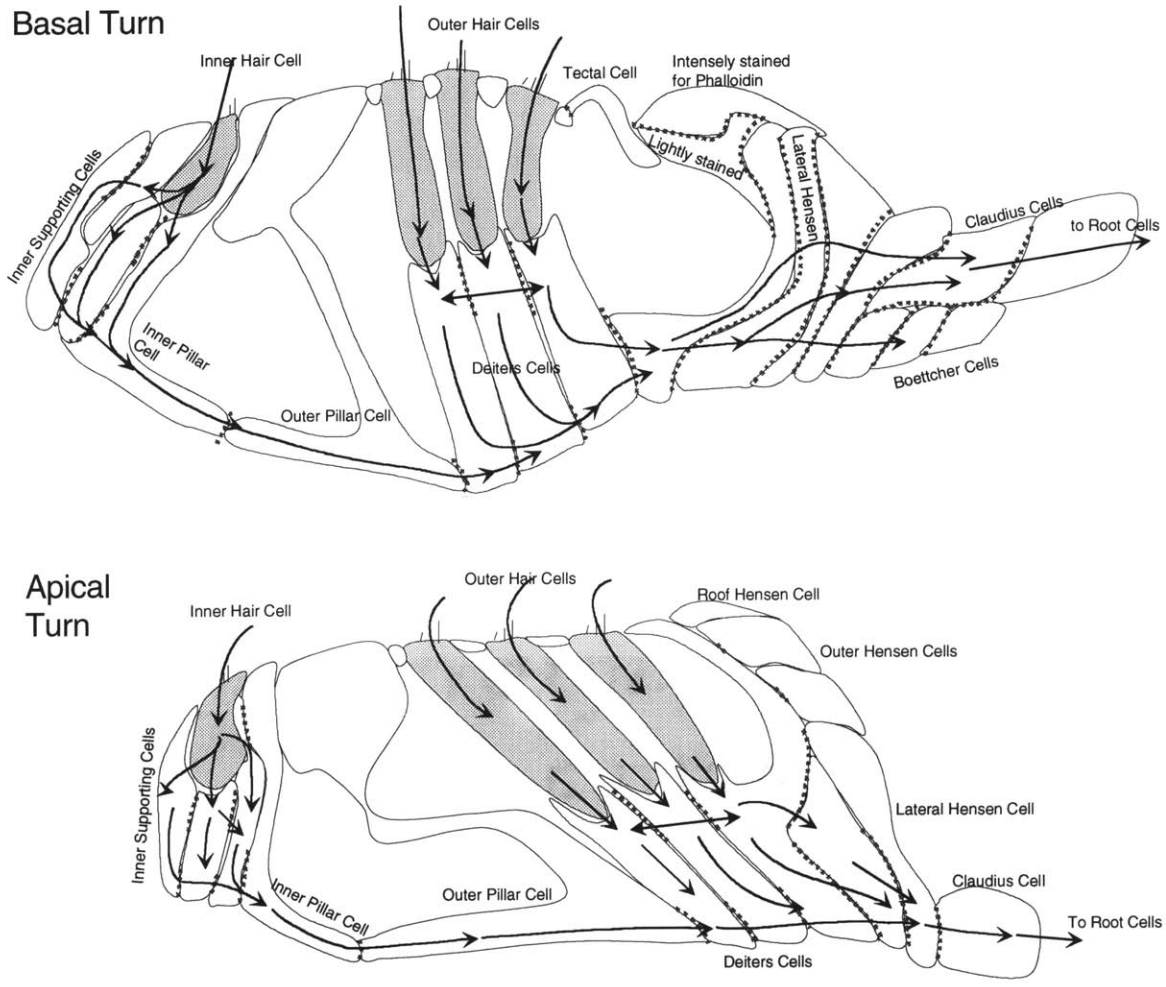

Figure 48. Schematic drawing of cross-sections from a basal turn and an apical turn. The dotted lines show locations where gap junctions were present at appositions between cells. The arrows indicate possible pathways by which potassium can flow within the cell network.

3.4 Discussion

Examination of the immunohistochemical localization of Cx26 by reconstructing images of the tissue at different planes of section provided greater detail in the arrangement of Cx26 at junctions within the organ of Corti than was previously reported. Immunostaining at appositions between non-sensory cells in the chinchilla organ of Corti was in agreement with previous reports of immunostaining in the rat (Kikuchi et al. 1995). In the present study, immunostaining was localized between cells in the organ of Corti including inner sulcus cells, inner border cells, inner phalangeal cells, inner pillar cells, outer pillar cells, Deiters cells, Hensen cells, Boettcher cells, Claudius cells, and root cells. These results extended previous reports (Forge 1984; Gulley 1976; Jahnke 1975a; Jahnke 1975b; Kikuchi et al. 1995) by identifying regions of dense immunostaining at specific sites, which suggests a high degree of coupling at those sites. A high degree of coupling between cell groups suggests that some cells may be organized into sub-networks of more strongly coupled cells. At some appositions, punctate staining was present, whereas at others junctions the staining looked like linear segments. This suggests that there may be different arrangements for gap junctional coupling and that the coupling is not uniform between cells. New observations of Hensen cells showed that they were in contact with many cells and that processes from these cells could project several cells lengths. Subtypes of Hensen cells did not have the same immunolocalization patterns or the same morphology, indicating different functions.

3.4.1 Relationship to physiological measurements

Physiological measurements of cell coupling (Chapters 1 and 2) suggest that cochlear supporting cells are not uniformly coupled to one another. The distribution of gap junctions immunostained for Cx26 in this study was consistent with some of the dye spread and electrophysiological results. Dye coupling experiments presented in Chapter 1 showed rapid and preferred longitudinal movement of dye from injected outer pillar cells to adjacent outer pillar cells. In the present study, a higher density of staining was seen between homotypical pillar cells than between outer pillar cells and Deiters cells. This could explain the apparently stronger coupling among pillar cells and the preferred longitudinal movement of dye. The longitudinal dye movement from inner pillar and inner supporting cells was consistent with denser Cx26

staining in the longitudinal direction among those cell types. Movement of dye in all directions from Claudius cells was consistent with the immunohistochemical localization of Cx26 along the entire surface of these cells where they contact other cells.

Not all movement of dye was consistent with the anatomical distribution of gap junctions. Limited dye movement from outer pillar cells to Deiters cells was consistent with the limited area of staining between these cells. However, immunostaining was not consistent with the finding that there was substantial dye movement from Deiters cells to outer pillar cells. This suggests rectification from Dieters cells to outer pillar cells. Simple rectification would to minimize the flow from pillar cells to Deiters cells, it would be inconsistent with the potassium recycling hypothesis presented in the Introduction. However, if the rectification were due to an electric field, then the anatomical findings would still be consistent with a potassium recycling hypothesis (see Discussion of Chapter 1). There was rapid movement of dye between inner and outer pillar cells, which have a limited area of immunostaining at the base of the cells, and sparse staining at the apex. Therefore, there may be different mechanisms for coupling at the inner-outer pillar junction than at the outer pillar-Deiters junction.

The complex structure of Hensen cells suggests that the number of cells that contact Hensen cells is highly variable. Deiters cells and pillar cells appear to contact just adjacent cells, so the number of cells they contact is less than 10. Hensen cells with processes can contact twice as many cells. The high degree of coupling implies that dye spread from these cells should be more diffuse. However, the results from Chapter 1 do not show any differences in the spread from Hensen cells when compared to Deiters cells. When LY was injected along with HRP, the LY spread to adjacent cells, but did not spread to tertiary cells. The lack of apparent spread may have been due low concentrations of LY in other cells that could not be imaged. An alternate explanation is that the Hensen cells that contact many other cells are sparse and the secondary cells that filled with dye may not have many contacts.

If Hensen cells are functionally coupled to all the cells they contact, then the electrical properties of the cell network in this region could be very different from other uniform coupling regions. The gap junction resistance computed from the mutual resistance measurements would be underestimated because for a unit of injected current, less current would pass to an adjacent cell, if a larger number of cells were coupled. Space constants computed from the mutual

resistance measurements would be smaller in the region of the Hensen cells. The space constants computed using sound-evoked responses depend on the amount of coupling since the model used to compute the space constant was based on a uniform square-grid network. As the number of connections increases, the approximation worsens. Furthermore, if more cells contact in the longitudinal direction, then the radial space constant measurements would not be accurate (see discussion in Chapter 2). This complex structure can account for the range of cell input resistance measured and could account for the variability in the mutual resistance measurements.

The present results offer and explanation of apparent conflicts in physiological studies. There were differences between previous measurements of sound-evoked responses of supporting cells (Oesterle and Dallos 1990) and electrophysiological measures of supporting cells (Santos-Sacchi 1987; Santos-Sacchi 1991), and the results presented in Chapters 1 and 2. Oesterle and Dallos found sound-evoked responses of Hensen cells to be smaller than extracellular responses measured in the outer tunnel of Corti. Mutual resistance between cells was larger in measurements made in Chapter 2 than *in vivo* coupling ratios between Hensen cells reported by Santo-Sacchi. Physiological measurements presented in Chapters 1 and 2 were performed in the base of the cochlea, whereas previous measurements were made using a lateral wall approach in more apical turns. In the present study, outer Hensen cells in the apical turns were found to have less immunostaining for Cx26 than basal Hensen cells. This suggests that apical Hensen cells are less coupled than Hensen cells in the basal turn. Hensen cells are the most accessible supporting cell in the lateral wall approach, so experiments using that approach were heavily biased with results from Hensen cells. The finding that there are differences in the staining density among subpopulations of Hensen cells provides one possible explanation for differences in the physiological measurements of the two studies. If the cells recorded from by previous investigators are less well coupled by gap junctions, as the present immunostaining results suggest, differences in coupling could account for differences in physiological results. The previous experiments were performed in a guinea pig cochlea, and it has not been established if the same change in staining pattern for Cx26 is present in Hensen cells in the guinea pig cochlea. But is it known that the Hensen cells in the apical turns of guinea pig are structurally different from the Hensen cells in the basal turn (Merchan et al. 1980), so differences in coupling could exist.

3.4.2 Implications for potassium recirculation

The hypothesized role of cochlear supporting cells in potassium recirculation has been presented previously (Kikuchi et al. 1995; Spicer and Schulte 1996), and in the Introduction, along with a diagram of the potassium currents in the cochlea (Figure 1). The model of potassium recycling assumes that supporting cells in the epithelial system take up potassium expelled from the hair cells, and release it near the lateral wall where the extracellular potassium concentration is thought to be at a lower level. The spatial organization of the gap junctional networks, together with other anatomical features such as the tight junctional barrier surrounding the stria vascularis (Jahnke 1975b; Kikuchi and Hilding 1966) and the presence of cells that are highly specialized for taking up potassium at the interface of the two gap junctional systems (Schulte and Adams 1989), suggested the hypothesis. The abundance of gap junctions, as indicated by high concentrations of Cx26 immunostaining between cells (Kikuchi et al. 1995), would enable spatial buffering of potassium by cochlear supporting cells in the epithelial cell network.

Several lines of evidence support the hypothesis that Deiters cells, inner phalangeal cells, and inner border cells take up potassium, much as do glial cells. Potassium has been shown to accumulate in the spaces of Nuel and tunnel during acoustic stimulation (Johnstone et al. 1989), which must be removed rapidly from the hair cell and neuronal regions to maintain good cochlear sensitivity. Intracellular electrical measurements showed a slowly depolarizing sound-evoked DC potential in supporting cells that is not present in hair cells. Similar depolarizing potentials have been recorded from Müller cells in response to potassium loading (Reichenbach et al. 1986). Potassium channels of the inward-rectifying type (Kir4.1) have been identified in the Deiters cells (Hibino et al. 1997) and these could be the mechanism by which Deiters cells accumulate potassium expelled by OHCs. There is little extracellular space between the base of the outer hair cells and Deiters cells, so localized regions of high potassium concentrations could develop by potassium leaving the hair cells. The increased extracellular potassium concentration could cause a potassium gradient across the Deiters cell membrane and a potassium current into the Deiters cells.

A summary of the immunostaining patterns in the basal turn and apical turn, shown in Figure 48, shows localization of Cx26 (dotted lines) to be present between most cells in the radial

direction. This figure also shows possible potassium currents and pathways based on the anatomical coupling. There is a complete intercellular pathway from Deiters cells and inner supporting cells to Claudius cells despite the findings that some Hensen cells are less well coupled in the apical turns.

The coupling pattern shows that there may be several different potassium pathways--one at the level of the Deiters cups and one through the base of the cells. The high density of Cx26 localized to membranes at the level of the Deiters cups would allow potassium to be rapidly cleared away from Deiters cells. Without rapid clearance of potassium from Deiters cells, the intracellular potassium concentration could increase such that less potassium enters the cell. In the present study, staining near Deiters cups appeared denser in the longitudinal direction, suggesting that potassium can be longitudinally buffered from regions of higher acoustic stimulation to lower stimulation regions. There was also dense localization of Cx26 at junctions between Deiters cells and Hensen cells at the level of the Deiters cups, which would allow for radial movement of potassium away from the hypothesized inward potassium current at the Deiters cups. Cx26 was localized between Hensen cells such that there is a complete pathway from Deiters cells to Claudius cells.

Dense staining at the base of the Deiters cells could provide a potassium pathway for potassium current taken up by the inner supporting cells. From the inner phalangeal cells all the way to the Hensen cells, there were high levels of staining at the base of adjacent cells (Figure 48). At the inner hair cell side of the organ of Corti, a potassium uptake mechanism may be present in the inner border cells and inner phalangeal cells. A high density of Cx26 localized between cells surrounding the inner hair cells suggests that potassium could be rapidly cleared away from those cells as well. It is not known where the potassium channels are located on the inner hair cells, but since the inner phalangeal cells and inner border cells are in intimate contact along the entire surface of the inner hair cell, they could take up potassium from any place it is expelled. The locations of gap junctions constrain potassium to flow through the feet of pillar cells from the inner supporting cells. The high density of staining in the base of Deiters cells allows for a direct path to the Hensen cells from the pillar cells.

3.4.3 Implications for cell signaling and trafficking

Some cells use gap junctions as a means to provide nutrients and energy to adjacent cells (Goodenough et al. 1980). Cytological studies have shown high concentrations of organelles including mitochondria, lysosomes, Golgi cisternae, and a rosette complex in the upper part of the Deiters cell body, above the level of the nucleus (Nakazawa et al. 1995; Okano et al. 1975; Spicer and Schulte 1993; Spicer and Schulte 1994a). The high density of Cx26 immunostaining among Deiters cells coincides with regions where there is a high density of organelles. If the organelles are involved with signaling molecules or molecules that need to be shared among the Detiers cells, then the high density of gap junctions at this location would provide a short pathway for these molecules. The strong coupling could also be a mechanism by which metabolites and nutrients are shared.

Certain locations where gap junctions were seen are unlikely to be playing a role in potassium recycling. For example, small punctate staining was found between the processes of the Deiters cells and the pillar cells at the reticular lamina. Gap junctions at this level suggest that the processes of cells may share small proteins, amino acids, or molecules since the cell body is remotely located. In the apical turns, outer Hensen cells often contain lipid globules. It has been suggested that these lipid globules are the source for providing nutrients to the other cells in the organ of Corti (Schiff and Christiensen-Lou 1967). The outer Hensen cells may be coupled to the Deiters cell processes through the roof cells or the third row of Deiters cells.

3.4.4 Subsets of Hensen cells

Hensen cells may have previously been inadequately classified because morphological studies failed to find differences between these cells. Hensen cells are generally regarded as the supporting cells lateral to the Deiters cells and the cells that form the outer tunnel. They extend from the endolymphatic surface of the organ of Corti to the basilar membrane (Lim 1980). Evidence from the present study suggests there are different types of Hensen cells. There is a significant difference in the morphology of cells classified as Hensen cells in the basal turns and in the apical turns (Merchan et al. 1980; Schiff and Christiensen-Lou 1967; Spicer and Schulte 1994a; Spicer and Schulte 1994b). The present work showed that there are further subpopulations of Hensen cells in both the apical and basal turns (Table 7).

The tectal cell, a cell type that forms the roof of the outer tunnel, was distinguished from the Hensen cells in the mustache bat (Henson and Henson 1979; Henson et al. 1983). Tectal cells were described as not having any contact with the basilar membrane, as having a thin process that attached to the phalangeal processes of the third row of Deiters cells, and as having a dark staining cytoplasm. The tectal cell has been studied in the mouse (Rueda et al. 1993) and gerbil (Spicer and Schulte 1994a; Spicer and Schulte 1994b). In the present study, it was found that the immunostaining pattern of tectal cells differed from other Hensen cells in that there was no evidence for gap junctional connections longitudinally. Few junctions were found between tectal cells and processes of third row Deiters cells. The dense cytoplasm and high density of mitochondria in the tectal cells suggest that they have an active function other than just forming the roof of the outer tunnel, possibly providing energy or nutrients to the processes of Deiters cells. The cytoplasm of the tectal cells is not as dense as the dark cells shown in Figure 45.

In addition to tectal cells, at least two other Hensen cell types in the basal turn were identified based on their staining with phallodin. The intensely stained cells formed peaks in the contour of the endolymphatic surface of the outer tunnel, whereas lighter cells were in the valleys. The intensely stained cells had fewer longitudinal connections (as determined by Cx26 staining), but they had strong Cx26-like staining at their basal surface at the apposition with lightly stained Hensen cells beneath them. It was not clear if processes of intensely stained cells extended to the basilar membrane or if they contact the tectal cells. The lightly stained cells showed a high concentration of longitudinal staining and they had processes that extended to the basilar membrane. Cells lateral to the intensely and lightly stained cells were classified as lateral Hensen cells. These cells had staining at their appositions with other cells along their entire cell surface.

Lipid globules are present in Hensen cells of the apical turns of many different mammalian species (Merchan et al. 1980; Schiff and Christiensen-Lou 1967). In this study, the cells which contain lipid globules were classified as the outer Hensen cells because they were on the lateral part of the cell mass that formed the outer tunnel. These cells showed a lower density of staining for Cx26, which implies that they are less coupled than other Hensen cells. All Hensen cells may not extend from the endolymphatic surface to the basilar membrane, as evidenced by the locations of their nuclei at several levels along this extent. The optical sections through the organ of Corti (Figure 42) showed cell nuclei at several levels. The cross-sectional area in the surface views of the cells remained constant, so if the cells extend to the basilar membrane, then they

must extend send thinner processes. This could be determined by filling the cells with dye to visualize their complete structure.

The present findings are the first report of processes extruding from Hensen cell bodies to Deiters cells. HRP-filled cells showed processes extending from Hensen cell bodies to Deiters cups as far as four cells in the longitudinal direction. At the bases of the cells, processes projected to and wrapped around the Deiters cell bases at their insertion into the basilar membrane. The Hensen cell processes wrapped around the Deiters cells in the region where Cx26 was localized at the base. However, tissue immunostained for Cx26 was not sectioned to determine if there were connections between the Hensen cell processes and the Deiters cells. Spread of LY from the Hensen cell to the Deiters cells suggested that these cells are coupled by gap junctions.

The role of the processes connecting these cells is not readily evident because not every Deiters cell is in contact with one of these processes and the processes occurred primarily at two planes of focus and extended to different sets of cells. The processes were commonly seen in plastic 2 μm serial sections. The Deiters cells that contacted the processes had no distinguishing features. The Hensen cell processes had a denser cytoplasm than the adjacent Hensen cells. Further examination of these cells, possibly at the untrastructural level, is needed to determine additional morphological properties of these cells.

There is evidence for innervation of some Deiters cells and Hensen cells in apical turns of guinea pig (Burgess et al. 1997; Eybalin et al. 1988; Fechner et al. 1998), rat (Merchan-Perez et al. 1993), cat (Liberman et al. 1990), and human (Nadol and Burgess 1994). Not all Hensen cells were found innervated, and they were more sparsely innervated in the basal turns. The ones that were innervated in the previous studies appear to correspond to the lateral Hensen cells found in the present study. These findings further support the idea that there are several different subpopulations of Hensen cells.

3.4.5 Staining for Phallodin

Much of the research on the morphology of cochlear supporting cells has been centered on the Deiters cells, pillar cells, and the Hensen cells because it was thought that their primary function was to provide mechanical structure for the hair cells. Phalloidin staining has been

localized to pillar cells, outer hair cells, and Deiters cells in the chinchilla (Attanasio et al. 1994), horseshoe bat (Kuhn and Vater 1995), Mongoalian geribil, and guinea pig (Flock et al. 1982; Pack and Slepecky 1995; Slepecky and Chamberlain 1983). In the chinchilla, there was a longitudinal gradient with greater phalloidin staining in the basal and middle turns (Attanasio et al. 1994).

In the present study, phalloidin was intended as a counterstain to identify cell types. More cells and cell processes were stained with phalloidin in the basal turns than in the apical turns. In addition to phalloidin staining at the base of the hair cells (presumed to be in the Deiters cells as previously reported by Attanasio et al. (1994)), phalloidin was found at the base of the Deiters cells near their insertion into the basilar membrane (Figure 41 F). This basal labeling may be part of the structural basis for the insertion into the basilar membrane since phalloidin is thought to stain for F-actin.

In addition to the presence of phalloidin staining in previously described locations—the pillar cells, hair cells, stereocila, and Deiters cells—phalloidin also stained the apical surface of the Hensen cells and the boundaries of Boettcher cells.[13] In the basal turn, certain Hensen cells appeared to have a stained sheath of staining along their endolymphatic surface, whereas other Hensen cells showed no staining. The presence of F-actin in some Hensen cells may provide rigidity to the outer tunnel. In the apical turns, the roof of the outer tunnel which was formed by the last row of Detiers cells was also stained by phalloidin, which indicates that F-actin may serve a common function, perhaps providing rigidity along the outer tunnel. However, the tectal cells did not show staining for phalloidin in the basal turn.

3.4.6 Summary

1. The high density of immunohistochemically localized gap junction proteins among pillar and inner supporting cells at their longitudinal appositions was consistent with the pattern of longitudinal movement of dye from among these cells.
2. Uniform localization of Cx26 at Claudius cell and Boettcher cell appositions was consistent with the uniform spread of dye from these cell types.

[13] Staining was seen in the root processes and external sulcus cells, but was not presented.

3. High concentrations of Cx26 were localized to regions near Deiters cups. Gap junctions at these locations could play a significant role in rapidly buffering potassium that is taken up by channels in the Deiters cups.
4. Non-uniform staining for Cx26, together with complex structures of some of the Hensen cells was consistent with the large range of electrophysiological coupling measurements among these cells.
5. The complex structure and morphology of Hensen cells, which had not been reported before, suggest multiple roles for the Hensen cells, for example in providing rigidity to the outer tunnel, and in ion regulation.

4 Effects of uncoupling agents on the properties of the gap junction networks in vivo

4.1 Introduction

Mutations in the connexin 26 (Cx26) protein, which is the predominant gap junction protein in the cochlea, cause a non-syndromic sensory hearing loss (Carrasquillo et al. 1997; Denoyelle et al. 1997; Kelsell et al. 1997; Zelante et al. 1997). One mutation is a deletion of the majority of the protein, including the region that forms the pore of the gap junction. This suggests that the gap junctions formed by Cx26 are not likely to be functional or patent. The Cx26 mutation is thought to occur in about one out of thirty people, and is believed to be the largest form of hereditary sensory neural hearing loss.

Physiological experiments in the previous chapters have shown that the gap junctions among the non-sensory cells in the organ of Corti are patent *in vivo*. It has also been suggested that the gap junctions allow the cells to function together to remove potassium from the regions near the hair cells and neurons. If the function of the non-sensory cells is critical to the function of the cochlea, then by uncoupling the gap junctions it may be possible to examine their role in maintaining normal hearing. Uncoupling the cells can also lead to some insight into pathologies and dysfunctions associated with the Cx26 mutations.

Gap junctions have reversibly been uncoupled using a variety of pharmacological agents and by altering the intracellular pH of the cells. Several studies showed that *in vitro*, cell aggregates of Hensen cells could be uncoupled reversibly using Octanol and by acidification of the extracellular fluids (Santos-Sacchi, 1992). Since these experiments were performed *in vitro*, it was not possible to determine the effect of uncoupling on hearing or cochlear function.

This chapter describes experiments that were aimed at reversibly uncoupling the gap junctions between non-sensory cells in the cochlea while measuring the physiological condition of the cells, hearing, and the condition of the cochlea. These uncoupling experiments were performed as a control for the physiological experiments in the previous chapters. The cochlea was perfused with artificial perilymph and a pharmacological agent that is known to uncouple

gap junctions while dye was injected into the cells, while electrical measures of impedance were made, or while sound evoked responses were measured from cells. The endochochlear potential (EP) and compound action potential (CAP) were also measured during the application of the uncoupling agents.

4.2 Methods

All procedures with animals were approved by the Animal Care and Use Committee of the Massachusetts Eye and Ear Infirmary. Chinchillas weighing between 300g and 600g were anesthetized with 65 mg/kg of sodium pentobarbital i.p. with boosters given every 2 hours or as needed. Young animals between 3 months and 1 year were used because the bony part of the cochlea was less calcified and easier to shave away than in older animals. After the animal was anesthetized, the trachea was intubated and the head was firmly fixed at the snout and roof of the mouth. The rectal temperature was maintained between 36° and 38° C. The skin and muscle over the back of the skull was removed to expose the bulla and the occipital bone. The pinna was removed to allow for the placement of a sound source into the external canal. To visualize the round window and the hook of the cochlea while leaving the middle-ear apparatus intact, the dorsal-lateral portion of the bulla and several septa were opened by shaving the bone to visualize the round window and the hook of the cochlea.

The procedures for the dye coupling and the electrophysiology experiments are described in Chapters 1 and 2. In this study, a perfusion system was added to the preparation such that scala tympani could be perfused with pharmocological agents. The perfusion system could not be used in conjunction with the on-line imaging system due to the spatial constraints of the system. Therefore, all the dye coupling was assessed after the tissue was fixed. The dye coupling and electrophysiological experiments were performed with a perfusion system. Normal physiology was measured while perfusing with artificial perilymph composed of (in mM): 120 NaCl, 3.5 KCl, 1.5 CaCl, 5.5 glucose, 20 HEPES; titrated with NaOH to pH 7.5; total Na+=130 mM. (Sridhar et. al., 1997), as a control for possible perfusion-related artifacts.

The opening to the cochlea was made slightly larger than in previous experiment, so a 33 gauge perfusion tube could be placed in scala tympani in addition to the recording electrode. The perfusion tube was advanced to within a few millimeters of the basilar membrane. The outflow

was allowed to come out the same opening. Attempts to make an outflow hole in the apex resulted in increased CAP thresholds. A flow rate between 5 and 20 µl/min perfusion of the artificial perilymph did not degrade the CAP thresholds. Gradually decreasing CAP thresholds within the first 30 minutes indicated a too high of a perfusion rate. As a control to verify that the perfuant was getting to the tissue, a 10 mM KCl in artificial perilymph was perfused. This caused a reversible change in the CAP thresholds by 10 to 20 dB SPL. Using the 10 mM KCl solution, it was determined that the perfusant was getting to the entire basal turn of the cochlea. The following perfusants were used: saturated solution of halothane in artificial perilymph (a.p.), saturated solution of octanol in a.p., 100 mM arachidonic acid in a.p., CO_2 bubbled a.p.

The procedure for measuring an effect on the coupling was as follows. First, a cell, usually a Claudius cell, was impaled during perfusion of artificial perilymph. The resting potential and sound-evoked responses to tones (see Chapter 2) were measured under baseline conditions. During normal a.p. perfusion, the baseline CAP thresholds were measured. The a.p. with the uncoupling agent was perfused through the cochlea, and measurements of the slow-DC potential were measured every minute during the perfusion. Every five minutes, CAP thresholds were measured. If there was a change in the slow-DC potential, the perfusant was switched back to the normal artificial perilymph to determine reversibility of the effects on the slow-DC and CAP thresholds.

4.3 Results

The effects of the halothane and octanol were very similar. On occasion, they both produced a decrement in the cell responses and CAP thresholds. The results were extremely variable and inconsistent. The arachidonic acid did not show any effects on the sound-evoked responses and occasionally caused the CAP thresholds to increase. Therefore, it was considered not to have an effect on the gap junctional coupling and those results will not be discussed.

4.3.1 Effects on CAP thresholds and EP

When the uncoupling agents were perfused through the cochlea, there was often a small change in the CAP thresholds. Most of the times the CAP thresholds increased by 20 dB SPL. When the increase was greater than 30 dB SPL or the thresholds were above 60 dB SPL, the

cochlea usually never recovered, and was considered to be irreversibily damaged. When the CAP thresholds increased by more than 5 dB SPL in the frequency range between 6000 and 12000 Hz, they usually never fully recovered to baseline measurements upon flushing out the uncoupling agents (Figure 49) and remained above the baseline measurements. This was taken to mean that the uncoupling agent had a permanent effect on the cochlear physiology. The results presented in the following section will be those in which the CAP thresholds did not increase by more than 10 dB in response to uncoupling agents.

In several experiments, the endocochlear potential (EP) was measured by passing the electrode through the organ of Corti (see Chapter 1 and 2). There was usually no change in the EP during perfusion of any of the uncoupling agents. If the uncoupling agents were affecting all the gap junctions in the cochlea, they would also uncouple the cells in the lateral wall. This would cause the flow of potassium into the intrastrial space to decrease, and thereby decrease the EP. In two cases, EP was reduced by about 55 mV during perfusion of uncoupling agents. In both of these cases, the drop in EP was accompanied by an increase in CAP thresholds of more than 40 dB SPL, and the cell resting potentials were reduced to near –30 to –40 mV. In these cases, no reversibility was observed, and the cause of the cochlear damage was not determined. In four other cases (three with octanol and one with halothane), it appeared that the EP increased by 10 mV. This was unusual since the EP is usually very stable during normal a.p. perfusions. The CAP thresholds often decreased when the EP increased, but the intracellular sound evoked responses were unchanged.

4.3.2 Effects on sound-evoked intracellular potentials and cell input resistance

There were several cases in which the perfusion of octanol or halothane caused a reversible decrease in the sound-evoked intracellular potentials. In these cases, the extracellular responses could not be measured because only a single electrode was placed in the cochlea. The time course of the change in one of the responses is shown in Figure 49.

In other cases, the input cell resistance was measured using a double barrel electrode during perfusion of halothane or octanol. The input impedance increased during the perfusion of the uncoupling agents. In one case the input cell resistance increased from 1.2 MΩ to 1.9 MΩ during perfusion of octanol. When the octanol was flushed out with normal a.p., the input impedance

returned to a level of 1.6 MΩ. In 4 cases when there was a change in the input impedance, it increased on average of 1.7 MΩ.

Six control measurements were made while holding cells for 1 hour while perfusing a.p. In one of these cases, the sound evoked responses decreased by as much as 30% with an increase in the impedance of 0.75 MΩ. These changes were attributed to a poor electrode. The electrode showed drifts of up to 10 mV in the extracellular space.

4.3.3 Dye coupling results

In five preparations, LY was injected into supporting cells after halothane was perfused in the organ of Corti. After injection of the dye into several cells, the cochleas were perfused with fixative, extracted, and the surface preparations were analyzed for dye spread (see Chapter 1). As a control, 1-2 cells were filled with dye before the uncoupling agents were perfused through the cochlea. In one preparation, no dye-filled cells were recovered, which was unusual since seven cells were injected with dye. In two cases, fewer cells were recovered than were injected with dye (10 out of 14 injected cells were recovered). The dye spread to 5-10 cells from the cells that were injected before the halothane, but the cells injected after the halothane appeared to have more limited spread 0-3 cells. In the last two experiments, the surface preparations showed that the dye spread to a substantial number of cells (greater than 20). In the last two preparations, the CAP thresholds increased by 10 dB SPL and the slow-DC potential was present in the supporting cell responses, but the on-DC potential was only slightly larger than the extracellular response. This suggests that the sound-evoked responses were reduced without altering the dye coupling.

4.3.4 Acidification of the artificial perilymph

In three preparations the pH of the artificial perilymph was decreased and perfused through the cochlea. The goal of this experiment was to cause an acidification of the supporting cells such that they would uncouple. CO_2 was bubbled through the artificial perilymph for 10 minutes, and the pH was measured right after the bubbling (5.0). The solution was perfused into the cochlea within 10 minutes of measuring the pH. The low pH a.p. did not significantly alter the CAP thresholds or the slow-DC potentials.

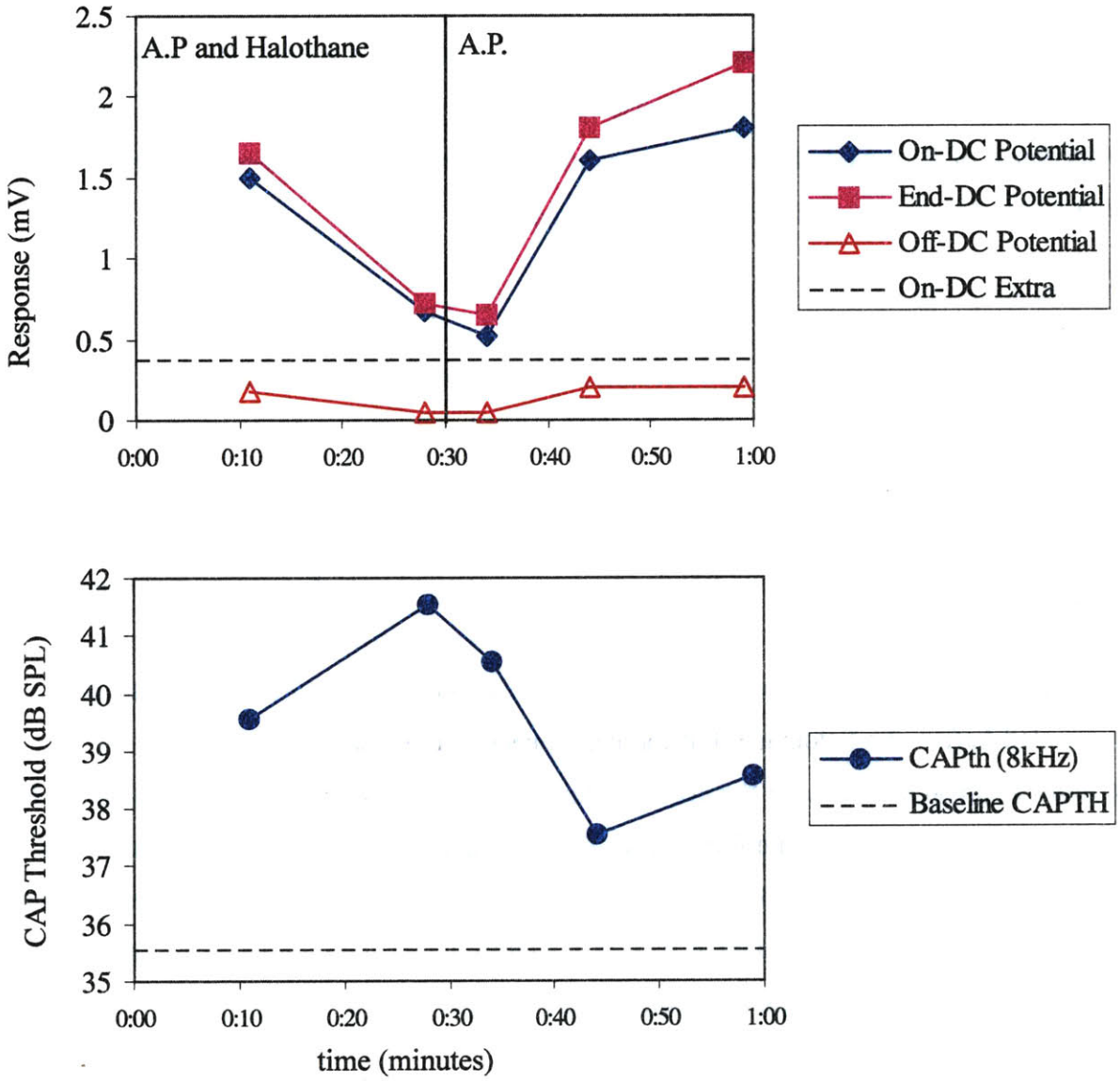

Figure 49. Responses to an application of a saturatated solution of halothane in artificial perilymph (A.P.) at t=0:00 min. The delay for the perfusion was 3:00 min. The perfusate was switched back to normal artificial perilymph at t=30:00 min. (TOP) Sound-evoked responses to an 8kHz, 50 msec tone burst was recorded. The on-DC (diamonds), end-DC (square), and off-DC (open triangle) were extracted from each of the measurements. The duration of the perfusion was 30:00 minutes, with a washout time of 3:00 minutes. The dashed line represents the on-DC and end-DC of the extracellular response measured after the halothane was washed out. The off-DC potential was -0.05 mV. (BOTTOM) The CAP threshold in response to 8kHz tones was elevated above the basline threshold (dashed lines). While there was some recovery during the washout, there was an irreversible threhsold shift..

4.4 Discussion

This study was an attempt to reversibly uncouple the gap junctions in the cochlea using known uncoupling agents. The results were very inconsistent, and definitive conclusions could not be made with the results from these studies. However, the attempt to determine cochlear physiology under uncoupled conditions is integral to understanding the physiology of the cell network and how it may play a role in normal cochlear functioning. Refinement of the experimental conditions may ultimately yield important information.

The uncoupling agents used in the present experiments have been used in other experiment to uncoupled gap junctions between cells. All previous uncoupling experiments were on isolated cell preparations or cell cultures *in vitro*. The present study was an attempt to use these agents *in vivo*. Several problems may account for the inconsistent results. First, since saturated solutions were used, there may have been inconsistent concentrations of the agents in the a.p. solution. The concentration of the octanol or halothane in saturated a.p. is not known. Second, the cells to be uncoupled were not directly accessed. The actual concentration of the uncoupling agents reaching the cells was unknown. Both octanol and halothane are thought to readily bind to extracellular matrix. The supporting cells rest on the basilar membrane, which is as much as 20 μm thick in the basal turn. The octanol or halothane could bind to the basilar membrane, diluting the perfusate or preventing it from reaching the supporting cells. Third, these agents are toxic and could damage other cellular systems that are vital for maintaining normal physiology of these cells. They could also alter the function of hair cells or auditory neurons, thereby altering the criterion used for normal hearing.

While the findings were inconsistent, there were several preparations in which it appeared that the octanol and halothane had some uncoupling effects. Both octanol and halothane appeared to have some effect on the cell responses, but did not appear to completely uncouple the cells. Dye coupling was present in several cases, and in some cases, the extent of the dye spread was reduced. Cell input resistances increased as much as five fold, but never to the approximate isolated cell input resistance (30-50 MΩ computed in Chapter 2). The on-DC and slow-DC potential decreased, but they never reached the level of the extracellular responses, so there may have been some residual hearing left. These results are not inconsistent with previous

reports. When halothane is used as an uncoupling agent, sometimes dye is no longer able to pass between cells, but the cells remain electrically coupled (Duncan et al.,1988)

It was not possible to convincingly uncouple the gap junctional network without knowing if the octanol or halothane affected the hair cells or auditory nerves. The change in CAP thresholds could be explained by a toxic effect of the octanol and halothane on both the hair cells and the auditory nerve. If the current through the hair cells was decreased because of the octanol or halothane, then the decrease in the supporting cell intracellular DC potentials could be due to a decrease in the total current and not uncoupling of the network. If the cells were uncoupled, the EP would be expected to change since the potassium could no long pass through the tight junctional barrier bounding the intrastrial space (see potassium recycling in the Introduction). Since the drugs were applied locally, the EP may have been maintained by other regions of the cochlea such that potassium was adequately supplied to the endolymph.

A different experimental design may be needed to test the effects of uncoupling the cell network. Measuring the cochlear microphonic as a measure of current through the hair cells would be an important addition to the experimental design. If cells were uncoupled through an internal mechanism, this would eliminate possible effects of the uncoupling agents on the hair cells and neurons.

In the initial dye coupling experiments, cells were often photobleached during the LY injection. In most of these cases, the LY did not spread to other cells. If the duration of the injection was longer than 2 minutes, then the cell resting potentials returned to zero, which indicated that the cell was killed. If the injection duration was kept to below 1 minute, the cell often remained viable, but there was still no dye coupling. These results suggest that the use of photobleaching may assist in uncoupling a portion of the network. An experiment could be done in the following way. First, the baseline measurements of sound-evoked measurements would be made from a radial sweep (Deiters cells, Hensen cells, and Claudius cells). Next, inject LY into a set of Hensen cells and confirm that the dye spreads to several Hensen cells in the longitudinal direction. After the dye has spread, photo-irradiate the cochlea such that the Hensen cells uncouple from the Deiters cells and the Claudius cells. This should create a break in the radial pathway. Since the break would be over a limited region of the cochlea, radial sweeps could then be performed to measure the responses of Deiters cells, Hensen cells, and Claudius cells in both

the disrupted region and an intact region. The results would show if the DC potentials are transmitted through the cell network through electrical coupling. If the segment of the organ of Corti is necessary for normal hearing then we might expect that there may be some damage to the hearing in that region of the cochlea where the cells are uncoupled.

5 Conclusion and Summary

This thesis employed complementary techniques to characterize the coupling properties of the epithelial gap junction network in the cochlea. The results from this thesis build upon what little is known about the properties of these cells and how they interact with each other. While these results did not demonstrate a potassium current within the epithelial cell network, they provide evidence that supports the hypothesized intercellular potassium current within the epithelial cell network. One of the main findings in this thesis is that the gap junctions are patent *in vivo*. Evidence suggests that there is a standing current between the supporting cells that may be a significant part of potassium recycling in the cochlea.

5.1 Patency of the epithelial cell network

This thesis has shown that the entire network is coupled from the inner supporting cells to the root cells *in vivo*. Movement of LY between cells confirmed that the gap junctions between the cells were patent *in vivo*. Injected neurobiotin spread throughout the entire epithelial cell network and tended to accumulate in the root cells. Modulation of the gap junctions and quantitative analysis of the amount of coupling could not be determined from these experiments. Therefore, electrophysiological experiments were employed to quantify the electrical coupling. Electrical coupling between supporting cells was confirmed by simultaneously impaling pairs of cells and measuring the responses in one cell from current injected into the other cell. These responses provided a quantitative measure of coupling and confirmed patency of gap junctional connectivity. A third proof of patency was the decrease in the AC and DC responses with increasing distance from the hair cell region. The intracellular responses were larger than the extracellular responses, which suggests coupling between the supporting cells. The fact that the intracellular AC and DC responses decreased in amplitude with distance from the hair cells without a change in the phase, suggests primarily resistive coupling between the supporting cells.

This thesis confirmed previous reports of slowly depolarizing DC potentials in supporting cells in response to sounds. However, the origins of these responses are still unknown. It is thought that the depolarizations are due to an increase in the extracellular potassium concentration in the spaces of Nuel, or potassium taken up by the Deiters cells. Since the

depolarization is has not been observed in hair cell responses, it appears that the response is due to potassium taken up by the supporting cells near the hair cells. If potassium redistribution is the mechanism by which the depolarizing DC potential is generated, then the response should not be present in the supporting cells that are not adjacent to the spaces of Nuel, such as Claudius cells. Therefore, the most likely mechanism by which the responses could be transmitted to the Claudius cells from Deiters cells is through electrical coupling.

5.2 Electrical properties of the epithelial cell network

In this thesis, two methods were employed to characterize the electrical properties of the epithelial cell network in the cochlea. By showing a gradient in the sound-evoked response as a function of distance from the hair cells, a measure of the space constant of the network was made, based on the assumption of a uniformly coupled network. Similar values for the space constant were obtained through measuring mutual resistance between pair of cells. This is the first measurement of its kind within the cochlea *in vivo*. From the measurements of the space constant and the mutual resistance measurements, a range of values for the gap junctional resistance between cells and the cell membrane resistance was obtained. While both of these values were highly variable, they were well within the known physiological range. These measurements were then used to determine amounts of current through the cells based on potential differences.

In this thesis, measurements were made from Claudius cells, which had not previously been studied. The resting potentials of these cells were found to be significantly different from the resting potentials of the Deiters cells and pillar cells. This is a key finding that suggests a standing current between the cells in the cell network. Prior to these measurements, only Deiters cells, Hensen cells, and pillar cells were examined, and no significant difference was found in their resting potentials.

5.3 Modulation of the gap junction network

If the slow-DC potential is transmitted through the supporting cell network, then it can be a useful parameter in quantifying the amount of coupling between the cells. If the network were

uncoupled, then the slow-DC measured in the Claudius cells and some Hensen cells should be reduced or eliminated. Attempts were made to reversibly uncouple cells using uncoupling agents, but the results were inconsistent. In some experiments, the slow-DC potential was reduced during the administration of the uncoupling agents, but they were not consistently reduced. One problem with the uncoupling studies was that the concentration of the agents could not be administered directly to the cells, and it was uncertain if the cells were being uncoupled. Another possible way to uncouple the network, which was not attempted, is to uncouple a portion of the cell network without affecting the sensitivity of the hearing. Such an experiment was presented in the discussion in Chapter 4.

5.4 Currents in the cochlea

One of the goals of the thesis was to examine the epithelial cell network for the purposes of determining if there was any intercellular potassium currents as proposed by the potassium recycling hypothesis. The experiments in this thesis were not able to directly measure potassium flow, but through indirect methods, evidence was presented that suggests the presence of an intercellular current that is likely to be carried principally by potassium.

5.4.1 Longitudinal Currents

The dye coupling experiments showed a strong longitudinal movement of dye when injected into many cell types. These findings were consistent with the anatomical findings of dense staining between homotypic cells in the longitudinal direction. The existence of a current could not be determined because there was no systematic measurement of coupling, resting, or sound-evoked responses in the longitudinal direction. The function of strong longitudinal coupling is not immediately apparent. The longitudinal movement of dye may be due to diffusion. If the negatively charged LY were impeded in moving in the radial direction, for example by a standing current which would promote the movement of cations towards the lateral wall, then the most likely direction for it to move would be in the longitudinal direction because of high density gap junctional connections in that direction.

5.4.2 Coupling to hair cells

Direct measures of coupling between hair cells and supporting cells was not performed, but there is substantial evidence which indicates that the hair cells are not directly coupled to the supporting cells. If the hair cells were coupled to the supporting cells, there should be dye coupling between them. A potassium current from the hair cells to the supporting cells would cause LY to tend to move from the supporting cells to the hair cells. Despite many cases where several Deiters cells or inner supporting cells were filled with LY, no cases of LY-filled hair cells were found. The sound-evoked responses provided further evidence for a lack of coupling between hair cells and supporting cells. The phase of the supporting cells was not similar to the hair cell responses, rather was similar to the extracellular spaces around the hair cells. The magnitude of the extracellular response near the hair cells was larger than that of the supporting cells, but smaller than the hair cell magnitude. Additionally, no immunolocalization of Cx26 was found between the hair cells and supporting cells. The immunostaining at the level of the Deiters cell cups was between adjacent Deiters cells and not between Deiters cells and hair cells.

5.4.3 Radial Intercellular Currents

Dye coupling was not able to conclusively show that there was an intercellular current. If a potential gradient or a current existed, there should be a preferential movement of dye in the radial direction. In most cases, a preferential radial movement of dye was not observed. First, since the dye-coupling was not very quantitative, concentrations of dye in a given cell could not be determined. A quantitative analysis of particle movement may have shown the dye moved via electrodiffusion. The experiments showed that there was some evidence of preferential movement of LY from Deiters cells to pillar cells. A high current density from pillar cells to Deiters cells, is consistent with such a pattern, but the resting potentials of pillar cells and Deiters cells did not appear to be significantly different. If the current exists from pillar cells to Deiters cells, then LY, but not NB would be impeded from moving to Deiters cells. Since the pillar cells are extensively coupled in the longitudinal direction, the dye would move longitudinally via diffusion. This was found to be the pattern of LY movement. NB would tend to move with the current, and in all cases of injected pillar cells, NB was found in Deiters cells and often extended as far as the root cells, indicating a preferred radial movement. Accumulation of NB in the root cells provided stronger evidence that this compound was being carried in part by a current. Since

the LY was not as permeable through the gap junctions and tended to bind to intracellular organelles, the LY did not spread far enough to determine preferential movement in many cases. The simultaneous injections of LY and NB did not convincingly show that the LY moved in the opposite direction of the NB because the amount of movement of the two dyes was very different.

The decrease in the resting potential and the AC and DC potential magnitudes from the supporting cells near the hair cells to the supporting cells near the lateral wall provide strong evidence for an intercellular current consistent with the hypothesized intercellular potassium current. It was shown that the most likely cause for such a gradient in the potentials is due to a current between the cells. Since potassium is the dominant cation, it is likely that this current is due to primarily a potassium current. These findings suggest that the intercellular pathway is more important for recycling potassium in the resting state than the extracellular pathway. During sound stimulation, the intracellular potentials did not appear to increase by much, and by measuring the differences in the potentials, there appeared to be no significant increase in current through the cells during sound stimulation.

The anatomical findings showed that there is a complete pathway from the supporting cells adjacent to the hair cells to the lateral wall, even thought some cells were more densely stained for Cx26 than other cells (Figure 48). What the anatomical findings also suggest is that there may also be intracellular currents within cells such as Deiters cells, pillar cells and Hensen cells since there are dense patterns of staining at different levels between these cells.

5.5 Potassium recycling

While much of the evidence supports the hypothesized potassium recycling pathways in the cochlea, the complete theory as not been proven or disproven. However, these findings provide important information concerning how homeostasis is maintained in the cochlea. It is known that humans with Cx26 mutation show sensory neural hearing losses. If the epithelial gap junction network is disrupted, then a major pathway for potassium recycling will be disrupted. While the size of scala tympani may be able to keep potassium levels low by diffusion, if the potassium leaving the hair cells is not removed, a high level of extracellular potassium could cause the auditory neurons and other cells to degenerate. The histopathology of cochleas of humans with

Cx26 mutations is not known, but when it is known, it may shed considerable light on the anatomical substrates of potassium recycling.

This work has shown the following to support the presence of intercellular potassium currents in the cochlea:

1. The epithelial gap junctional network in the cochlea is patent.
2. The gradient in the resting potentials suggests the existence of a standing intercellular current between the cells.
3. The decrease in the sound evoked potentials from the cells with increasing distance from hair cells suggests the existence of a sound evoked current between the cells.
4. The intercellular impedance was found to be less than the cell membrane impedance. Therefore, potassium taken up by the network would tend to move intercellularly.
5. The amount of potassium current accounted for by intercellular currents was calculated to be greater than that accounted for by extracellular currents.

There are still many facets of this hypothesis that have not been shown:

1. It is not been shown directly how the supporting cells adjacent to the hair cells take up potassium, or if they take up potassium at all.
2. It is not known if the intercellular potential differences give rise to a potassium current, or movement of other ions.
3. Charge neutrality is needed, so a counter-ion flow must be mapped to determine how the cochlea maintains equilibrium in response to movement of potassium from the hair cells to the stria vascularis.

6 Bibliography

Aschner, M. 1998a. Astrocytes as mediators of immune and inflammatory responses in the CNS. *Neurotoxicology* 19: 269-81.

Aschner, M. 1998b. Astrocytic functions and physiological reactions to injury: the potential to induce and/or exacerbate neuronal dysfunction--a forum position paper [see comments]. *Neurotoxicology* 19: 7-17; discussion 37-8.

Attanasio, G., V. P. Spongr, and D. Henderson. 1994. Localization of F-actin and fodrin along the organ of Corti in the chinchilla. *Hear Res* 81: 199-207.

Barbour, B., H. Brew, and D. Attwell. 1991. Electrogenic uptake of glutamate and aspartate into glial cells isolated from the salamander (Ambystoma) retina. *J Physiol (Lond)* 436: 169-93.

Bassnett, S., J. R. Kuszak, L. Reinisch, H. G. Brown, and D. C. Beebe. 1994. Intercellular communication between epithelial and fiber cells of the eye lens. *J Cell Sci* 107: 799-811.

Bennett, M. V., and V. K. Verselis. 1992. Biophysics of gap junctions. *Semin Cell Biol* 3: 29-47.

Bennett, M. V., X. Zheng, and M. L. Sogin. 1994. The connexins and their family tree. *Soc Gen Physiol Ser* 49: 223-33.

Benveniste, E. N. 1992. Inflammatory cytokines within the central nervous system: sources, function, and mechanism of action. *Am J Physiol* 263: C1-16.

Bhat, N. R. 1995. Signal transduction mechanisms in glial cells. *Dev Neurosci* 17: 267-84.

Bologa, L., J. Sharma, D. Dahl, and E. Roberts. 1987. Buffers and H2O2 reduce neuronal death and/or enhance differentiation of neurons and astrocytes in dissociated mouse brain cultures. *Brain Res* 411: 282-90.

Brew, H., and D. Attwell. 1985. Is the potassium channel distribution in glial cells optimal for spatial buffering of potassium? *Biophys J* 48: 843-7.

Brew, H., P. T. Gray, P. Mobbs, and D. Attwell. 1986. Endfeet of retinal glial cells have higher densities of ion channels that mediate K+ buffering. *Nature* 324: 466-8.

Brown, M. C., and A. L. Nuttall. 1984. Efferent control of cochlear inner hair cell responses in the guinea- pig. *J Physiol (Lond)* 354: 625-46.

Brown, M. C., A. L. Nuttall, and R. I. Masta. 1983. Intracellular recordings from cochlear inner hair cells: effects of stimulation of the crossed olivocochlear efferents. *Science* 222: 69-72.

Bruzzone, R., and C. Ressot. 1997. Connexins, gap junctions and cell-cell signalling in the nervous system. *Eur J Neurosci* 9: 1-6.

Burgess, B. J., J. C. Adams, and J. B. Nadol. 1997. Morphologic evidence for innervation of Deiters' and Hensen's cells in the guinea pig. *Hearing Research* 108: 74-82.

Carrasquillo, M. M., J. Zlotogora, S. Barges, and A. Chakravarti. 1997. Two different connexin 26 mutations in an inbred kindred segregating non-syndromic recessive deafness: implications for genetic studies in isolated populations. *Hum Mol Genet* 6: 2163-72.

Celesia, G. G. 1988. Anatomy and physiology of visual evoked potentials and electroretinograms. *Neurol Clin* 6: 657-79.

Charles, A. 1998. Intercellular calcium waves in glia [In Process Citation]. *Glia* 24: 39-49.

Dallos, P. 1996. Overview: Cochlear Physiology in P. Dallos, A. N. Popper, and R. R. Fay, eds. *The Cochlea*. Springer-Verland, New York.

Denoyelle, F., D. Weil, M. A. Maw, S. A. Wilcox, N. J. Lench, D. R. Allen-Powell, A. H. Osborn, H. H. Dahl, A. Middleton, M. J. Houseman, C. Dode, S. Marlin, A. Boulila-ElGaied, M. Grati, H. Ayadi, S. BenArab, P. Bitoun, G. Lina-Granade, J. Godet, M. Mustapha, J. Loiselet, E. El-Zir, A. Aubois, A. Joannard, C. Petit, and et al. 1997. Prelingual deafness: high prevalence of a 30delG mutation in the connexin 26 gene. *Hum Mol Genet* 6: 2173-7.

Detwiler, P. B., and A. L. Hodgkin. 1979. Electrical coupling between cones in turtle retina. *J Physiol (Lond)* 291: 75-100.

Deutsch, D. E., J. A. Williams, and D. I. Yule. 1995. Halothane and octanol block Ca2+ oscillations in pancreatic acini by multiple mechanisms. *Am J Physiol* 269: G779-88.

Donaldson, P., R. Eckert, C. Green, and J. Kistler. 1997. Gap junction channels: new roles in disease. *Histol Histopathol* 12: 219-31.

Duncan, G., S. Stewart, A. R. Prescott, and R. M. Warn. 1988. Membrane and junctional properties of the isolated frog lens epithelium. *J Membr Biol* 102: 195-204.

Enkvist, M. O., and K. D. McCarthy. 1994. Astroglial gap junction communication is increased by treatment with either glutamate or high K+ concentration. *J Neurochem* 62: 489-95.

Eybalin, M. C., M. Parnaud, M. Geffard, and R. Pujol. 1988. Immunoelectron microscopy identifies several types of Gaba-containing efferent synapses in the guinea pig organ of Corti. *Neuroscience* 24: 29-38.

Fechner, F. P., B. J. Burgess, J. C. Adams, M. C. Liberman, and J. B. Nadol. 1998. Dense Innervation of Deiters' and Hensen's Cells Persists after Chronic Deefferentation of Guinea Pig Cochleas. *The Journal of Comparative Neurology* .

Flock, A., A. Bretscher, and K. Weber. 1982. Immunohistochemical localization of several cytoskeletal proteins in inner ear sensory and supporting cells. *Hear Res* 7: 75-89.

Forge, A. 1984. Gap junctions in the stria vascularis and effects of ethacrynic acid. *Hearing Res.* 13: 189-200.

Goodenough, D. A. 1978. Gap junction dynamics and intercellular communication. *Pharmacol Rev* 30: 383-92.

Goodenough, D. A., J. S. d. Dick, and J. E. Lyons. 1980. Lens metabolic cooperation: a study of mouse lens transport and permeability visualized with freeze-substitution autoradiography and electron microscopy. *J Cell Biol* 86: 576-89.

Goodman, D. A., R. L. Smith, and S. C. Chamberlain. 1982. Intracellular and extracellular responses in the organ of Corti of the gerbil. *Hear Res* 7: 161-9.

Gulley, R. L. R., T.S. 1976. Intercellular junctions in the reticular lamina of the organ of Corti. *J. Neurocytol.* 5: 479-507.

Henson, M. M., and O. W. Henson, Jr. 1979. Some aspects of structural organization in the cochlea of the bat, Pteronotus parnellii. *Scan Electron Microsc* 3: 975-82.

Henson, M. M., D. B. Jenkins, and O. W. Henson, Jr. 1983. Sustentacular cells of the organ of Corti--the tectal cells of the outer tunnel. *Hear Res* 10: 153-66.

Hibino, H., Y. Horio, A. Inanobe, K. Doi, M. Ito, M. Yamada, T. Gotow, Y. Uchiyama, M. Kawamura, T. Kubo, and Y. Kurachi. 1997. An ATP-dependent inwardly rectifying potassium channel, KAB-2 (Kir4. 1), in cochlear stria vascularis of inner ear: its specific subcellular localization and correlation with the formation of endocochlear potential. *J Neurosci* 17: 4711-21.

Hoffmann, E. K. 1992. Cell swelling and volume regulation. *Can J Physiol Pharmacol* 70: S310-3.

Ichimiya, I., J. C. Adams, and R. S. Kimura. 1994. Immunolocalization of Na+,K+-ATPase, Ca++-ATPase, calcium-binding proteins, and carbonic anhydrase in the guinea pig inner ear. *Acta Otolaryngol.* 114: 167-176.

Ikeda, K., and T. Morizono. 1989a. Electrochemical profile for calcium ions in the stria vascularis: cellular model of calcium transport mechanism. *Hear Res* 40: 111-6.

Ikeda, K., and T. Morizono. 1989b. Electrochemical profiles for monovalent ions in the stria vascularis: cellular model of ion transport mechanisms. *Hear Res* 39: 279-86.

Iurato, S., K. Franke, L. Luciano, G. Wermbler, E. Pannese, and E. Reale. 1976a. Intercellular junctions in the organ of Corti as revealed by freeze fracturing. *Acta Otolaryngol* 82: 57-69.

Iurato, S., K. Franke, L. Luciano, G. Wermbter, E. Pannese, and E. Reale. 1976b. Fracture faces of the junctional complexes in the reticular membrane of the organ of corti. *Acta Otolaryngol* 81: 36-47.

Jahnke, K. 1975a. The fine structure of freeze-fractured intercellular junctions in the guinea pig inner ear. *Acta Otolaryngol.(supp.)* 336: 1-.

Jahnke, K. 1975b. [Intercellular junctions in the guinea pig stria vascularis as shown by freeze-etching (author's transl)]. *Anat Embryol Berl* 147: 189-201.

Johnstone, B. M., R. Patuzzi, J. Syka, and E. Sykova. 1989. Stimulus-related potassium changes in the organ of Corti of guinea-pig. *J Physiol (Lond)* 408: 77-92.

Johnstone, B. M., and G. K. Yates. 1974. Basilar membrane tuning curves in the guinea pig. *J Acoust Soc Am* 55: 584-7.

Kazemi, H., and L. Choma. 1977. H+ transport from CNS in hypercapnia and regulation of CSF [HCO3-]. *J Appl Physiol* 42: 667-72.

Kelsell, D. P., J. Dunlop, H. P. Stevens, N. J. Lench, J. N. Liang, G. Parry, R. F. Mueller, and I. M. Leigh. 1997. Connexin 26 mutations in hereditary non-syndromic sensorineural deafness. *Nature* 387: 80-3.

Kempski, O., S. von Rosen, H. Weigt, F. Staub, J. Peters, and A. Baethmann. 1991. Glial ion transport and volume control. *Ann N Y Acad Sci* 633: 306-17.

Khanna, S. M., M. Ulfendahl, and C. R. Steele. 1998. Vibration of reflective beads placed on the basilar membrane. *Hear Res* 116: 71-85.

Kiang, N. Y., R. R. Pfeiffer, W. B. Warr, and A. S. Backus. 1965. Stimulus coding in the cochlear nucleus. *Trans Am Otol Soc* 53: 35-58.

Kikuchi, K., and D. A. Hilding. 1966. The development of the stria vascularis in the mouse. *Acta Otolaryngol (Stockh)* 62: 277-91.

Kikuchi, T., R. S. Kimura, D. L. Paul, and J. C. Adams. 1995. Gap junctions in the rat cochlea: immunohistochemical and ultrastructural analysis. *Anat. Embryol.* 191: 101-118.

Konishi, T., P. E. Hamrick, and P. J. Walsh. 1978. Ion transport in guinea pig cochlea I. Potassium and Sodium Transport. *Acta Otolaryngol* 86: 22-34.

Kreutzberg, G. W. 1996. Microglia: a sensor for pathological events in the CNS. *Trends Neurosci* 19: 312-8.

Kuhn, B., and M. Vater. 1995. The arrangements of F-actin, tubulin and fodrin in the organ of Corti of the horseshoe bat (Rhinolophus rouxi) and the gerbil (Meriones unguiculatus). *Hear Res* 84: 139-56.

Laffon, E., and E. Angelini. 1996. On the Deiters cell contribution to the micromechanics of the organ of Corti. *Hear Res* 99: 106-9.

Lamb, T. D., and E. J. Simon. 1976. The relation between intercellular coupling and electrical noise in turtle photoreceptors. *J Physiol (Lond)* 263: 257-86.

Liberman, M. C., L. W. Dodds, and S. Pierce. 1990. Afferent and efferent innervation of the cat cochlea: quantitative analysis with light and electron microscopy. *Journal of Comparative Neurology* 301: 443-460.

Lim, D. J. 1980. Cochlear anatomy related to cochlear micromechanics. A review. *J Acoust Soc Am* 67: 1686-95.

Mammano, F., S. J. Goodfellow, and E. Fountain. 1996. Electrophysiological properties of Hensen's cells investigated in situ. *Neuroreport* 7: 537-42.

Marcus, D. C. 1986. Nonsensory electrophysiology of the cochlea: stria vascularis. Pages 123-137 in R. A. H. Altschuler, D.W.; Bobbin, R.P., ed. *Neurobiology of Hearing: The Cochlea*. Raven Pres, New York.

Marcus, D. C., N. Y. Marcus, and R. Thalmann. 1981. Changes in cation contents of stria vascularis with ouabain and potassium-free perfusion. *Hear Res* 4: 149-60.

Melichar, I., and J. Syka. 1987. Electrophysiological measurements of the stria vascularis potentials in vivo. *Hear Res* 25: 35-43.

Merchan, M. A., J. A. Merchan, and M. D. Ludena. 1980. Morphology of Hensen's cells. *J Anat* 131: 519-23.

Merchan-Perez, A., P. Gil-Loyzaga, J. Lopez-Sanchez, M. Eybalin, and F. J. Valderrama. 1993. Ontogeny of gamma-aminobutyric acid in efferent fibers to the rat cochlea. *Dev. Brain Res.* 76: 33-41.

Merchant, S. N., S. D. Rauch, and J. B. Nadol, Jr. 1995. Meniere's disease. *Eur Arch Otorhinolaryngol* 252: 63-75.

Mizuta, K., M. Adachi, and K. H. Iwasa. 1997. Ultrastructural localization of the Na-K-Cl cotransporter in the lateral wall of the rabbit cochlear duct. *Hear Res* 106: 154-62.

Mobbs, P., H. Brew, and D. Attwell. 1988. A quantitative analysis of glial cell coupling in the retina of the axolotl (Ambystoma mexicanum). *Brain Res* 460: 235-45.

Mountian, I., P. E. Declercq, and W. Van Driessche. 1996. Volume regulation in rat brain glial cells: lack of a substantial contribution of free amino acids. *Am J Physiol* 270: C1319-25.

Muller, T., T. Moller, J. Neuhaus, and H. Kettenmann. 1996. Electrical coupling among Bergmann glial cells and its modulation by glutamate receptor activation. *Glia* 17: 274-84.

Nadol, J. B., and B. J. Burgess. 1994. Supranuclear efferent synapese on outer hair cells and Deiters' cells in the human organ of Corti. *Hearing Research* 81: 49-56.

Nadol, J. B., M. J. Mulroy, D. A. Goodenough, and T. F. Weiss. 1976. Tight and gap junctions in a vertebrate inner ear. *Amer. J. Anat.* 147 No.3: 281-302.

Nagasawa, A., R. V. Harrison, R. J. Mount, and Y. Harada. 1993. Three-dimensional cytoskeletal structures of the chinchilla organ of Corti: scanning electron microscopy application of the polyethylene glycol method. *Scanning Microsc* 7: 897-906.

Nakazawa, K., B. A. Schulte, and S. S. Spicer. 1995. The rosette complex in gerbil Deiters cells contains gamma actin. *Hear Res* 89: 121-9.

Nedergaard, M. 1994. Direct signaling from astrocytes to neurons in cultures of mammalian brain cells. *Science* 263: 1768-71.

Nedergaard, M., A. J. Cooper, and S. A. Goldman. 1995. Gap junctions are required for the propagation of spreading depression. *J Neurobiol* 28: 433-44.

Newman, E., and A. Reichenbach. 1996. The Muller cell: a functional element of the retina. *Trends Neurosci* 19: 307-12.
Norenberg, M. D. 1994. Astrocyte responses to CNS injury. *J Neuropathol Exp Neurol* 53: 213-20.
Oberoi, P., and J. Adams. 1996. Intracellular transport between supporting cells of the organ of corti. *Midwinters meeting of the Association for Research in Otolaryngology*, St. Petersburg, FL.
Oberoi, P., and J. Adams. 1998. In vivo measurements of dye-coupling among non-sensory cells in the organ of Corti. *Midwinters Meeting of the Association for Research in Otolaryngology*, St. Petersburg, FL.
Oesterle, E., and P. Dallos. 1986. Intracellular recordings from supporting cells in the organ of Corti. *Hear Res* 22: 229-32.
Oesterle, E. C., and P. Dallos. 1989. Intracellular recordings from supporting cells in the guinea-pig cochlea: AC potentials. *J Acoust Soc Am* 86: 1013-32.
Oesterle, E. C., and P. Dallos. 1990. Intracellular recordings from supporting cells in the guinea pig cochlea: DC potentials. *J Neurophysiol* 64: 617-36.
Offner, F. F., P. Dallos, and M. A. Cheatham. 1987. Positive endocochlear potential: mechanism of production by marginal cells of stria vascularis. *Hear Res* 29: 117-24.
Okano, Y., T. Yamashita, and H. Iwai. 1975. In vitro morphological study of cochlear epithelium. *Arch Otorhinolaryngol* 209: 151-8.
Pack, A. K., and N. B. Slepecky. 1995. Cytoskeletal and calcium-binding proteins in the mammalian organ of Corti: cell type-specific proteins displaying longitudinal and radial gradients. *Hear Res* 91: 119-35.
Palay, S. L. 1991. The general architecture of sensory neuroepithelia. *Ciba Found Symp* 160: 3-17.
Pappas, C. A., M. G. Rioult, and B. R. Ransom. 1996. Octanol, a gap junction uncoupling agent, changes intracellular [H+] in rat astrocytes. *Glia* 16: 7-15.
Pasantes-Morales, H., J. Moran, and A. Schousboe. 1990. Volume-sensitive release of taurine from cultured astrocytes: properties and mechanism. *Glia* 3: 427-32.
Pasantes-Morales, H., and A. Schousboe. 1989. Release of taurine from astrocytes during potassium-evoked swelling. *Glia* 2: 45-50.
Paul, D. L. 1995. New functions for gap junctions. *Curr Opin Cell Biol* 7: 665-72.
Ransom, B. R., and R. K. Orkand. 1996. Glial-neuronal interactions in non-synaptic areas of the brain: studies in the optic nerve. *Trends Neurosci* 19: 352-8.
Reichenbach, A. 1989. Attempt to classify glial cells by means of their process specialization using the rabbit retinal Muller cell as an example of cytotopographic specialization of glial cells. *Glia* 2: 250-9.
Reichenbach, A. 1991. Glial K+ permeability and CNS K+ clearance by diffusion and spatial buffering. *Ann N Y Acad Sci* 633: 272-86.
Reichenbach, A., B. Nilius, and W. Eberhardt. 1986. Potassium accumulation by the glial membrane pump as revealed by membrane potential recording from isolated rabbit retinal Muller cells. *Neurosci Lett* 63: 280-4.
Reichenbach, A., J. U. Stolzenburg, W. Eberhardt, T. I. Chao, D. Dettmer, and L. Hertz. 1993. What do retinal muller (glial) cells do for their neuronal 'small siblings'? *J Chem Neuroanat* 6: 201-13.

Rhode, W. S. 1971. Observations of the vibration of the basilar membrane in squirrel monkeys using the Mossbauer technique. *J Acoust Soc Am* 49: Suppl 2:1218+.
Rhode, W. S. 1974. Measurement of vibration of the basilar membrane in the squirrel monkey. *Ann Otol Rhinol Laryngol* 83: 619-25.
Rhode, W. S. 1978. Some observations on cochlear mechanics. *J Acoust Soc Am* 64: 158-76.
Richter, C. P., B. N. Evans, R. Edge, and P. Dallos. 1998. Basilar membrane vibration in the gerbil hemicochlea. *J Neurophysiol* 79: 2255-64.
Robinson, S. R., E. C. Hampson, M. N. Munro, and D. I. Vaney. 1993. Unidirectional coupling of gap junctions between neuroglia [see comments]. *Science* 262: 1072-4.
Rueda, J., J. J. Prieto, M. E. Rubio, A. Gutierrez, and J. A. Merchan. 1993. Development of the tectal cells in the mouse cochlea. *Anat Embryol (Berl)* 187: 425-32.
Russell, I. J., and M. Kossl. 1991. The voltage responses of hair cells in the basal turn of the guinea-pig cochlea. *J Physiol (Lond)* 435: 493-511.
Russell, I. J., and P. M. Sellick. 1978. Intracellular studies of hair cells in the mammalian cochlea. *J Physiol Lond* 284: 261-90.
Russell, I. J., and P. M. Sellick. 1983. Low-frequency characteristics of intracellularly recorded receptor potentials in guinea-pig cochlear hair cells. *J Physiol (Lond)* 338: 179-206.
Sakaguchi, N., J. J. Crouch, C. Lytle, and B. A. Schulte. 1998. Na-K-Cl cotransporter expression in the developing and senescent gerbil cochlea. *Hear Res* 118: 114-22.
Salt, A. N., N. Inamura, R. Thalmann, and A. Vora. 1989. Calcium gradients in inner ear endolymph. *Am J Otolaryngol* 10: 371-5.
Salt, A. N., and T. Konishi. 1986. The cochlear fluids: perilymph and endolymph. Pages 123-137 in R. A. H. Altschuler, D.W.; Bobbin, R.P., ed. *Neurobiology of Hearing: The cochlea.* Raven Pres, New York.
Salt, A. N., I. Melichar, and R. Thalmann. 1987. Mechanisms of endocochlear potential generation by stria vascularis. *Laryngoscope* 97: 984-91.
Santos-Sacchi, J. 1986. Dye coupling in the organ of Corti. *Cell Tissue Res* 245: 525-9.
Santos-Sacchi, J. 1987. Electrical coupling differs in the in vitro and in vivo organ of Corti. *Hear Res* 25: 227-32.
Santos-Sacchi, J. 1991. Isolated supporting cells from the organ of Corti: some whole cell electrical characteristics and estimates of gap junctional conductance. *Hear Res* 52: 89-98.
Santos-Sacchi, J., and P. Dallos. 1983. Intercellular communication in the supporting cells of the organ of Corti. *Hear Res* 9: 317-26.
Santos-Sacchi, J., G. J. Huang, and M. Wu. 1997. Mapping the distribution of outer hair cell voltage-dependent conductances by electrical amputation. *Biophys J* 73: 1424-9.
Schiff, M., and H. Christiensen-Lou. 1967. The nature of lipid globules in Hensen's cells. *Ann Otol Rhinol Laryngol* 76: 624-37.
Schubert, J., and J. Adams. 1997. Immunolocalization of a Na+-K+-2Cl--cotransporter within the cochlear and vestibular labyrinth. *Midwinter Meeting of the Association for Research in Otolaryngology*, St. Petersburg, FL.
Schulte, B. A., and J. C. Adams. 1989. Distribution of immunoreactive Na+,K+-ATPase in gerbil cochlea. *J. Histochem. Cytochem.* 37: 127-134.
Sellick, P. M., R. Patuzzi, and B. M. Johnstone. 1982. Measurement of basilar membrane motion in the guinea pig using the Mossbauer technique. *J Acoust Soc Am* 72: 131-41.
Shao, Y., and K. D. McCarthy. 1994. Plasticity of astrocytes. *Glia* 11: 147-55.

Slepecky, N., and S. C. Chamberlain. 1983. Distribution and polarity of actin in inner ear supporting cells. *Hear Res* 10: 359-70.
Somjen, G. G. 1979. Extracellular potassium in the mammalian central nervous system. *Annu Rev Physiol* 41: 159-77.
Spicer, S. S., and B. A. Schulte. 1991. Differentiation of inner ear fibrocytes according to their ion transport related activity. *Hearing Res.* 56: 53-64.
Spicer, S. S., and B. A. Schulte. 1993. Cytologic structures unique to Deiters cells of the cochlea. *Anat Rec* 237: 421-30.
Spicer, S. S., and B. A. Schulte. 1994a. Differences along the place-frequency map in the structure of supporting cells in the gerbil cochlea. *Hear Res* 79: 161-77.
Spicer, S. S., and B. A. Schulte. 1994b. Ultrastructural differentiation of the first Hensen cell in the gerbil cochlea as a distinct cell type. *Anat Rec* 240: 149-56.
Spicer, S. S., and B. A. Schulte. 1996. The fine structure of spiral ligament cells relates to ion return to the stria and varies with place-frequency. *Hear Res* 100: 80-100.
Spray, D. C., A. P. Moreno, and A. C. Campos-de-Carvalho. 1993. Biophysical properties of the human cardiac gap junction channel. *Braz J Med Biol Res* 26: 541-52.
Spray, D. C., R. L. White, F. Mazet, and M. V. Bennett. 1985. Regulation of gap junctional conductance. *Am J Physiol* 248: H753-64.
Sridhar, T.S., M. C. Brown, and W. F. Sewell. 1997. Unique Postsynaptic Signaling at the Hair cell Cell Efferent Synapse Permits Calcium to Evoke Changes on Two Time Scale. *J. Neurosci* 17: 428-437.
Stankovic, K. M., D. Brown, S. L. Alper, and J. C. Adams. 1997. Localization of pH regulating proteins H+ATPase and Cl-/HCO3- exchanger in the guinea pig inner ear. *Hear Res* 114: 21-34.
Steinhauser, C., and V. Gallo. 1996. News on glutamate receptors in glial cells. *Trends Neurosci* 19: 339-45.
Tasaki, I., and C. S. Spyropoulos. 1959. Stria vascularis as source of endocochlear potential. *J. Neurophysiol.* 22: 149-155.
Verkhratsky, A., and H. Kettenmann. 1996. Calcium signalling in glial cells. *Trends Neurosci* 19: 346-52.
Verkhratsky, A., R. K. Orkand, and H. Kettenmann. 1998. Glial calcium: homeostasis and signaling function. *Physiol Rev* 78: 99-141.
Vernadakis, A. 1988. Neuron-glia interrelations. *Int Rev Neurobiol* 30: 149-224.
Verselis, V. K., C. S. Ginter, and T. A. Bargiello. 1994. Opposite voltage gating polarities of two closely related connexins. *Nature* 368: 348-51.
Wangemann, P., J. Liu, and D. C. Marcus. 1995. Ion transport mechanisms responsible for K+ secretion and the transepithelial voltage across marginal cells of stria vascularis in vitro. *Hear Res* 84: 19-29.
Weiss, T. F. 1996. *Cellular Biophysics: Transport.* MIT Press, Cambridge.
Weiss, T. F., D. W. Altmann, and M. J. Mulroy. 1978. Endolymphatic and intracellular resting potential in the alligator lizard cochlea. *Pflugers Arch* 373: 77-84.
Weiss, T. F., M. J. Mulroy, and D. W. Altmann. 1974. Intracellular responses to acoustic clicks in the inner ear of the alligator lizard. *J Acoust Soc Am* 55: 606-19.
Zahs, K. R., and E. A. Newman. 1997. Asymmetric gap junctional coupling between glial cells in the rat retina. *Glia* 20: 10-22.

Zelante, L., P. Gasparini, X. Estivill, S. Melchionda, L. D'Agruma, N. Govea, M. Mila, M. D. Monica, J. Lutfi, M. Shohat, E. Mansfield, K. Delgrosso, E. Rappaport, S. Surrey, and P. Fortina. 1997. Connexin26 mutations associated with the most common form of non-syndromic neurosensory autosomal recessive deafness (DFNB1) in Mediterraneans. *Hum Mol Genet* 6: 1605-9.

Zidanic, M., and W. E. Brownell. 1990. Fine structure of the intracochlear potential field. I. The silent current. *Biophys J* 57: 1253-68.

Zidanic, M., and W. E. Brownell. 1992. Fine structure of the intracochlear potential field. II. Tone-evoked waveforms and cochlear microphonics. *J Neurophysiol* 67: 108-24.

Zwislocki, J. J., and E. J. Kletsky. 1980. Micromechanics in the theory of cochlear mechanics. *Hear Res* 2: 505-12.

Zwislocki, J. J., N. B. Slepecky, L. K. Cefaratti, and R. L. Smith. 1992. Ionic coupling among cells in the organ of Corti. *Hearing Res.* 57: 175-194.